FS SONNE
FAHRTBERICHT SO159
CRUISE REPORT SO159

SALIERI

SOUTH AMERICAN LITHOSPHERIC TRANSECTS
ACROSS VOLCANIC RIDGES

GUAYAQUIL - GUAYAQUIL
AUGUST 21 - SEPTEMBER 17, 2001

Edited by
Ernst R. Flüh, Jörg Bialas, and Philippe Charvis
with contributions of cruise participants

GEOMAR
Forschungszentrum
für marine Geowissenschaften
der Christian-Albrechts-Universität
zu Kiel

KIEL 2001

GEOMAR REPORT 101

GEOMAR
Research Center
for Marine Geosciences
Christian Albrechts University
in Kiel

Redaktion dieses Reports:
Ernst R. Flüh, Jörg Bialas und Philippe Charvis

Editors of this issue:
Ernst R. Flüh, Jörg Bialas, and Philippe Charvis

GEOMAR REPORT
ISSN 0936 - 5788

GEOMAR REPORT
ISSN 0936 - 5788

GEOMAR
Forschungszentrum
für marine Geowissenschaften
Wischhofstr. 1-3
D - 24148 Kiel
Tel. (0431) 600-2555, 600-2505

GEOMAR
Research Center
for Marine Geosciences
Wischhofstr. 1-3
D - 24148 Kiel
Tel. (49) 431 / 600-2555, 600-2505

Table of Content

Abstract

The SALIERI experiment is a cooperation between GEOMAR and GEOAZUR to study the Carnegie Ridge and the active margin of Ecuador and Colombia. The cruise started on 22 August in Guayaquil on-board R/V Sonne and ended on 16 September in Guayaquil. During this cruise ~4000 nautical miles (nm) of multibeam bathymetry were acquired most of them together with magnetics. Two wide-angle seismic lines were shot on the Carnegie Ridge, three in the Gulf of Guayaquil and one on the Colombian margin for a total of 130 OBS deployments. Profiles P02, P05 and P06 were shot along pre-existing multichannel seismic reflection lines acquired during the SISTEUR cruise in 2000.

Most of the OBS data are of excellent quality with clear arrivals at offsets greater than 100 km on the oceanic crust. Two approximately N-S lines were shot across the Carnegie Ridge. The western profile (PO1) on Carnegie Ridge exhibits a 16-km thick crust whereas the eastern one, immediately west of the subduction zone, shows a crust as thick as 25 km. Modelling indicates that crustal thickening is mainly related to a thickening of oceanic layer 3. Velocity structures resemble those described beneath other oceanic plateaus formed near a spreading centre especially the Cocos and Malpelo ridges.

'In the Gulf of Guayaquil the dip seismic line P02 constrains deep structures of the overriding plate and the subducting oceanic plate. On the margin the thick Guayaquil sedimentary basin imaged from MCS during the Sisteur cruise is at least 6 km thick. The crust of the South American plate extends westwards almost to the trench with seismic velocities increasing from ~4.0 km/s to ~4.5 km/s. A clear shadow zone (0.5 to 1.0 s of offset along PO3) possibly outlines sediments subducted beneath the margin.

Profile P06 across the North Ecuadorian-Southwest Colombian margin exhibits clear arrivals from the upper plate and the down-going plate, which will allow to model the convergent margin using both wide-angle and previous SISTEUR MCS data.

Multibeam bathymetry acquired during the cruise show that the Carnegie Ridge is a highly asymmetric dome feature with a steep, faulted northern flank and a gently sloping southern one intruded locally by large, flat-topped and elongated seamounts. Among the most conspicuous features on the Ridge are fields of circular closed depressions distributed over its flanks at depths of 1500 to 2600m, and two EW-trending alignments of reflective basement highs outlining a graben-like structure in its eastern part. These data also show that the inner trench slope off Guayaquil (latitude 3°S) is unstable, affected by mass wasting and incised by a major canyon carrying sediment into the trench. Incipient accretion is evident at the toe of the margin. The Grijalva Fracture Zone is marked by an overall N50E scarp with a narrow linear N60E trending Ridge. Offshore Esmeraldas near 1° 40'N, the upper margin section is smooth and sub-horizontal. Its lower section has a rough morphology and is deeply incised by a major canyon dumping sediment into the Colombia trench to form a noticeable sedimentary fan. Between 1° 40'N and 0° 30 N, incipient accretion is locally evident along a generally non-accretionary margin.

Magnetic anomalies across Carnegie Ridge are generally related to the topography, in particular large seamounts and local volcanic domes and basement faults. South of the Carnegie Ridge possible seafloor spreading anomalies are observed. The margin profiles in SW Colombia and the Gulf of Guayaquil are magnetically quiet presumably due to the homogeneous and weak magnetic composition of the upper plate.

Zusammenfassung

Die Ausfahrt SALIERI ist ein Gemeinschaftsexperiment der Forschungsinstitute GEOMAR und GEOAZUR um das ozeanische Plateau des Carnegie Rückens und des aktiven Kontinentalrandes vor Equador und Kolumbien zu untersuchen. Die Reise an Bord des FS SONNE begann am 22 August in Guayaquil und endete dort am 16. September. Während dieser Reise wurden annähernd 4000 Seemeilen (sm) Kartierung mit dem Fächerecholot gefahren, der größte Teil davon gemeinsam mit Magnetik. Zwei seismische Weitwinkellinien wurden über den Carnegie Rücken, drei im Golf von Guayaquil und eine am kolumbiansichen Kontinentalrand mit 130 OBS Stationen vermessen. Die Profile P02, P03 und P06 wurden wurden dabei entlang der vorliegenden Linien mit Mehrkanalseismik aus dem SISTEUR Projekt von 2000 aufgenommen.

Zum größten Teil sind die OBS Daten von sehr guter Qualität, auf der ozeanischen Kruste mit klaren Einsätzen bis zu Distanzen von über 100 km. Zwei Linien wurden nahezu N-S verlaufend über den Carnegierücken geschossen. Das westliche Profil (P01) auf dem Carnegierücken zeigt eine 16 km mächtige Kruste, wohingegen das östliche, direkt westlich der Subduktionszone gelegene Profil eine 25 km mächtige Kruste aufweist. Modellierungen belegen das die Krustenverdickung im wesentlichen im ozeanischen Layer 3 stattfindet. Die Geschwindigkeitstruktur spiegelt ein solche Verteilung wieder, wie sie von anderen ozeanischen Plattformen bekannt ist, die in der eines Spreizungszentrums gebildet wurden, besonders trifft dies auf den Cocos- und den Malpelorücken zu.

Die quer zum Streichen verlaufende Linie P02 im Golf von Guayaquil zeigt tiefe Strukturen der überschiebenden und der subduzierenden Platte. Am Kontinentalrand erreicht das mächtige Guayaquil Sedimentbecken eine Tiefe von 6 km, die auch in der Mehrkanalseismik aus dem SISTEUR Projekt gut belegt ist. Die Kruste der südamerikanischen Platte erstreckt sich weiter wetswärts, nahezu bis zum Graben, wobei die seismsiche Geschwindigkeit von ~4.0 km/s auf ~4.5 km/s zunimmt. Eine deutliche Schattenzone (P03, 0.5 s - 1.0 s Versatz) mag ein Anzeichen für subduzierte Sedimente sein.

Das Profil 06 über den nordequadorianischen-südwestkolumbischen Kontinentalrand zeigt klare Einsätze, sowohl der oberen, als auch der nach unten gehenden Platte. Diese werden es erlauben in Verbindung mit der Mehrkanalseismic der SISTEUR Daten ein Modell für den konvergenten Kontinentalrand zu erstellen.

Bathymetrische Vermessung mit dem Fächerlot zeigt den Carnegierücken als stark asymmetrische Aufwölbungsstruktur mit einer steilen gefalteten nördlichen und einer leicht geneigten südlichen Flanke, die von lokalen gestreckten Seamaounts mit ebener Kuppe durchdrungen wird. Zu den überraschensten Strukturen auf dem Rücken zählen Felder kreisrunder geschlossener Vertiefungen, die über die Flanken in Tiefen von 1500 m bis 2600 m verteilt sind. Ebenso zwei EW verlaufende reflektierende Hochs des Basement, die im östlichen Teil eine grabenähnliche Struktur anzeigen. Die Daten zeigen ebenfalls, das der inner Hang vor Guayquil (3° Grad S) instabil ist, beeinflußt durch Materialablagerungen und unterstützt durch einen prominenten Canyon, der Sediment bis in den Trench transportiert. Beginnende Akkretion kann am Fuß des Hanges beobachtet werden. Die Grijalva Zone ist durch eine 50° NE verlaufende Stufe mit einem schmalen 60° NE verlaufenden Rücken gekennzeichnet. Seewärts von Esmeralda, bei etwa 1°40´N ist der obere Kontinentalrand glatt und horizontal. Der unter Teil weist eine rauhe Morpholgie auf und ist durch einen markanten Canyon, der Sediment bis in den kolumbischen Tiefseegraben transportiert und einen bemerkenswerten Fächer bildet, tief eingeschnitten. Zwischen 1°40´N und 0°30´N ist eine anfängliche Akkretion an einem sonst nicht akkretierenden Kontinentalhang zu sehen.

Magnetische Anomalien über dem Carnegierücken sind im allgemeinen an die Topographie gebunden, insbesondere im Bereich von Seamounts, lokalen Vulkankegeln und Basementbrüchen. Südlich des Carnegierücken wurden vermutlich Spreadinganomalien gemessen. Die Profile über den Kontinentalrand in SW Kolumbien und im Golf von Guayaquil sind vermutlich aufgrund der homogenen und gering magnetisierten oberen Platte magnetisch ruhig.

Résumé

La campagne SALIERI est une coopération entre GEOMAR et GEOAZUR pour l'étude de la ride volcanique de Carnégie et de la marge convergente d'Équateur et de Colombie. La campagne a débuté le 22 Août à Guayaquil, à bord du N/O Sonne et s'est terminée le 16 Septembre à Guayaquil. Pendant cette campagne environ 4000 milles nautiques de bathymétrie multifaisceau ont été enregistrés, le plus souvent simultanément avec le champ magnétique. Deux profils de sismique grand-angle furent tirés à travers la ride de Carnégie, trois dans le Golfe de Guayaquil et un sur la marge Colombienne avec au total 130 déploiements d'OBS. Les profils P02, P05 et P06 furent tirés sur des profils de sismique réflexion multitrace acquis pendant la campagne SISTEUR en l'an 2000.

Les données sont en général d'excellente qualité avec des arrivées claires pour des offsets supérieurs à 100 km sur la croûte océanique. Deux profils approximativement nord-sud furent tirés à travers la ride de Carnégie. Le profil Ouest montre une croûte de 16 km d'épaisseur alors que sous le profil Est, situé immédiatement à l'Ouest de la fosse de subduction, elle atteint 25 km. L'épaississement crustale est principalement lié à l'épaississement de la couche 3 (croûte inférieure). La loi de vitesse est comparable à celle observée sous d'autres rides volcaniques construites au voisinage d'un axe d'expansion et particulièrement les rides de Cocos et de Malpelo.

Dans le Golfe de Guayaquil, le profil perpendiculaire à la marge (P02) a permis la modélisation de la plaque chevauchante et la plaque océanique subduite. Sur la marge, l'épais bassin sédimentaire de Guayaquil, imagé par sismique réflexion, atteint au moins 6 km d'épaisseur. La croûte de la plaque Sud-Américaine s'étend vers l'ouest jusqu'à la fosse avec des vitesse sismique augmentant de ~4,0 à ~4,5 km/s. Une zone d'ombre, avec un décalage de 0,5 à 1,0 s (P03) correspond probablement à des sédiments subduits sous la marge.

Le profil P06 sur la marge Colombienne montre clairement des arrivées réfractées et réfléchies dans les plaques chevauchantes et plongeantes qui vont permettre une modélisation des données coincidantes de sismique réflexion (campagne SISTEUR) et réfraction.

Les données de bathymétrie multifaisceau enregistrée pendant cette campagne montrent que le ride de Carnégie est une structure très dissymétrique avec un flanc nord abrupt, affecté de failles, et un flanc sud en pente douce mais localement affecté de grands volcans allongés dont le sommet est plat. Parmi les structures caractéristiques observées sur la ride, des zones parsemées de dépressions circulaires fermées distribuées sur les flancs de la ride entre 1500 et 2600 m de profondeur, et deux alignements Est-Ouest de hauts du socle, réflectifs, soulignant des structures en graben à l'Est. Les données montrent que le mur interne de la fosse, au large de Guayaquil, est instable, affecté par des glissements sédimentaires et entaillé par des canyons qui assurent le transport des sédiments vers la fosse. Un début d'accrétion apparaît à l'extrémité de la marge. La zone de fracture de Grijalva est marquée par un escarpement N50°E avec une ride étroite de direction N60°E. Au large d'Esmeraldas, vers 1° 40'N, le haut de la marge est lisse et subhorizontal. Le bas de la marge présente au contraire une topographie accidentée et est profondément entaillée par des canyons majeurs assurant le transport des sédiments vers la fosse où se développe un delta profond. Entre 1° 40'N et 0° 30' N, un début d'accrétion est évident le long d'une marge globalement en érosion.

Les anomalies magnétiques à travers la ride de Carnégie sont en général associées à la topographie du socle, en particulier les principaux monts sous-marins, les petits dômes volcaniques et les failles affectant le socle. Les profils de la marge au sud-ouest de la Colombie et dans le Golfe de Guayaquil sont magnétiquement calmes sans doute à cause de la composition homogène et peu magnétique de la plaque chevauchante.

Resumen

El experimento SALIERI es una cooperación entre GEOMAR y GEOAZUR para estudiar la cordillera oceánica de Carnegie y el margen activo de Ecuador y Colombia. El experimento, realizado a bordo del buque oceanográfico alemán R/V Sonne, comenzó el 22 de agosto y terminó el 16 de septiembre en Guayaquil. Durante la campaña se adquirieron ~4000 millas náuticas (nm) de batimetría multihaz, la mayoría junto con datos magnetismo. También se dispararon dos perfiles de sísmica de gran ángulo a través de la cordillera de Carnegie, así como tres en el Golfo de Guayaquil y otro en el margen colombiano, lo cual supuso un total de 130 despliegues de sismómetros e hidrófonos de fondo oceánico (OBS/OBH). Los perfiles P02, P05 y P06 se dispararon a lo largo de tres líneas de sísmica multicanal (MCS) adquiridas durante la campaña SISTEUR en 2000.

La mayoría de los datos de los OBS/OBH son de excelente calidad, con claras llegadas hasta distancias de más de 100 km de los receptores en la corteza oceánica. Dos líneas aproximadamente N-S fueron disparadas a través de la cordillera de Carnegie. El perfil oeste (P01) de Carnegie exhibe una corteza de 16 km de espesor, mientras que el perfil este, junto a la zona de subducción, muetra un espesor cortical de hasta 25 km. La modelización de los datos indica que el engrosamiento cortical está relacionado básicamente con el engrosamiento de la Capa 3 oceánica. La estructura de velocidades se parece a la descrita en otras cordilleras oceánicas formadas cerca de una dorsal, y muy especialmente a la de Cocos y Malpelo.

La línea P02 del Golfo de Guayaquil restringe la estructura profunda de la placa subducida y del basamento del margen. En el margen se ha constatado que la capa sedimentaria que se observa en las líneas de MCS de Sisteur tiene al menos 6 km de espesor. La corteza de la placa Suramericana se extiende hacia el oeste casi hasta la fosa y presenta velocidades que aumentan desde ~4.0 km/s hasta ~4.5 km/s. Una clara zona de sombra (entre 0.5 s y 1 s a lo largo del perfil P03) delimita posiblemente la existencia de sedimentos subducidos bajo el margen.

El perfil P06, a través del margen norte ecuatoriano – suroeste colombiano exhibe claras llegadas de la placa superior y de la subducida, que permitirán modelizar el margen convergente utilizando estos datos de gran ángulo y la sísmica multicanal de Sisteur.

La batimetría multihaz adquirida durante el experimento muestra que la Cordillera de Carnegie es una estructura fuertemente asimétrica, la cual presenta un flanco norte escarpado y fallado y un flanco sur de pendiente más suave, con intrusión de grandes montes submarinos de cima plana y forma oblonga. Una de las características más notables de esta cordillera es la existencia de densos campos de depresiones circulares distribuidos en sus flancos entre 1500 y 2600 m de profundidad, y dos alineamientos de altos reflectivos del basamento que delimitan una estructura de tipo *graben* en la parte este. Estos datos también muestran que la pendiente interna de la fosa de Guayaquil (latitud 3° S) es inestable, está afectada por derrumbamientos y muestra un cañón principal por donde se transportan los sedimentos hacia la fosa. Es asimismo evidente la existencia de acreción incipiente en la parte frontal del margen. La zona de fractura de Grijalva está marcada por un escarpe principal que transcurre en dirección N50E y una estrecha cordillera orientada N60E. Al frente de Esmeraldas, hacia 1° 40'N, la sección superior del margen es suave y cuasi-horizontal. La sección inferior, en cambio, muestra una morfología rugosa cruzada por un profundo cañón que ha llevado los sedimentos hacia la fosa hasta formar un destacable abanico sedimentario. Entre 1° 40'N y 0° 30 N se evidencia la existencia de zonas de acreción incipiente a lo largo de un margen que no es acrecional en general.

Las anomalías magnéticas a través de la cordillera de Carnegie están relacionadas principalmente con la topografía, en particular con los montes submarinos, los domos volcánicos y las fallas del basamento. Al sur de Carnegie se observan posibles anomalías de expansión oceánica. Los perfiles del margen suroeste de Colombia y del Golfo de Guayaquil son magnéticamente poco activos debido presumiblemente a la composición homogénea y de débil magnetización de la placa superior.

Foreword

Philippe Charvis and Ernst Flüh

The SALIERI cruise is a french-german cooperation based on the exchange of ship time between research vessels of the European fleet. A call for proposal was opened in France in January 2000 for a 1 month cruise on-board Sonne in the southeastern Pacific Ocean.

The cooperation between GÉOAZUR and GEOMAR in this study area started in 1999 with the participation of GÉOAZUR to the PAGANINI cruise conducted by GEOMAR on-board R/V Sonne. During this experiment several wide-angle seismic lines were shot across the Cocos and Malpelo ridges using both GEOMAR and GÉOAZUR ocean bottom sensors. In 2000 during the SISTEUR cruise conducted by GÉOAZUR on-board R/V Nadir and Orion with the participation of GEOMAR (IHP, Access to Large scale facilities), 6000 km of multichannel seismic data and 1250 km of wide angle seismic data were recorded on the Colombian and Ecuadorian margin.

The SALIERI cruise is the continuation of this program with several wide-angle lines shot across the Carnegie volcanic Ridge and on the Colombian and Ecuadorian margin most of them superposed to MCS lines shot during he SISTEUR experiment.

1. Introduction

(E. Flueh, Ph. Charvis, M.-A. Gutscher)

Along convergent continental margins an oceanic plate descends beneath the continental plate, typically generating intense seismicity. The margin of northwestern South America has been the site of several great subduction thrust earthquakes in the 20th century (Fig. 1.1). Their occurence is thought to be controlled by the degree of coupling along the plate interface or "seismogenic zone" (Ruff, 1992; Ruff and Tichelaar, 1996). The seismogenic zone represents that portion of the plate boundary subject to elastic (brittle) failure and generally lies between depths of 10 and 40 km. It is the target of a major international research initiative the "SEIZE" (SEIsmogenic Zone Experiment) program. As this target (the rupture zone) is generally situated offshore, marine technologies must be applied to study it in detail. It has been suggested that interplate coupling may be locally increased by the presence of asperities (positive topographic features) on the downgoing plate, such as seamounts or oceanic plateaus (Cloos, 1996; Cloos and Shreve, 1996, Scholz and Small, 1997). The subduction of such oceanic plateaus can strongly affect the structure, deformation, seismicity and magmatism of the upper plate at convergent margins (Pilger, 1981; McGeary et al., 1985).

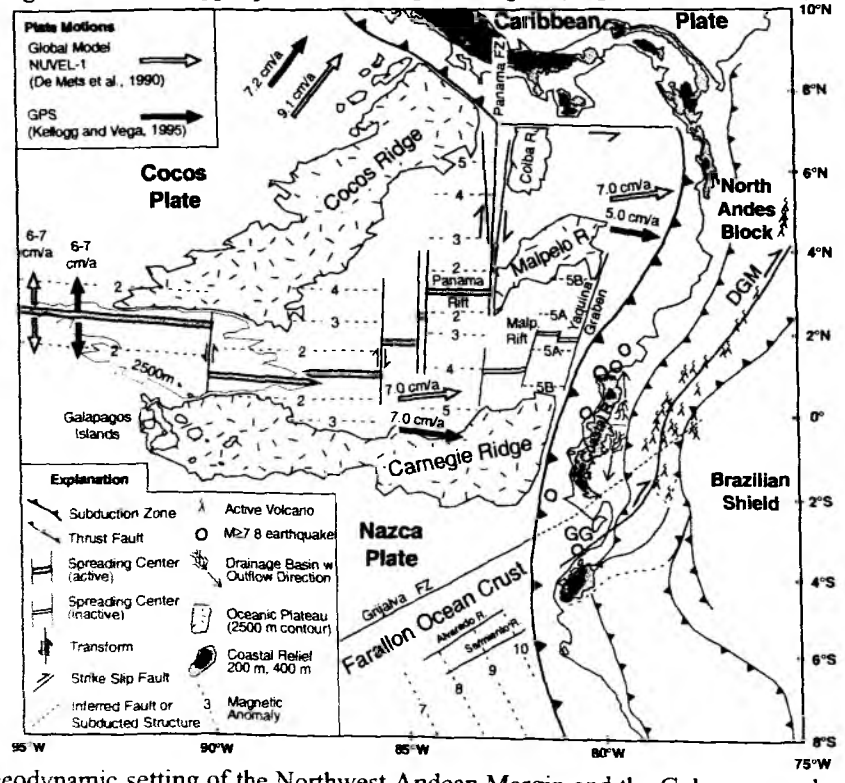

Figure 1.1 : Geodynamic setting of the Northwest Andean Margin and the Galapagos volcanic province on the Nazca and Cocos Plates (after Gutscher et al., 1999)

The northernmost Nazca Plate and adjacent Cocos Plate include several blocks of thickened oceanic crust (oceanic plateaus) thought to have originated from an interaction between the Galapagos hotspot and the Cocos - Nazca spreading center, the most prominent being the Cocos, Malpelo and Carnegie Ridges (Fig. 1.1). While the Cocos Ridge is presently subducting beneath Costa Rica (Gardner et al., 1992), the Carnegie Ridge is subducting beneath the Ecuador convergent margin (Pennington, 1981; Gutscher et al., 1999). Each has produced a segmentation of the upper plate margin expressed in lateral variations of uplift, seismicity, deformation, as well as arc magmatism.

The scientific objectives of the SALIERI cruise are twofold. The first is to constrain the deep crustal structure of the Carnegie Ridge, and compare it to the crustal structure of other products of Galapagos hotspot volcanism (Cocos, Galapagos Platform, Malpelo) where wide-angle seismic data have been recently acquired during the PAGANINI Cruise SO-144. The second is to study the plate interface beneath the Ecuador margin and to determine the effect on margin structure due to subduction of Carnegie Ridge.

1.1 Hotspot - Ridge interaction and formation of the Panama Basin

(V. Sallares and M.-A. Gutscher)

Tectonic Evolution

The generally accepted tectonic model for the formation of the oceanic crust of the Panama basin suggests that a major plate reorganization took place around 25 Ma, breaking the Farallon Plate into the Cocos and Nazca plates to the south and the Juan de Fuca plate farther to the north (Hey, 1977). Due to differential stresses on the northeastward subducting Cocos Plate and the eastward subducting Nazca Plate, spreading was initiated about 23 Ma between the two plates in the vicinity of the Galapagos hotspot and later evolved into the current day Cocos-Nazca spreading center with N-S spreading (Hey, 1977; Lonsdale and Klitgord, 1978) (Fig. 1.2).

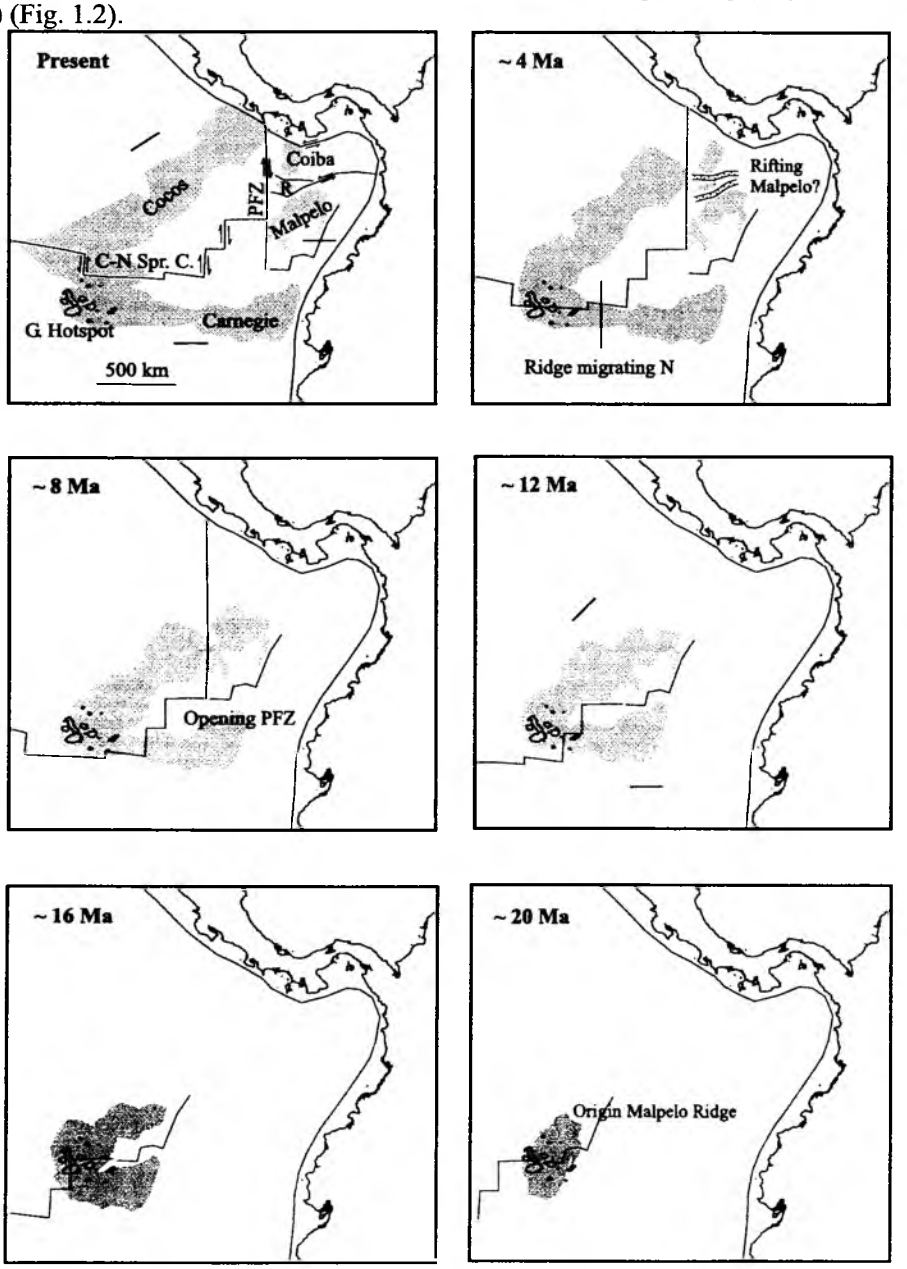

Figure 1.2 : Schematic evolution of the Cocos - Carnegie Ridge System as a result of interaction of the Galapagos Hotspot with the Cocos - Nazca Spreading Center since 20 Ma.

The Grijalva scarp, an old N 60 E fracture zone in the Farallon Plate, is interpreted to represent the southern half of the scar where the Nazca plate tore off. Carnegie and Cocos Ridges are thus mirror image hot spot traces formed by the NE motion of the Cocos Plate and the eastward motion of the Nazca Plate over the Galapagos hotspot (Pennington, 1981; Kolarsky et al., 1995). The age of Cocos Ridge at the trench is 14-16 Ma based on recent radiometric dating (Hoernle et al., 2000), whereas the age of Malpelo Ridge and Carnegie Ridge at the trench is believed to be 20 Ma based on available magnetic anomalies. Dredge samples acquired during the recent PAGANINI 3 cruise will provide radiometric constraints on these ages.

Kinematic reconstructions suggest Malpelo Ridge is a former continuation of Cocos Ridge separated by dextral motion along the N-S trending Panama F.Z. at about 8 Ma (Hey, 1977; Lonsdale and Klitgord, 1978). Malpelo and Carnegie Ridges separated from one another during a period of rifting and seafloor spreading from ca. 17 - 8 Ma (Hey, 1977; Pennington, 1981; Hardy, 1991). Both active and extinct rifts as well as the transform faults associated with them are morphologically expressed in the E-W and N-S structural grain of the Panama Basin seafloor, respectively (Fig. 1.1).

Deep Crustal Structure of the Cocos and Malpelo Ridges

Wide-angle seismic data were recently acquired during the PAGANINI (SO144) and SISTEUR cruises on oceanic plateaus from the Galapagos volcanic province (Fig. 1.3).

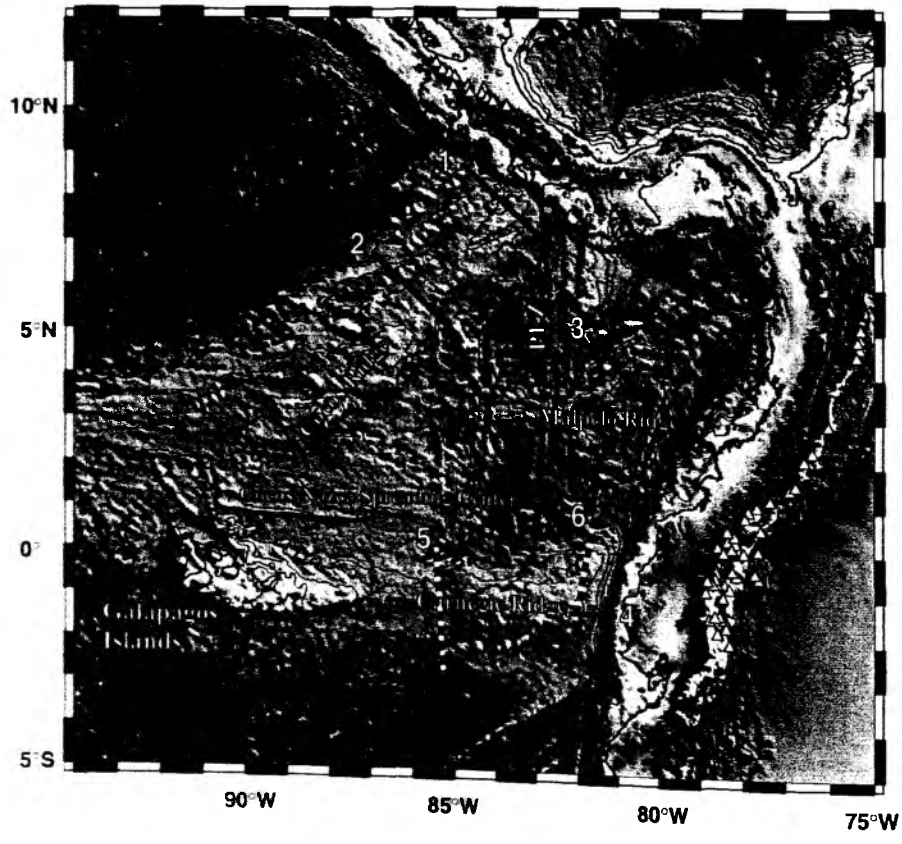

Figure 1.3 : Shaded hill relief map of the Cocos - Carnegie Ridge area with active arc volcanoes (triangles). Locations of wide-angle seismic profiles acquired during recent cruises. PAGANINI Cruise SO144 are shown (solid black lines): 1 - Northern Cocos, 2 - Central Cocos, 3 - Malpelo Ridge. SISTEUR Cruise : 4 - Carnegie Ridge margin profile. Wide angle profiles acquired during the current SALIERI Cruise SO159 are also shown (dashed lines): 5 - Central Carnegie Ridge, 6 - Northeast Carnegie Ridge

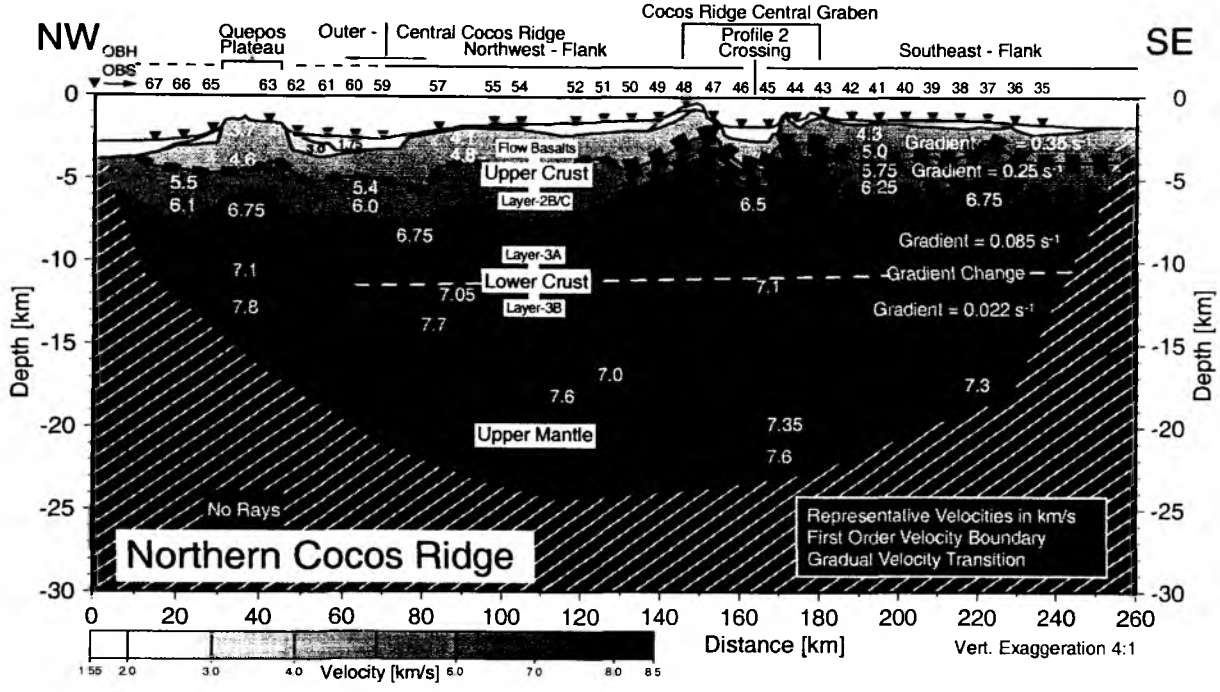

Figure 1.4 : Velocity model based on raytracing of wide-angle data from the Northern Cocos Ridge (see profile 1 on Figure 1.3) acquired during the Paganini Cruise SO-144. (Walther et al., subm.)

The crustal structure of the Cocos and Malpelo Ridges has been constrained along three profiles during the Paganini cruise. Results indicate that maximum crustal thickness along the three profiles range from 18 km at the northern Cocos Ridge (Fig. 1.4) to 16 km at the central Cocos Ridge (Fig. 1.5a) to 19 km on Malpelo Ridge (Figure 1.5b). The thickness of oceanic Layer 2 is quite uniform regardless of the variations in total crustal thickness, and thus crustal thickening is mainly accomodated by variations in the thickness of Layer 3. Seismic velocities of Layer 3 are similar in all profiles. Several low velocity anomalies in the long-wavelength structure (up to ~ 6.8 km/s) have been found, which lead to an overall anticorrelation between crustal thickness and bulk lower crustal velocities. The Moho geometry of the central Cocos profile is highly asymmetric. The steep transition into a normal oceanic crust in the easternmost segment of this profile can be associated with the presence of the Inca Fracture Zone, part of the current Cocos-Nazca Spreading Center. The rapid thinning of the northernmost segment of Malpelo Ridge can be most likely related with a rifting process that split the ancient Malpelo Ridge into Regina and Malpelo Ridges after the initiation of the movement along the Panama Fracture Zone.

In the SALIERI experiment two new wide-angle profiles will be acquired across the Carnegie Ridge (Fig. 1.3). These profiles are located at the conjugate positions to the Southern Cocos profile and the Malpelo profile. One of the objectives is to determine the deep crustal structure of this ridge in order to better understand the influence of the Galapagos hotspot on both sides of the Cocos-Nazca Spreading Center at a given period of time (at about 12 Ma and 20 Ma). This information may allow us to determine if the variations on the crustal thickness are due to temporal variations in the hotspot activity and/or to variations on the relative position of the hotspot and the spreading center.

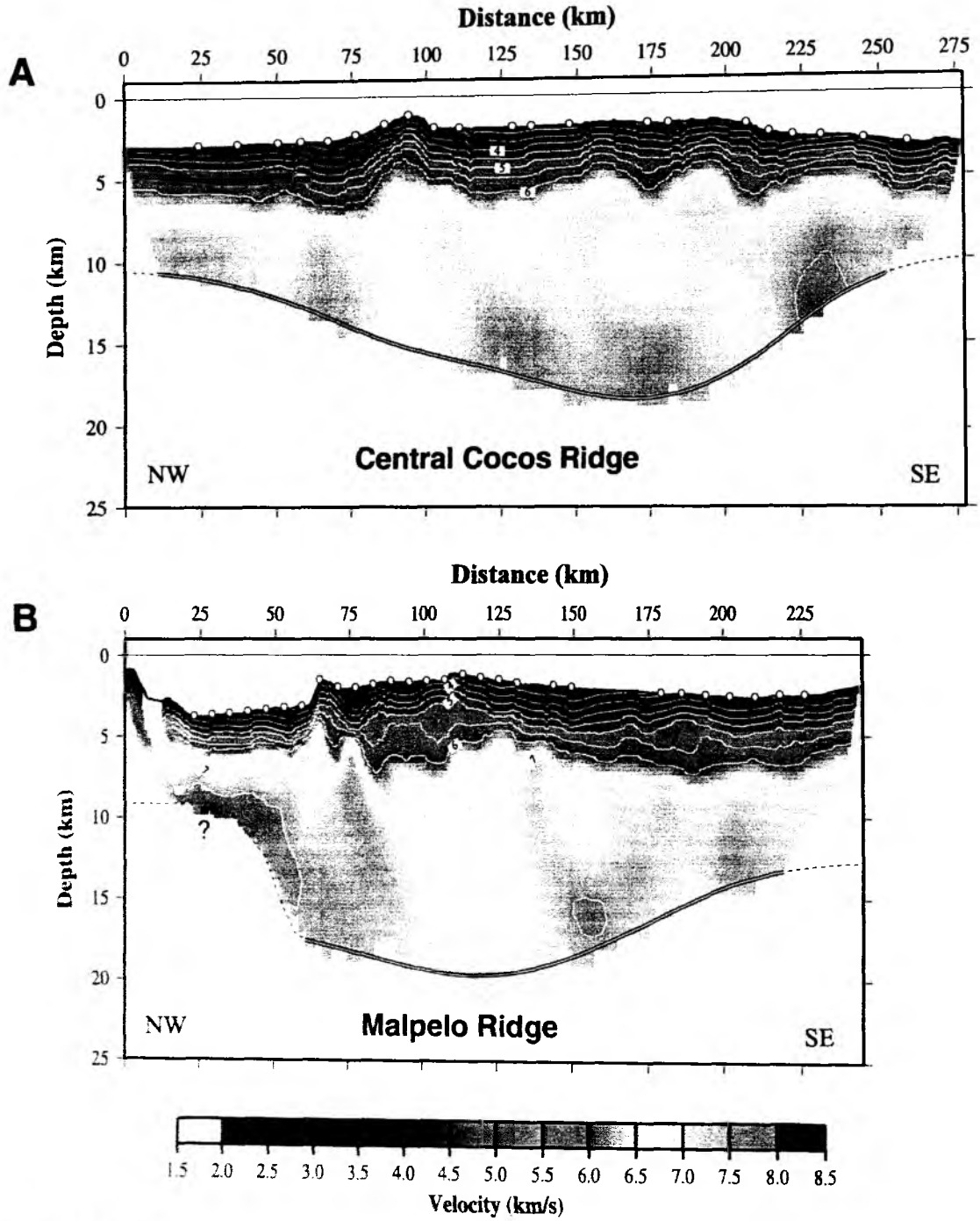

Figure 1.5 : Velocity model based on inversion of seismic data acquired during the PAGANINI Cruise SO-144 (Bialas et al., 1999, Sallares, et al., 2001) a: Central Cocos Ridge (see profile 2 on Figure 1.3) and b: Malpelo Ridge (see profile 3 on Figure 1.3)

1.2 The Colombia - Ecuador Margin

(J.-Y. Collot and M.-A. Gutscher)

Geological setting

Along the northwestern Andean margin the Nazca Plate subducts eastwards beneath Ecuador and Colombia (Fig. 1.1). The Colombia-Ecuador margin belongs to the North Andean block, which extends from the Pacific coast to the Eastern Cordillera and includes the oceanic terranes of the Western Cordillera and coastal block. The oceanic terranes were accreted against the western flank of the metamorphic eastern cordillera of the Andes during three major tectonic events. The initial accretion event occurred during the late Jurassic-Early Cretaceous (140-130 Ma) and involve both continental and oceanic terranes (Aspden and Litherland, 1992). Remnants of these rocks crop out at the western flank of the Eastern Cordillera. The second event involved oceanic plateaus and island arcs that were accreted during the Late Cretaceous (85-65 Ma) (Reynaud et al., 1999). These rocks are found along the inter-Andean valley and Western Cordillera as far south as the inland side of the Gulf of Guayaquil. The third event ended with the early Cenozoic (58-38 Ma) accretion of other oceanic plateau and island arc terranes, which presently form part of the Western Cordillera and the coastal block basement of Ecuador and southern Colombia (Jaillard et al., 1995). As indicated by neotectonic data in Ecuador (Winter et al., 1993), and Colombia (Taboada et al., 2000), and analysis of earthquake analysis (Guiller et al., in press) majors faults such as the Pallatanga and the Chingal-Sophia faults reactivate with a dextral strike-slip movement part of the accreted terranes sutures zones. These faults are part of the Dolores-Guayaquil-Pallatanga fault zone system that marks the eastern boundary of the North Andean block (Lavenu et al., 1995; Ego et al., 1996).

The oceanic basement of the coastal block is overlain by thick sedimentary sequences with deposition starting during the upper Cretaceous-early Paleocene between the Cayo and San Lorenzon island arcs. After arc-continent collision occurred in the late Paleocene, a turbiditic fore-arc basin developed on the coastal block. During lower to middle Eocene, the basin was unconformably overlain by thick shelf sediments. These sediments were deformed, truncated and covered with shore and continental deposits during the middle to upper Eocene final docking phase of the oceanic terrane. From late Oligocene to Miocene, thick sedimentary basins, such as the Progresso, Manabi, Borbon and Tumaco basins developed in both Colombia and Ecuador forearcs. From the Miocene time to Present the Gulf of Guayaquil basins have remained major depot centers, whereas the other basins have been mostly uplifted and exposed.

The Colombia - Ecuador margin is marked by an active volcanic arc from 5°N to 2°S (Fig. 1.1 and Fig. 1.3). Whereas the arc is narrow in Colombia, it widens considerably in Ecuador to form three distinct parallel chains, situated 250 - 400 km from the trench. Two of these volcanoes, the Pichincha next to Quito and Tungurahua (near Riobamba) have shown recent activity and disrupted aviation traffic through Plinian columns and ashfalls. The andesitic and dacitic stratovolcanoes of Ecuador show an unusual geochemical signature said to be "adakitic". These arc magmas are highly depleted in heavy rare earth elements which has been interpreted as indicating a contribution of direct melting of the subducted oceanic crust (Gutscher et al., 2000).

Kinematics

The relative motion of the Nazca Plate along the Ecuador - Colombian margin is eastward at a rate of 5-7 cm/a (DeMets et al., 1990; Kellogg and Vega, 1995) (Fig. 1.1). GPS data indicate the North Andean block is being displaced northeastward at a rate of approximately 1 cm/a along the Dolores Guayaquil Megashear (Kellogg and Vega, 1995) (Fig. 1.6). This movement results in transpressional deformation in the inter-Andean Valley and transtension at the southern termination in the Gulf of Guayaquil (Ego et al., 1996) (see also below). This northeastward displacement, combined with the ENE orientation of Carnegie Ridge, implies the point of intersection between the ridge and margin has been moving gradually southwards (Fig. 1.7).

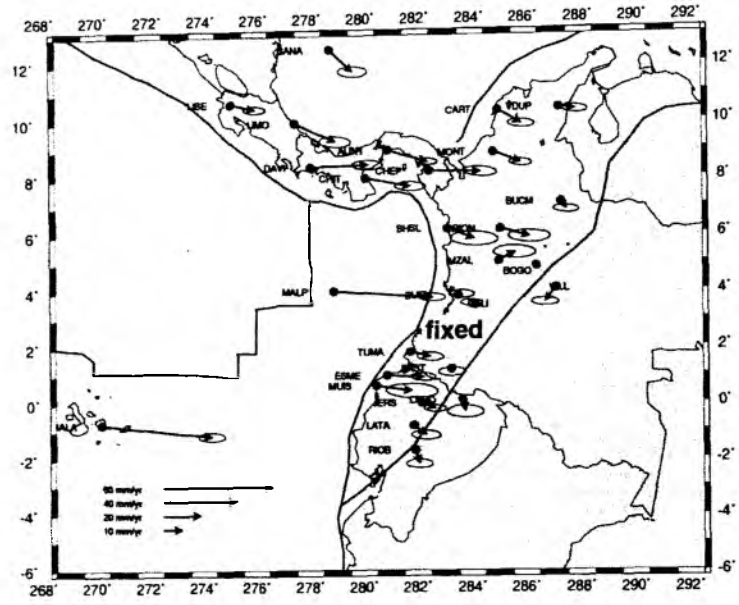

Figure 1.6 : Displacement vectors observed by GPS stations of the CASA network (Kellogg and Vega, 1995; Kellogg and Trenkamp, 1998) showing relative plate motions with respect to a fixed North Andean Block. Note the relative displacement between the North Andean block and Brazilian shield along the Dolores-Guayaquil strike slip fault.

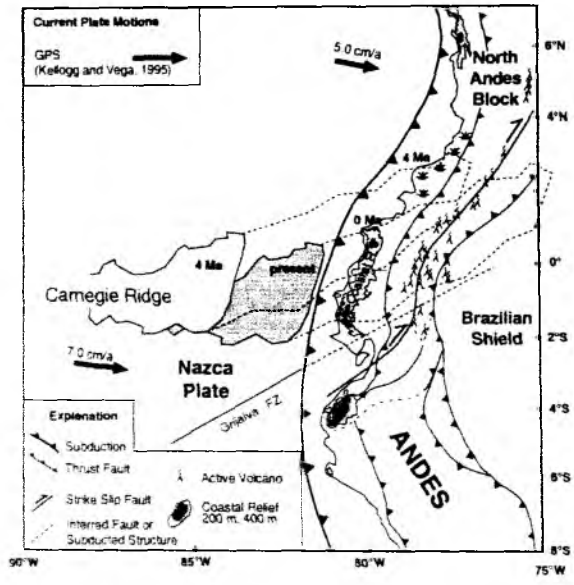

Figure 1.7 : Schematic diagram indicating relative motion between the Carnegie Ridge and Ecuador - Colombia margin since 4 Ma. Subsidence in SW Colombia, marked by the presence of mangrove swamps, is consistent with a general southward migration of the trench - ridge intersection.

Recent coastal uplift facing Carnegie Ridge is indicated by Pliocene marine terraces (Tablazos) exposed at 200-300 m elevations (DeVries et al., 1988; Dumont et al., 1996). The Pacific Margin of SW Colombia appears to be subsiding as shown by the presence of mangrove swamps along a margin reentrant with a very low coastline. It has been suggested that this recent vertical deformation is due to uplift and subsidence due to the relative southward migration of Carnegie Ridge (Gutscher et al. 1999).

Seismicity

The North Andean margin in the vicinity of Carnegie Ridge has produced 4 great ($M \geq 7.8$) subduction earthquakes in the 20th century. The largest in 1906 ($M_W = 8.8$) had an estimated rupture zone of ca. 500 km length, partially reactivated in three subsequent events from south to north, in 1942, 1958 and 1979 (Beck and Ruff, 1984; Swenson and Beck, 1996) (Fig. 1.8). The objective of the SISTEUR cruise in Sept. 2000 was to investigate the asperity which ruptured during the great 1979 earthquake and to study the coupling along the plate interface in the vicinity of Carnegie Ridge. The focal mechanism of the 1979 event is clearly an eastward dipping low-angle thrust and relocation work done on the older events combined with the spatial distribution of aftershocks indicate all earthquakes were of a similar type (Swenson and Beck, 1996).

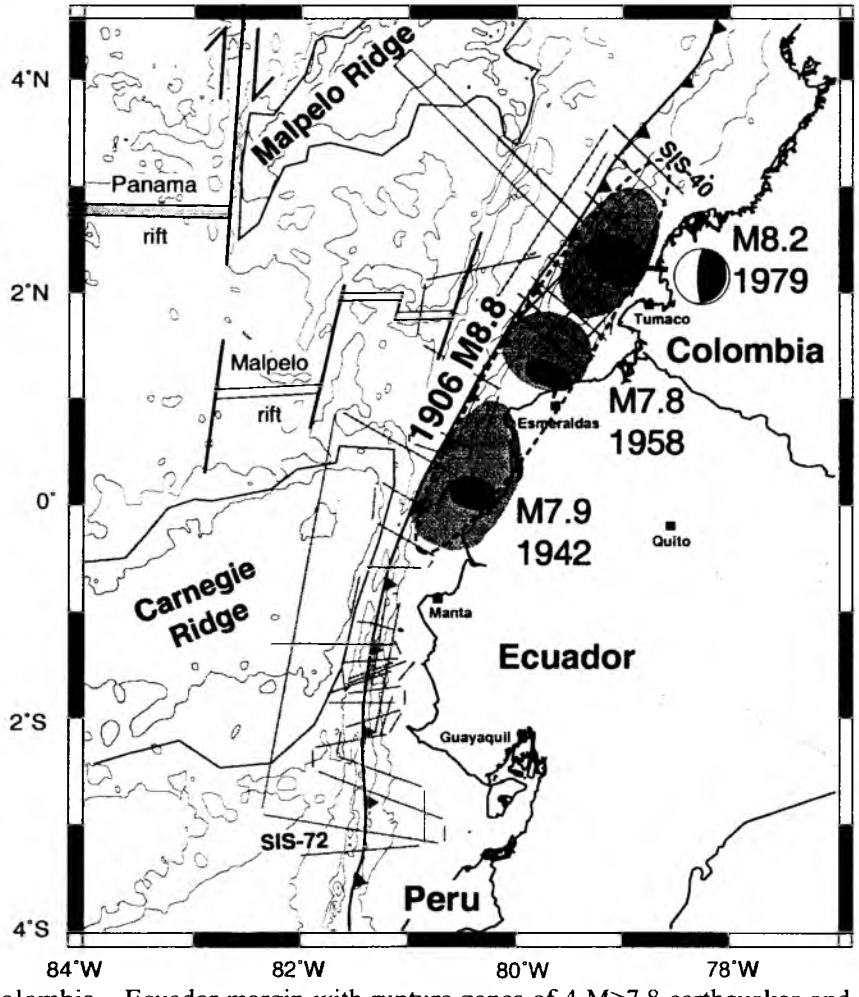

Figure 1.8 : Colombia - Ecuador margin with rupture zones of 4 $M \geq 7.8$ earthquakes and CMT (Harvard) focal mechanism for the 1979 Great Colombia earthquake. The positions of the multichannel seismic profiles acquired during the SISTEUR cruise are also shown.

Upper plate seismicity is also high in the Inter-Andean valley where transpressional deformation occurs along the DGM system with on average 3 M6 earthquakes occuring per century (Gutscher et al. 1999). Teleseismically recorded intermediate depth (70 - 300 km) seismicity, with magnitude ≥ 4 (Engdahl et al., 1998) is observed in southern Colombia and in southern Ecuador and northern Peru, but is nearly absent in the prolongation of Carnegie Ridge, a phenomenon observed in other similar geodynamic settings (subduction of oceanic plateaus) (Pilger, 1981; McGeary et al., 1985)

Evolution from erosion to accretion

Preliminary results from the SISTEUR cruise indicate strong longitudinal variations of the margin structure (Collot, Charvis et al., submitted). From the Carnegie Ridge-Trench junction to the Gulf of Guayaquil, the Ecuadorian margin shows trenchward-dipping reflectors and acoustic basement being truncated downward at the plate interface, suggesting that the margin underwent severe tectonic erosion (Fig. 1.9a).

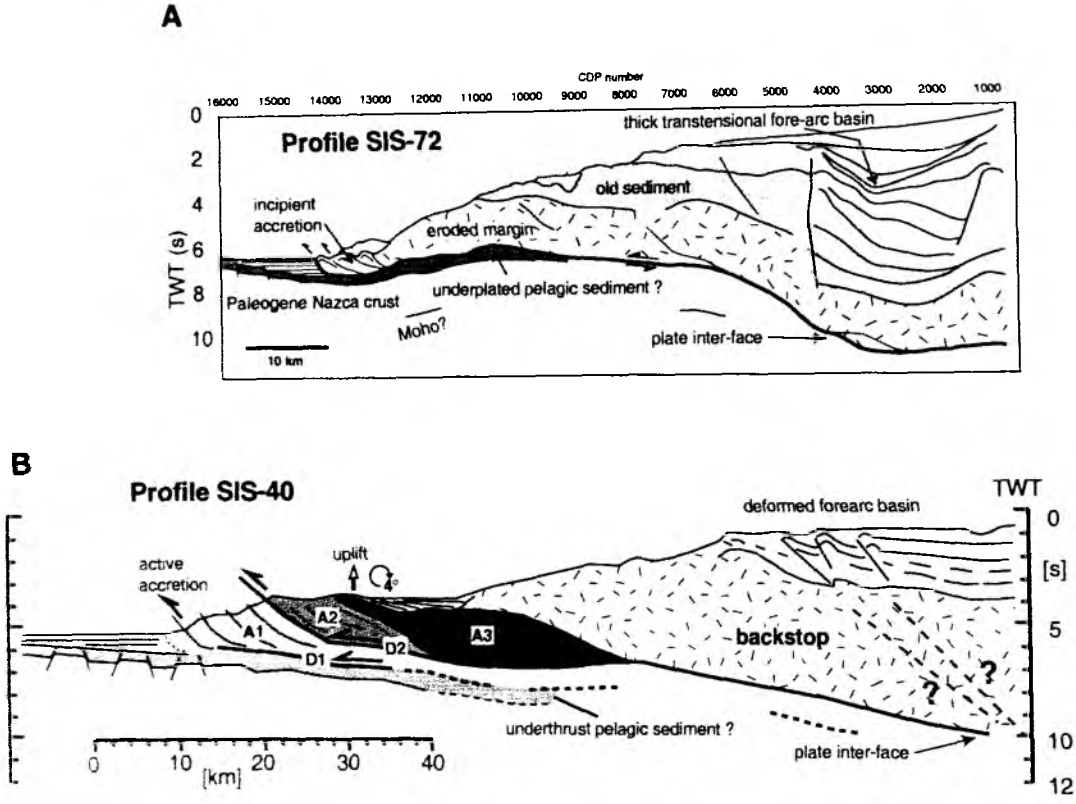

Figure 1.9 : Line drawings of multi-channel seismic profiles acquired during the SISTEUR cruise in Sept. 2000 (Collot, Charvis et al., subm.) Profile locations shown in Fig. 1.8. a: Profile SIS-72 of the Gulf of Guayaquil margin, b: Profile SIS-40 of the SW Colombian margin

Where the Carnegie ridge is subducting, the trench is devoid of turbidites and its outer slope is chopped by flexural normal faults. The slope margin is locally unstable and deformed by large rotational slumps, and subducting seamounts. There, the subduction channel may contain both deforming pelagic sediment and highly reflective and stratified Carnegie Ridge rocks. OBS data exhibit deep reflections (PmP) beneath the Ecuador margin, possibly from the base of the subducting Carnegie ridge crust. A shadow zone observed on most OBSs and land seismometers on the margin could be related to a low velocity layer, possibly associated with the subduction process. West of the Gulf of Guayaquil, trench fill sediment, up to 0.7 s TWT thick, is offscraped to form an incipient 8 km wide accretionary wedge locally overlain by mass wasting deposits, whereas the 0.5 s thick Nazca Plate pelagic sediments underthrust the margin over a minimum distance of ~25 km (Fig. 1.9a). In Southern Colombia, the subduction channel consumes the pelagic sediments and locally part of the trench fill, which reaches 2.7 s in thickness. As a result, a ~30 km wide accretionary wedge (Fig. 1.9b) has developed north of 3°N as previously reported (Westbrook et al., 1995; Mountney and Westbrook, 1997), whereas, a nascent (<10 km-wide) or no accretionary wedge characterizes the margin segment between 1°N and 2.5°N, despite thick trench fill. Thus, the lower margin appears to consist of imbricated and previously eroded basement and older sediment. In this area, the OBS signal to noise ratio is low likely due to the highly deformed sedimentary cover, and a strong attenuation in the uppermost crust. Nevertheless PmP reflections mark the base of the subducting oceanic crust, and a shadow zone is also

observed on some OBSs on the Colombia margin. Therefore results from the SISTEUR cruise indicate that forearc structures vary from subduction erosion along the Ecuador margin with incipient accretion off the Gulf of Guayaquil (Fig. 1.9a), through sediment subduction beneath an eroded margin at 1°N, to active accretion at 3°N (Fig. 1.9b). These variations may be interpreted in terms of the temporal evolution of the margin as the ridge sweeps gradually southward along the trench (Fig. 1.10). This evolution is similar to that described for the southward migrating Nazca Ridge at the southern Peru Trench (von Huene et al., 1996).

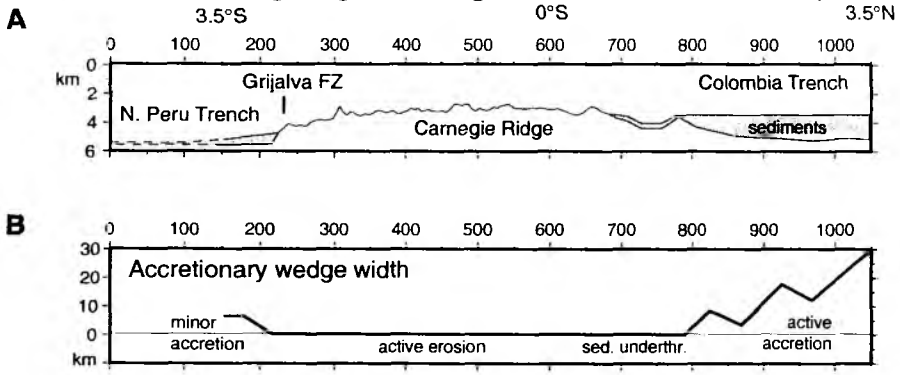

Figure 1.10 : Schematic diagram showing longitudinal variations along the Colombia - Ecuador margin. a: Axial trench profile with sediment thickness at the trench, b: Schematic diagram showing variations in accretionary wedge thickness and /or the presence of tectonic erosion along the margin.

Northern Margin Study Area 1°-3 N°

The northern Ecuador-southern Colombia margin segment shows a ~600-1000 m deep and 90 km wide morphological reentrant, bounded landward by a generally subsiding coastal area. The trench floor is about 3200 m deep and contains up to 2.7 s TWT of turbidite, whereas a 3 s TWT-thick fore-arc basin is 50 km wide in the south and narrows northward to 20 km, where its borders appear affected by active deformation (Fig. 1.9b). Across this segment, abundant sediment derived from the Andean Cordilleras reaches the margin and the Colombia trench through major rivers such as the Esmeraldas River in the South and the Patia River in the North. The northernmost OBS line (Profile 6) acquired during SO159 is coincident with MCS line SIS-44. This line shows strong reflections returned form the plate interface at a depth of 10-11 sTTW near the eastern end of the line. The wide fore arc basin extends across 2/3 of the line and tectonic deformation concentrates near the front of the margin where a major landward dipping ramp-like fault cuts through the margin. A minor accretionary wedge may be developing in this region where the lowermost trench fill appears to be subducting. Thrust faults beneath the margin front could reveal an imbricated margin. A recent, gently seaward sloping sedimentary fan is related to turbidites from the Esmeraldas River deposited in the trench at the toe of the margin.

Evolution of the Gulf of Guayaquil :

The Gulf of Guayaquil is a deep transtensional basin in a fore arc position (Shepherd and Moberly, 1981) . It contains the thickest (>10 km) neogene sedimentary basins of the Ecuadorian fore-arc, near the boundary with the Peru margin. Results of the SISTEUR cruise indicate as much as 7 s TWT of reflective sediments. Together with the Progresso, Manabi and Borbon basins, the Gulf of Guayaquil Basin recorded the geodynamic evolution of the Andes since the Oligocene time. Its central region has been the locus of intense hydrocarbon prospection by oil companies from 1968 to 1983. The 5000 km of industry multichannel seismic lines and 5 drill sites allowed identification of its major structures and history and led to the discovery of the Amistad gas field.

The Gulf of Guayaquil is located near the junction between the trench and the southern extremity of the Dolores-Guayaquil-Pallatanga megashear (Fig. 1.11), which further north serves as the tectonic boundary between the Coastal block-western cordillera and the Brasilan shield (Ego et al., 1996). The fault zone cuts Puna Island and deforms the region of Santa Clara Island separating the gulf into the Jambeli basin to the east and the Gulf of Guayaquil basin sensu-stricto to the west. The trenchward prolongation of the fault zone is not precisely known. It seems, however, to be marked by a transpressive accommodation zone marking the SE tectonic boundary of the basin (Dumont et al., 1996). The basin developed northward against the

structural bock of Elena-Posorja, from which it is separated by a WNW trending, steeply south dipping normal fault. This fault has been interpreted as Eocene-Paleocene structure reactivated during the Neogene basin formation (Deniaud, 1999).

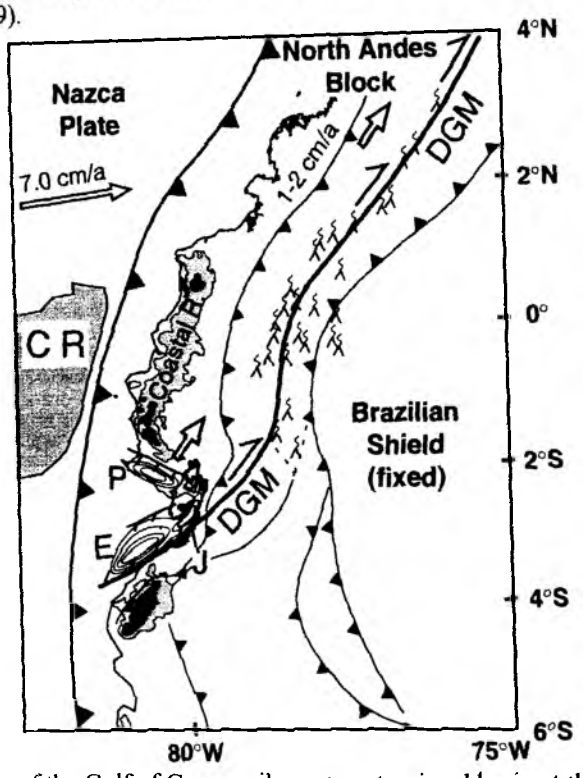

Figure 1.11 : Tectonic setting of the Gulf of Guayaquil as a transtensional basin at the southern termination of the Dolores - Guayquil Megashear (DGM) due to NNE motion of the North Andean block. Three basins are shown with schematic sediment isopachs, E - Esperanza Basin, J - Jambeli Basin, and P - Progreso Basin.

The western boundary of the basin is marked by diapiric intrusions as indicated by industry and SISTEUR MCS lines (Collot, Charvis et al., 2001). The inner trench slope is underlain by trenchward-dipping reflectors and acoustic basement that are truncated downward at the plate interface, suggesting that the margin underwent tectonic erosion. The trench proper contains flat lying sediment, up to 0.7s TWT-thick, that is offscraped to form an incipient 8-km-wide accretionary wedge locally overlain by mass wasting deposits.

SISTEUR MCS lines, image the plate interface beneath the Gulf of Guayaquil as a series of acoustically strong, discontinuous reflectors dipping landward from the trench, over a distance of 90-100 km, and to a maximum depth of 10-11 s TWT. Its section deeper than ~5 s.bsf is resolved by a set of strong reflectors 0.2-0.6 s thick that steepens abruptly near the Gulf of Guayaquil basin and appears subhorizontal beneath it in the time sections (Fig. 1.10a). Within 10-20 km from the trench, the shallow section of the plate inter-face show that the 0.5 s-thick Nazca Plate pelagic sediments underthrust the margin over a minimum distance of ~25 km (Fig. 1.10a). The forearc basement forms a wedge of rocks that thickens from near the trench, up to 5-6 s TWT at the basin western edge, where the basement drastically thins to ~3 s TWT beneath the basin, suggesting that the development of the Gulf of Guayaquil basin was controlled by crustal rupture and thinning processes in relation with the northward migration of the Andean block. In addition, crustal deformation in the Gulf of Guayaquil was affected by oblique subduction of the Grijalva Fracture Zone fault scarp, as well as by Neogene oceanic crust on the scarp hanging wall, and Paleogene crust on its foot wall. The crustal nature and velocities of the margin are however unknown beneath the Gulf of Guayaquil. At this location, the crust could either be oceanic as in coastal Ecuador or continental as beneath the Peru margin. Objectives of the dip and strike OBS lines are to obtain crustal velocities, real depth structures and nature of the margin crust, subducting Grijalva Fracture zone, and oceanic crusts.

2. Participants

Scientists – Leg SO159

Flüh	Ernst	GEOMAR	Chief-Scientist
Charvis	Philippe	GEOAZUR - IRD	Co-Chief Scientist
Agudelo	William Mauricio	GEOAZUR - UPMC	
Anglade	Alain	GEOAZUR - CNRS	
Berhorst	Arnim	GEOMAR	
Bialas	Jörg	GEOMAR	
Broser	Anne	GEOMAR	
Collot	Jean-Yves	GEOAZUR - IRD	
Fekete	Noémi	GEOMAR	
Gailler	Audrey	GEOAZUR - UPMC	
Gutscher	Marc André	IUEM	
Hello	Yann	GEOAZUR - IRD	
Liersch	Petra	GEOMAR	
Michaud	Francois	GEOAZUR - UPMC	
Müller	Meino	UHB	
Osorio Naranjo,	Jairo Alonso	INGEOMINAS	
Ravaut	Celine	GEOAZUR - UPMC	
Sallarés	Valentí	GEOAZUR - IRD	
Steffen	Klaus-Peter	KUM	
Thierer	Peter Oliver	GEOMAR	
Walther	Christian	GEOMAR	
Yates	Ben	UTIG	

GEOMAR = Forschungszentrum für Marine Geowissenschafter der CAU, Kiel
KUM = Umwelt und Meerestechnik Kiel GmbH
IRD = Institut de Recherche pour le Développement
CNRS = Centre National de la Recherche Scientifique
IUEM = Institut Universitaire Europeen de la Mer
UPMC = Université Pierre et Marie Curie (Paris)
UTIG = University of Texas, Institute for Geophysics
UHB = Universität Bremen, Sektion Geowissenschaften

Crew – Leg SO159

Andresen	Hartmut	Master
Baschek	Walter	1st Officer
Göldner	Frank	1st Officer
Köthe	Wolfgang	Radio Officer
Ingo	Naeve	Surgeon
Neumann	Peter	Chief Engineer
Rex	Andreas	2nd Engineer
Lindhorst	Norman – Clemens	2nd Engineer
Dammann	Thorsten	Electrician
Hoffmann	Hillmar	Electronic Engineer

Leppin	Jörg	Electronic Engineer
Wintersteller	Paul	System Operator
Wenz	Christian	System Operator
Rosemayer	Rainer	Fitter
Kunze	Christian	Motorman
Lange	Gerhard	Motorman
Von Arronet	Johannes	Motorman
Fromme	Lothar	Motorman
Hermann	Klaus	Chief Cook
Ernst	Arnold	2nd Cook
Horzella	Ernst	Chief Steward
Götze	Reiner	2nd Steward
Hoppe	Jan	2nd Steward
Lohmüller	Karl – Heinz	Boatswain
Rosin	Peter	A. B.
Becker	Siegfried	A. B.
Schachel	Dirk	A. B.
Krüger	Helmut	A. B.
Bosselmann	Norbert	A. B.
Becker	Michael	A. B.

Addresses of Participating Institutions

GEOMAR: GEOMAR
Forschungszentrum für
Marine Geowissenschaften der
Christian-Albrechts-Universität zu Kiel
Wischhofstr. 1-3
24148 Kiel
Germany
Tel.: 0049 – 431 – 600 – 2327
Fax.: 0049 – 431 – 600 – 2922
e-mail: INAME@geomar.de
INAME = First Initial followed by name
web site: http: www.geomar.de

GEOAZUR: GeoAzur (CNRS, IRD, UPMC, UNSA)
2 Quai de la Darse, BP 48
06235 Villefranche-sur-mer Cedex
France
Tel.: 0033 – 4 93 – 76 – 37 – 40
Fax.: 0033 – 4 93 – 76 – 37 – 68
e-mail: surname.name@obs-vlfr.fr
Web site: http: www.geoazur.unice.fr

KUM: K.U.M.
Umwelt- und Meerestechnik Kiel GmbH
Wischhofstr. 1 – 3, Geb. D5
24148 Kiel
Germany
Tel.: 0049 – 431 – 7209 – 220
Fax.: 0049 – 431 –7209 – 244
e-mail: KUM.Umweltmeerestechnik@t-online.de
web site: http://www.kum.de

UEM: Université de Bretagne Occidentale
Institut Universitaire Europeen de la Mer
UMR 6538 Domaines Oceaniques
Place Nicolas Copernic
29280 Plouzane
France
Tel.: 0033 – 298 – 49 – 87 – 27
Fax.: 0033 – 298 – 49 – 87 – 60
e-mail: name@univ-brest.fr
web site: http://www.univ-brest.fr/IUEM

UTIG: University of Texas
Institute for Geophysics
4412 Spicewood Springs Rd
Austin, TX 78759
USA
Tel.: 001 – 512 – 471 – 0492
Fax.: 001 – 512 – 471 – 8844
e-mail: name@utig.ig.utexas.edu
web site: http://www.ig.utexas.edu

UHB: Universität Bremen
Sektion Geowissenschaften
Klagenfurter Str.
28334 Bremen
Germany
Tel.: 0049 – 421 – 218 – 7165
Fax.: 0049 – 421 – 218 – 7163
e-mail: surname@geophys32.uni-bremen.de
web site: http://www.

INGEOMINAS: National Geologic Service
Diagonal 53 No 34 – 53
Bogotá - Colombia
Tel.: 0057 – 122 – 000 – 41
Fax.: 0057 – 122 – 204 – 38
e-mail: INAME@ingeomin.gov.co
web site: http://www.ingeominas.gov.co

Figure 2.1: The Salieri Scientific Crew.

3. Agenda of the cruise SO 159 SALIERI

Sonne left the pier in Puerto Maritimo of Guayaquil at 20:15 on August 22. After leaving the 3nm-terrotorial border of Ecuador at 02:00 on August 23, the Simrad system was activated and the magnetometer was deployed on the transit to the Ecuadorian trench. Here, in water depth of 4200 m the release systems of the Geomar ocean bottom hydrophones (OBH) aand seismometers (OBS) were tested using W6 winch. Also a CTD was run to full water depth to obtain a velocity profile to be used for swathmapping. Also a prototype of a broadband OBS was deployed. We then continued our transit to the center of Carnegie Ridge at around 85°W, with the magnetometer being deployed during transit. A second test of the release systems was made in the afternoon of August 24.
Along the first seismic line S1 at 85° West a total of 37 OBS were deployed on August 25. An additional CTD was made during deployment of OBS on the top of Carnegie Ridge. Shooting along this line with two airguns started at 06:00 the following day and continued without interruption to 02:00 on August 28. The streamer was damaged soon after deployment and could not be repaired during the cruise.
Recovery of the instruments was made until August 30, with three instruments not recovered. The time needed to wait for the preset time release was used for additional profiles to cover a larger area with swathmapping, and the transit back to the coast was chosen such that we covered a wide area of Carnegie Ridge.
The second seismic profile, S2, a dip line from the oceanic crust to the Ecuadorian shelf was covered with 21 OBS, being deployed September 01. Shooting with 3 guns operational terminated at 10:00 September 02, and recovery of the instruments lastet until September 03, but was interrupted for the deployment of 8 OBS along a short strike line S3, along which 2 airguns were deployed for shooting. Three additional instruments could not be recovered.
An additional strike line, S4, was covered with 21 instruments and shooting along this 80 nm long line was made with one to three airguns and the magnetometer being deployed during the night 04/05 September. Two instruments could not be recovered, and the time available before the time release was to be activated was used to deploy 24 instruments along a north-south oriented profile, S5 across the northern part of Carnegie Ridge. Also, the prototype broadband OBS was recovered on September 07. The time release of the not recovered instrument also failed, increasing the number of lost instruments to eight. We received notice that one of them had apparently been released earlier and was picked up by a fishing vessel, which returned the instrument on land.
Shooting along profile S5 started at 08:00 on September 08 and terminated 13:00 the following day. Recovery of the 24 instruments was completed at 14:00 on September 10. During the transit to the north for our final seismic line, S6, the magnetometer was deployed. S6 is another strike line across the margin, and 24 instruments were deployed 11.09. Shooting using three airguns started at 17:00 and terminated 10:00 on September 12. All instruments except one were recovered by 07:00 September 13, this terminated the seismic programme. Along the six profiles 130 OBS deployment were made, with nine instruments unfortunately not recovered. Two of these were recovered by fishermen before the end of the cruise.
On the transit back to Guayaquil two more CTD stations were made, another magnetic profile was observed to 0:35´S, and the remaining course was set such that gaps in the bathymetric maps could be filled using the Simrad system. Sonne docked at Puerto Maritimo de Guayaquil at 11:30 on September 16 after cruising for 4580 miles.
A trackchart of the cruise is shown in Figure 3.1.

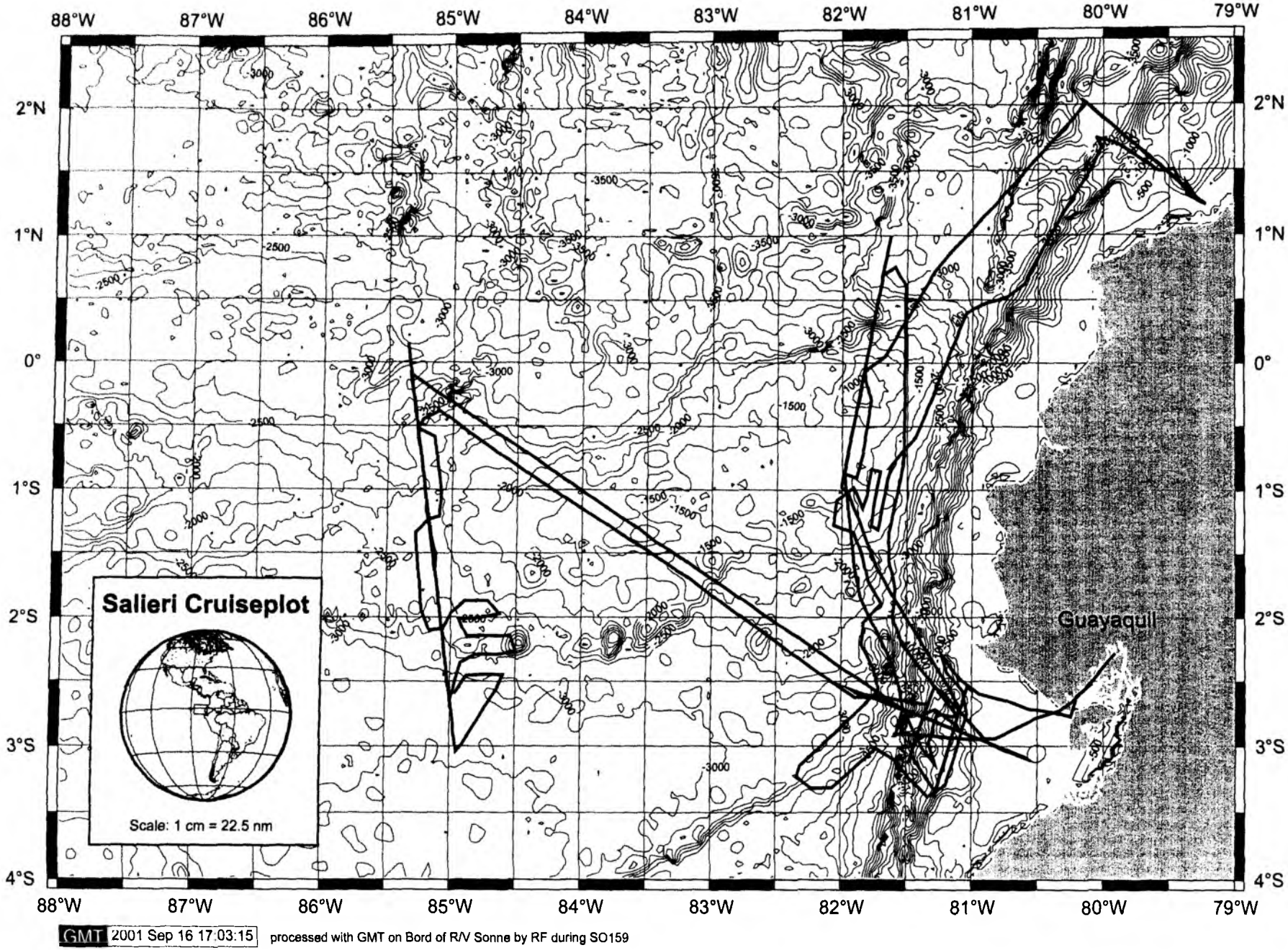
88°W
87°W
86°W
85°W
84°W
83°W
82°W
81°W
80°W
79°W
2°N
1°N
0°
1°S
2°S
3°S
4°S
Salieri Cruiseplot
Scale: 1 cm = 22.5 nm
Guayaquil
GMT 2001 Sep 16 17:03:15
processed with GMT on Bord of R/V Sonne by RF during SO159

Figure 3.1

4. Scientific Equipment

4.1 Shipboard Equipment

4.1.1 Simrad EM120 swathmapping bathymetry system

(F. Michaud, P. Wintersteller, C. Wenz)

Data Aquisition

During the SO159 cruise, the Simrad EM120 Multibeam echosounder was used for a continous mapping of the seafloor. This system has replaced the former echo sounder HYDROSWEEP of the R/V SONNE since June 2001 and this was the third cruise with acquisition of bathymetric data using the Simrad system.

The Simrad echosounder system consists of several units. A transmit and a receive transducer array is fixed in a Mills cross below the keel of the vessel. A preamplifier unit contains the preamplifiers for the received signals. The transducer unit contains the transmit and receive electronics and processors for beamforming and control of all parameters with respect to gain, pingrate and transmit angles. It has serial interfaces for vessel motion sensors, such as roll, pitch and heave, external clock and vessel position. A high performance Sun-workstation is used as an Operator station. The Operator station processes the collected data, applying all corrections, displays the results and logs the raw data to internal or external disks. The EM120 system has an interface to a sound speed sensor in the onboard thermosalinograph.

Simrad EM120 uses a frequency of about 12 KHz with a whole angular coverage sector of up to 150° (75° per port-/starbordside). One ping is sent and the receiving signal is formed into 191 beams by the transducer unit through the hydrophones in the receiver unit. The beam spacing can be defined as equidistant or equiangular, or a mix of both. The pingrate depends on the water depth and the runtime of the signal through the water column. The variation of angular coverage sector and beam pointing angles was set automatically.

4.1.2 PARASOUND

(F. Michaud, P. Wintersteller, C. Wenz)

The PARASOUND system works both as a low-frequency sediment echosounder and as a high-frequency narrow beam sounder to determine the water depth. It utilizes the parametric effect, which produces additional frequencies through nonlinear acoustic interaction of finite amplitude waves. If two sound waves of similar frequencies (here 18 kHz and e.g. 22 kHz) are emitted simultaneously, a signal of the difference frequency (e.g. 4 kHz) is generated for sufficiently high primary amplitudes. The new component travels within the emission cone of the original high frequency waves, which are limited to an angle of only 4° for the equipment used. Therefore, the footprint size of 7% of the water depth is much smaller than for conventional systems and both vertical and lateral resolution are significantly improved.

The PARASOUND system is permanently installed on the ship. The hull-mounted transducer array has 128 elements within an area of ~ 1 m^2. It requires up to 70 kW of electric power due to the low degree of efficiency of the parametric effect. In 2 electronic cabinets, beam formation, signal generation and the separation of the primary (18, 22 kHz) and secondary frequencies (4 kHz) is carried out. Using the third electronic cabinet located in the echosounder control room, the system is operated on a 24 hour watch schedule.

Since the two-way travel time in the deep sea is long compared to the length of the reception window of up to 266 ms, the PARASOUND System sends out a burst of pulses at 400 ms intervals, until the first echo returns. The coverage in this discontinuous mode is dependent on the water depth and also produces non-equidistant shot distances between bursts.

The main tasks of the operators are system and quality control and to adjust the start of the reception window. Because of the limited penetration of the echosounding signal into the sediment, only a short time window close to the sea floor is recorded.

In addition to the analog recording features with the b/w DESO 25 device, the PARASOUND System is equipped with the digital data acquisition system ParaDigMA, developed at the University of Bremen. The data is stored on removable hard disks using the standard, industry-compatible SEGY-format. The 486-processor based PC allows for buffering, transfer and storage of the digital seismograms at high repetition rates. Of the emitted series of pulses, usually only every second pulse can be digitized and stored, resulting in recording

intervals of 800 ms for a given pulse sequence. The seismograms were sampled at a frequency of 40 kHz, with a typical registration length of 266 ms for a depth window of ~200 m. The source signal was a band limited, 2-6 kHz sinusoidal wavelet with a dominant frequency of 4 kHz and duration of 1 period (~250 μs total length). Data was stored on DAT-tapes using Windows NT backup software.

During the entire cruise SO159 the combined PARASOUND/ParaDigMa system worked without significant problems. From time to time the tape drives had to be cleaned. We did not record continously with ParaDigMa system, and only a few select profiles were recorded digitally.

4.1.3 Navigation

(J. Bialas)

A crucial prerequisite for all kinds of marine surveys is the precise knowledge of position information (latitude, longitude, altitude above/below a reference level). Since 1993 the global positioning system (GPS) is commercially available and widely used for marine surveys. It operates 24 satellites in synchronous orbits, thus at least 3 satellites are visible anywhere at any moment (Seeber, 1996). The full precision of this originally military service yields positioning accuracies of a few meters, yet this is restricted to military forces and usually unaccessible to commercial users (Blondel and Murton, 1997). For civilian purposes the precision is in the order of 100 meters.

The resolution of GPS can be enhanced with the Differential GPS (D-GPS) scheme (Blondel and Murton, 1997, Knickmeyer, 1996). Using several reference stations the determination of the ship's position can be corrected in real time and enhanced to a 1 m to 5 m accuracy. Since the cruise SO-109 (1996) D-GPS service is available onboard R/V SONNE. The ships ASHTEC system provides a validated accuracy better than 5 - 10 m in the area of the Salieri investigations.

D-GPS values were available from the ships navigation data base and could be extracted by a PC based end user interface program. Out of all ships sensor values the user could select the wanted variables and specify the output in various formats. The amount of data could be controlled by the desired interval of extracted values which could be as short as one second. Stored on the "wiss-data" directory the extracted ASCII file was acessable from every workstation connected to the shipboard network via ftp or volume access. Surprisingly the output data format writes decimal values separated by a colon instead of the standard american dot notation. According to information of the ships operator this is due to the chosen set up of the desktop program on the PC. Therefore a reformating program must be written prior to further computational use of the values.

During preparing discussion it turned out that the coordinates stored within the data base were provided by the *Atlas ANP 2000* system which does not copy the exact GPS time values but adds time stamps of its internal uncontrolled clock to the high precision coordinates of the DGPS system. Accuracy of the time values is mainly dependend on the operators skills by manually setting the ANP clock to GPS time. A somewhat conservative method compared to the efforts of precise positioning. To enable the most accurate GPS related time stamps within the ANP system prior to each seismic survey the system operates were informed to reset the ANP.

4.1.4 CTD data

(F. Michaud, P. Wintersteller, C. Wenz)

To obtain accurate sound velocity profiles needed for bathymetric swathmapping we used the SEABIRD CTD 911 plus on board of RV SONNE which is additionally equipped with an oxygen sensor. Date collection and post processing was done with the SEABIRD software. Down and up cast were stored separately. Winch speed was 1 m/s. All data was stored as SEABIRD raw data files and ASCII files.

We acquired two CTD profiles. The first was taken at the northern Peru Trench down to 4000 m. Here the northward flowing Humboldt current brings cold Antarctic waters up along the west coast of South America. Surface water temperatures are cold, 18°C and these cold upwelling water appears to have unusual acoustical properties.

This first CTD profile was applied during the first transit to the northwest and produced a strong tunneling artifact in the seafloor bathymetry. Thus we used Simrad Sound Velocity Probe together with the CTD at a second position in 2500 m water depth over the central Carnegie Ridge. Surface water temperatures north of the Carnegie Ridge are 23-25°C.

The Simrad Probe was lowered down to a water depth of 1500 m at a velocity 1 m/s measuring the sound speed in-situ continuously. The curve calculed with the CTD data and the curve measured directly by the Simrad Probe are almost identical and yield an accurate velocity profile. Upon application of the new water velocity profile, to the previously acquired bathymetric data the tunneling artifact disappeared. This profile was used for subsequently acquired data as well. A total of 3 Seabird CTD's and two Simrad sound velocity profiles were acquired during SO159 (Fig. 4.1 and 4.2).

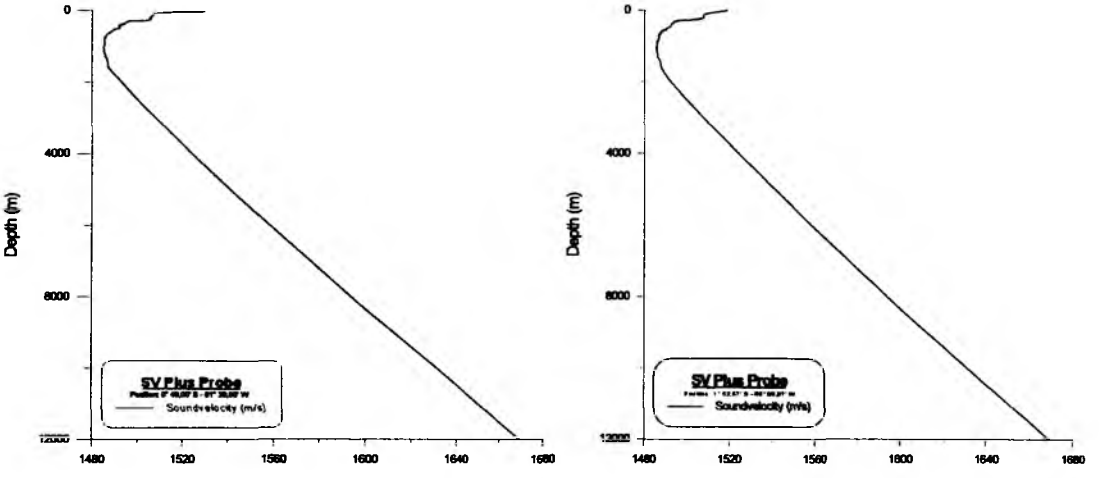

Figure 4.1 : Sound velocity profiles acquired with Simrad velocity probe

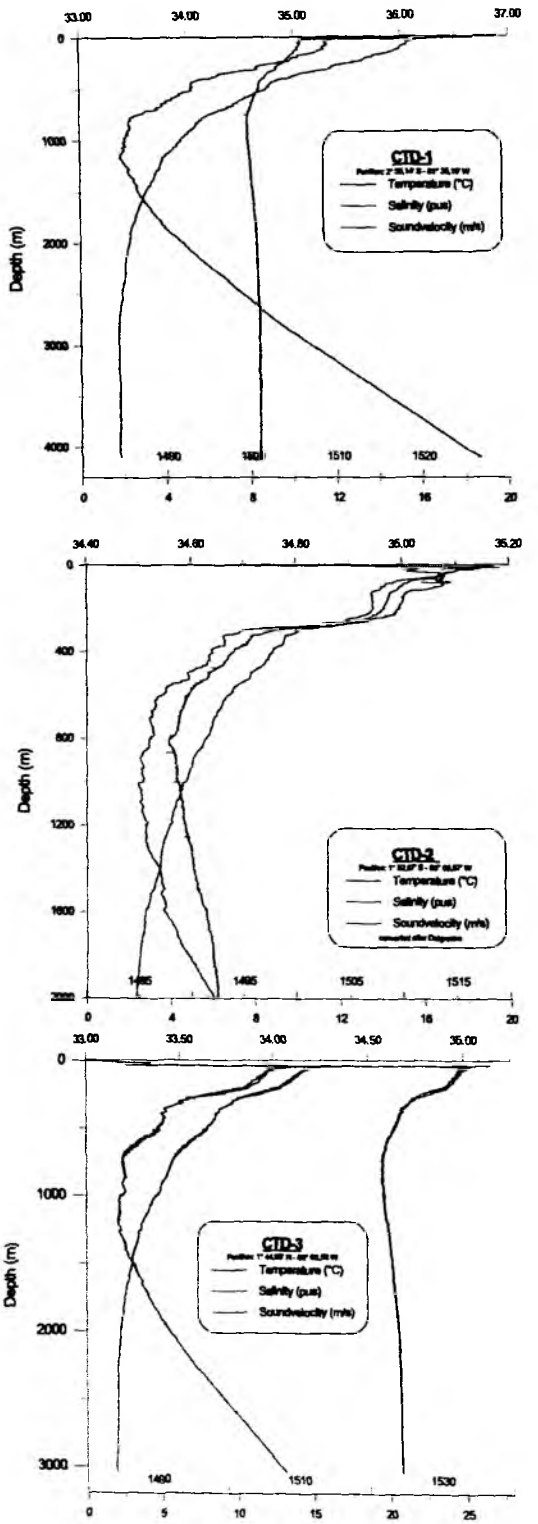

Figure 4.2 : CTD Profiles acquired with the SeaBird probe

4.2 COMPUTER FACILITIES

The experiments and investigations during SO159 required special computing facilities in addition to the existing shipboard systems. For programming of ocean bottom stations, processing of seismic data and analysis of SIMRAD recordings several workstations were installed from the groups.

Due to the large amount of data transfer GEOMAR installed a workstation cluster onboard comprising the following systems:

1	"moho"	SUN Sparc 20	2 CPU, 256 MB memory	10 GB disks, DAT, CD	Sun Solaris 5.8
2	"devonia"	SUN Ultra 60	2 CPU 1 GB memory	130GB disks, 2.3 GB MO, 2x DAT, 2x Exabyte	Sun Solaris 5.6
3	"galicia"	SUN Sparc 10	1 CPU, 96 MB memory	12 GB disks, DAT, Methusalem	SunOS 4.1.4
4	"coiba"	Pentium II 700 MHz	1 CPU, 128 MB memory	64 GB disks, 3x PCMCIA	Windows2000
5	"pinta"	Pentium II 700 MHz	1 CPU, 128 MB memory	64 GB disks, 3x PCMCIA	Windows2000
6	PowerMacintosh G3/300 MHz				
7	PowerMacintosh 8200/120				

In addition to these computers, two X-Windows-Terminal were included in the network. A further Sun workstation was included to the ships network as this unit should stay onboard for future cruises. Due to the extended network ports in the cabins several laptops/powerbooks were used in addition

For plotting and printing two HP Postscript Laserprinters (papersize A3 and A4) as well as the shipboard color plotters were available.

The workstation cluster was placed in the Reinlabor and Magnetiklabor where it was set up according to a "client-server" model, with "moho" being the server (fig. 4.2.1). In the Magnetiklabor a 10/100Mbit hub was kindly provided from the WTD onboard SONNE. The complete network onboard SONNE provides two ports in each laboratory which are all configurable via a switch board. Therefore the two hubs used to build the network in the Reinlabor and Magnetiklabor could easily be connected and allow to extend the GEOMAR LAN across two laboratories. All important file systems from the main server at GEOMAR were duplicated onto the "moho"-disks. Using NFS-, NIS-, and automounter services the computing environment was identical to that at GEOMAR so every user found his/her familiar user interface. The convenience of network mounted file systems has to be paid for with a heavy network load, particularly during playback of OBH-data from tape to disk (c.f. SO123 cruise report, Flueh et al., 1997). This required

a high-performance network, which was accomplished by a switched twisted-pair ethernet. A 12-port ethernet switching-hub (3COM-SuperstackII 1000) with an uplink connection of 10 Mbps to the server "moho" and dedicated 10 Mbps ports for the client workstations maintained the necessary network performance. In order to keep the shipboard network undisturbed by the workstation cluster, but to allow for communication between them, the server "moho" was equipped with two network interfaces and served as a router. This provided the additional benefit of a simplified network configuration. Considerable setup work was dedicated to "moho", while the other workstations used the same IP-addresses and network configuration as at GEOMAR.

This network setup showed a reliable and stable performance. A breakdown of one system disk within "devonia" could be passed by as all disks were mirror-doubled within the workstation. One of the Macintosh failed after three days due to a hard disk crash and could not be reactivated during the cruise.

GeoAzur OBSs are programmed before being deployed through a RS232 serial port using laptop computers that are also used for clock drift measurements and predeployment tests. The data stored on a 1.2 Gbytes SCSI hard disk are copied simultaneously on two 70 Gbytes UNIX hard disks and processed using in-house programs running on SUN workstations.

Tehuelche : SUN Blade		128 Mbytes RAM 20 Gbytes HD	Data transfer Quality control
Vega : SUN Ultra 10	Softwares: OBSTOOL, Seismic Unix, GMT	512 Mbytes RAM 140 Gbytes HD Exabyte drive	Seismic data processing and archiving OBS relocation clock correction merging with navigation data generating Seg-Y files Data modelling
Manta : SUN Ultra 10	Caraïbes™, GMT	512 Mbytes RAM 36 Gbytes HD	Multibeam data processing

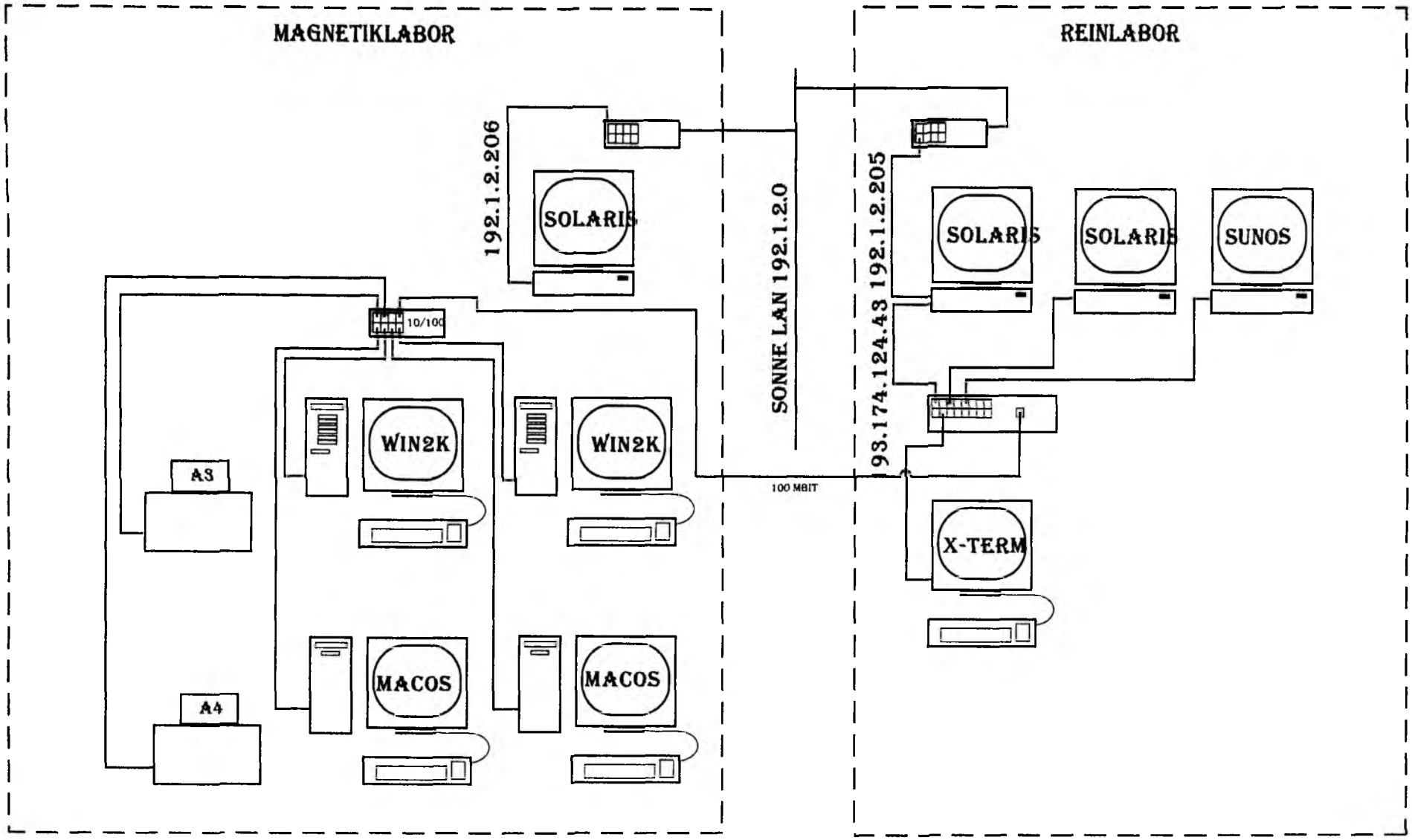

FIGURE 4.2.1 : NETWORK PLAN FOR THE ONBOARD GEOMAR LAN 193.174.124.0
MOHO OPERATES AS DEFAULTROUTER BETWEEN SONNE AND GEOMAR LAN´S ENABLING TELNET AND FTP CONNECTIONS BETWEEN BOTH NETWORKS

4.3 The GEOMAR Ocean Bottom Hydrophone / Seismometer (OBH/S)

The Ocean Bottom Hydrophone

The first GEOMAR Ocean Bottom Hydrophone was built in 1991 and tested at sea in January 1992. This type of instrument has proved to have a high reliability; in fact more than 1600 successful deployment were carried out since. A total of 22 OBH and 2 OBS instruments were available for SO159. Altogether 76 sites were occupied during the SO159 cruise.

The principle design of the instrument is shown in Figure 4.3.1, and a photograph showing the instrument upon deployment can be seen in Figure 4.3.2. The design is described in detail by Flueh and Bialas (1996).

The system components are mounted on a steel pipe which holds the buoyancy body on its top. The buoyancy is made of syntactic foam and is rated, as are all other components of the system, for a water depth of 6000 m, except for the pressure cylinders holding the recording electronics. Here, various models are available for variable depths (2500 m, 3000 m, and 6000 m). Attached to the buoyant body are a radio beacon, a flash light, a flag and a swimming line for retrieving from aboard the vessel. The hydrophone for the acoustic release is also mounted here. The release transponder is a model *RT661CE* made by *MORS Technology*. Communication with the instrument is possible through the ship's transducer system, and even at maximum speed and ranges of 4 to 5 miles release and range commands are successful. For anchors, we use pieces of railway tracks weighing about 40 kg each. The anchors are suspended 2 to 3 m below the instrument. The sensor is an *E-2PD* hydrophone from *OAS Inc.*, and the recording device is a *MBS recorder of SEND GmbH*, which is contained in its own pressure tube and mounted below the buoyant body opposite the release transponder (see Figures 4.3.1 and 4.3.2). During this cruise a prototype hydrophone was provided from *HighTech Inc.*, USA, which worked satisfactorily.

The Ocean Bottom Seismometer

The Ocean Bottom Seismometer (OBS) construction (Bialas and Flueh, 1999; Fig. 4.3.3) is based on the experiences with the GEOMAR OBH. For system compatibility the acoustic release, pressure tubes, and the hydrophone are identical to those used for the OBH. Syntactic foam was used as floatation again but of larger diameter due to the increased payload. In contrast to the OBH the OBS has three legs around a center post to which the anchor weight is attached (Fig. 4.3.4). While the OBH is floating about 1 m above the sea bottom, the OBS is positioned on the sea bottom to avoid collisions between the the seismometer cable and the anchor. The sensible seismometer is deployed about 1 m to the side of the system once the OBS lands on the sea floor. During descent to the ocean bottom, the footplate of the seismometer release lever is about one meter below the base of the anchor and therefore hits the seafloor first. At touch down the baseplate forces an upward movement of the lever which lays out the seismometer hook until the seismometer anchor is about 0.5 m above the seafloor. At about 45 degrees to the vertical the seismometer is released from its hook and falls to the sea floor from about 1 m height, ensuring coupling between the seismometer and the sea floor. At this time the only connection from the seismometer to the instrument is a cable and an attached wire which retracts the seismometer during ascent to the sea surface. An oscillation of the instrument caused by possible currents is therefore not transmitted mechanically to the seismometer. All three channels are preamplified within the seismometer housing and recorded by the standard Methusalem recorder as used in the OBH units. Parallel to these three channels the standard hydrophone is recorded on the fourth channel.

Beside the standard OBS type used for active seismic recording a broadband seismometer was available for test purposes and routinely deployed within the profiles. Two different types of sensors were attached to the instrument. The "Spahr Webb" type seismometer is based on *Mark-L4* sensors which are operated with a feedback loop to enable recordings of frequencies as low as about 60 sec. As the sensors are

sensitive to horizontal or vertical adjustment the complete construction is fully gimbaled. Tilt is measured at selected intervals and two electric motors are used to adjust and fix for a proper positioning. The second sensor is a *PMD-113* which has a flat frequency responce curve from 95 sec. up to 30 Hz. This sensor type operates on the base of measuring levels within electrolytical tubes. This principle is less sensitive to ist horizontal adjustment. The sensor is fixed like a pendulum while ist lower third is surrounded by a viscose oil filling that gives freedom to very slow movements (within a circle of 18°) and could be assumed to be solid within the measured frequency range. Both systems are mounted within a 17" glas sphere with an additional weight at the bottom (20 kg weight in water) which should ensure a good coupling to the ground. The above discribed lever system was not able to handle this size of sensor and therefore a slide system was designed (Fig. 4.3.5) which allows to deploy the sensor about three meters to the side of the instrument carrier. A clock controled burning wire is used first as release of the slide. Then the sensor is pulled by an elastic rope along the slide until he falls off at the end of the boom. Secondly the clock releases the sledge itself to enable deployment of the sensor even if it does not drop off the slide for any reason. Both sensors are recorded by use of the *Marine Longtime Recorder (MLS)* which is manufactured by *SEND GmbH* and specially designed for longtime recordings of low frequency bands. Together with the broadband sensors the fourth channel record a Differential Pressure Gauge (DPG) build by Spahr Webb at SCRIPPS.

Marine Broadband Seismic Recorder (MBS)

The so-called *Marine Broadband Seismic recorder (MBS;* Bialas and Flueh, 1999*)*, manufactured by *SEND GmbH*, was developed based upon experience with the DAT based recording unit Methusalem (Flueh and Bialas, 1996) over the last few years. This new recorder avoids a mechanically driven recording media, and the PCMCIA technology enables static flash memory cards to be used as unpowered storage media. Read/write errors due to failure in tape handling operations should not occur with this system. In addition, a data compression algorithm is implemented to increase data capacity. Redesign of the electronic layout enables a decreased power consumption (1.5 W) of about 25% compared to the *Methusalem* system. Depending on the sampling rate, data output could be in 16 to 18 bit signed data. Based on digital decimation filtering, the system was developed to serve a variety of seismic recording requirements. Therefore, the bandwidth reaches from 0.1 Hz for seismological observations to the 50 Hz range for refraction seismic experiments and up to 10 kHz for high resolution seismic surveys. The basic system is adapted to the required frequency range by setting up the appropriate analog front module. Alternatively, 1, 2, 3 or 4 analogue input channels may be processed. Operational handling of the recording unit is similar to the *Methusalem* system or by loading a file via command or automatically after power-on. The time base is based on a DTCXO with a 0.05 ppm accuracy over temperature. Setting and synchronizing the time as well as monitoring the drift is carried out automatically by synchronization signals (DCF77 format) from a GPS-based coded time signal generator. Clock synchronization and drift are checked after recovery and compared with the original GPS units. After software preamplification the signals are low-pass filtered using a 5-pole Bessel filter with a -3 dB corner frequency of 10 kHz. Then each channel is digitised using a sigma-delta A/D converter at a resolution of 22 bits producing 32-bit signed digital data. After delta modulation and Huffman coding the samples are saved on PCMCIA storage cards together with timing information. Up to 4 storage cards may be used. Currently, up to 440 MB per card are available. Data compression allows more than 2 GB data capacity. Recently technical specifications of flashdisks (disk drives of PCMCIA technology) have been modified to operate below 10 °C, therefore 1 GB drives are now available for data storage. After recording the flashcards need to be copied to a PC workstation. During this transcription the data are decompressed and data files from a maximum of four flash memory are combined into one data set and formatted according to the PASSCAL data scheme used by the *Methusalem* system. This enables full compatibility with the established processing system. While the *Methusalem* system did provide 16 bit integer data, the 18 bit data resolution of the *MBS* can be fully utilized using a 32 bit data format.

The Marine Longtime Seismograph

For the purpose of low frequent recordings such as seismological observations of earthquakes during long term deployments of about one year time a new data logger, the Marine Longtime Seismograph (MLS) was developped by *SEND GmbH* under direction of GEOMAR.

The MLS is again a four channel data logger whose input channels have been optimized for 3-component seismometers and one hydrophone channel. The modular design of the analogue front end allows to adopt for different seismometers and hydrophones or pressure sensors. Currently front ends for the Spahr Webb, PMD and Guralp seismometers as well as for a differential pressure gauge (DPG) and the OAS hydrophone are available. With these sensors we are able to record events between 50 Hz and 120 s. The very low power consumption of 250 mW during recording together with a high precision internal clock (0.05 ppm drift) allows data acquisition for one year. Data storage is done on up to 12 PCMCIA type II flashcards. The instrument can be parameterized and programmed via a RS232 interface. After low pass filtering the signals of the input channels are digitized using Sigma-Delta A/D converters. A final decimating sharp digital low-pass filter is realized in software by a Digital Signal Processor. The effective signal resolution depends on the sample rate and varies between 18.5 bit at 20 ms and 22 bits at 1 s. Playback of the data is done under the same scheme as described for the MBS above. After playback and decompression the data is provided in PASSCAL format from where it could be easily transformed into standard seismological data formats.

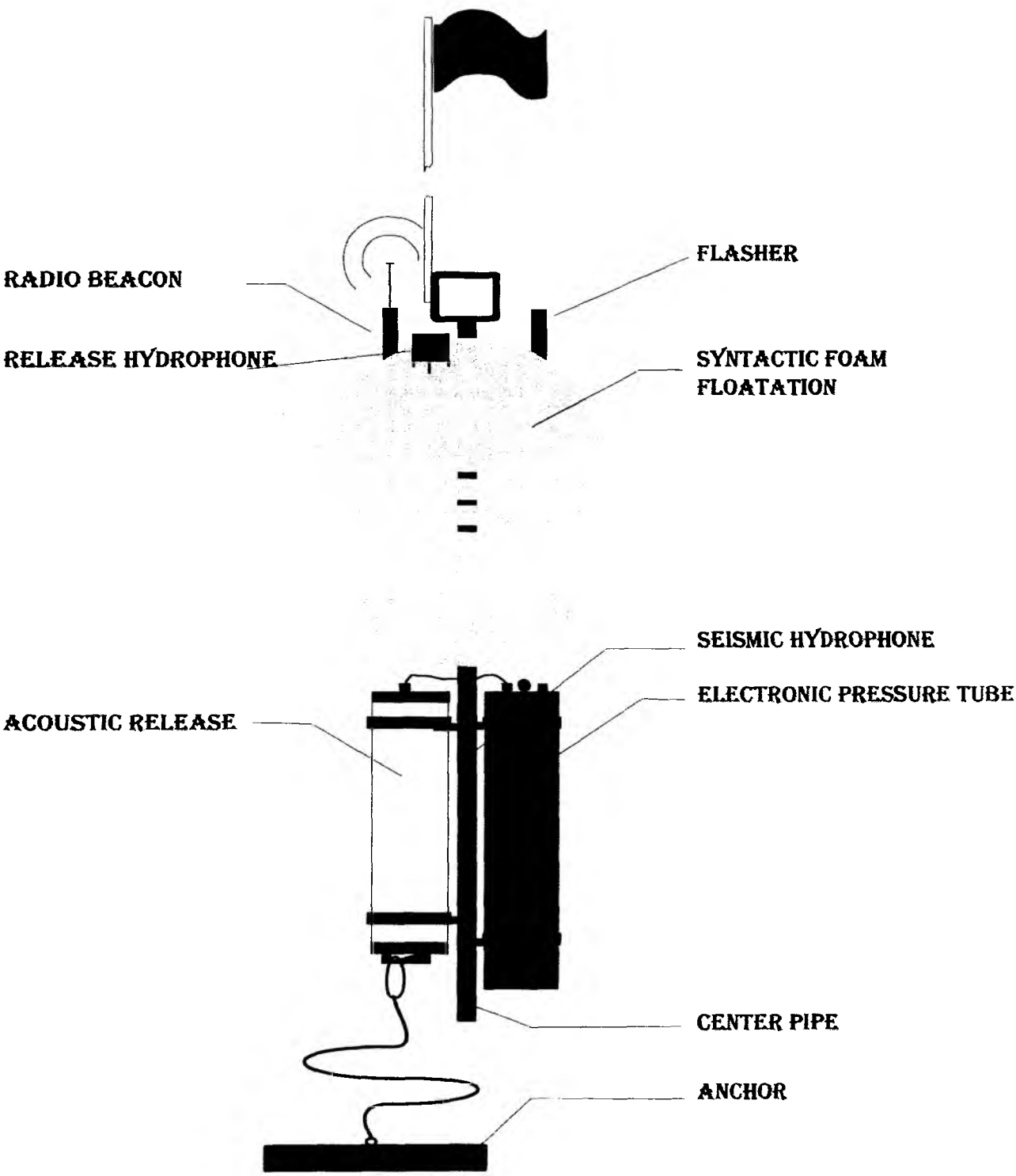

Figure 4.3.1: Principle design of the GEOMAR OBH (after Flueh and Bialas, 1996)

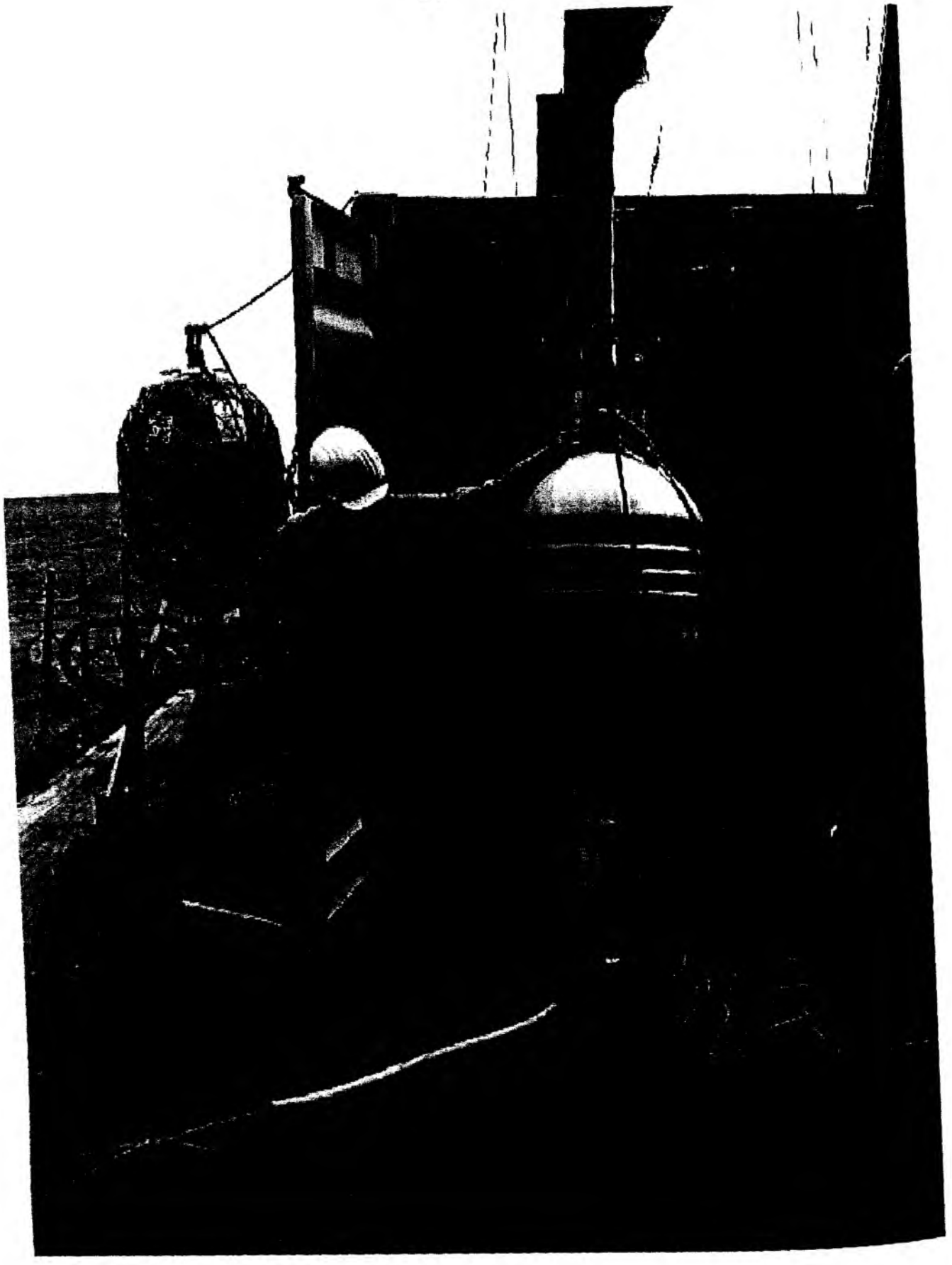

FIGURE 4.3.2: THE GEOMAR OBH READY FOR DEPLOYMENT
BACKGROUND LEFT: GEOMAR OBS
BACKGROUND RIGHT: OBH CONTAINER

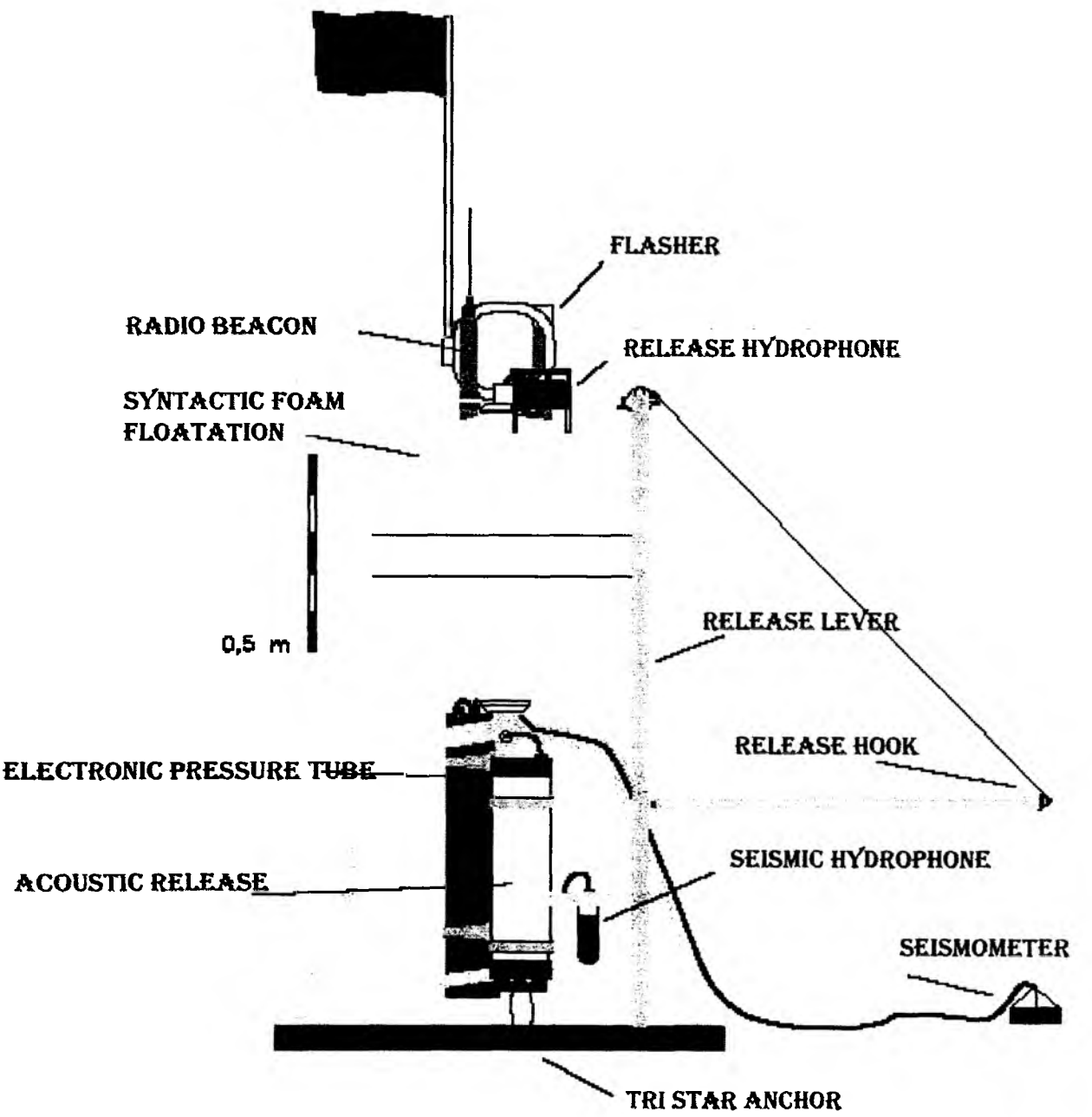

FIGURE 4.3.3: PRICIPLE OF THE GEOMAR OBS (AFTER BIALAS AND FLUEH, 1999)

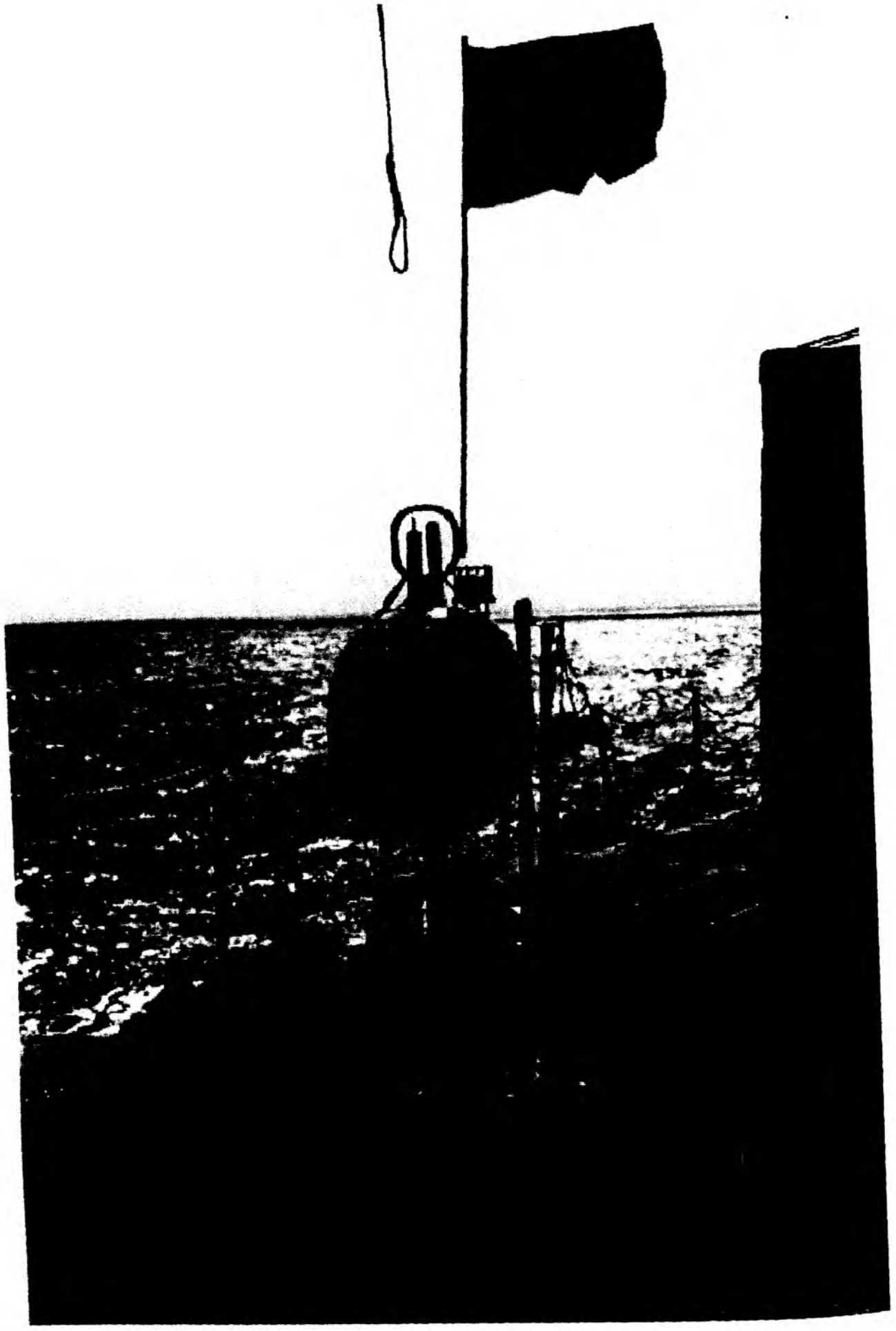

Figure 4.3.4: The GEOMAR OBS ready for deployment

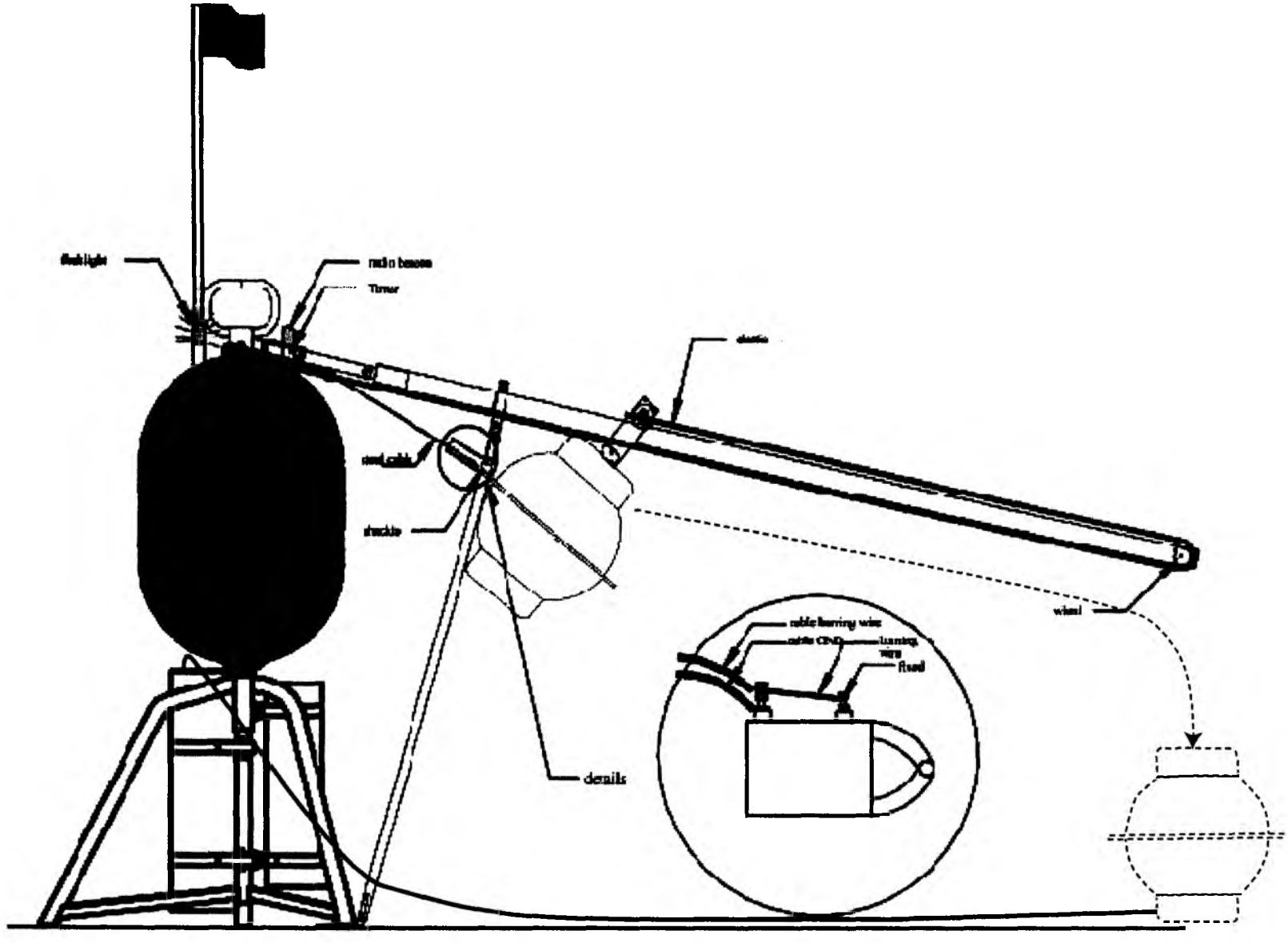

Figure 4.3.5: Scetch of GEOMAR broadband seismometer
dashed lines indicate deployment of the external broadband sensor at the seafloor

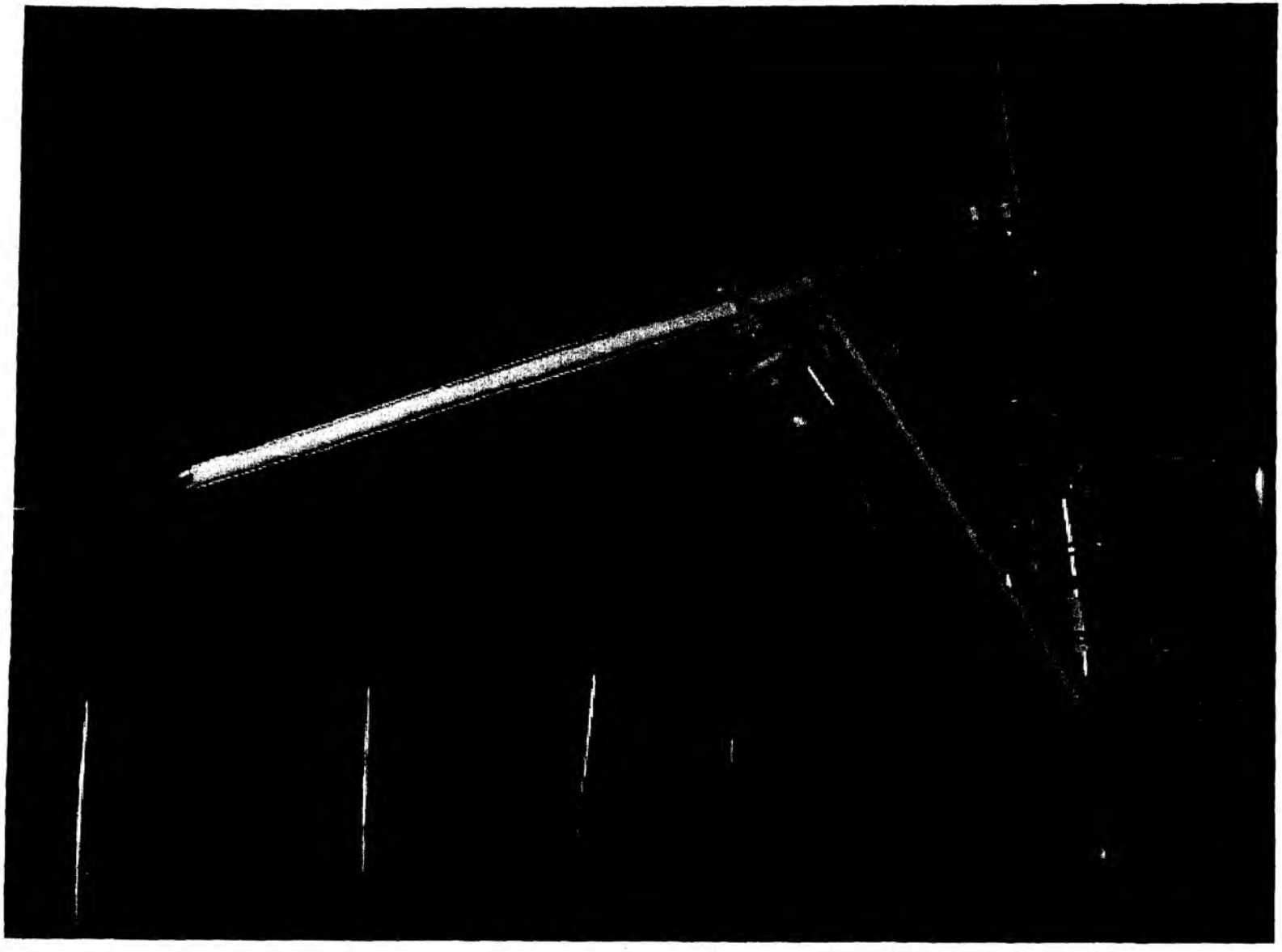

FIGURE 4.3.6: THE GEOMAR BROADBAND SEISMOMETER EQUIPPED WITH WEBB SEISMOMETER AT DEPLOYMENT

4.4 The Géosciences Azur Ocean Bottom Seismometers

4.4.1 Equipment and Facility

Our laboratory: the "Unité Mixte de Recherche (UMR) Géosciences Azur" share a pool of 26 Ocean Bottom Seismographs (OBS) with UTIG (University of Texas, Institute for Geophysics). These OBSs were developed and built in the framework of a long-term cooperation between IRD (Institut de Recherche pour le Développement) and UTIG, and have been successfully used in numerous experiments. Some early versions of the instrument are described in Nakamura et al. [1987] and Nakamura and Garmany [1991].

These instruments consist of a single glass sphere, used as the flotation device and pressure case, which contains the acquisition system and three gimballed geophones. A radio beacon, used for recovery, and a hydrophone are fixed outside the glass sphere (Figures 1). This unit, fastened to an anchor frame for deployment, is released from the anchor at the end of the recording phase.

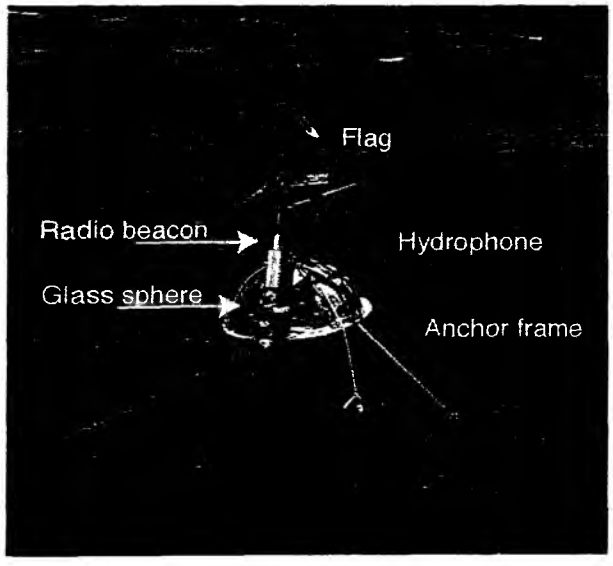

Figure : 1 deployment of an OBS during the Salieri experiment

We are fully equipped to support servicing of these instruments and to provide extensive computer facilities for processing and analysis of the acquired seismic data. This include laptop computers to program OBSs before deployment and to measure clock-drift and SUN workstations with hard disks and tape drives for on-board quality control, processing and archiving of data.

4.4.1.1 Acquisition system

Developed at UTIG (Nakamura and Garmany, 1991) the acquisition system is based on a C44 Bus, and controlled by a low power CPU-80C88 microprocessor. A 4 channel preamplifier also ensure filtering of the analog data. The cut-off frequency of anti-alias filter is selectable by replacing plug-in resistor blocks. The data are stored temporarily in the 512 Kbytes RAM and then transferred to the SCSI 1.2 Gbytes hard disk. The real-time clock (TCXO) is compensated for temperature ranging from 0 to 30°C with a precision of 0.3×10^{-6}. For more details see Table 1.

4.4.1.2 Sensors

A set of 3 gimballed 4.5 Hz geophones is installed in the inner part of the bottom half sphere. An optional hydrophone is fixed outside the sphere for wide-angle seismic profiling. The OBS is fastened to the anchor frame using bungy cords connected to a stainless steel wire triangle on the top of the sphere. The bungy cords are tightened to their limit of elasticity to ensure a proper coupling of the OBS to the anchor frame.

4.4.1.3 Release

The OBS is released from the anchor by the rupture of a stainless steel wire triggered by an acoustic release. Electrolytical phenomena of current in salt water will break the steel wire after approximately 5 minutes and liberate the bungy cords which fasten the glass sphere to its anchor frame allowing the OBS to rise up to the surface at ~1m/s.

Table 1: main characteristics of the IRD-UTIG Ocean Bottom Seismometers

Sensors	3-component gimballed geophones and a hydrophone
Pass Band	4.5 - 100 Hz
Alias filter	selectable with plug-in resistor blocks
Filter roll-off	-24 dB/oct
Sensitivity	1.2 nm/s Mark Products L-15B geophones
Dynamic range	126 dB theoretical, 112 dB re rms electronic noise
Analog/Digital converter	14 bits plus dynamic gain ranging
Sample interval	1 to 255 ms at 1 ms steps
Number of channel	1, 2, 3 or 4
Timing accuracy	0.3 ppm with a temperature compensated crystal (TCXO)
Instrument location accuracy	10 m, from post-recovery analysis of water-wave arrival data
Instrument orientation accuracy	5° from post-recovery analysis of water-wave arrival data
CPU	80C88
Temporary data memory	RAM 512 Kbytes standard, 4 Mbytes optional
Acquisition	Continuous record length 675 s (4 channels @ 10 ms sampling rate)
Transfer rate to recorder	90 Kbytes/s
Data gap	22 s for 512 Kbytes transfer to 1.2 Go IBM hard disk
Recording capacity	1.2 Gbytes on IBM 2.5" hard disk
Autonomy	6 months dormant; 50 days recording (3 channels @ 20 ms samp. r.)
Batteries	24 to 37 lithium or alkaline D cells
Pressure case	43 cm diameter glass sphere
Weight at deployment	85 kg
Weight at recovery	35 kg
Overall dimension at deployment	128 x 128 x 145 cm
Maximum depth of deployment	8 km
Method of instrument recovery	Timed release from anchor controlled by acoustic release.

Operations at sea are summarised in Figure 2 and in Hello et al. (1992) and Hello and Charvis (1998).

Figure 2 : operating OBSs at sea

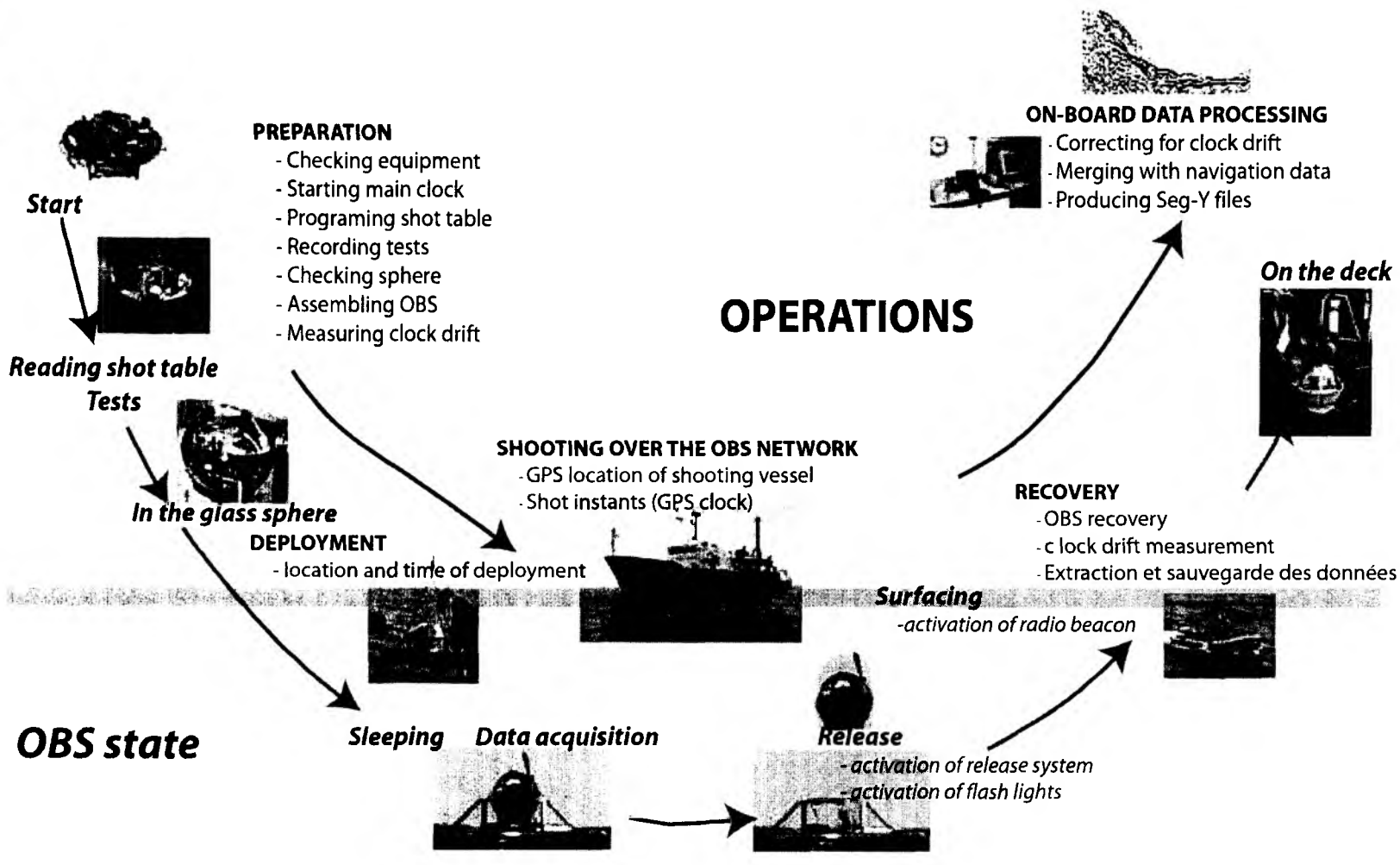

4.4.2 Operation at sea

Operations at sea are described in Nakamura et al. (1987) and Hello et al. (1992), and summarised in (Figure 2) they consist mainly in:

preparation and programming of acquisition system

closing the glass sphere

tests and clock drift measurements using GPS time

deployment of the OBSs fastened to the anchor

shooting of seismic lines over the network of recording OBSs

recovery of OBS at surface after release from anchor

post-recovery clock drift measurement

opening the glass sphere

data transfer and back-up

4.4.3 Data processing and analysis plan

The acquired seismic data, recorded on a hard disk mounted on each OBS, are first transferred to a hard disk on a SUN work station on board the ship and, together with shot times and navigation data, are processed using an in-house-developed proprietary software package OBSTOOL [Christeson, 1995]. OBSTOOL will allow automatic picking of water-wave arrivals, inversion of these arrival times and amplitudes to calculate precise location of each instrument on the ocean floor, correction for clock drift, and generation of SEG-Y format files (Barry et al., 1975) for further processing and analysis of the data.

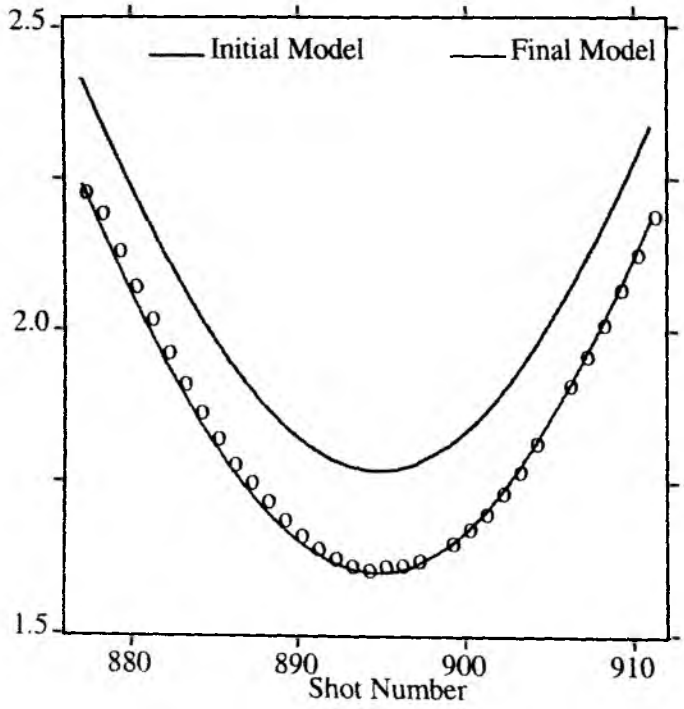

Figure 3 : result of the inversion of the location of OBS 27 on the bottom. Change from initial x,y: 138 m, 1 m. Initial water velocity: 1500 m/s; Final water velocity: 1497 m/s. Initial clock correction: 0.000 sec; Final clock correction: 0.172 sec. Initial Error: 0.168 s; Final Error: 0.005 s

Further processing of the data may include band-pass filtering, deconvolution, and f-k filtering to enhance arrivals. The processed data will be displayed in the form of record sections to be used for analysis.

The processed data are analyzed to produce crustal seismic wave-speed model. For this analysis, we plan to use seismic ray inversion code developed by Zelt and Smith [1992] and tomography code by Zelt and Barton [1998].

4.4.3.1 OBS clock correction

Pre-deployment and post-recovery clock drift measurements allow to correct for clock drift during data acquisition phase.

Table 2: Seg-Y Trace Header Fields (Barry et al., 1975). Major fields in bold.

1	trace sequence number within line	[1-4]	37	mute time--start	[111-112]
2	trace sequence number within reel	[5-8]	38	mute time--end	[113-114]
3	field record number	[9-12]	39	number of samples in this trace	[115-116]
4	trace # within field record (channel)	[13-16]	40	sample interval in micro-seconds	[117-118]
5	energy source point number	[17-20]	41	gain type of field instruments code	[119-120]
6	CDP ensemble number	[21-24]	42	instrument gain constant	[121-122]
7	trace number within CDP ensemble	[25-28]	43	instrument early or initial gain	[123-124]
8	trace identification code	[29-30]	44	correlated	[125-126]
9	number of vertically summed traces	[31-32]	45	sweep frequency at start	[127-128]
10	# of horizontally summed traces	[33-34]	46	sweep frequency at end	[129-130]
11	data use	[35-36]	47	sweep length in ms	[131-132]
12	distance from source to receiver (m)	[37-40]	48	sweep type code	[133-134]
13	receiver group elevation from sea	[41-44]	49	sweep trace length at start in ms	[135-136]
14	source elevation from sea	[45-48]	50	sweep trace length at end in ms	[137-138]
15	source depth (positive)	[49-53]	51	taper type: 1=linear, 2=cos^2, 3=other	[139-140]
16	datum elevation at receiver group	[53-56]	52	alias filter frequency if used	[141-142]
17	datum elevation at source	[57-60]	53	alias filter slope	[143-144]
18	water depth at source (m)	[61-64]	54	notch filter frequency if used	[145-146]
19	water depth at receiver group (m)	[65-68]	55	notch filter slope	[147-148]
20	scale factor for previous 7 fields	[69-70]	56	low cut frequency if used	[149-150]
21	scale factor for next 4 coordinates	[71-72]	57	high cut frequency if used	[151-152]
22	X source coordinate	[73-76]	58	low cut slope	[153-154]
23	Y source coordinate	[77-80]	59	high cut slope	[155-156]
24	X group coordinate	[81-84]	60	year data recorded	[157-158]
25	Y source coordinate	[85-88]	61	day of year	[159-160]
26	coordinate units	[89-90]	62	hour of day (24 hour clock)	[161-162]
27	weathering velocity	[91-92]	63	minute of hour	[163-164]
28	subweathering velocity	[93-94]	64	second of minute	[165-166]
29	uphole time at source	[95-96]	65	time basis	[167-168]
30	uphole time at receiver group	[97-98]	66	trace weighting factor	[169-170]
31	source static correction	[99-100]	67	GPN* of roll switch position one	[171-172]
32	group static correction	[101-102]	68	GPN of first trace	[173-174]
33	total static applied	[103-104]	69	GPN of last trace within original field record	[175-176]
34	lag time A in ms	[105-106]			
35	lag time B in ms	[107-108]	70	gap size (total nb of groups dropped)	[177-178]
36	delay recording time in ms	[109-110]	71	overtravel taper	[179-180]

* GPN = geophone group number,; # = number

4.4.3.2 Relocation and orientation of the instrument on the bottom

Using the arrival time of the water wave recorded either on the hydrophone or on the vertical geophone, and the polarity of horizontal components it is possible to calculated, from a least-square fitting (Figure 3):

the actual location of the instrument on the bottom relative to shot locations

the actual orientation of horizontal components

the residual clock correction when passing over the OBS

4.4.3.3 SEG-Y file generation

It consists in merging the navigation file: time, location and water depth at each shot with the seismic data. In the Salieri project, for each shot a window of 20 s is stored, for each component of the OBS, with a shift with distance of 6 km/s. The shot number, the component number (1= vertical; 2 and 3 = horizontal; 4 = hydrophone), the distance between source and receiver, the delay recording time (delay in ms between the shot and the first sample of the trace), the number of samples per trace and the sampling interval are the main parameters stored in the trace header (see table 2 and Barry et al., 1978).

4.5 Seismic Sources

4.5.1 32 l BOLT Airguns

The seismic signals were generated by three Model 800 CT *BOLT* airguns (one on loan from UTIG); a photo of one of the guns is shown in Figure 4.5.1.1. Each gun has a volume of 32 liters (2000 inch^3), and generates a signal with a main frequency centered around 6 to 8 Hz and including higher harmonics (see also 4.9.1). Two guns were towed attached to blocks on the outer side of the A-frame, with two pier winches controlling the towing. The third gun was towed through the center block of the A-frame using the W6 deep sea cable. Trigger cables and airhoses were deployed manually. Each gun was suspended on two floats with an additional float attached to the supply lines to prevent contact between the gun and the towing wire. A sketch of the towing configuration is shown in Figure 4.5.1.2. The guns were towed 60 m behind the vessel and operated at 145 bar in 7 to 8 m depth. While onboard the port and starboard side guns could not be stored inside the A-frame as the assisting winches on the A-frame were not available this time. Due to good weather conditions the handling of the guns was smooth all the time. Nevertheless a higher wave state during the last recovery operation showed that the limited space on the outer sides of the A-frame with this large guns leave not much safety area for the crew members. Availablility of the assisting winches from the A-frame is therefore needed to allow gun operations from the inside of the A-frame which has been proven as safe and easy procedure during previous cruises (SO146, SO150). Due to the large distance needed for safety reasons between guns and the rear of the vessel the outer guns tend to drift to the center, leaving no space to have the third gun in between. Unfortunately no boom was available to take the force of the towing cable and provide a larger distance between port and starbord side gun. However the small boom used to lower the core carrier on starbord side which was extended by app. one meter recently provided excellent help keeping the hoses away from the towing cable. The recently replaced magnetic boom on port side were used to hold pressure hoses and trigger cables farther to the side which helps prevent them from being damaged by the towing cable. Unfortunately the blocks used for towing the gun hoses and to lift the leading rolls of the magnetometer cable with the old boom were not available. It is highly recommended to replace them (at about 2/3rd and 50 cm before the end of the boom). The center gun was towed about 50 m behind the vessel to keep clear of the other two guns. This configuration is probably not appropriate during weather conditions with high sea state. Booms at the aft capable to take the tow forces of the guns are necessary to further spread the guns away from each other.

During cruise SO159 SALIERI, the guns were used along six seismic profiles. Besides line 1 and 3 (two guns) all lines were shot with three guns, despite shorter intervals needed for repair. The total operation time was about 130 hours, with more than 7100 shots being fired, always at a 60 s shot interval. Line 3 was shot at 40 sec interval, due to the wrap around effect at closer distances from the ocean bottom receivers this shot interval was not repeated on the following lines. The ship's compressor system worked smoothly and caused no delays or interruptions.

External Trigger

The trigger signal was supplied from the ships *Ashtech* GG24 GPS/Glonass receiver, and was available in the Geology Lab and the Seismic Lab. The receiver can provide a one millisecond long 5 V-TTL pulse at intervals between 0.2 and 999 s. The impulse should be stable to within the accuracy of the GPS Time, which is 70 nanoseconds. The impulse was delivered to the *BOLT* Par Airgun Firing Circuit FC300. The shotbreaks, necessary for subsequent data processing and instrument location, were stored on a MBS recorder and displayed in real time to double check. For this process the same time basis was used that is used for the OBH (see chapter 4.4) and the trigger signal was converted into a 5 V TTL pulse of 250 ms length by a circuit provided from the ships technical support staff (WTD). Exact position calculation for the shot time should be done by later post-processing using shot time and UTC time values stored with DGPS coordinates in the ship's data base. As kwon from earlier cruises the coordinates stored within the data base were provided by the *Atlas ANP 2000* system, which does not copy the exact GPS time values but adds time stamps of its internal uncontrolled clock to the high precision coordinates of the DGPS system. Accuracy of the time values mainly depends on the operators skills by manually setting the ANP

clock to GPS time. This is clearly a somewhat conservative method compared to the efforts of precise positioning. To enable the most accurate GPS related time stamps within the ANP system prior to each seismic survey the system operates were informed to reset the ANP.

Figure 4.5.1.1: Photograph of a Bolt PAR 800 CT airgun with 32 l chamber

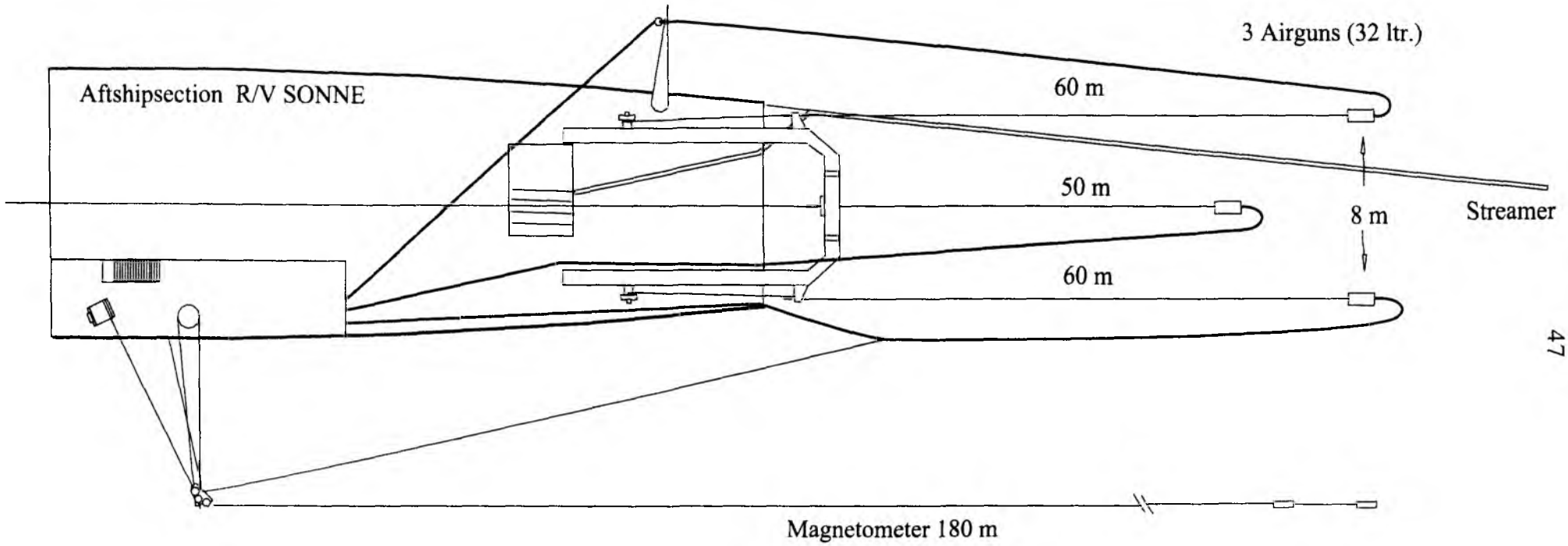

Figure 4.5.1.2: Scetch of tow configuration at the stern of R/V SONNE
3 * 32 l BOLT airgun, streamer and gradiometer

4.6 Multichannel Seismic Data Acquisition

It was planed to record all shots additionally by a short streamer during this cruise. It is a three channel unit originally build by Prakla-Seismos, Hannover, Germany for the Deutsches Hydrographisches Institut in 1979. Unfortunately the PVC tube of the active and stretch section has lost ist flexibility and became brittle. Intense repair and oil refill could reactivate the streamer. Back in water data recording continued for about 15 min when a saltwater break in caused short cuts of the hydrophones again. It turned out that the tube material was to much altered to be repaired onboard and therefore MCS recording could not be done.

The system comprises three parts, a 50 m long active length, a 50 m long stretch length and a 150 m long towing cable. The active length is separated into three groups of 16 HHOC type hydrophones. Construction of the first and third group are identical while the middle one has a smaller hydrophone separation. Within group one and three the hydrophones are 1.2 m apart building a 18 m long unit. This selection results in an antenna directivity which is sensitive to high frequency wavefronts impinging from the near vertical. The -3 dB point is found to be at 48 Hz for wavefronts traveling at 90° (measured from the vertical), 66 Hz / 30°, 190 Hz / 11.5° and 380 Hz / 5.7°. The central group is only 6 m long with 16 hydrophones each 0.4 m apart. The -3 dB point is found at 110 Hz / 90°, 220 Hz / 30 °, 550 Hz / 11.5° and 1.1 kHz / 5.7°. Adding all three groups together the total directivity is (-3 dB) 18 Hz / 90°, 36 Hz / 30°, 90 Hz / 11.5°, 180 Hz / 5.7°. At the tail a depth sensor is installed which indicates the actual depth moduulated as frequency changes. With a base frequency of 990 Hz at the surface it increases by 100 Hz per bar (100 Hz per 10 m). The whole unit is stored and operated from a hydraulic winch at the stern of RV SONNE, in between the two airgun arrays (see 4.6.1).

For recording the data one of the four channel MBS recording units (see 4.3) was used, one such unit having with the high frequency license kit installed which enables sampling intervals up to 10 kHz. This unit was choosen to record the streamer signals with 1000 Hz sampling interval resulting in a Nyquist frequncy of 300 Hz, which is well above the expected maximum energy of 100 Hz. Together with the use of the standard OBH preamplifiers a suitable signal recording was achieved. An oscilloscope connected to a separate output of the channel separator enables online control of each channel.

4.7 The Magnetometer

During cruise SO159 we used a GeoMetrics G801/3 Marine Proton Magnetometer. This unit uses a gasoline-filled sensor with 350 m marine cable and a control unit. During a polarisation cycle an electric current generates a strong magnetic field in the coil and forces the magnetic moments of the protons to be aligned for a short time parallel to the existing field. During the following measuring cycle, i.e. when the electric current is turned off, the previously excited field is removed and the protons "try" to realign themselves with the Earth's magnetic field. According to the moment preservation law, this happens by precession of the protons with a certain frequency, which is directly proportional to the intensity of the Earth's magnetic field. Basically, this frequency is measured as AC electric current created by magnetic induction in the coil, amplified, counted and transformed to the magnetic field intensity values (measuring unit: 10^{-9} Tesla = 1 nT), which are recorded.

In order to minimize the influence of the ship's hull, the sensor of the Magnetometer is towed 180 m behind the ship. This distance of the sensor from the ship was long enough, so that the magnetic influence of the vessel could not produce any disturbances in the recorded magnetic field, so we achieved a resolution of about 5 nT.

On board of RV SONNE, the winch was placed on the port back deck and the sensor was towed to the port side of the vessel. A boom leads the cable about 7 m to the side of the ship in order to prevent it from being tangled with the ship. After having some minor problems at the beginning, the system worked well throughout the trip.

The measured values of the total intensity magnetic field were displayed on a console and written as digital output coded in BCD values. The system was set to deliver one data value every 3 seconds via digital multiport interface to a PC, where a special software was used to store the data together with UTC-time in ASCII tables.

After data backup the files were transferred to a SUN workstation. GPS coordinates and time were taken from the ship's navigation system and assigned to each magnetic stamp on the basis of the recorded time. The magnetic and the navigation data were resampled to 10 s interval. After optional median filtering they were displayed using GMT plot routines (Wessel and Smith, 1995).

4.8 DATA PROCESSSING

4.8.1. OBS/OBH Wide-Angle Seismics

Introduction

The work during the SO-159 Salieri cruise was mainly devoted to the acquisition and processing of wide-angle seismic data. A total of 130 GEOMAR and IRD OBS/OBH deployments were made along six profiles located at four different zones. The location of the lines and deployment sites are shown in Figures 5.3.1.1 to 5.3.6.1, while details on the instrumentation are given in chapters 4.3 and 4.4. The length of the profiles range from 100 km (Profile 03) to 360 km (Profile 01), all of them covered by a densely spaced set of receivers, with OBH/OBS spacing ranging from 5 to 12 km. The seismic source array was constituted by up to three 2000 cubic inch airguns, but in the first profile only two of the guns were used. The shot interval for the profiles was generally set at 60 s, though in part of the Guayaquil slope line (P03) it was reduced to 40 s in order to improve resolution at the topmost crustal levels. After shooting each line, all the GEOMAR instruments and most of the IRD ones were recovered using the acoustic release, but several others had to be recovered with the automatic time release.

All collected seismic data were played out, processed and plotted during the cruise. They were stored in standard SEG-Y format and several copies of the complete data set were provided to each participating institution. The excellent cooperation between the different scientific parties on board, the OBS/OBH technical groups and the ship's crew enabled a smooth and fast operation. Most of the data are of very good quality, especially those along the Carnegie Ridge lines (P01 and P05), in which very clear first arrivals (Pg, Pn) and Moho reflections (PmP) were recorded up to ~140 km distance. The data from the Guayaquil margin lines (P02 to P04) have a lower quality, due to the higher noise level associated with the shallower water depth and to the attenuation related with the extremely thick sedimentary cap.

Preliminary models and interpretations were performed for the first 5 profiles. In this chapter we describe the applied processing and modelling techniques. In chapter 5.3 the most outstanding results from all available profiles are also shown and discussed. The basic processing consisted of butterworth filtering and automatic gain. Predictive deconvolution and whitening have been also applied to several data in order to obtain a better signal-to-noise ratio. The modelling have been done following two independent techniques. On one hand, classical forward modelling has been applied to obtain 2D velocity-depth models along all the profiles. On the other hand, a joint refraction/reflection traveltime inversion method has been used with data from profile P01 to obtain the 2D velocity field and Moho geometry. Finally, a new combined approach of first arrival traveltime and waveform inversion has been also tested with several OBS/OBH from the same profile.

OBH/OBS-data Processing

Deconvolution: To improve the temporal resolution of the seismic data a deconvolution is applied to compress the basic seismic wavelet. The recorded wavelet has many components, including the source signature, recording filter, and hydrophone/geophone response. Ideally, deconvolution should compress the wavelet components and leaving only the earth's reflectivity in the seismic trace. The deconvolution algorithm which was applied is the Wiener deconvolution in successive trace segments, based on the following assumptions:

1. The earth's reflectivity is 'white'.
2. The wavelet shows the minimum-delay phase behavior.

As in this wide-angle data the amplitude spectra of the seismic traces vary with time and offset (e.g. reflected and refracted phases), the deconvolution must be able to follow these time and offset variations. Each trace is therefore divided into 3 s data gates with 1 s overlap, in which time invariant deconvolution operators are computed from the autocorrelation function of the data segment and applied to account for the nonstationarity of the seismic signals. The overall deconvolved trace results from a weighted merging of the independently deconvolved gates.

Input for the deconvolution process is raw data. As several recordings were influenced by a DC shift, a 0-3 Hz high-pass Kaiser frequency filter in minimum delay characteristic with 60 dB attenuation between the pass and reject zone was applied prior to deconvolution in order to center the amplitudes around zero. A predictive length of 100 ms and an operator length of 200 ms was chosen for the data which is a compromise between temporal resolution and signal-to-noise ratio.

After deconvolution an offset- and time-variant Ormsby filter with minimum delay characteristic was applied. As the seafloor depth changes along the seismic lines, each trace was statically corrected to a fixed seafloor travel time of 11 s based on the water depth before filtering. This information is available in the trace headers. After this filter was applied, the data were shifted back to their original travel times.

- **Final processing sequence**
  - Input: SEGY-data, 8/10 ms sampling rate with complete geometry information.
  - Tapering the first 0.5 s to zero to reduce the response of the debias filter operator.
  - Kaiser highpass (debias).
  - Resampling from 10 to 5 ms.
  - Gated Wiener deconvolution: gate length 3 s, overlap 1 s, length of merge region 1 s, operator length 200 ms (prediction interval excluded), prediction interval 100 ms.
  - Static correction to a fixed seafloor traveltime of 11 s.
  - Time and offset-dependent Ormsby frequency filter.

On time-shifted traces with a reduced time scale of 6 or 7 km/s the following filter parameters were used:

lower stop/pass	upper pass/stop (Hz)	offset(m)	beginfull(s)	endfull(s)
3/5	28/48	0	0	12.8
		8000	0	12.6
		48000	0	0
3/5	23/38	0	13.7	14.3
		8800	13.5	14.4
		13200	13.0	13.9
		52000	1.0	2.0
		107000	0	0
3/5	18/28	0	15.3	16.8
		11700	15.1	16.6
		19200	14.8	16.3
		61700	7.0	10.1
		114000	2.0	3.0
		152000	0	0
3/5	13/18	0	19.0	trace length
		20000	18.4	trace length
		130000	3.5	trace length

Modelling

2-D Forward Modelling: For seismic forward modeling conventional 2-D raytracing was applied using the program MacRay [Luetgert, 1992]. This program runs under the Mac OS system and allows the interactive manipulation of a velocity model. A model is defined by two or more interfaces extending across the whole model. Any pair of successive interfaces describes a layer, within which the velocity must be defined at the top and bottom. Within any layer the velocity may be inhomogeneous but has to be continuous. First or second order discontinuities in velocity may occur at interfaces. A raytracing algorithm is used, that calculates the propagation of rays within a layer by

stepwise integration of a system of first order differential equations [Cerveny et al., 1977]. Lithologic interfaces are represented in the model as first or second order velocity discontinuities. When an interface is encountered in the calculation of a ray, Snell's law is applied and the calculation is continued. The MacRay program is very useful for quickly manipulating velocity models.

The initial models were set up with an uppermost layer of water, velocity=1.5 km/s. The sea level is at 0 km depth, sea floor and OBH/S locations are provided by the UKOOA file. Model depth is positive downward.

A layer-stripping strategy was applied, modeling from top to bottom. The models are developed by trial and error. To ease this procedure first order boundaries were assumed, although some record sections reveal a more gradual transition between two traveltime branches. Usually a constant vertical layer gradient was applied.

The traveltimes of the most prominent phases were picked on UNIX workstations with the interactive plotting and picking program for seismic data ZPLOT [Zelt, 1994] and transformed to the MacRay format.

Inverse Modelling: Together with the forward modelling techniques, two different tomographic methods have been applied. The first one is a recent method of joint refraction/reflection traveltime inversion which was succesfully used with a similar data set in the Greenland margin [Korenaga et al., 2000]. This method employs an hybrid ray-tracing scheme based on the graph method with a local ray-bending refinement. This allows to obtain accurate ray tracing and forward travel time calculation of refracted and reflected waves across an arbitrarily dense mesh of velocity nodes. Node spacing can vary laterally and vertically. An independent set of depth nodes is used to define a floating reflector. The final 2D velocity field and the floating reflector geometry (Moho) are achieved by using smoothing and damping constraints to regularize a simultaneous iterative inversion. The perturbations of the model parameters in each iteration are calculated by least squares minimization of the (sparse) linear system using the LSQR solver. This code was implemented into a SUN UltraSparc Workstation, and phases (Pg-first arrivals and PmP) were picked using the program PLOTSEGY.

The second one is a seismic tomographic approach based on combined first arrival traveltimes tomography and waveform inversion. This approach is subdivided in two steps. The first one consists on a classical finite differences traveltime inversion where the first traveltime arrivals are computed by solving eikonal equation using the algorithm of Podvin Lecomte. The rays are traced a posteriori following the inverse of gradient traveltimes. This first step gives a first low frequency velocity model of the medium, used as an initial model for waveform inversion. The waveform inversion is nonlinear linearised in the frequency domain . The forward problem is resolved by solving the wave propagation equation by finite differences in the frequency domain (Stekl, 1997). The perturbations are computed using a conjugated gradient method as described in Pratt [1996]. The inversion proceeds from low frequency to high frequency in order to reduce the non linearity of the inverse problem. These second step allows to recover a higher resolution velocity model of the medium. These method is currently developed and tested in Geosciences Azur by C. Ravaut and S. Operto. Only the first step of these method was implemented during the cruise into a SUN UltraSparc Workstation using the first arrival traveltimes picked on the recorded sections using the program PLOTSEGY.

4.8.2 Simrad Data Processing

(F. Michaud, P. Wintersteller, C. Wenz)

Software on board

The collected data were processed onboard with the coverage software EM 120. The postprocessing was done on two other workstations by the accessory software Neptune and Cfloor (Roxa, Smedvig Tech., Oslo). The Neptune software, used by the System Operators of R/V SONNE converted the raw data in 9 different files which contains informations about position, status, depth, sound velocity and other parameters and are stored in Simrad's own binary format.

Using the Neptune software, the first step of data cleaning was to assign the correct navigational positions to the data without map projections. The second step was the depth corrections, for which a depth threshold was defined to eliminate erratic data points. In the third part of postprocessing statistical corrections were applied. Therefore a multitude of statistical functions are available in a so called BinStat window where the data are treated by calculating grid cells with an operator choosen range in x and y direction. Each kind of treatment is stored as rule and has an undo option. For the calculation the three outermost beams (1-3 and 188-191) were not considered. Also a noise factor, filtering and a standard deviation were applied to the calculated grid. The Cfloor software was used to generate maps and digital elevation models from the cleaned database. Thus, the Cfloor software also offers possibilities to clean the data for an better representation.

CARAIBES software

The acquired data were also processed simultaneously using CARAIBES software. The CARAIBES software is developed by IFREMER (CARtography Adapted to Imagery and BathymEtry of Sonars and multibeam echosounders). The CARAIBES software used on board by the scientists converted the EM120 raw data into 2 differents files : one with the position information (navigation) and a second with depth, sound velocity, backscatter and other parameters. It is composed of two software programs : CARAIBES-RT which combines real time operations for bathymetry and reflectivity data acquisition, visualization and archiving, CARAIBES-PP for post-processing: This last one was used during the S0159 cruise.

The software is adapted to many sounders (SIMRAD, SEABEAM, FURUNO, THOMSON, ATLAS, MGD77, etc.) and can be easily interfaced with other multibeam echosounders or sidescan sonars. Bathymetric DTM 3D visualisation CARAIBES-PP provides full processing of bathymetry and reflectivity data from multibeam echosounders and sidescan sonars. Available processing ranges from importing raw data to visualizing processed data (DTM, image mosaics), as well as filtering,
smoothing and various corrections.

Using the CARAIBES software, a systematic processing was applied after cutting several of the outermost beams to each side. As a first step we produced a grid with half the cell-grid size (80 m) of the final calculated grid. From this first grid we created asmoothed grid (with a spline function) and with a double cell-grid size (160)m. We compared this smoothed grid with the data in order to apply a filter. Data with amisfit greater than 80-m were eliminated (approximately 2-3 % of the data). As a last step, after cleaning data we generated the final calculated grid (160m grid-cell size).

All this work was mainly done both by the System Operators of R/V SONNE in charge of the Neptune software and by scientists in charge of the Caraibes software. After the postprocessing the data was exported as an ASCII file in x,y,z format with header information.

4.8.3 Magnetics

Quality control, preliminary data processing and presentation were done onboard. In order to process the magnetic data, ASCII files of raw data were transferred to a Sun workstation. Processing consisted of resampling and merging the magnetic data with the differential GPS navigation from the ship. The anomalies were plotted along track after merging with navigation. No corrections for diurnal variations have been carried out during the cruise.

5 Experiments completed and preliminary results

5.1 Bathymetry

(F. Michaud, J.-Y. Collot, M.-A. Gutscher)

5.1.1 Performance of the Simrad EM 120 system and data quality

During SO159 multibeam bathymetry was recorded continously whenever the vessel was outside the near coastal zones. Simrad mapping was used onboard to obtain the correct depth and topography along the OBS wide-angle profiles and for the correlation of magnetic anomalies with depth. Transits and short surveys (between OBS deployment and seismic acquisition) were selected to complement existing bathymetric data recorded during previous cruises by the R/V Atalante, R/V Sonne and R/V Jean Charcot, especially along the Ecuador margin and across the Carnegie ridge. All these data were merged with Caraibes software and fit together very well. This allows us to compare the various acquisition systems. For example along a ship track, between 3000 m and 4000 m, the area covered by the EM120 of the R/V Sonne is similar in width to the area covered by the EM12 dual of the R/V Atalante. No interference was observed with the 96 l air-gun array during acquisition of wide-angle seismic profiles. Real-time control of newly acquired data with existing data was not possible (as available from CARAIBES-RT software) and this explains why between some swaths data gaps exist. Total bathymetric coverage acquired during SO159 is shown in Figure 5.1. In order to present the most complete bathymetric coverage available, data from other cruises has been integrated with the newly acquired SO159 data as shown in Figure 5.2

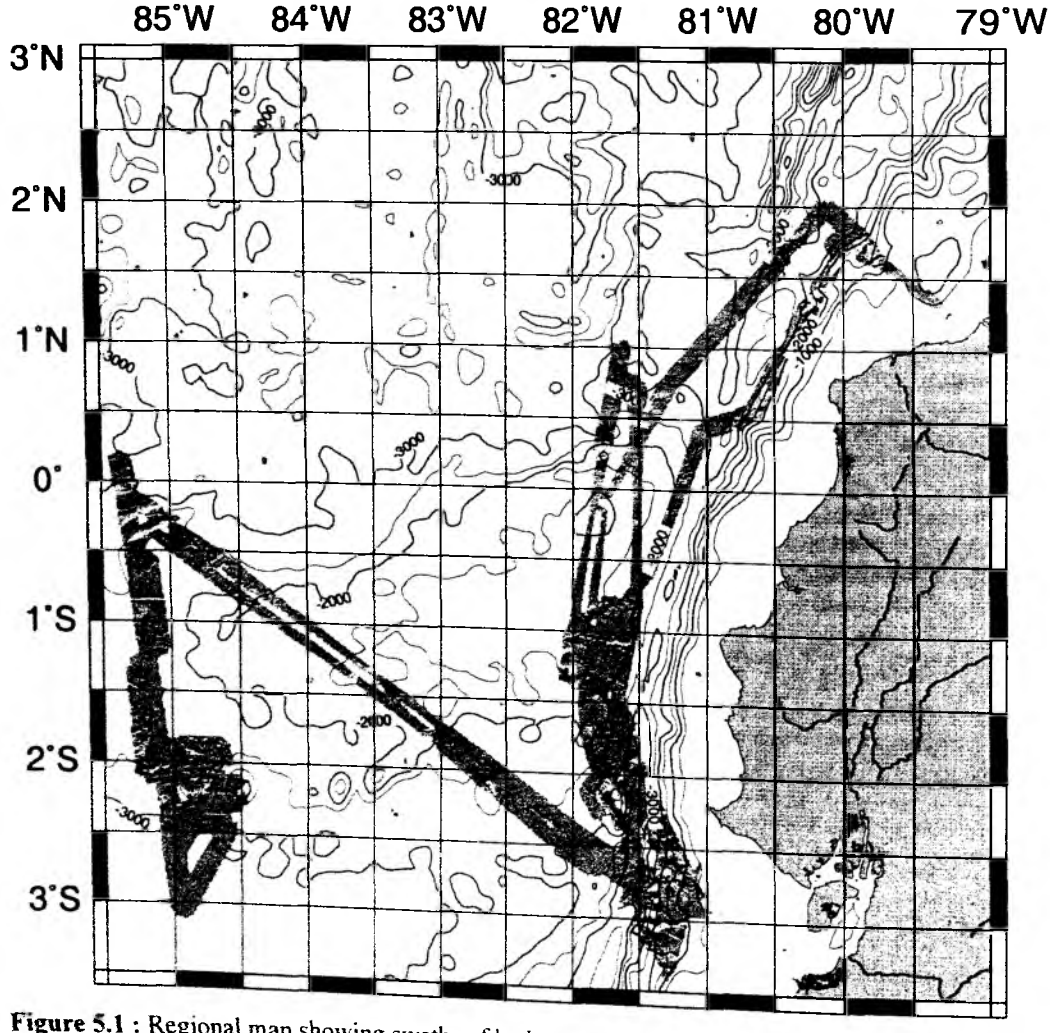

Figure 5.1 : Regional map showing swaths of bathymetric data acquired during SO159

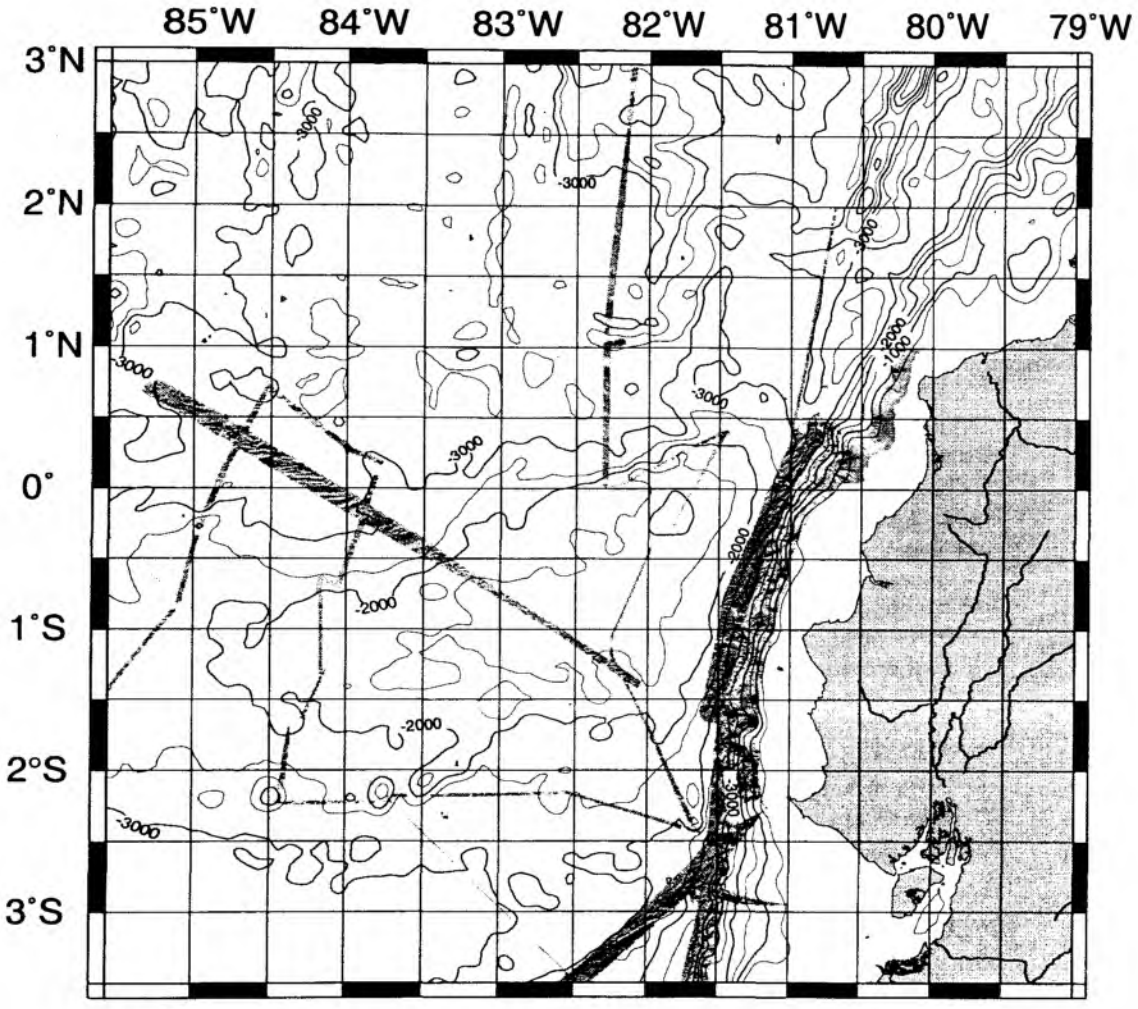

Figure 5.2 : Regional map showing previous multibeam bathymetric coverage in the SO159 study area. (SEAPERC, J. Charcot, 1986 ; PUGU Atalante, 1997 ; PAGANINI, SO-144, 1999 ; Megaprint Cruise SO-158).

5.1.2 Observations and preliminary results

Central Carnegie Ridge (85°W)

Multibeam bathymetric data were acquired on the low relief segment of the Carnegie Ridge near 85° W longitude (Fig. 5.3). Here the oceanic plateau and its flanks can be morphologically defined as a doming seafloor, at an average depth of 2400 m, extending between the 3000 m contour in the south and 3200m in the north, thus providing a ~270 km width.

Immediately north of the Carnegie Ridge the oceanic crust is rugged and shows an EW-trending structural grain at depths of 3200-3500m, and a major, north-trending horst-like feature that we interpret as a Fracture Zone.

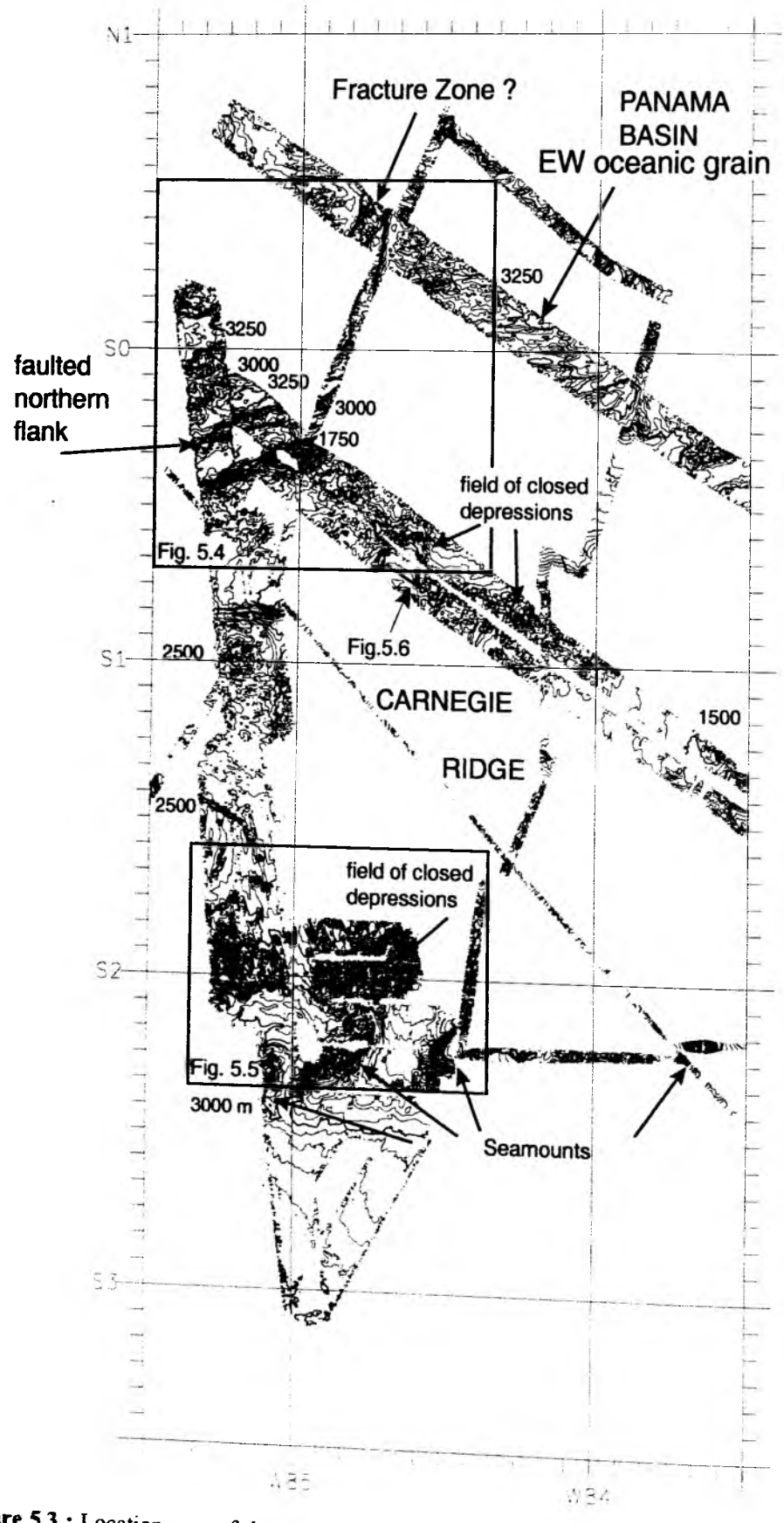

Figure 5.3 : Location map of the Central Carnegie Ridge showing multibeam bathymetric coverage and distinct morphologic provinces described in detail below (processed and drafted with Caraibes Software).

The northern flank of the plateau is steep and irregular. It comprise an ENE-trending, 4-5 km wide, 1500-2000m shallow ridge overhanging two flat platforms, 5 to 10 km wide at depths of 2700 m and 3100m respectively. The ridge and platforms are separated by steep, NW facing linear scarps suggesting northwestward-dipping normal faults. These likely formed during a period of NW-SE extension which rifted the northern flank of Carnegie Ridge, separating it from the SE flank of Cocos Ridge. At the conjugate position on Cocos Ridge N60E structures are also observed as well as a steep SE dipping seafloor and a marked asymmetry in the crustal root, all consistent with rifting of an ancestral Cocos-Carnegie Ridge.

- The summit surface of the ridge is generally smooth, suggesting a tectonically undeformed sediment cover. This pattern is locally disrupted by narrow E-W or N-S trending ridges and a N-120 trending low, apparently basement highs and faults of volcanic origin.

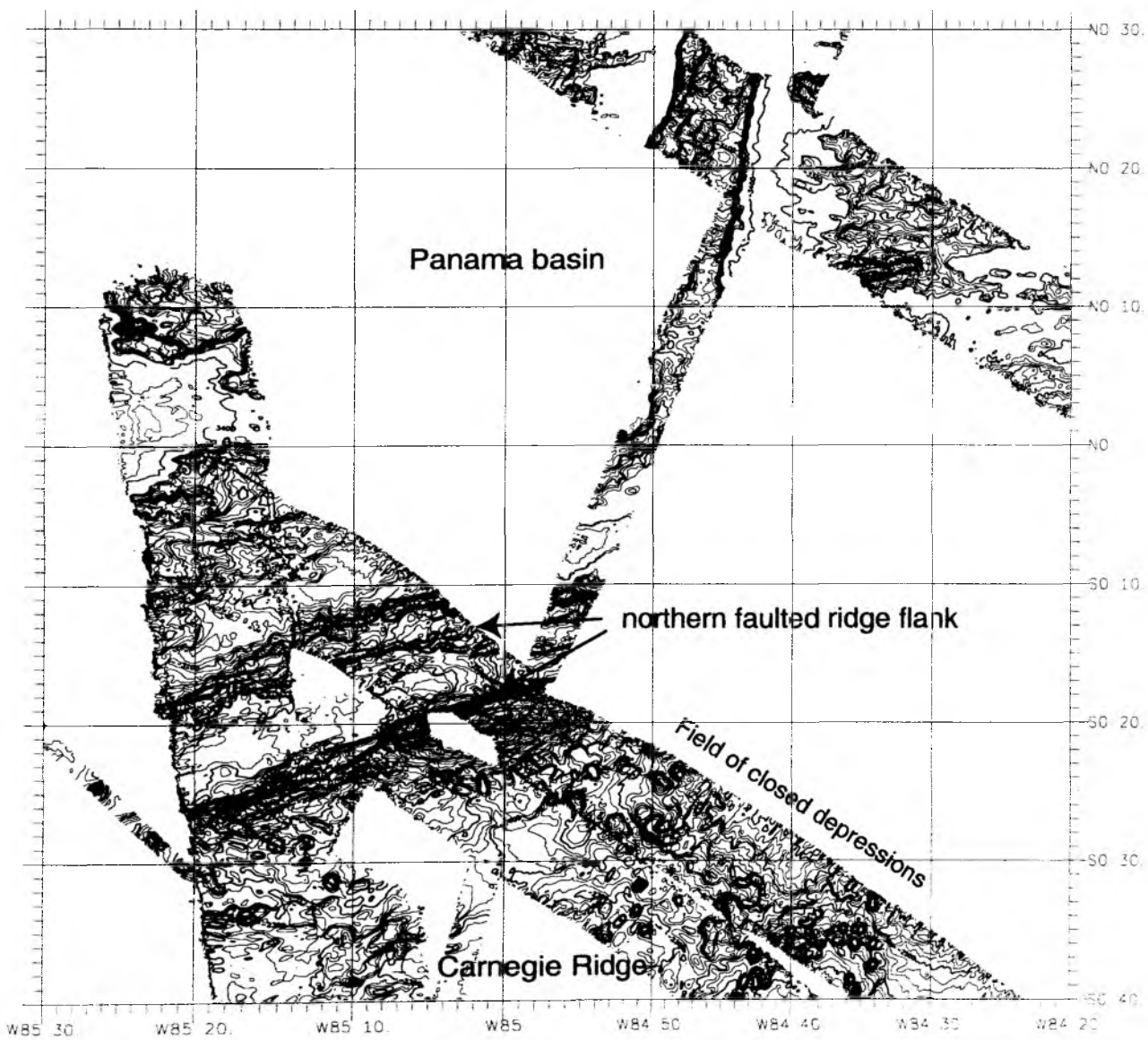

Figure 5.4 : Close-up of the northern flank of the Central Carnegie Ridge showing steep N60E scarps, E-W structural grain of the Panama Basin and a field of closed depressions (processed and drafted with Caraibes Software)

The southern ridge flank shows a gentle slope from 2500 m to 3000 m. Large seamounts are located at the junction between the abyssal plain and the plateau southern flank. They are 10-20 km long, ...m high, and trend N-30-40°E. Some are flat-topped, suggesting a period of wave-based erosion followed by thermal subsidence. Others show numerous peaks and crests. Their elongated shape and orientation suggest they resulted from fissural volcanism.
The most interesting and puzzling features we observed are a series of curved elongate and circular depressions (Fig. 5.5). These are most common at depths of 2000 to 2600m on both the northern and southern flanks of the Carnegie Ridge. These will be described in detail below.

We distinguish three classes of depressions :
1) Curved hook shaped depressions about 4 km wide, 200-500 m deep and some 20-30 km in length, wrapped around the base of 10-20 km wide 1-1.5 km high seamounts. We interpret these features to be curved valleys carved by the scouring action of deep sea currents eroding the sedimentary cover on the seafloor around the base of these volcanic edifices.
2) Fairly isolated 2 km wide 50 - 300 m deep circular or crescent shaped depressions on the upper slope of the ridge. These commonly contain a central high, not higher than the local seafloor depth. These are typically associated with wispy N-S trending tails strongly suggesting the effects of erosion of a N-S basal current.
3) Concentrations of circular depressions, 1-4 km wide and typically 100 - 300 m deep. Almost all are flat floored and some are so densely packed as to almost present a honeycomb pattern. These are typically located along the mid-slope of the flanks of Carnegie Ridge at seafloor depths of 2000-2600 m. Several hypotheses can be advanced to explain their shape and abundance. A) They are scouring features on the seafloor, carved by local eddies of a basal current in the soft underlying sedimentary cover and are thus similar to 1 and 2. B) They are volcanic in origin, representing late stage explosive eruptions similar to volcanic maars on land and which blasted 200 m deep craters out of the seafloor and then later covered by a thin sedimentary cover preserving the volcanic depression in the seafloor. C) A combination of A and B, the crater like depressions are the surface of the volcanic basement, which has been swept clean of overlying sediments by basal currents. The third hypothesis C can be ruled out, because parasound observations (Fig. 5.6) made in this region shows sedimentary cover of at least 50 m thickness on the highs between the depressions and ~20-40 m inside them. D) A pockmark origin due to gas release is unreasonable in view of the dimension and abundance of these structures and the lack of biogenic sediment to produce gas. E) These depressions are karst type features, the result of dissolution of carbonate sediments. As portions of the juvenile Carnegie Ridge were likely emerged above sea level, carbonate rich sediments may have been deposited in shallow water depths (500-1000m). The paleo platform then subsided by roughly 1.5 km bringing it below the CCD (carbonate compensation depth) and the carbonate rich layers would have dissolved. This hypothesis is attractive because it offers an explanation for the spatial distribution of the depressions. This would imply a similar sedimentary composition around the present day Galapagos Platform.

Figure 5.5 (following page): Close-up of the southern flank of the Central Carnegie Ridge showing three styles of closed depressions, including a densely packed field of circular depressions (processed and drafted with Caraibes Software).

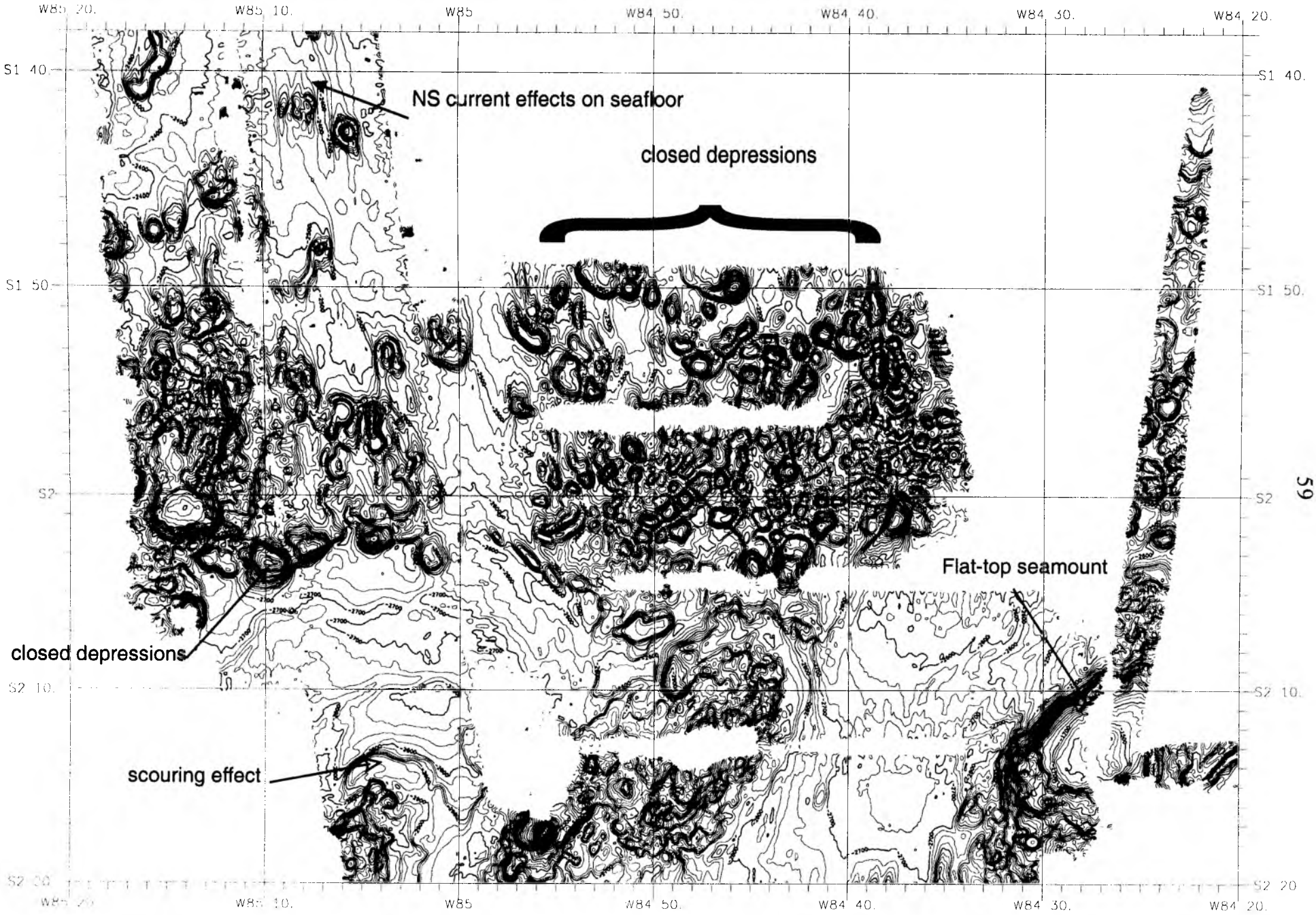
W85 20.
W85 10.
W85
W84 50.
W84 40.
W84 30.
W84 20.
S1 40.
S1 50.
S2
S2 10.
S2 20
NS current effects on seafloor
closed depressions
Flat-top seamount
closed depressions
scouring effect

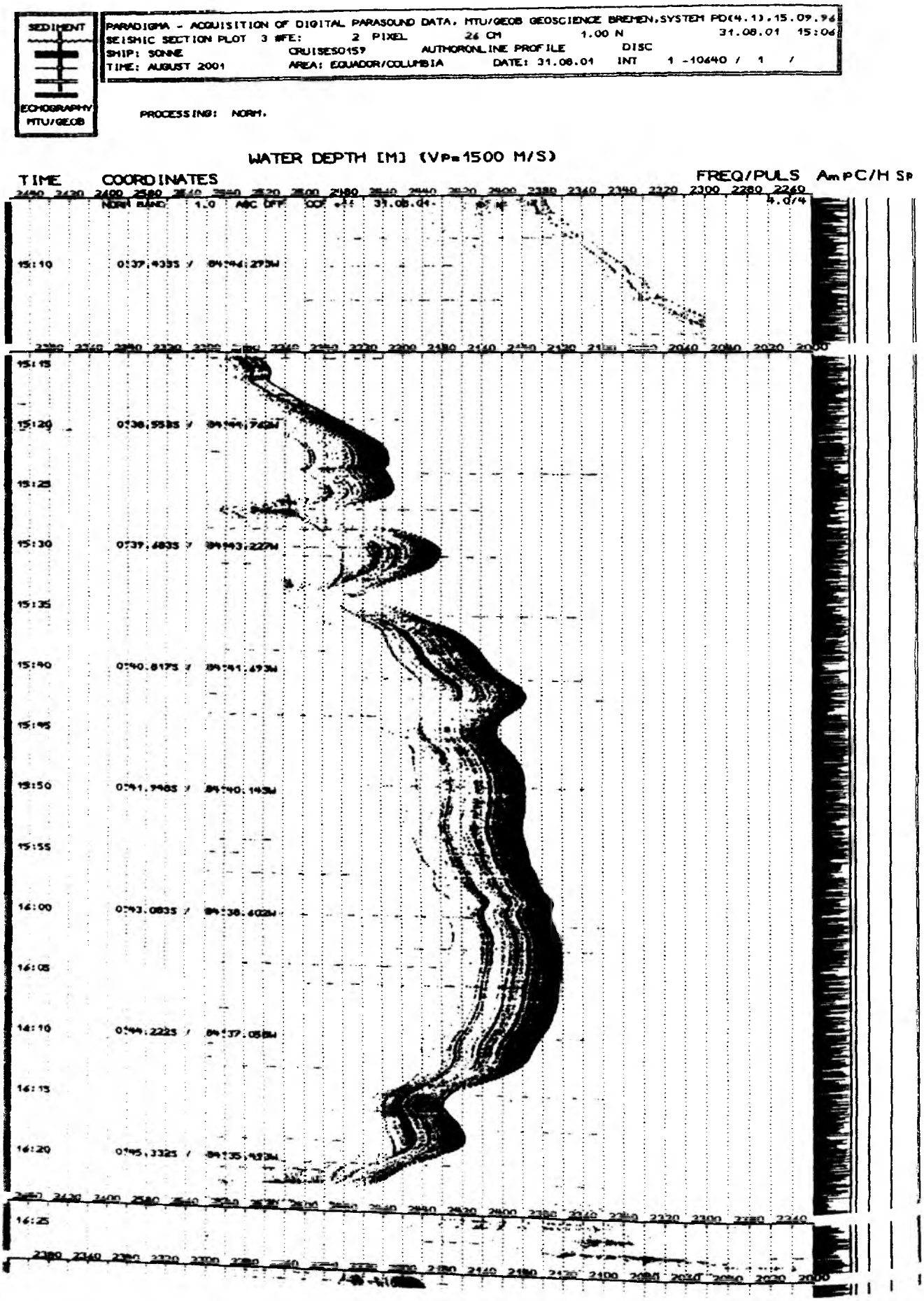
SEDIMENT
ECHOGRAPHY
MTU/GEOB
PARADIGMA - ACQUISITION OF DIGITAL PARASOUND DATA, MTU/GEOB GEOSCIENCE BREMEN,SYSTEM PD(4.1).15.09.96
SEISMIC SECTION PLOT 3 #FE: 2 PIXEL 26 CM 1.00 N 31.08.01 15:06
SHIP: SONNE CRUISES0159 AUTHORONLINE PROFILE DISC
TIME: AUGUST 2001 AREA: EQUADOR/COLUMBIA DATE: 31.08.01 INT 1 -10640 / 1 /
PROCESSING: NORM.
WATER DEPTH [M] (Vp=1500 M/S)
TIME
COORDINATES
FREQ/PULS AmpC/H Sp
NORM BAND 1.0 AGC OFF
15:10
15:15
15:20
15:25
15:30
15:35
15:40
15:45
15:50
15:55
16:00
16:05
16:10
16:15
16:20
16:25

Figure 5.6 (preceding page): Parasound observations of sedimentary cover in the field of closed depressions on the northern flank of the Central Carnegie Ridge (for location see Fig. 5.4)

Eastern Carnegie Ridge (82°W)

Multibeam bathymetric data were acquired on the eastern part of the Carnegie Ridge near 82° W longitude, crossing the summit of the plateau at a water depth of ~750 m (Fig. 5. ?). The morphology will be described from south to north. There is a general asymmetry, similar to that observed on the Central Carnegie Ridge at 85°W, with a gentle southward dipping southern flank and a steep northern flank.

At the southeast corner of Carnegie Ridge the seafloor rises from a base level of >3000 m to <2000 m water depth in an irregular fashion. The undisturbed oceanic crust between Grijalva and Carnegie Ridge (between 3°10'S and 2°40'S) is situated at a mean water depth of 3100 m. North of this limit the seafloor climbs gently norththward by 400 m before reaching a subhorizontal platform between 2600 m and 2400 m. This platform is shown on the SISTEUR multichannel seismic profile to be a 0.7 s TWT thick sediment basin which pinches out to the south along the gentle slope.

Within this domain on the southern flank (between 3000 m and 2400 m water depth) a series of circular to elongate seamounts are observed. The longest, adjacent to the trench is 50 km long, 10 km wide, and composed of N-S to N30W trending segments. Two of the roughly circular seamounts (at 82°40'W, 2°10S and 81°55, 1°45'S) have curved hook shaped depressions at their base as described for seamounts south of the Central Carnegie Ridge study area (see above).

Further north above 2400 m depth, the seafloor morphology is more disturbed and a series of closed circular depressions and elongate depressions are observed. These can be seen in the multichannel profile to be depressions within the southward sloping sedimentary cover. Between 1°10'S and 1°00'S, the seafloor is rough, marked by isolated circular basement highs (which we interpret to be volcanic cones) and E-W trending linear ridges. Sedimentary cover is nearly absent here. North of about 1°S the seafloor is smooth and flat, at a mean depth of 1400 m and covered by a a 0.7 s TWT thick layer of sediments.

North of 0°20'S the seafloor rises abruptly to <1000 m depth and the summit of Carnegie Ridge is reached. The seafloor surface is rough, marked by E-W linear ridges and is seen to have little to no sedimentary cover in the seismic profile. North of the Equator a field of closed circular and elongate depressions is observed between 1500 m and 2000 m and the seafloor dips northwards.

At about 0°10'N a series of steep N70E to E-W trending north facing scarps are observed. These are interpreted to be north dipping normal faults at the rifted northern flank of Carnegie Ridge as in the Central Carnegie Ridge study area. A scarp bounded seafloor high at 0°20'N adjacent to a conical seamount appears to be a local horst structure.

North of 0°30'N seafloor depths of 3000 – 3200 m are reached and the basement appears to be undisturbed oceanic crust formed at the fossil Malpelo Rift. The E-W trending axis of this extinct spreading center is seen at 82°15', 1°00'N and at

Figure 5.7 (following page): Location map of the Eastern Carnegie Ridge showing a compilation of multibeam bathymetric coverage acquired during SO159 and the PUGU survey with R/V Atalante in 1997. Distinct morphologic provinces are described in detail above (processed and drafted with Caraibes Software).

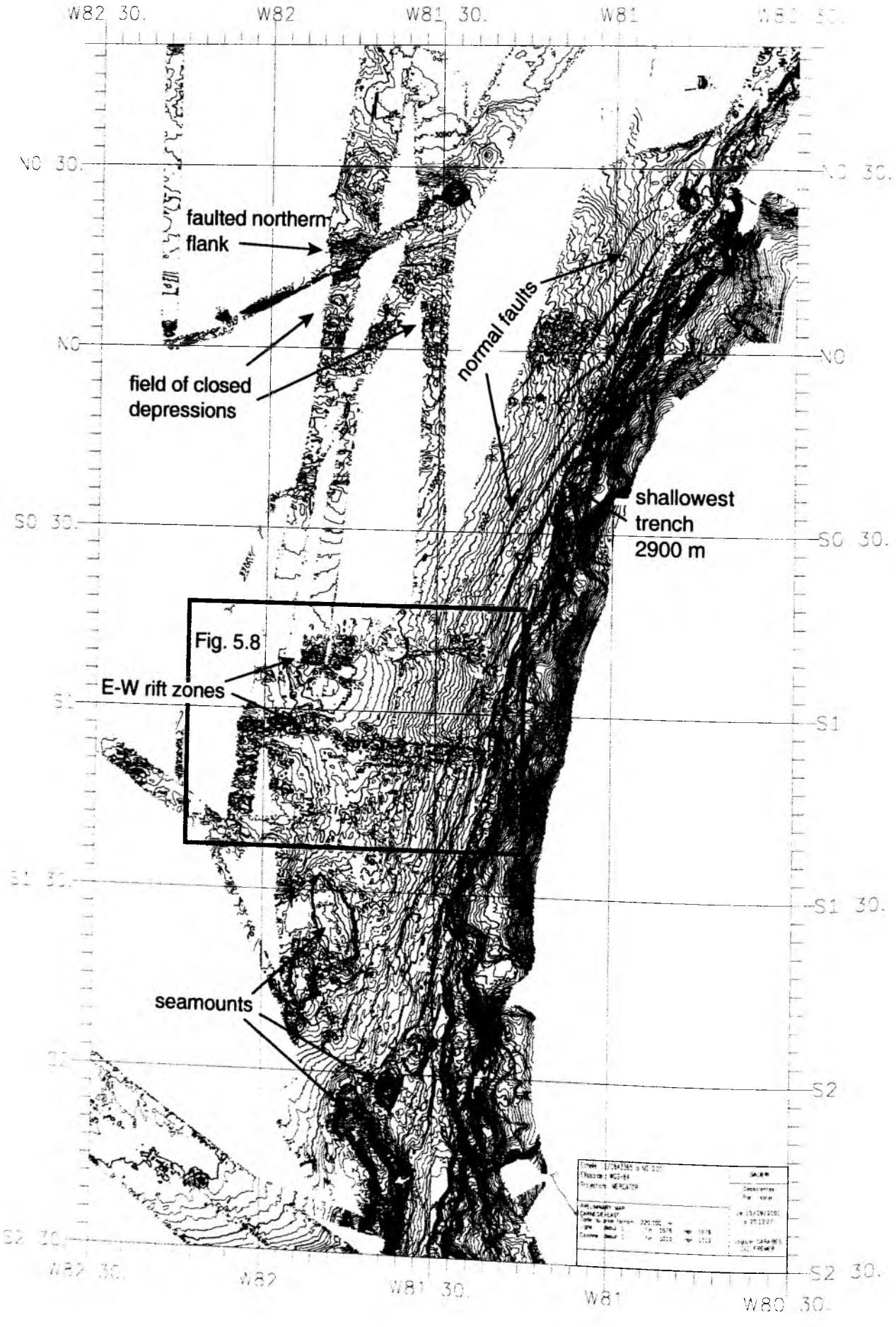
W82 30.
W82
W81 30.
W81
W80 30.
N0 30.
N0
S0 30.
S0
S1 30.
S1
S2 30.
S2
faulted northern flank
field of closed depressions
normal faults
shallowest trench 2900 m
Fig. 5.8
E-W rift zones
seamounts

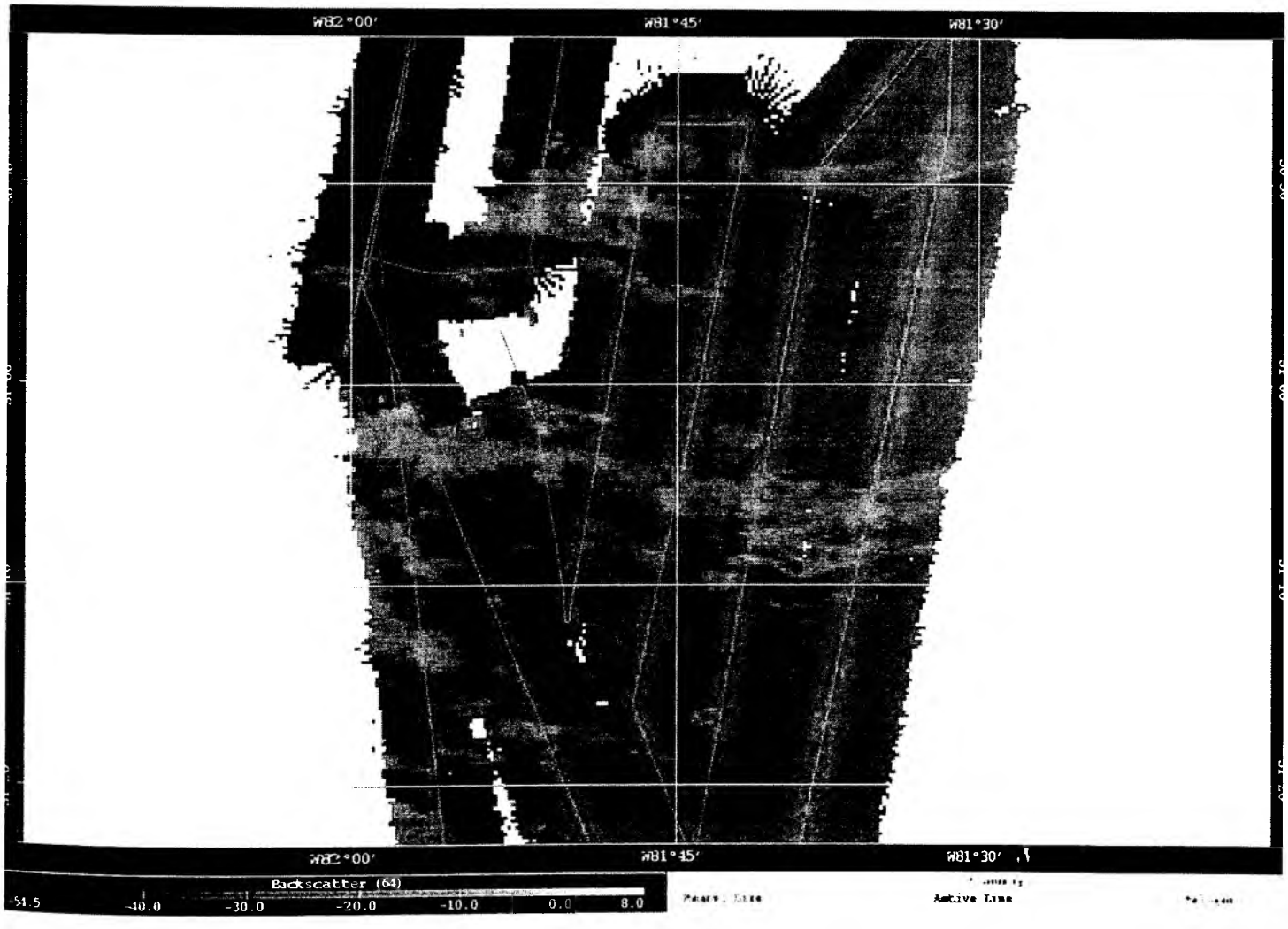

Figure 5.8 : Backscatter sonar image of the the eastern sector of Carnegie Ridge showing E-W trending basement highs as regions of high reflectivity and darker regions indicating sedimented areas. These correspond to areas of rough seafloor and smooth seafloor topography, respectively (see Fig. 5.7).

Gulf of Guayaquil Area

Multibeam bathymetry acquired in this area covers several morphologic domains to be discussed below : 1) the northernmost Peru Trench, 2) the Grijalva Scarp, 3) the Gulf of Guayaquil Margin, 4) the southwestern Ecuador Margin facing the Carnegie Ridge.

1) The Northern Peru Trench narrows northward from about 30 km at 3°S to <10 km width north of 2°40'S. A slight widening to 20 km is also observed from 2°10' S to 2°20' S where closed bathymetric contours indicate a local sub-basin. At these locations where the trench is wider, the trench floor is flat and is covered by a few hundred m of turbiditic trench fill as shown by multichannel seismic data acquired during the SISTEUR cruise. In all places the seafloor of the oceanic Nazca Plate steepens towards the east due to flexure upon entering the subduction zone. Generally eastward facing fault scarps are observed at numerous locations along the western rim of the trench, and are known from seismic profiles to be east dipping normal faults due to lithospheric flexure. North of 2°15' S the trend of the normal faults is N-S to N20E. Between 2°30'S and 3°S, normal faults are oriented N20E to N45E, especially at the Grijalva – trench intersection. The trench north of 2°15' S is the shallowest along the margin at a mean depth of 3200 m and appears to be nearly devoid of trench fill. The shallow depth is due to the presence of the subducting Carnegie Ridge. Here normal faults are prominent and can be followed to within a few km of the defrmation front at the base of the continental slope.

2) Bathymetric data from the Grijalva Scarp were acquired during the previous Megaprint Cruise SO-158. They reveal a series N45E trending offset in the seafloor depth, from about 3000 m to the NW down to 4000 m to the SE. This offset is taken up by two to three N45E trending, SE facing scarps, including a steep N60E trending linear ridge splaying off the main scarp.

3) The Gulf of Guayaquil margin will be described from top to bottom. The shallowest portion we sampled is at 100 - 200 m water depth. Here the margin is very flat floored. Below 200 m a gentle westward slope is observed. Cutting into this gentle slope is a canyon, beginning near 81°W and 3°S. It trends west-southwestward before joining with a tributary canyon and proceeding in serpentine fashion down to the trench. This lowermost portion of the canyon has steep side walls cutting 1000 - 1200 m into the substratum over a lateral distance of about 4 km (a mean slope of about 17°). Other canyons can be seen at 3°15'S and at 2°15'S. A major irregular crescent shaped depression is located at 2°40' S extending 20 km into the margin. Its origin may be due to confluence of paleocanyons or a major slump scar due to graviatational instabilities. Steep embayments are observed at the base of the slope in numerous locations, the most prominent at 2°55'S. These give the base of the margin a scalloped type of appearance suggesting bites having been taken out of a stable rigid substratum. From SISTEUR multichannel seismic lines this substratum appears to be in a state of tectonic erosion. Beneath this scalloped lower margin scarp a small bench at a waterdepth of 4100 - 3700 m can be seen, extending from 3°S to 2°15'S. It is bounded to the west by a linear, continuous, N-S trending 300 - 400 m high scarp. As shown by SISTEUR MCS lines this bench and associated scarp represent a single thrust slice with emergent thrust fault at the deformation front cutting through a 400 - 500 m thick sediment layer at the trench. South of 3°S this bench widens into a series of 2-3 individual steps with a more discontinuous deformation front. Here, where the trench fill is deepest, incipient accretion is occurring (e.g. see Fig. 1.9a)

4) The southwestern Ecuador Margin facing the Carnegie Ridge is marked by a short steep continental slope descending from 700 m to the trench at 3200 m over a distance of about 25 km (for a mean slope of about 6°). A large embayment is observed at 1°42'S. The lower slope is covered by by mass wasting deposits and the margin has been shown to be unstable and affected locally by seamount subduction. (Villamar, 2001).

Figure 5.9 (following page): Location map of the Gulf of Guayaquil Margin study area showing : the northernmost Peru Trench, the Grijalva Scarp, the Gulf of Guayaquil with its incised margin, a seamount province at the southeastern corner of Carnegie Ridge (processed and drafted with Caraibes Software).

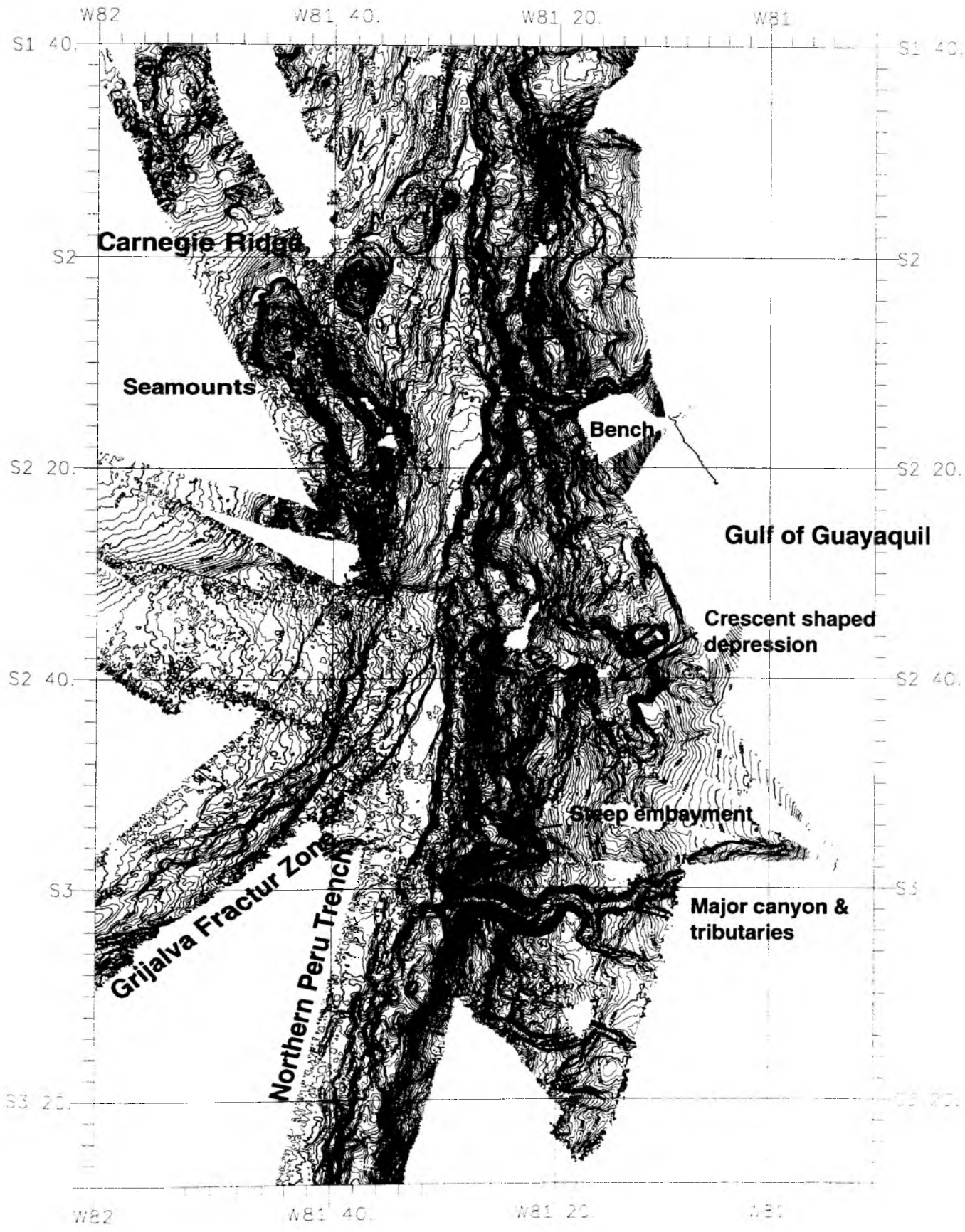
W82
W81 40.
W81 20.
W81
S1 40.
S2
S2 20.
S2 40.
S3
S3 20.
Carnegie Ridge
Seamounts
Bench
Gulf of Guayaquil
Crescent shaped depression
Steep embayment
Major canyon & tributaries
Grijalva Fractur Zone
Northern Peru Trench

Northern Margin Study Area (0-2.5°N)
Multibeam bathymetric data were acquired perpendicular to the margin along OBS Profile 6 and during transits, including the base of the continental slope at the border to the southernmost Colombia Trench.

The northwesternmost transit (from 1°N, 81°W to 2°N) samples undisturbed oceanic crust formed at the extinct Malpelo Rift sytem. It reveals a smooth surface, apparently due to a few hundred m of pelagic sediments, as known from SISTEUR MCS data. The SE flank of a large seamount (summit at 1400 m depth) is crossed and then a series of parallel, N-S trending east facing scarps as seafloor depth increases to 3100 m and the western edge of the Colombia trench is reached.

The trench perpendicular profile begins at about 300 m depth on the shelf with a gentle NW slope down to a flat domain, with a smooth seafloor at about 700 - 900 m water depth. This corresponds to the >2.5 s TWT thick forearc basin observed in SISTEUR MCS data. At about 1°35'N lat. the seafloor becomes rougher. First a minor WSW ward draining canyon is crossed, then the seafloor shallows and descends again and a major N-S trending canyon is crossed at 79°50'W. The seafloor steepens along a few NW facing scarps, the last dropping some 400 m to the trench floor commencing at about 2900 m depth. Here a gentle cone shaped slope is observed descending radially to 3100 m water depth. We interpret this to be a fan of turbidites caused by the sediment influx from the major N draining canyon which enters the trench at about 79°50'W.

The trench parallel profile was selcted to cover the lowermost part of the continental slope and a part of the floor of the trench. From 1°48'N to 1°25'N a series of 1-3 subparallel trench facing scarps are observed at the base of the slope, commonly separating flat bench like areas. They are typically 200-400 m in height and the lowermost of these may represent thrust slices, marking the beginning of accretion in this sector. They strike N30 to N60E parallel to the regional continental slope. A SISTEUR MCS line at 1°42'N shows an incipient thrust at the deformation front, which we also observed in the parasound data. It connects structurally with a major scarp to the southwest indicating a well developed imbricate thrust slice. Over this same sector the trench deepens slightly from 2900 m to 3200 m. Higher up the slope at 2500 - 1500 m water depth there are prominent highs (< 1500 m depth) at 1°35'N and 1°23'N separated by a flat floored reentrant. These structures show a strong N40E - N60E structural grain as expressed by steep bounding scarps. The reentrant may mark a slump scar left by the passage of a subducting seamount. South of 1°25'N the dominant trend of the continental slope becomes N-S to N30E and trench parallel faultscarps become discontinuous and less common. The floor of the trench deepens substantially to >3900 m and narrows to < 10 km width. This suggests minor amounts of trench fill and an underfilled trench with respect to the 40 - 50 km wide Colombia Trench north of 1°50'N. To the north the 2.5 s TWT of sediments at the trench axis from SISTEUR MCS lines indicates about a 3 km thickness. An MCS profile at 1°10'N indicates < 800 m of sediments at the trench axis.

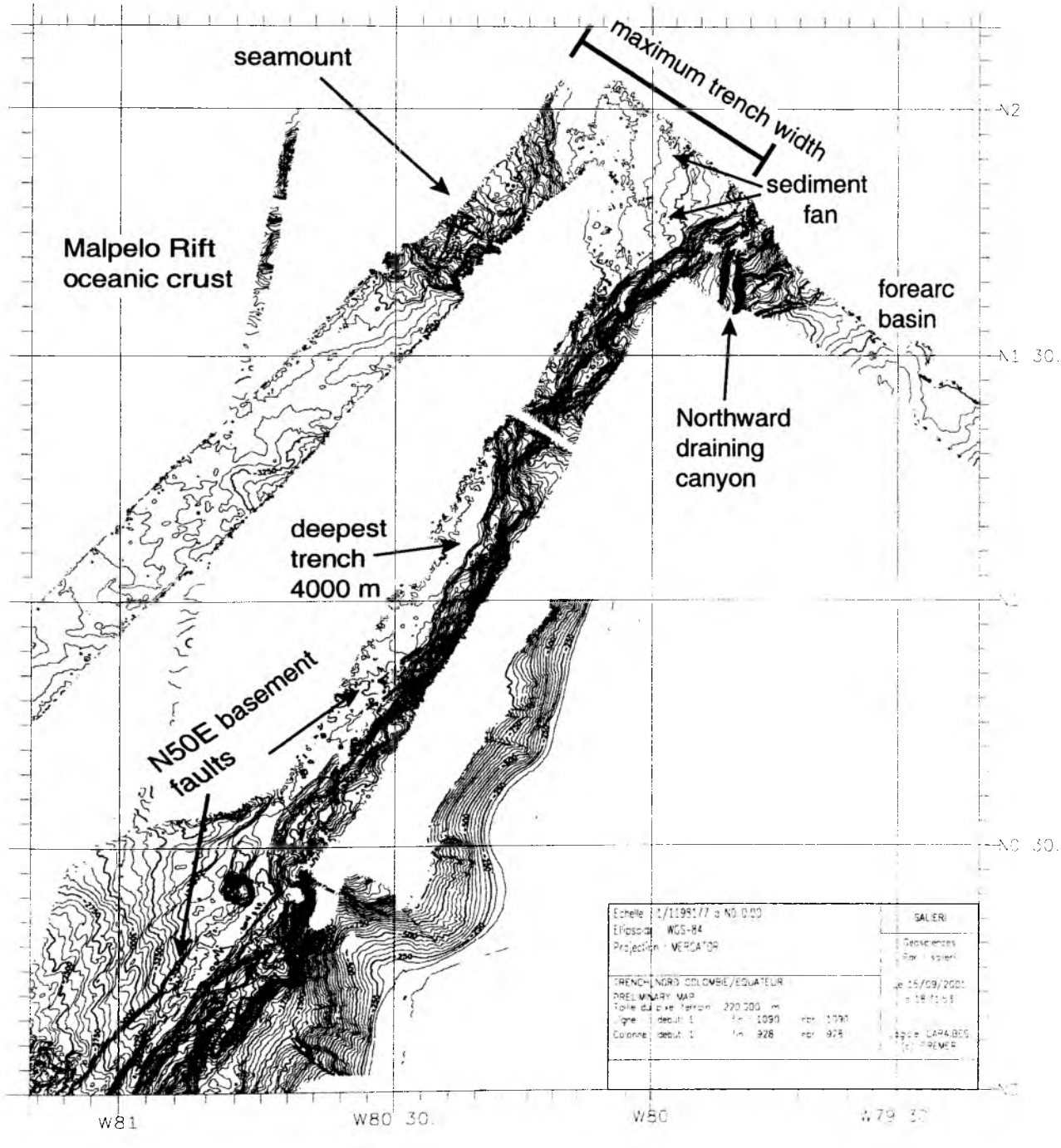

Figure 5.10 : Location Map of northern margin study area (0° - 2.2°N) with multibeam bathymetric data acquired, including digitized data from coastal hydrographic maps (processed and drafted with Caraibes Software).

5.2 Magnetics

(Peter Oliver Thierer)

During the cruise SO159 of R/V SONNE, about 1700 km of magnetic profiles were acquired. The magnetic profiles are based on measurements done during shooting seismic refraction profiles as well as on transit sections. Interpretation has been done on the total field magnetic raw data, no corrections as e.g. latitude correction was done. Therefore interpretations are of preliminary character. However, the neighbored seismic lines and corresponding modeling was used to keep the framework.

First Results – Magnetic Profile SO 159, S01

Profile S01 (figure 5.2.1) is orientated SSE-NNW (roughly 3,00° S and 84.95° W to 0,17° N and 85,36° W) and crosses the Carnegie Ridge (see seismic model of line S01, figure 5.5.1.33). Its overall length is about 354 km.
The magnetic field strength ranges from about 29500 nT in the outermost south up to about 31100 nT in the outermost north. The magnetic profile can be divided into three different subsections:

1. Northern Section (west of 85,3° W): The highest magnetic field strength is observed in the northern part of the line. Variations in magnetic anomalies are well distinct and of relative short frequency, the amplitude changes are of about 500 nT. However, changes in magnetic field strength well correlate to the observed topography. They may be coincident with magmatic intrusions connected to rifting processes which occurred at the northern flank of the Carnegie Ridge, indicated on bathymetry data.
2. Central Section: This section corresponds to the bathymetric high of the Carnegie Ridge. Variations in magnetic field strength are weak and of low values, amplitudes are of about 350 nT. Between 85,22° W and 85,24° W, a sharp distinct magnetic anomaly of about 400 nT can be observed. This well correlates to a fault observed in bathymetric data. The magnetic anomaly there may be linked to intruded magmatic rocks at the fault. Furthermore to the east (85,08 ° W and 85,2° W), two other magnetic anomalies are observed. They coincident with two seamounts as the detailed bathymetric map shows.
3. Southern Section (east of 85,02° W): The lowest magnetic field strength is observed in the southern part of the line. The magnetic anomalies are of about 400 nT and the corresponding half wavelength of the anomaly is about two kilometers. It does not correlate with sea floor topography, so the anomaly can be interpreted as resulting from a oceanic spreaded crust.

First Results – Magnetic Profile SO 159, S02

Profile S02 (figure 5.2.2) is orientated WNW-SES (roughly 3,08° S and 80,56° W to 2,61° S and 81,83° W) and crosses the Ecuadorian Slope and the Guayaquil basin (see seismic model of line S02, figure 5.3.2.17). Its overall length is about 150 km.
The magnetic field strengths range from about 29300 nT in the outermost east up to about 29800 nT in the outermost west. Due to air in the sensor, the data quality of the western section of profile P02 is noisy and exhibits only few details.

Variations in magnetic field intensity are very low. However, the intensity of the total field intensity is slightly increasing toward the west. Only in the western part of the magnetic section very few anomalies reaching amplitudes of 150 nT are observed. They coincident with the down going oceanic Nazca Plate. In the eastern part of the profile, no magnetic anomalies can be observed. This may be linked to the huge thickness of the sedimentary layer in the Guyaquil basin and the deep underthrusting oceanic crust.

First Results – Magnetic Profile SO 159, S03

Profile S03 (figure 5.2.3) is orientated SSW-NNE (roughly 3,08° S and 81,47° W to 2,54° S and 81,28° W) and strikes parallel to the Ecuadorian Margin (see seismic model of line S01, figure 5.####). Its overall length is about 62 km.
The magnetic field strength ranges from about 29400 nT in the outermost south up to about 29600 nT in the outermost north. The maximum field intensity is located to the north of the profile. There are almost no variations of magnetic field strength along the magnetic line. The profile appears very similar compared to the upper part of the perpendicular crossing profile S02.
The north of the profile is situated in a bathymetric higher position than the south, therefore the northern part of the profile is cutting the slope closer to the continent.

The geological interpretation is linked to the geometry of the subduction zone. At this place, the subducted plate appears in a deeper position as indicated from the refraction seismic model of this profile. Therefore, the magnetic influence of the oceanic crust on the overall magnetic field is less.

First Results – Magnetic Profile SO 159, S04

Profile S04 (figure 5.2.4) is situated parallel to the east of profile S03. It is orientated SSW-NNE (roughly 2,53° S and 81,03° W to 3,38° S and 81,28° W) and strikes parallel to the Ecuadorian Margin, too. Its overall length is about 100 km.
Profile S04 looks similar to profile S03. The magnetic field strength ranges from about 29300 nT in the outermost south up to about 29500 nT in the outermost north and is therefore about 100 nT less than on profile S03. The maximum field intensity is located to the north of the profile. As described on profile S03, there are almost no variations of magnetic field strength along the magnetic line. The profile appears very similar compared to the upper part of the perpendicular crossing profile S02, too.

First Results – Magnetic Profile SO 159, S05

Profile S05 (figure 5.2.5) is orientated SSE-NNW (roughly 0,83° S and 81,97° W to 1,00° N and 81,63° W) and crosses the eastern part of the Carnegie Ridge. Its overall length is about 223 km.
The magnetic field strength ranges from about 30300 nT in the outermost south up to about 31200 nT in the outermost north. The magnetic profile can be divided into three different subsections:

1. Southern Section (west of 81,90° W): The highest magnetic field strength is observed in the southern part of the line. Variations in magnetic anomalies are there of low amplitude, reaching up to 150 nT. These changes in magnetic field strength do not fit to bathymetry. Therefore it is supposed that a thick sedimentary layer is overlaying an irregular volcanic basement and obscure the clear shape of expected magnetic anomalies.
2. Central Section: This section corresponds to the bathymetric high of the eastern Carnegie Ridge. Variations in magnetic field strength are weak and of low but short frequent amplitudes ranging to about 100 nT. This western section of the Carnegie Ridge coincide with a rough volcanic topography. Its prolongation towards the north is dominated by a sharp faulted flank of the ridge which is only very few influencing the magnetic anomalies.
3. Northern Section (east of 81,76° W): The northern section comprises the bathymetric low of the profile. Between 81,80° W and 81,76° W, a distinct magnetic anomaly of about 600 nT can be observed. This well correlates to a volcanic horst like bloc detected on the bathymetry data. Further magnetic anomalies can be observed to the east of the volcanic block with amplitudes of about 250

nT. The coincident bathymetry is flat shaped. Therefore these magnetic anomalies are interpreted as oceanic spreaded crust; its corresponding half anomaly wavelength is about two kilometers. Possible therefore they are interpreted as spreading anomaly crust.

First Results – Magnetic Profile SO 159, S06

Profile S06 (figure 5.2.6) is orientated NW-SE (roughly 1,29° N and 79,29° W to 2,03° N and 80,16° W) and strikes orthogonal to the Ecuadorian/ Colombian Margin. Its overall length is about 127 km.
The magnetic field strength ranges from about 31500 nT in the outermost west up to about 31000 nT in the outermost east. The maximum field intensity is located in the west of the profile. Variations in magnetic anomaly almost not exist, neither in the oceanic basin nor on the continental slope.
The homogeneous appearance of the magnetic field on the upper slope may be linked to the huge sedimentary thickness of the sedimentary basin and a very homogeneous magnetic continental crust.

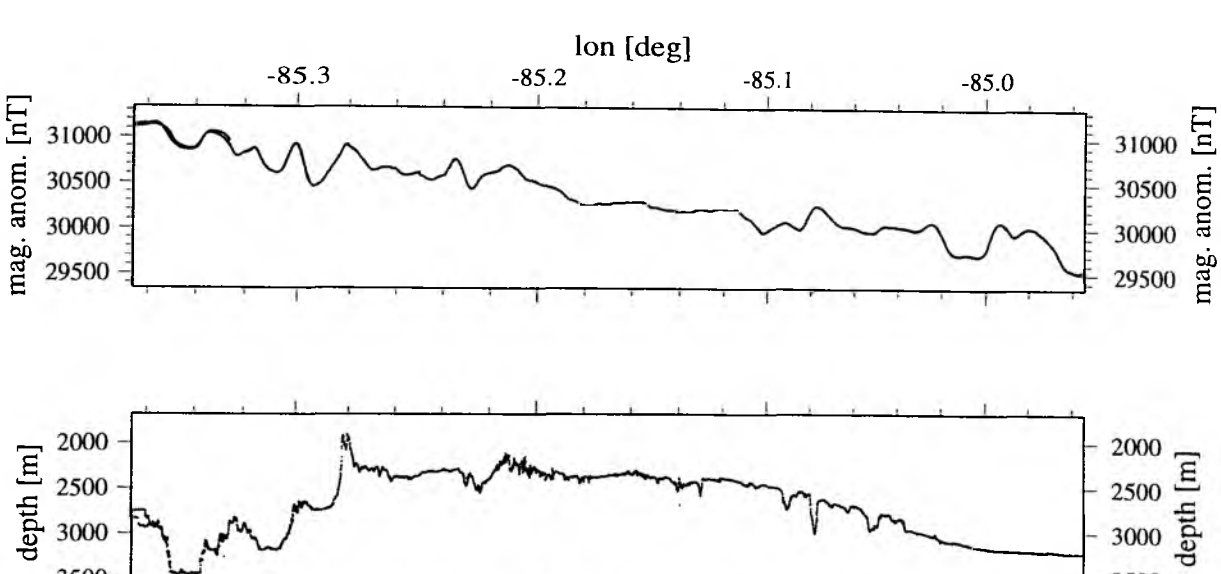

SO159 Profile 01

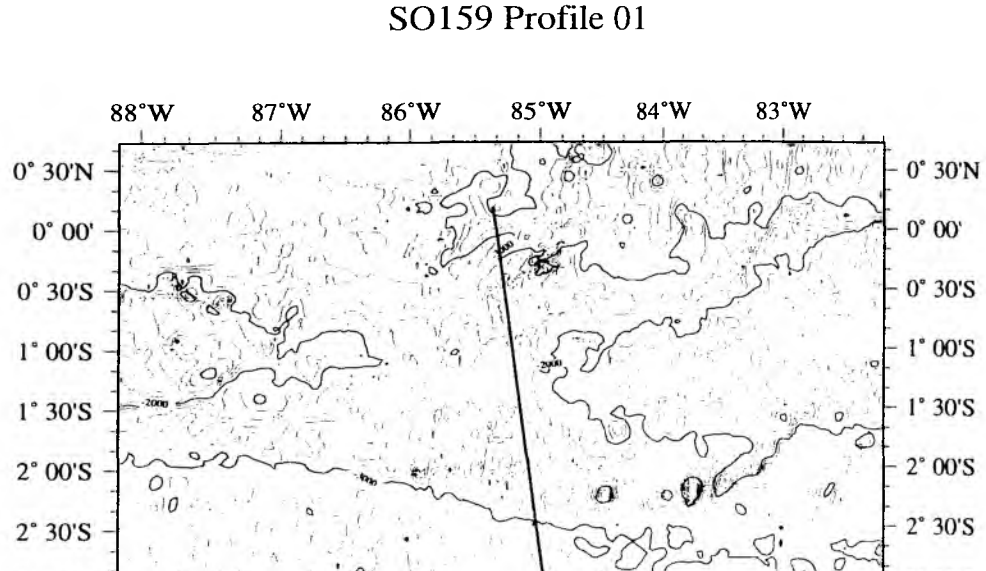

Figure 5.2.1 :
Magnetic field strength, bathymetry and track line SO159 Profile 01. The data was acquired twice from the end of the profile to 85°32 when returning to recover the deployed OBH/S after shooting the profile.

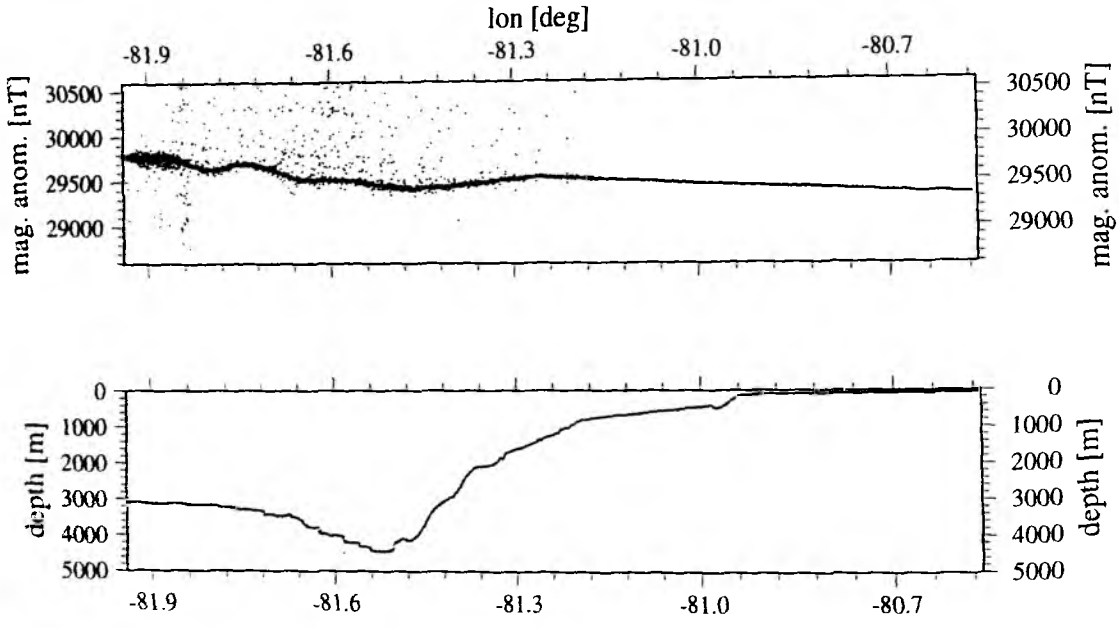

SO159 Profile 02

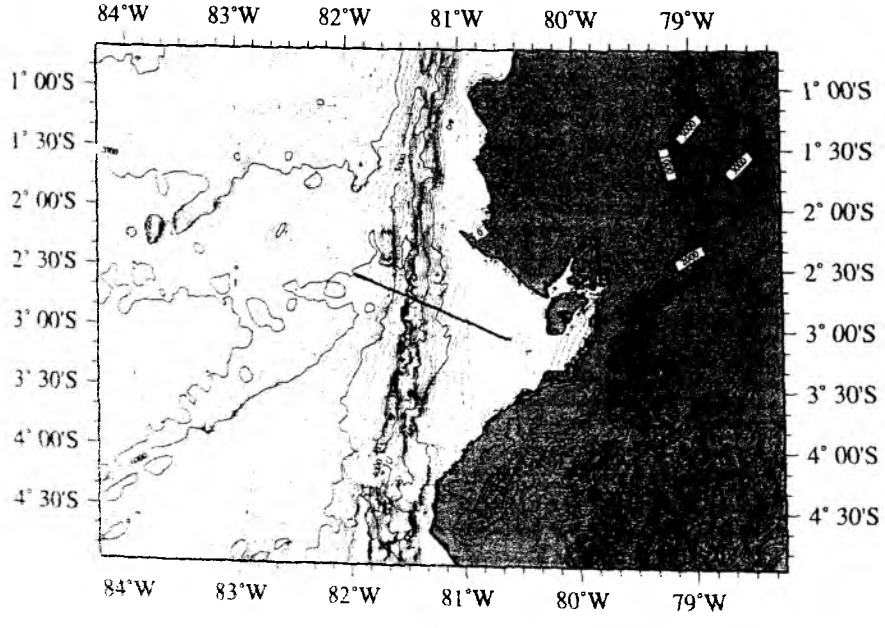

Figure 5.2.2 :
Magnetic field strength, bathymetry and track line SO159 Profile 02.

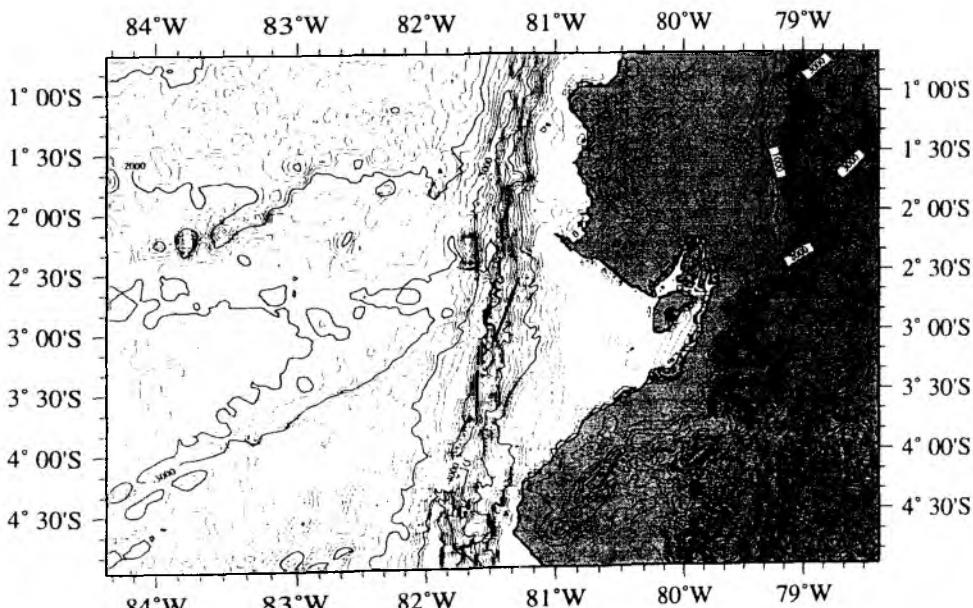

Figure 5.2.3 :
Magnetic field strength, bathymetry and track line SO159 Profile 03.

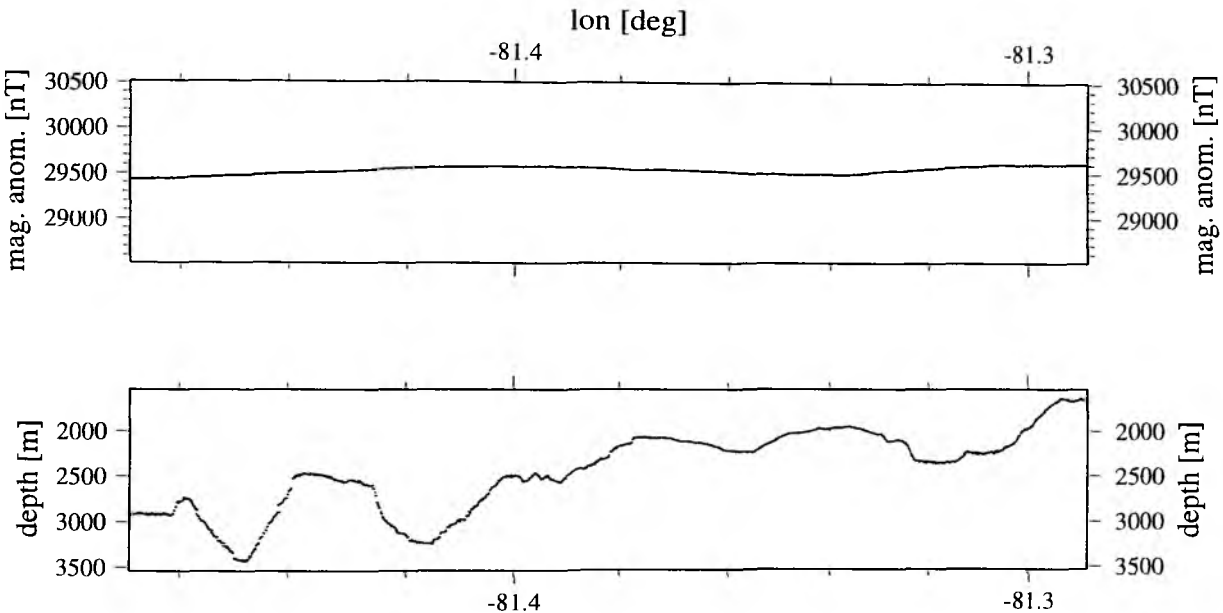
lon [deg]
-81.4
-81.3
mag. anom. [nT]
30500
30000
29500
29000
depth [m]
2000
2500
3000
3500

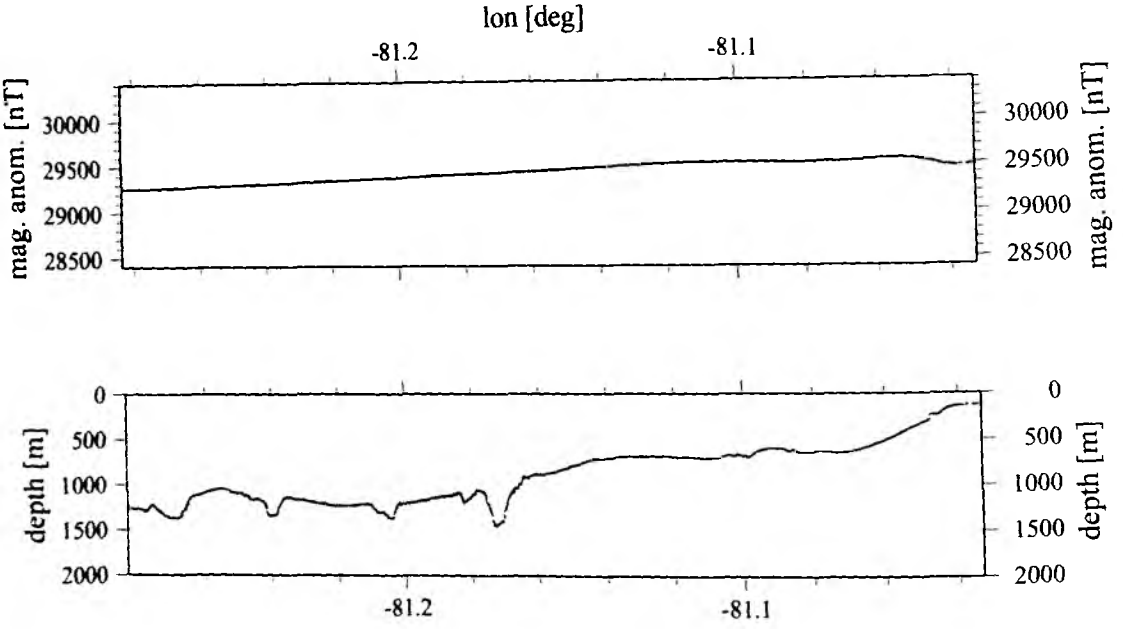

SO159 Profile 04

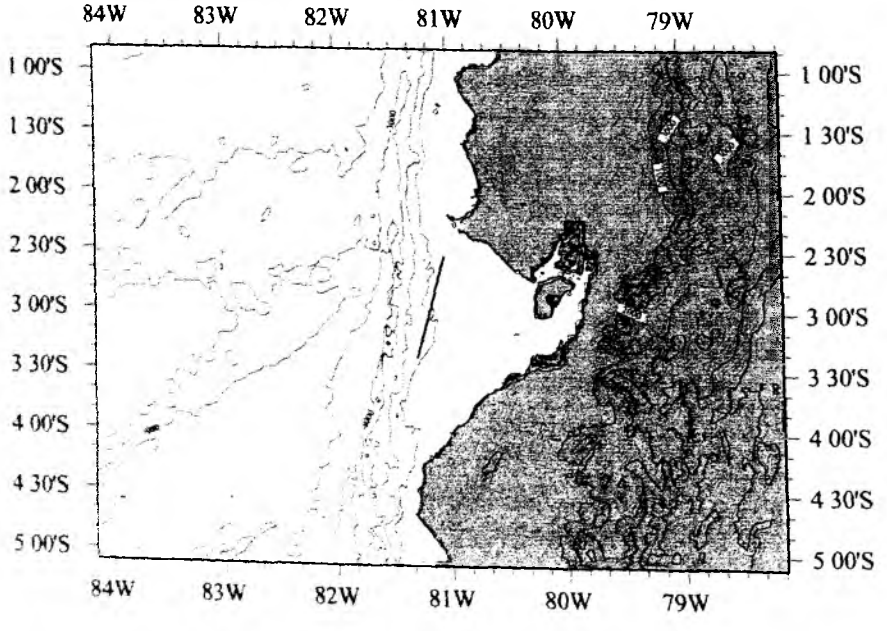

Figure 5.2.4 :

Magnetic field strength, bathymetry and track line SO159 Profile 04.

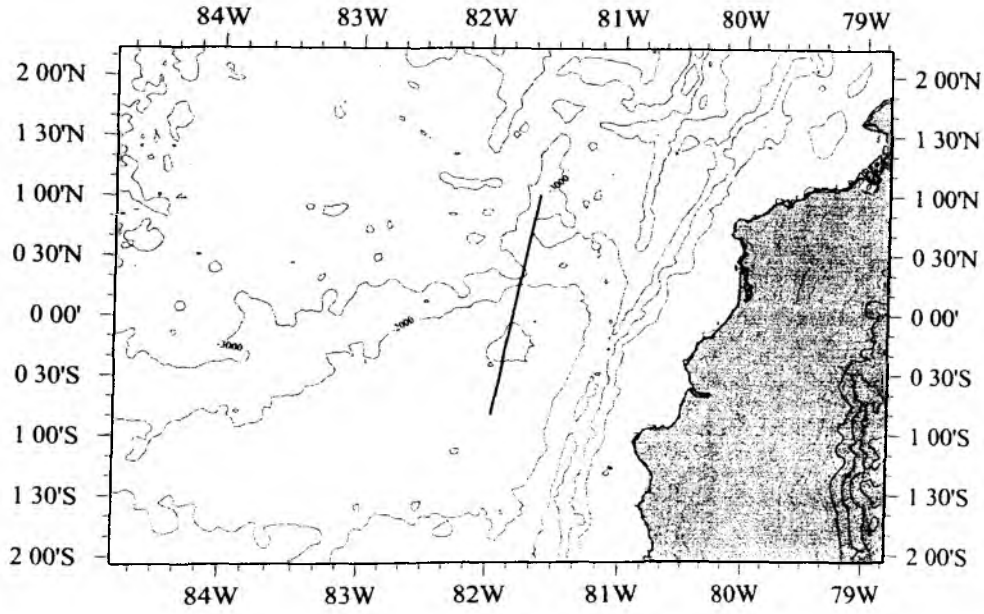

Figure 5.2.5 :
Magnetic field strength, bathymetry and track line SO159 Profile 05.

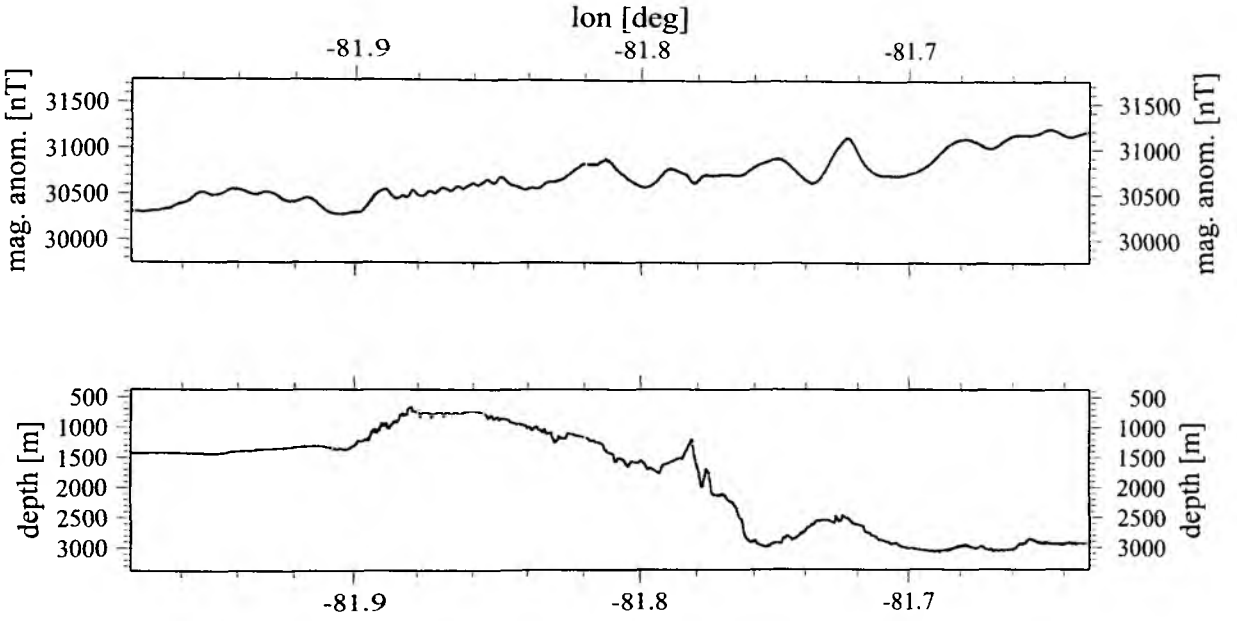
lon [deg]
-81.9
-81.8
-81.7
mag. anom. [nT]
31500
31000
30500
30000
depth [m]
500
1000
1500
2000
2500
3000

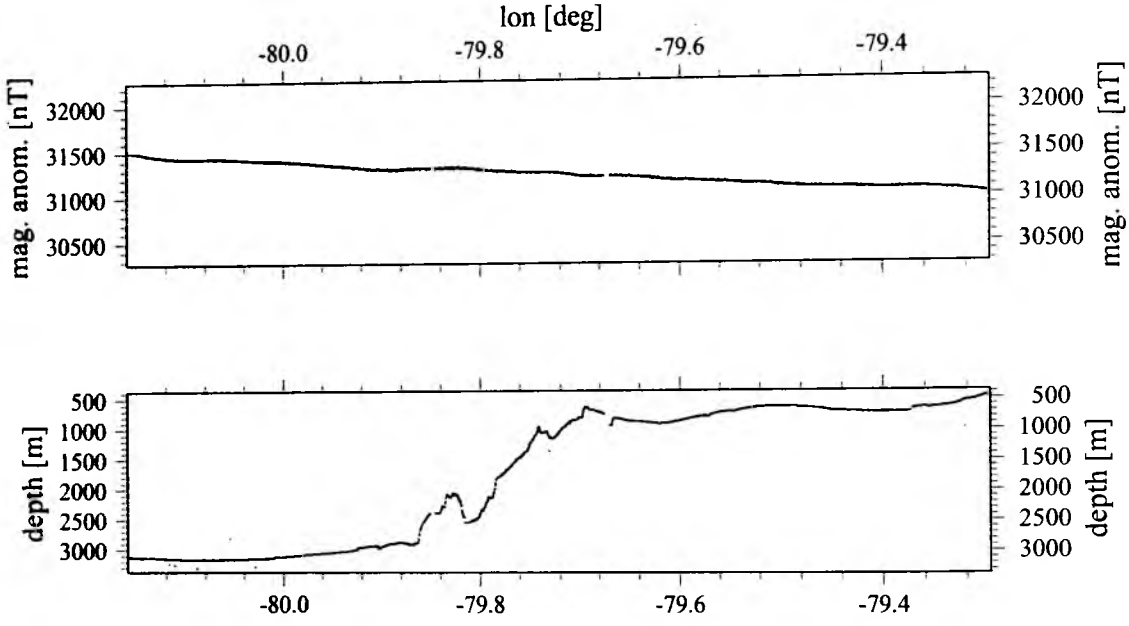

SO159 Profile 06

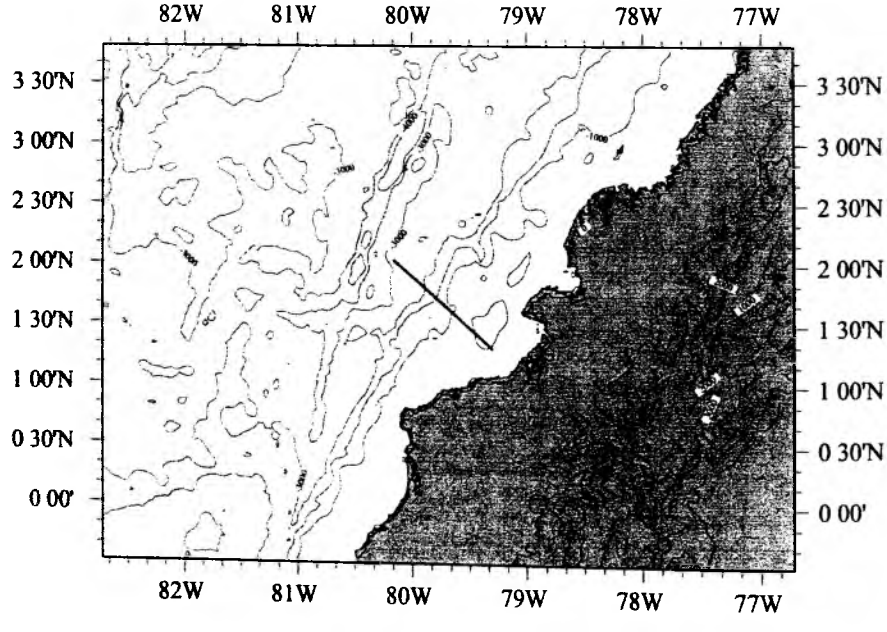

Figure 5.2.6 :

Magnetic field strength, bathymetry and track line SO159 Profile 06.

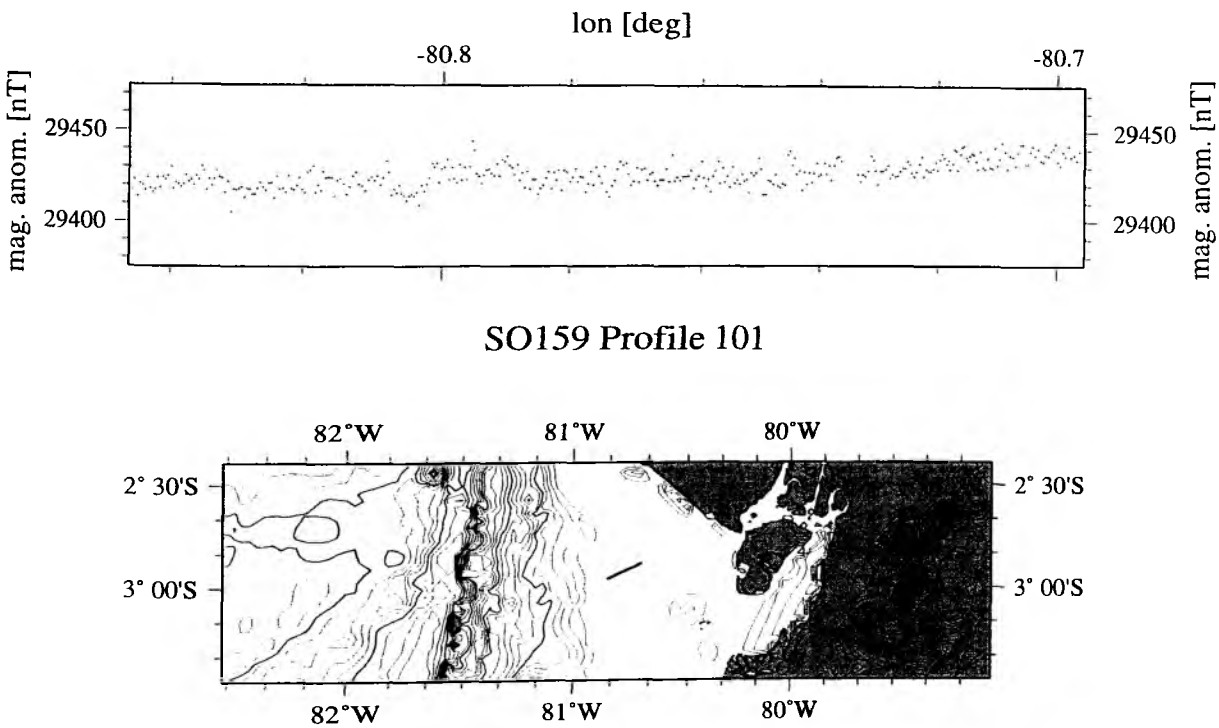

Figure 5.2.7 :
Magnetic anomaly and track line SO159 Profile 101.

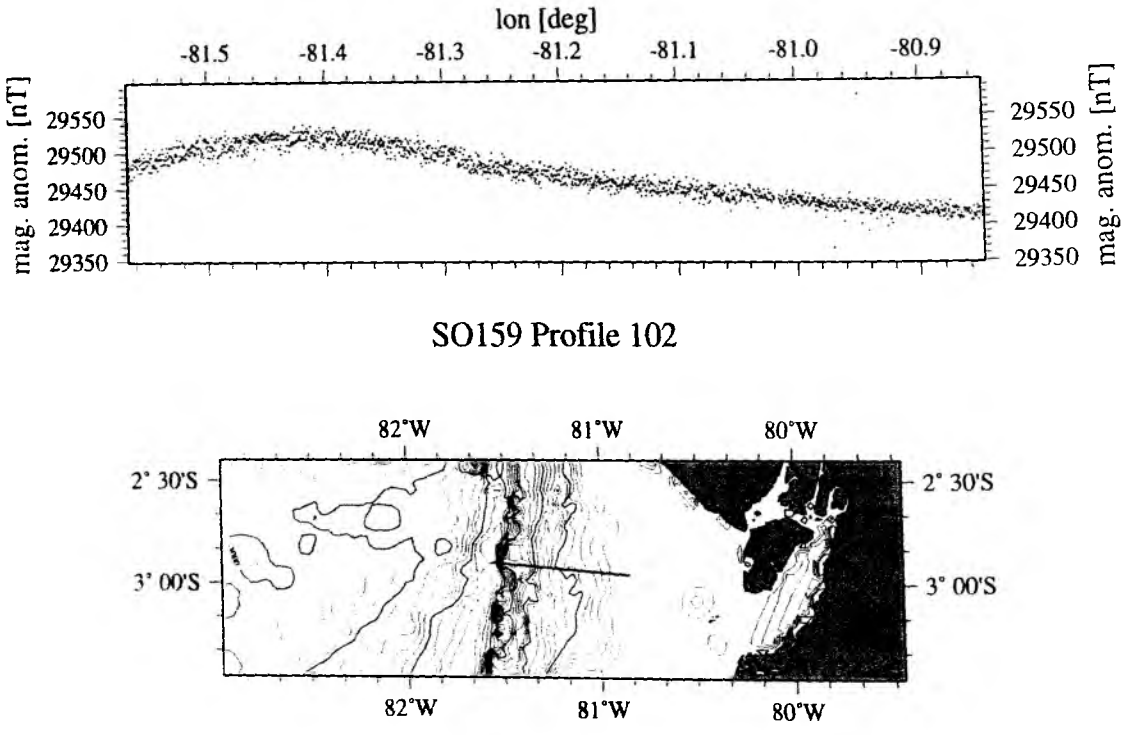

Figure 5.2.8 :
Magnetic anomaly and track line SO159 Profile 102.

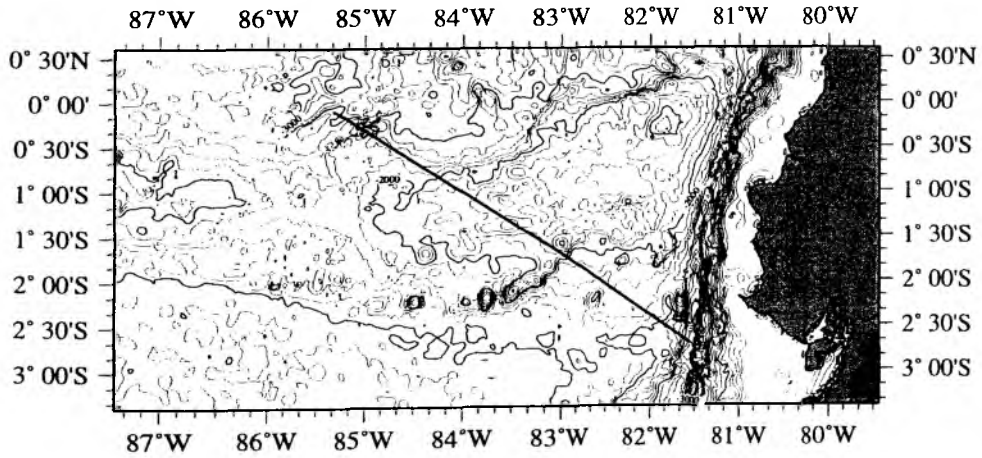

Figure 5.2.9 :
Magnetic anomaly, bathymetrie and track line SO159 Profile 103.

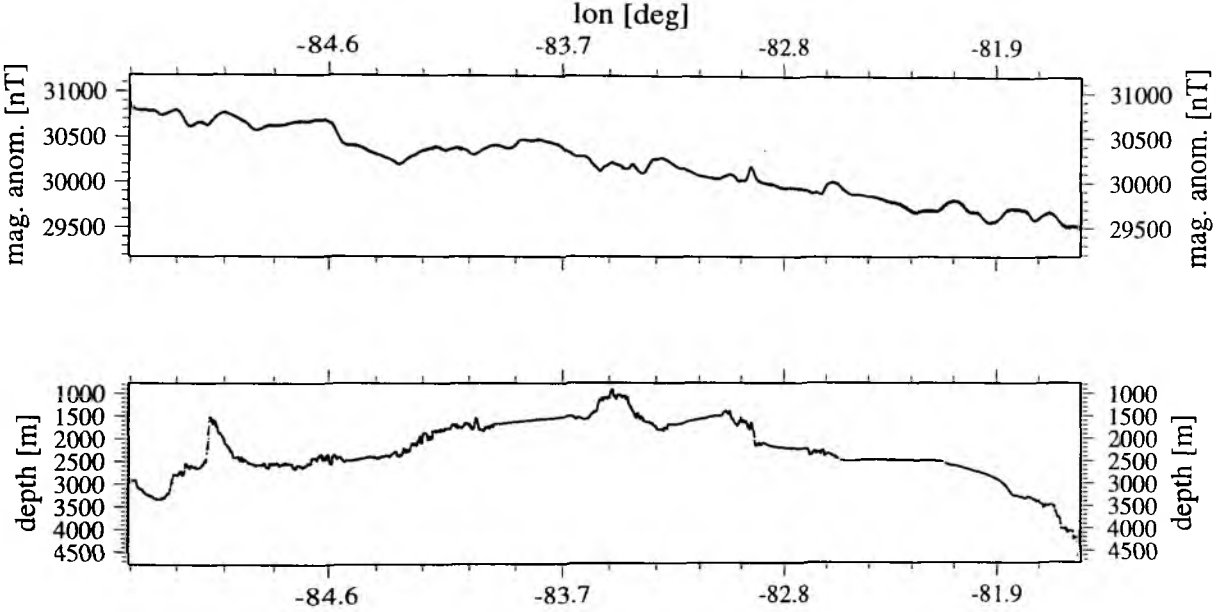

SO159 Profile 103

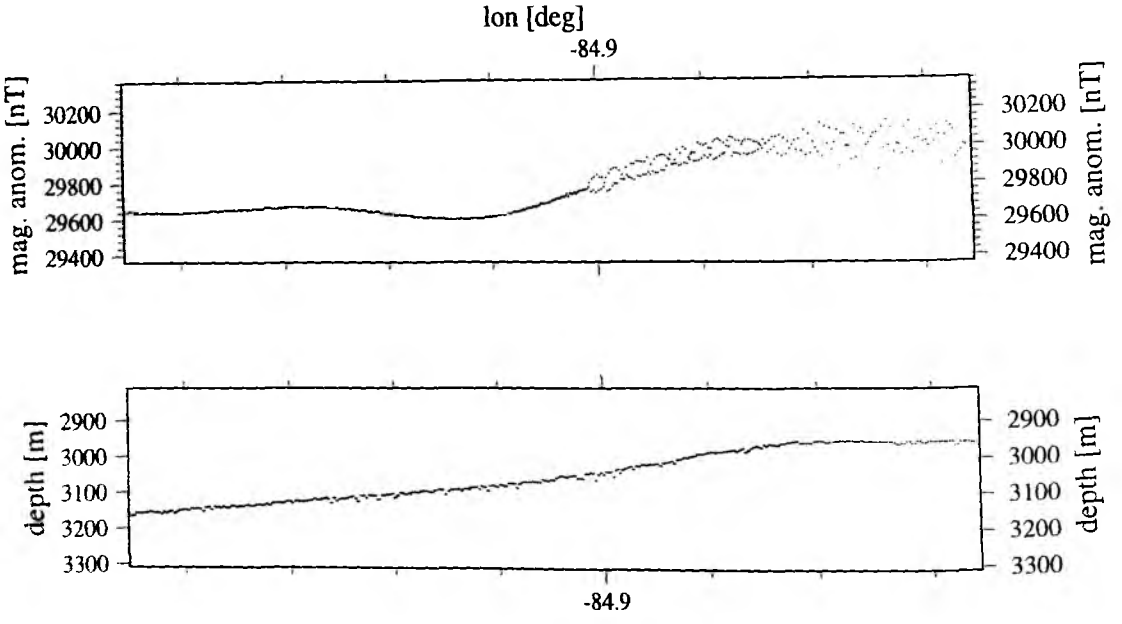

SO159 Profile 105

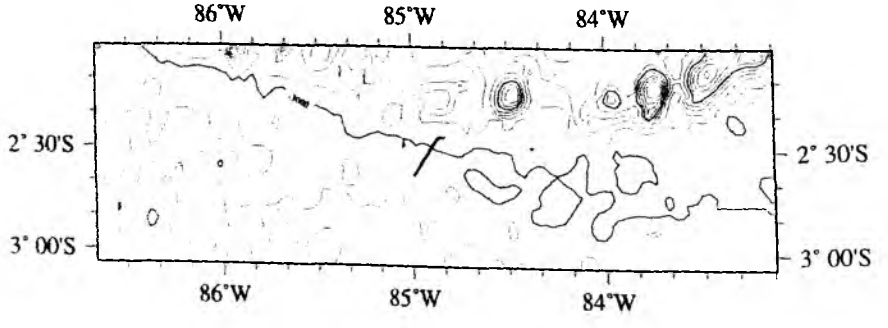

Figure 5.2.10 :

Magnetic anomaly, bathymetrie and track line SO159 Profile 105.

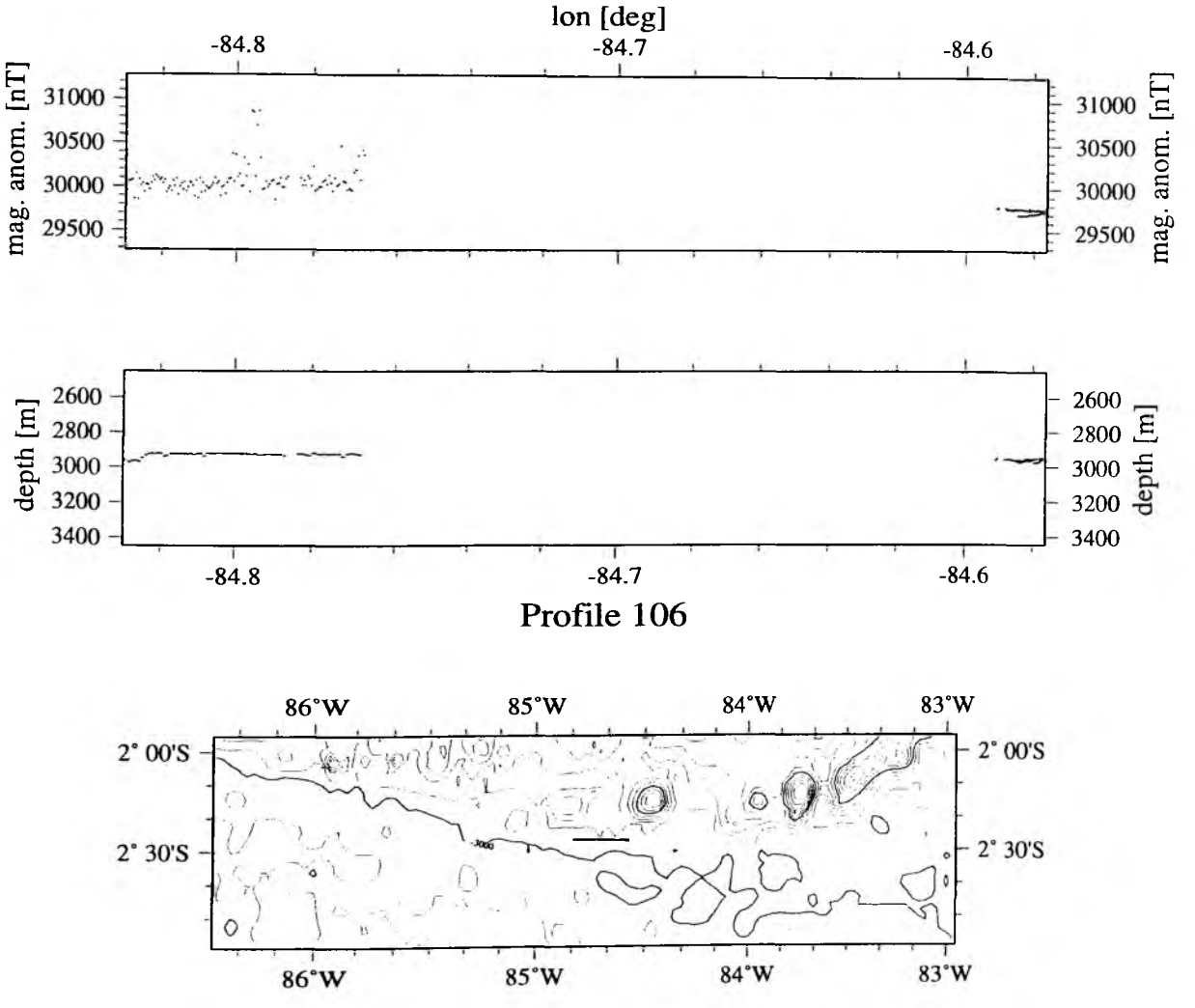

Figure 5.2.11 :
Magnetic anomaly, bathymetry and track line Profile 106.
Data gap due to maintainance of magnetometer.

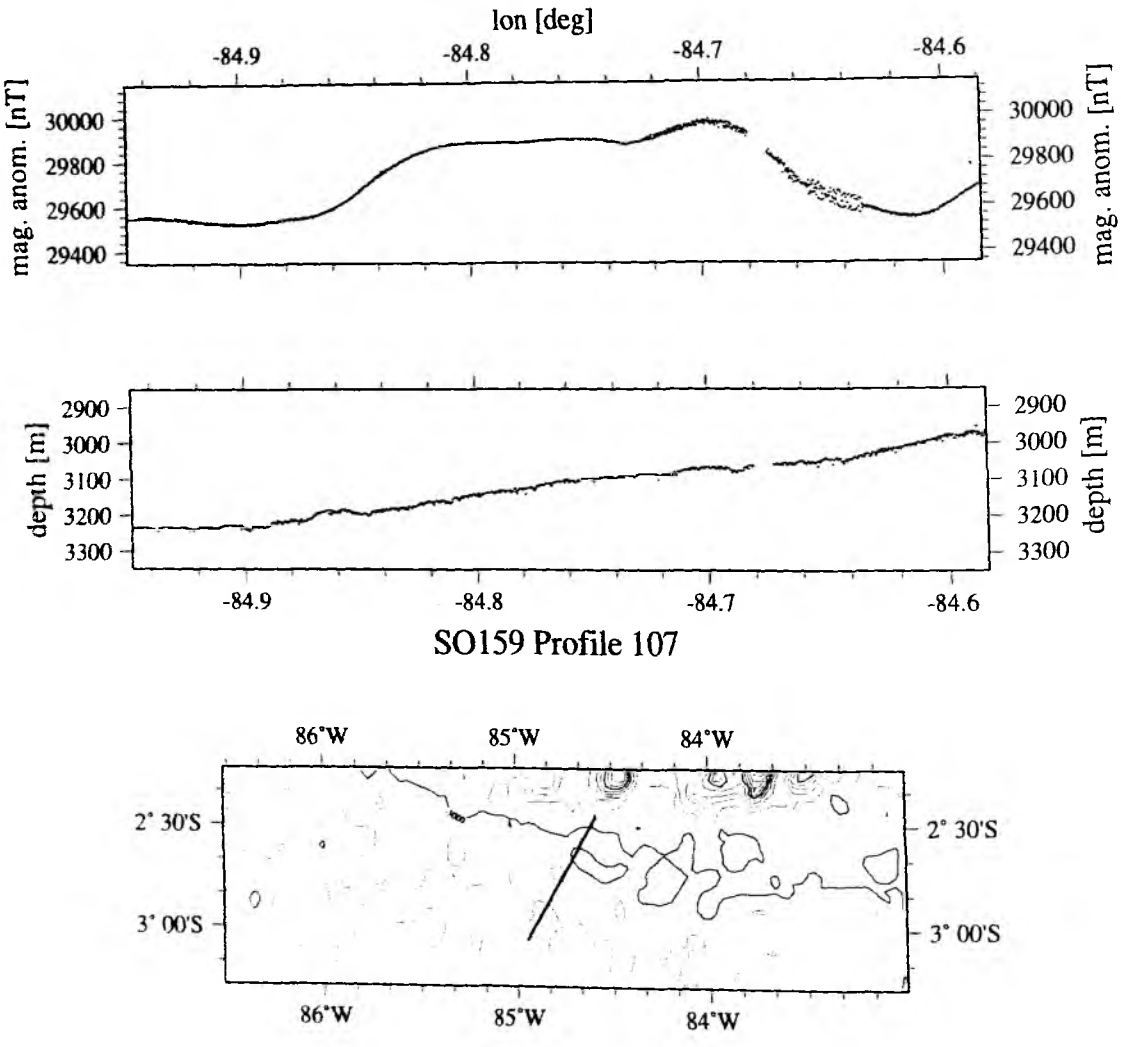

Figure 5.2.12 :

Magnetic anomaly, bathymetrie and track line SO159 Profile 107.

5.3 Wide angle Seismics

5.3.1 Profile SO 159-01

(C. Walther, V. Sallarès, A. Berhorst)

Profile 01 crosses the Carnegie Ridge in a location where it is bathymetrically least pronounced. In total 37 OBH/S where deployed at 4.5 nm intervalls on 25. August. The location of the profile and deployment sites are shown in Figure 5.3.1.1. Shooting along this 190 nm long profile was made at 4.5 kn, with two airguns deployed and operational without any major disruption. Unfortunately, the streamer was badly damaged after a few hours and could not be repaired onboard. The data recorded by the streamer are shown in Figure 5.3.1.2.

Recovery of the instruments was made on August 28/29, but three instruments could not be recovered. Even at their preprogrammed release time the instruments did not surface. A few other instruments had recording failures (see Appendix II-1), which reduced the number of successful record to 30. These record sections are shown in Figures 5.3.1.3 to 5.3.1.32.

The quality of the record sections is generally quite good, showing energy propagation of first arrivals (Pg waves) and Moho reflections (PmP) in excess of 100 km. A preliminary interpretation of this dastaset was attempted at sea.

Model description from 2-D forward modeling

A preliminary model of the crustal velocity structure of the this profile is presented in Figure 5.3.1.33 and reveals the following features.

Hemipelagic sediment. No sediment phase can be observed in the record sections due to a low velocity and thickness. No MCS data are available nor any streamer data for most of the profile. The only constraints for the sediment thickness come from the near offset onset of the first refracted waves from the uppermost basement and the apparently low velocity, which does not stand out against the water wave and is modeled with 1.6 to 1.8 km/s. The modeled thickness of the sediment does not exceed 1 km. It has mainly accummulated at the outer flanks of the Carnegie Ridge, even in the NNW part, where topography is rough and partly shallower. The central ridge is almost bare of sediment.

Oceanic crust. The first arrivals preceding the water wave belong to a refraction travelling through the uppermost oceanic crust. They form the beginning of the most prominent phase Pg, which lasts till 60 to 80 km offset. The bending of this branch appears to be discontinuous on most OBH/S, showing two or three distinct parts of different increasing apparent velocities, but some OBH/S, especially between OBH/S 18 and 22, show only one single traveltime branch bending almost continuously.

The highly increasing velocities in the near offset range of the Pg-phase are reflected in the model by an upper crustal layer, oceanic layer-2. Velocities in the upper part lie around 4.7 km/s and increase to 5.4 to 5.7 km/s in the lower part. This is well in the range of typical values for oceanic basalts. Between OBH/S 14 and 19 higher velocities of 5.8 km/s are encountered in the lower part of this layer, but are still in the range of basaltic lithology. The upper crustal thickness varies between 1 and 2 km in the outer parts of the Carnegie Ridge, which is normal compared to global compilations of oceanic crust. The thickness of this layer increases considerably towards the ridge center between OBH/S 08 and 35, where it is more than doubled and reaches 4 km.

The far offset part of the phase Pg appears to be only slightly bended and emerges in the model from a lower crustal layer, oceanic layer-3. Upper velocities of this crustal unit range on average from 6.5 to 6.75 km/s, with a remarkable increase to 6.9 to 7.0 km/s in the SSE part of the model. The resulting velocity contrast between upper and lower crust may be too strong in the model compared to the observed reflectivity and should be more gradually modelled including a transition zone. Lower crustal velocities range from 6.8 km/s in the NNW outer ridge to 7.2 to 7.3 km/s in the central part at about 12 km depth and reach 7.45 km/s in the deepest crustal part below OBH 16 in 18 km depth. All these velocities and the low gradient $< 0.1\ s^{-1}$ are typical for a normal gabbroic or olivine gabbroic composition of the lower crust. The thickness of this edifice steadily increases from 3.5 km in the outer ridge to almost 8 km below OBH 10 and OBH 20. Between these two OBH an additional bulge is observed, where the crust mantle bounary (MOHO) further drops to 18 km depth and the maximal lower crustal thichness is reached with 12 km.

Crust-mantle boundary and uppermost mantle. The far offset end of the Pg-phase merges asymptotically with a strong reflection, PmP, from the crust-mantle boundary (OBH 14, 24 and 26 are excellent examples). These OBH also emphasize that there appears to be no refraction, Pn, travelling through the uppermost mantle, at least in the central ridge area. In the outer ridge parts, on OBH/S 01, 03, 06 and 08 to NNW and on OBH 36 and 37 to SSE, a weak phase with high apparent velocity of about 8 km/s may be interpreted as Pn and can be modeled with an uppermost mantle velocity of 7.8 km/s and a low gradient. Due to the pronounced PmP but missing Pn in the central ridge area, a strong velocity contrast at the MOHO and a negative velocity gradient in the uppermost mantle is infered.

These preliminary results will surely be altered and more reliably modeled in the future, but what will certainly remain and is a clear result of the first modeling, is the huge thickened crust of the Carnegie Ridge, which reaches almost 16 km, and the close resemblance of its velocity structure to other hotspot related ridges formed in an on- or near-axis condition, especially the Cocos Ridge [Walther, submitted].

2-D inverse modelling

Inverse modelling using a simultaneous refraction/reflection traveltime inversion code was also attempted on board. Outcomes were satisfactory, but unfortunatelly no figures of the models are available due to the occurence of unrecoverable hard disk problems in the workstation.

In any case, four different inversions were done with the data from this profile. In the first one we only used the Pg and PmP phases from the German instruments (16 stations, basically even numbers in Figure 5.3.1.1), and in the second one we used the same phases from the French OBS only (14 stations, odd numbers in Figure 5.3.1.1). These phases were picked by three different persons using two different codes (Plotsegy for French data and Zplot for German data), and thus both data sets are completely independent. However, the results from these two inversions are extremely similar, showing the same velocity anomalies ($\Delta v \leq 0.15$ km/s), especially at mid-lower crustal levels, and a very similar Moho geometry along the whole model ($\Delta z \leq 1$ km). At upper crustal levels we found several local discrepances ($\Delta v \sim 0.25$ km/s) basically due to the uneven sampling of this layer from each data set alone. These results indicate that, without any doubt, both data sets are compatible, which means that they contain a self-consistent velocity-depth information.

The third and fourth inversions were done using the full set of OBS and OBH , and they confirmed the results of the first two inversions. In the third one, we used only first arrivals to estimate the velocity field. Due to the good coverage of first arrivals up to great distances from receivers (> 100 km), the velocity information is well constrained up to lower crustal levels from this phase alone. Hence, the trade-off between lower crustal velocities and Moho depth for PmP traveltime inversion is confirmed to be small. Therefore, a fourth inversion with the complete data set was performed (Pg and PmP), showing the next results: the maximum crustal thickness is ~15 km in the central part of the ridge, gently thinning towards the Southern end of the profile. In this point the crustal thickness reaches 8-9 km. In the Northern end the transition is sharper, and crustal thickness seems to be only 5-6 km. This is in agreement with the observations from multibeam bathymetry in the same profile, which indicate the possible existence of a rifted segment in the Northern flank of the ridge. Upper crustal thickness (Sediments + Layer 2) is quite uniform along most of the profile, but shows a pronounced thinning in the rifted flank. Averaged Layer 3 velocities are lower in the most thickened part of the profile (up to ~ 6.8 km/s) than in the more normal Southern half (~ 7.0 km/s).

Note the close similarity of these results with those obtained in Malpelo and Cocos Ridges with data from the former Paganini cruise (Figure 1.5).

MCS data

An approximately 65 km long multi channel seismisc (MCS) section was acquired before the mini streamer broke. Due to an intresting bathymetrical feature, the "curved hook shaped depressions", an enhanced processing was performed on this final dataset of the streamer. The seismic traces were high-pass frequency filtered with a 0-3 Hz Kaiser filter to remove a DC shift. Channel 3 recorded a much greater dynamic range than channel 2, while the first channel showed only noise. Large amplitude noise at identical travel-times but different polarity in channel 2 and 3 was completely removed by stacking. These suspicious events were probably a first sign of the later short circuit.

Some bad traces were replaced by a dip-dependent trace interpolation. A static correction because of swell and shot time uncertainties was introduced where necessary. To improve the temporal resolution of the seismic data, a roll-along deconvolution which uses autocorrelograms averaged over a number of traces is applied to compress the basic seismic wavelet. To account for the variable amplitude spectra of the seismic traces, the deconvolution operator was calculated for several timegates and applied individually. The overall deconvolved trace results from a weighted merging of the independently deconvolved gates. After deconvolution a time-variant Ormsby frequency filter with minimum delay characteristics was applied to enhance the signal-to-noise ration. Additionally a notch filter of 49-51 Hz was used for some traces to remove electronic noise. Prior to time migration, the CMP distance was reduced from 137 m to 34 m by a dip-dependent trace interpolation, to minimize aliasing effects. The energy loss due to geometrical spreading was compensated by a spherical divergence correction. A finite difference time migration was used to enhance the spacial resolution. Finaly the interpolated traces were removed and an automatic-gain-control was applied to improve the visualisation.

The 65 km long MCS profile (Fig. 5.3.1.2) has registrated the first part of the airgun-shots of the refraction profile 01. It is situated on the normal oceanic crust in a water depth of 3150 m up to the southern flank of the Carnegie Ridge with a depth of 2900 m. The bathymetry reveals that the northern part of the profile is situated in a curved hook shaped depression about 5.5 km wide, 150 m deep and more then 20 km long, wrapped around the base of a seamount (see chp. 5.1.2). The seismic section shows well stratified sediments overlying a strong reflective bumpy basement. Structures in the basement are masked by noise, possibly due to peg-leg multiples from within the sediments, side scatterer from the rough basement and the refraction of the seismic waves along the irregular basement topography with a strong velocity contrast from about 1.8 km/s in the sediments to 4.7 km/s (from forward modeling) in the upper basement. Therefore no clear reflections can be imaged in the basement. The thickness of the sediments varies from 320 m in the south to about 520 m in the north for an assumed velocity of 1.75 km/s. The lower part of the sedimentary column, up to a well visible discontinuity (marked with arrows on Fig. 5.3.1.2) has a relative uniform thickness and a parallel layering. Only the very northern part of this unit shows a lack of stratification. For the sediments above the unconformity, only the sediments on the southern half of the profile have a similar thickness, while the sedimentary column on the northern side increases continuously. Below OBH37 several reflectors are pinching out from the discontinuity, forming a triangle shaped sedimentary body towards the north, where they are terminated by a northward dipping reflector which creates a depression structure below OBS33. A local high between OBH35 and OBS33 is related to a NW to SE trending 20 m high step in the bathymetry.

The observations suggest an undisturbed sedimentary deposit before reaching the unconformity. Afterwards an additional sediment supply from the Carnegie Ridge thickens the sediments towards the north. On this profile, the sedimentary layer in the curved hook shaped depression (between OBH35 and OBS33) is thicker than on the adjacent oceanic plate. This observation did not fit with the interpretation of these features as curved valleys which are carved by the scouring action of deep sea currents eroding the sedimentary cover on the seafloor around the volcanic edifices (see chp. 5.1.2). This remark is limited by the fact, that the MCS profile is quite short and it is well visible that the sedimentary history in this northern part of the profile is fare more complex then in the southern half.

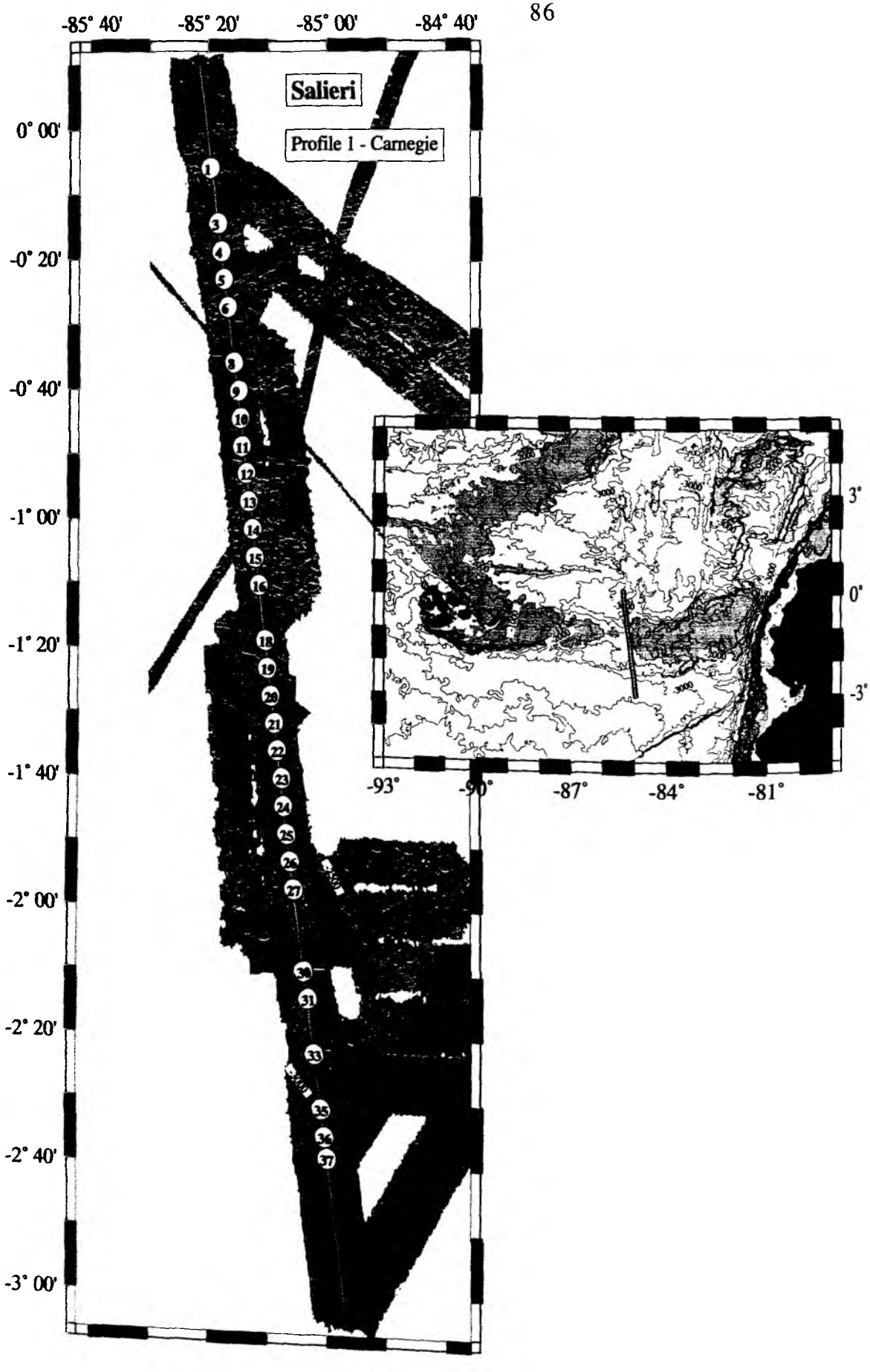

Figure 5.3.1.1. Location map and OBS/OBH locations for Profile SO 159 - P01

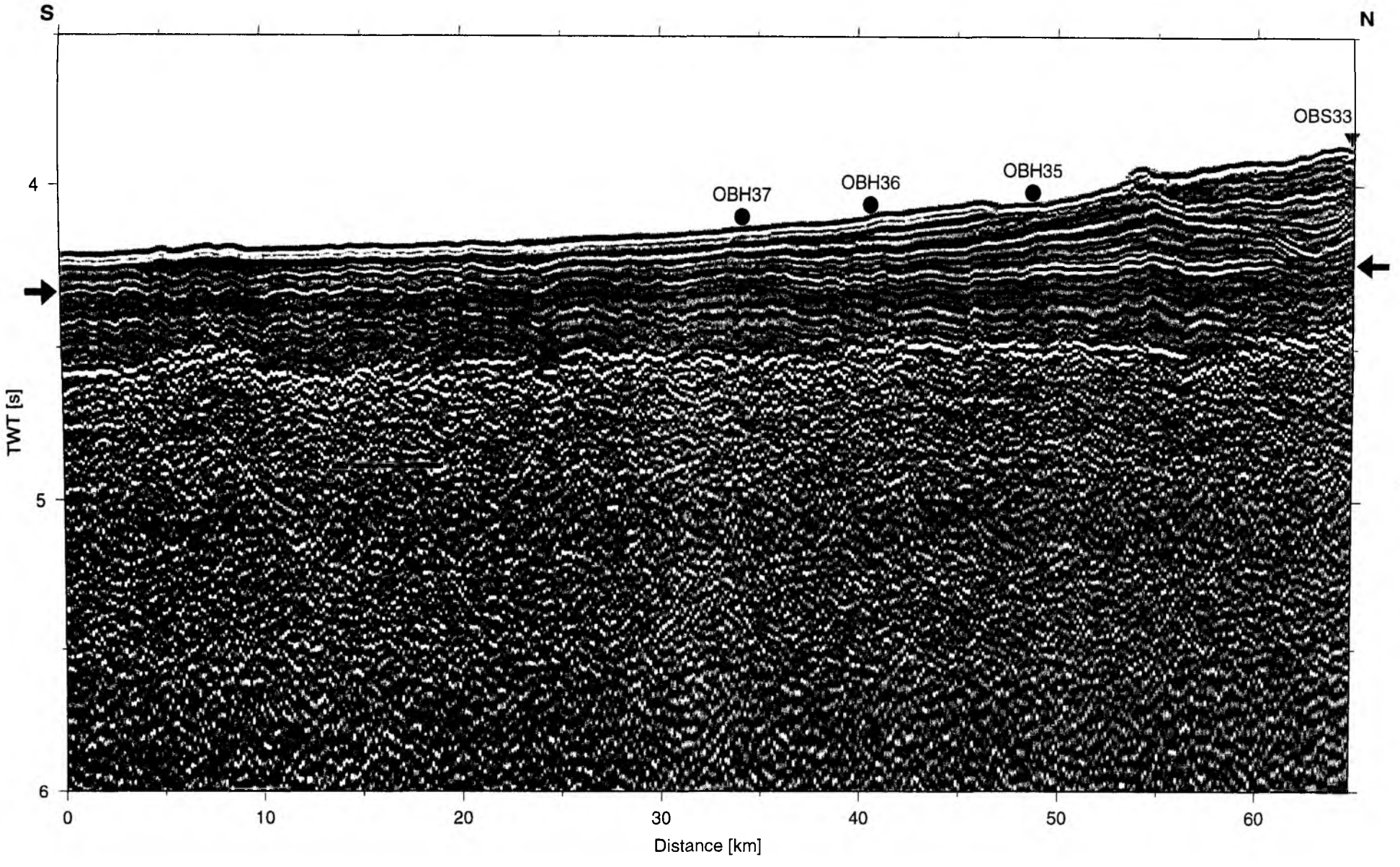

Figure 5.3.1.2: Time migration of MCS Profile 01. A discordant reflector is marked by arrows.

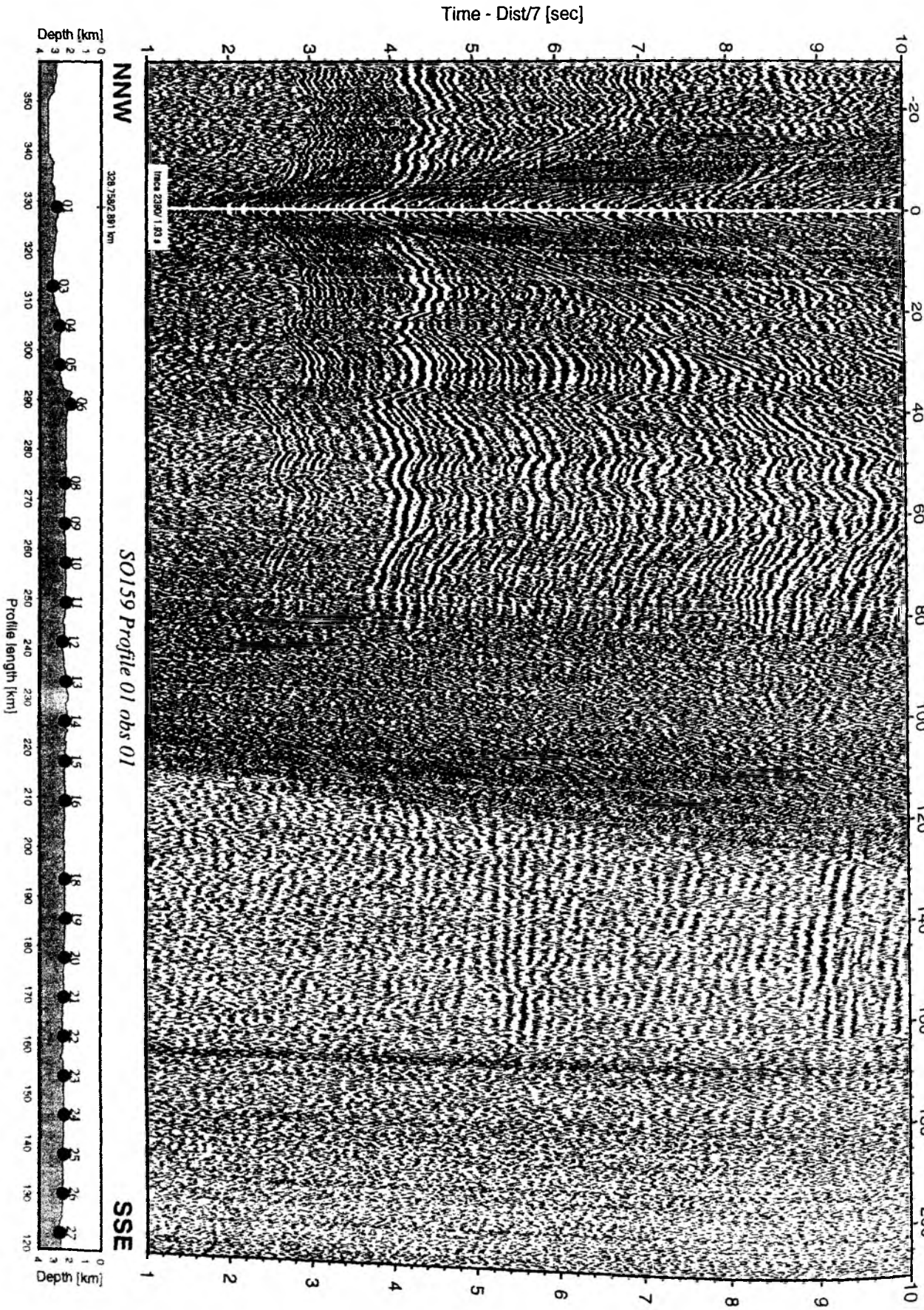

Figure 5.5.1.3: Record section from obs 01 vertical component, Profile 01.

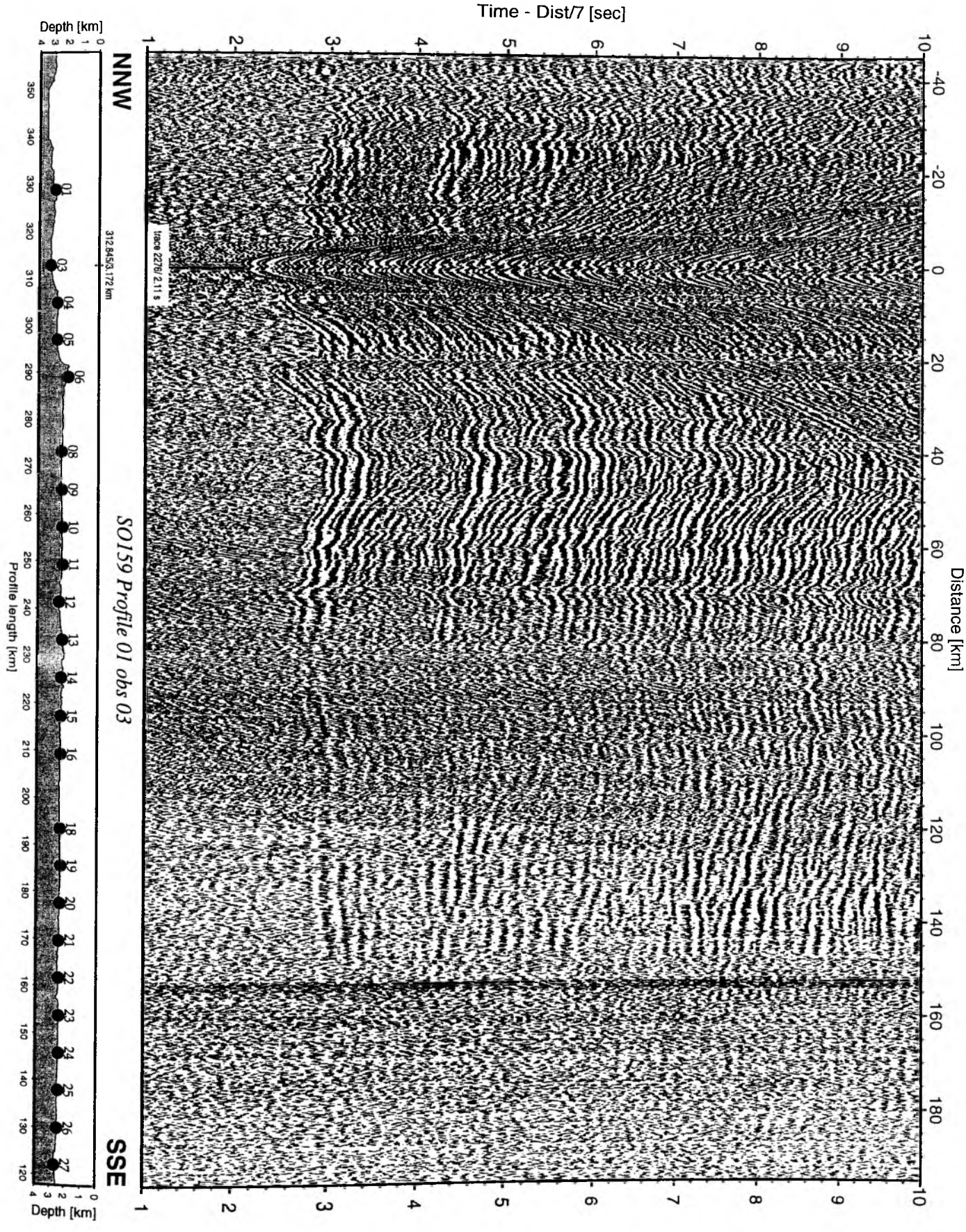

Figure 5.5.1.4: Record section from obs 03 vertical component, Profile 01.

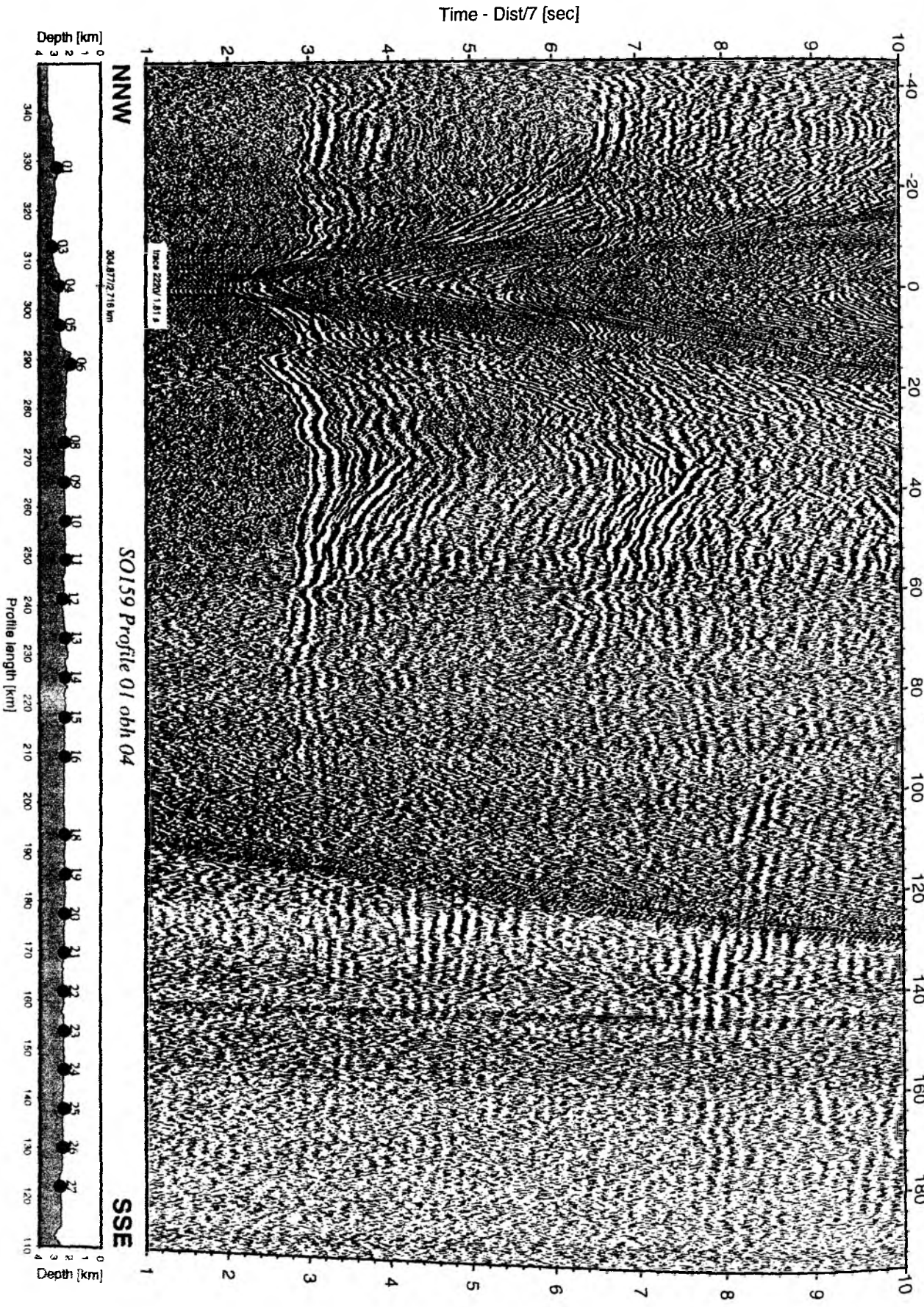

Figure 5.5.1.5: Record section from obh 04 , Profile 01.

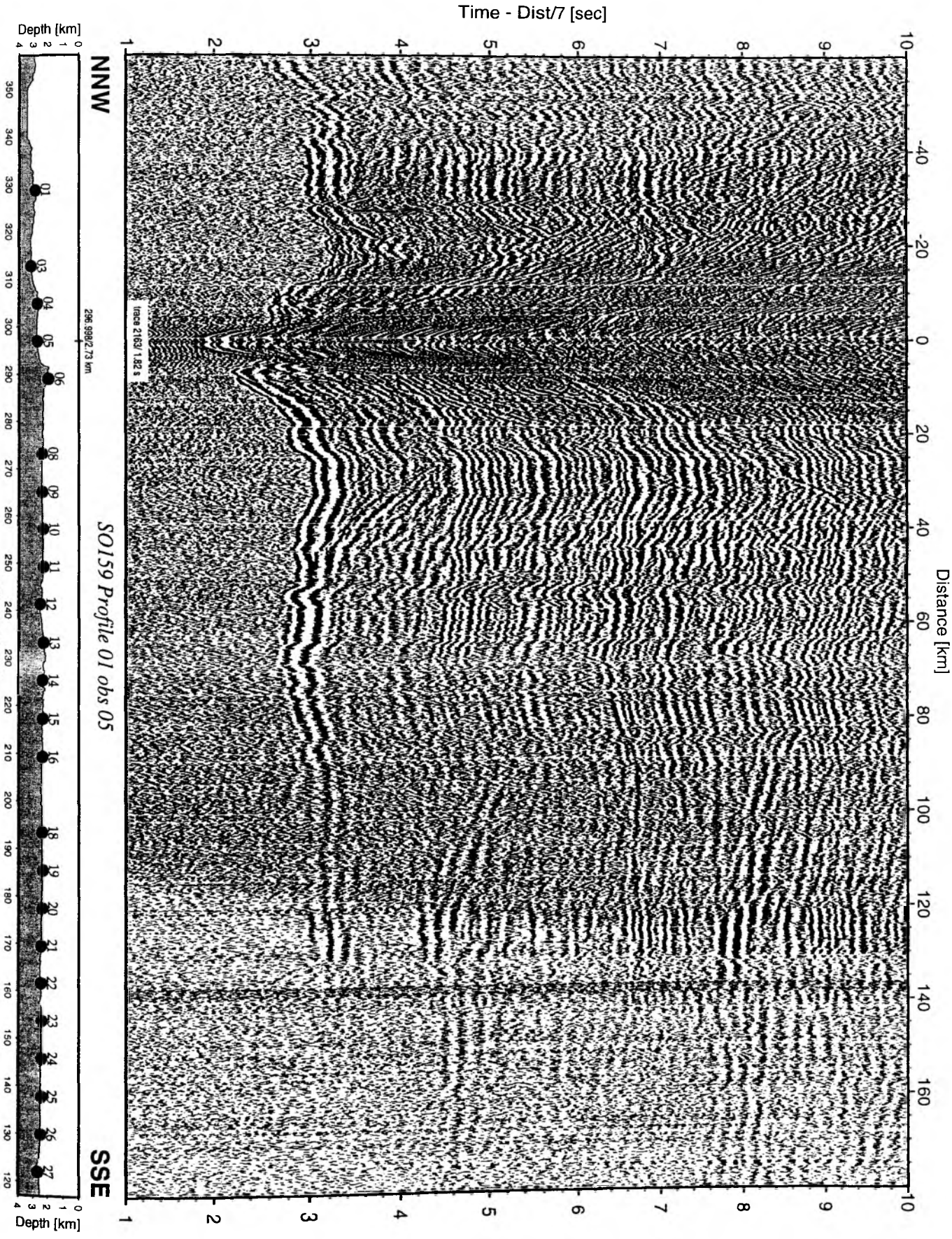

Figure 5.5.1.6: Record section from obs 05 vertical component, Profile 01.

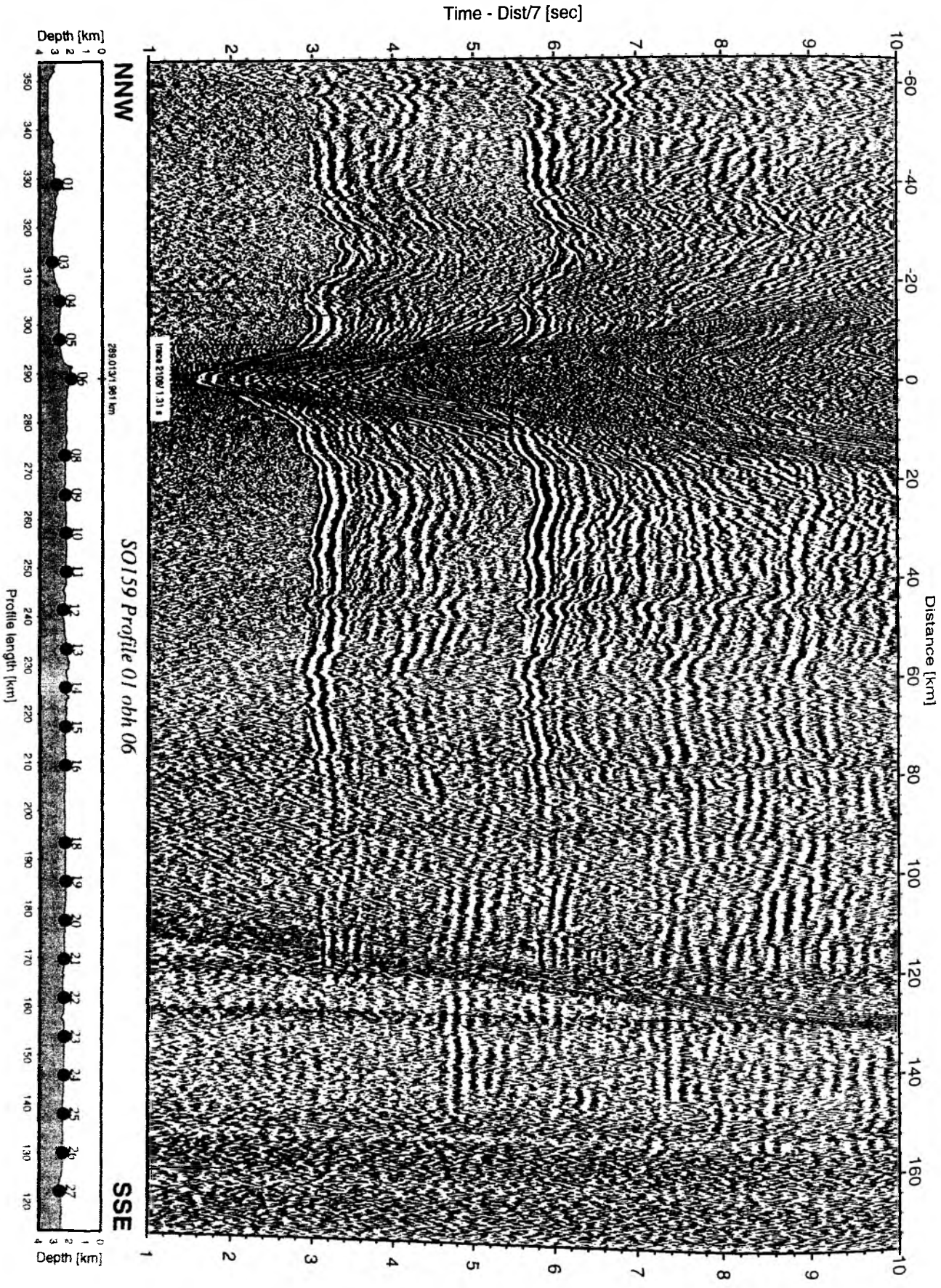

Figure 5.5.1.7: Record section from obh 06 , Profile 01.

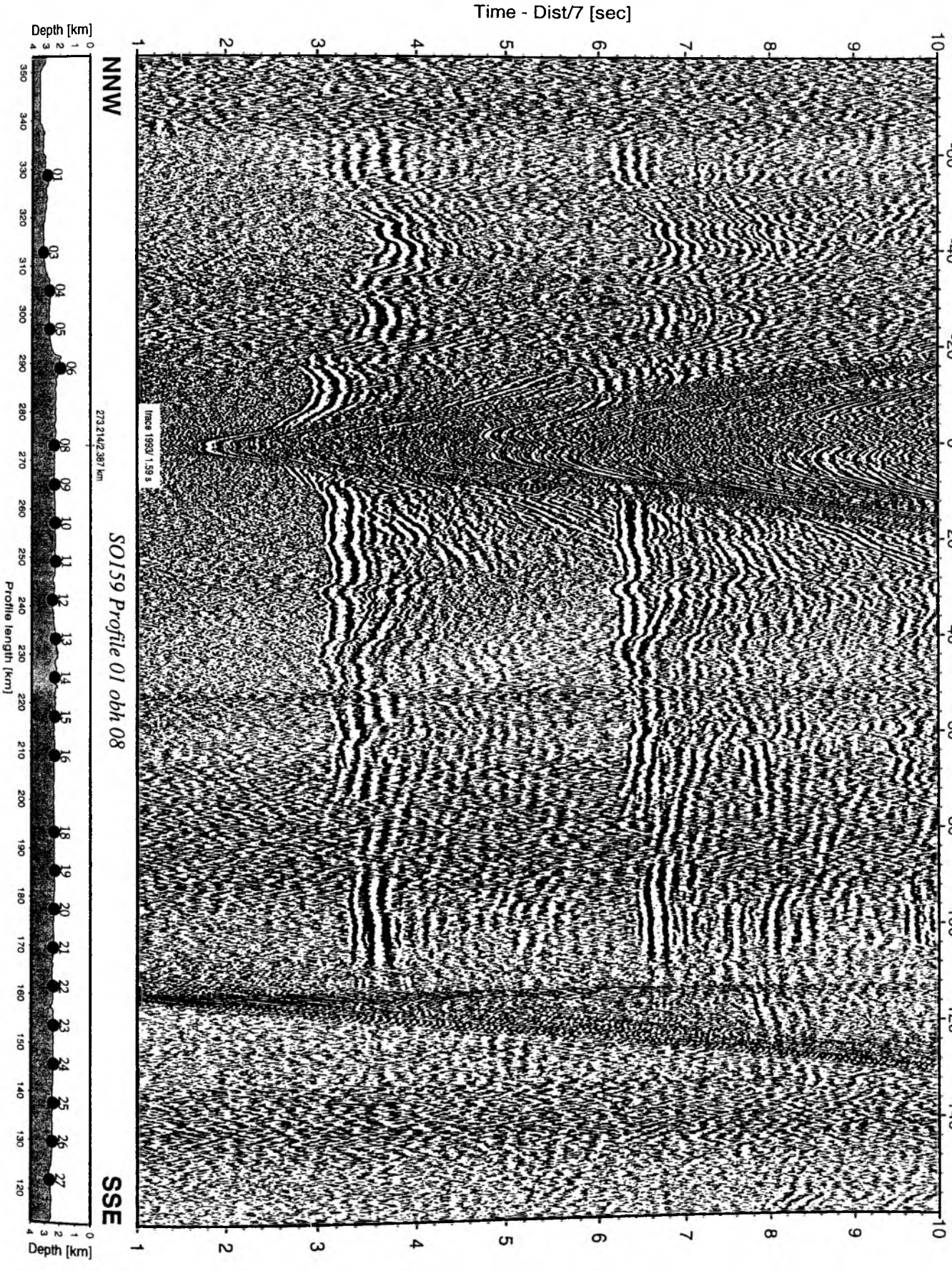

Figure 5.5.1.8: Record section from obh 08 , Profile 01.

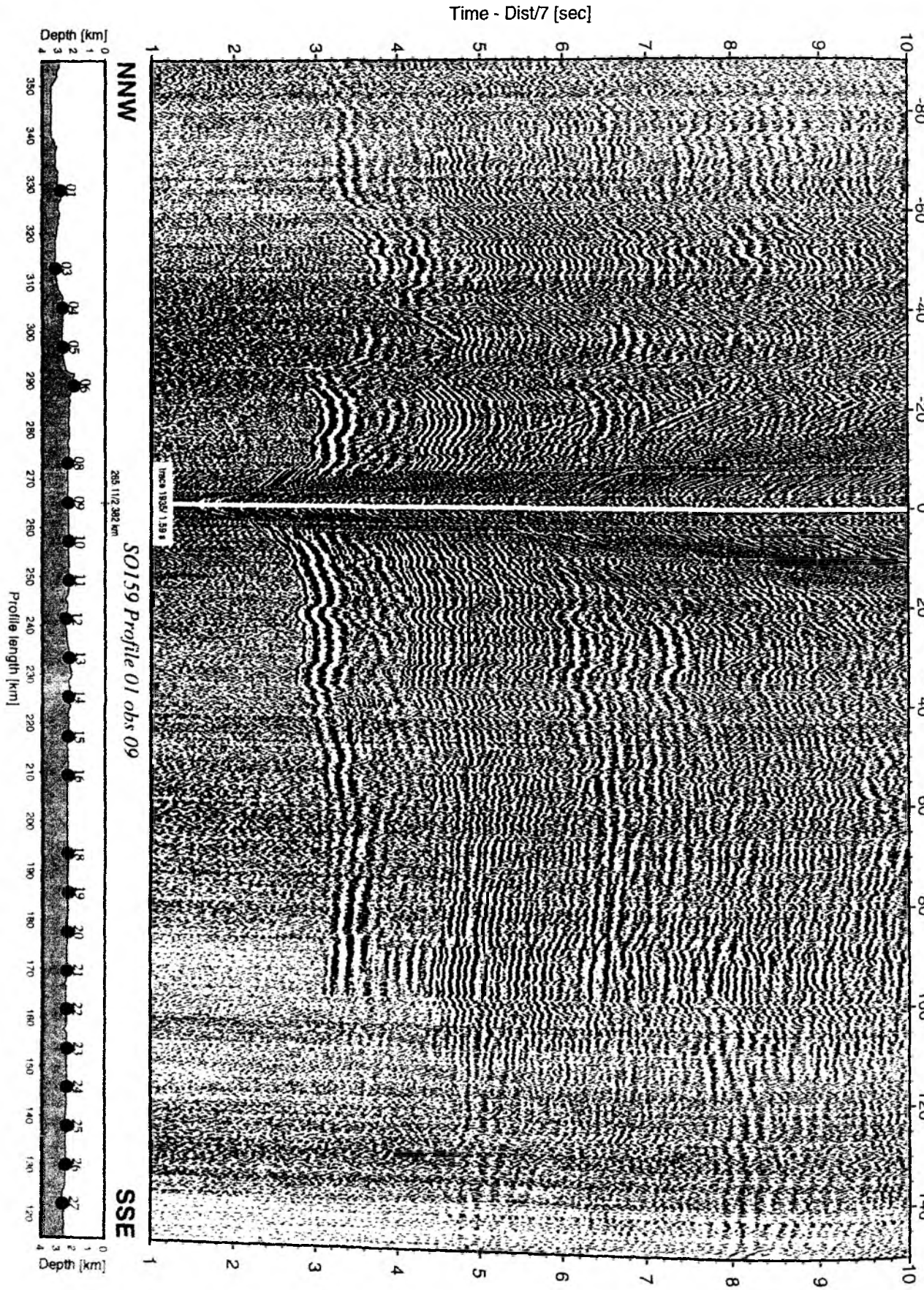

Figure 5.5.1.9: Record section from obs 09 vertical component, Profile 01.

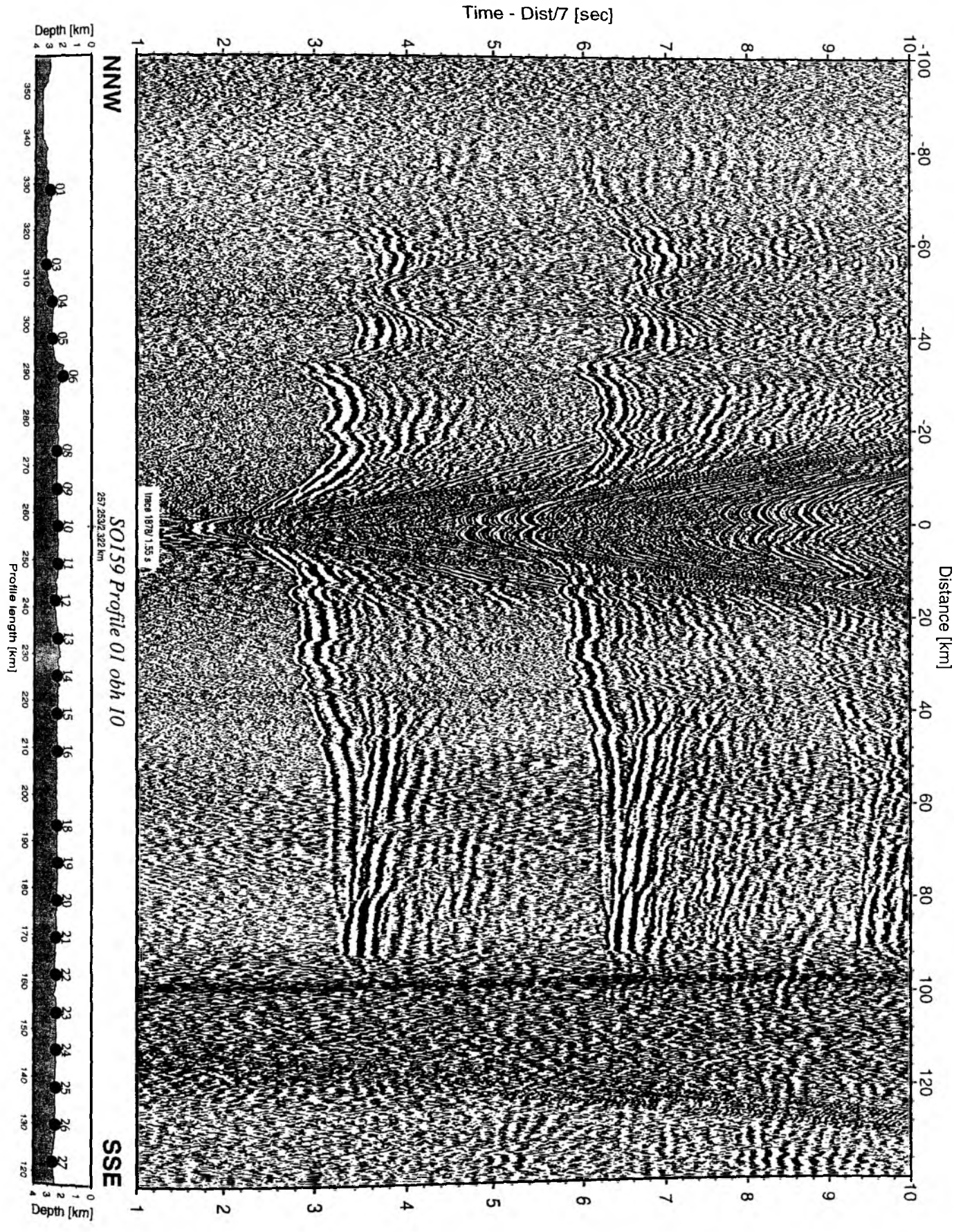

Figure 5.5.1.10: Record section from obh 10 , Profile 01.

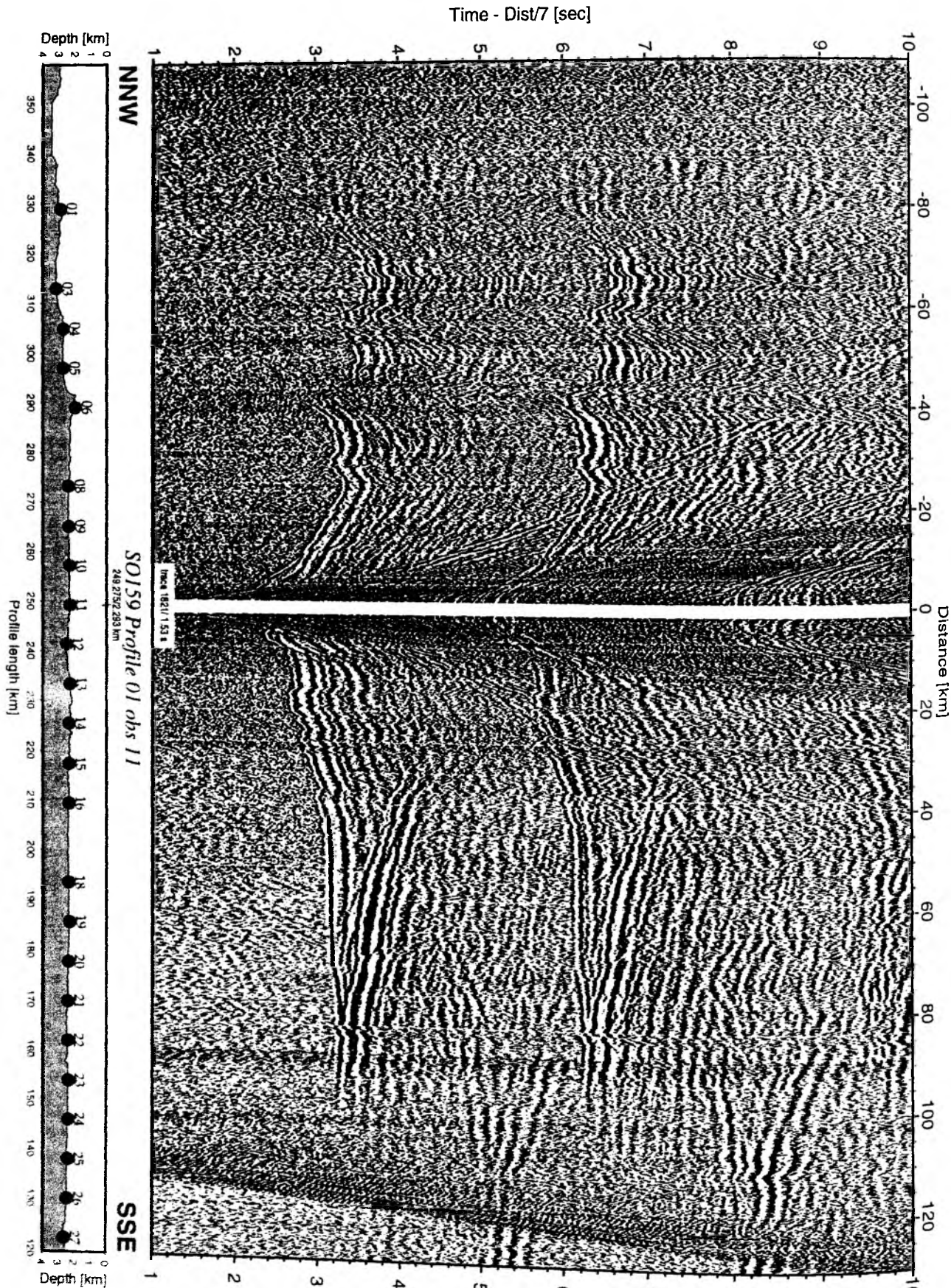

Figure 5.5.1.11: Record section from obs 11 hydrophone, Profile 01.

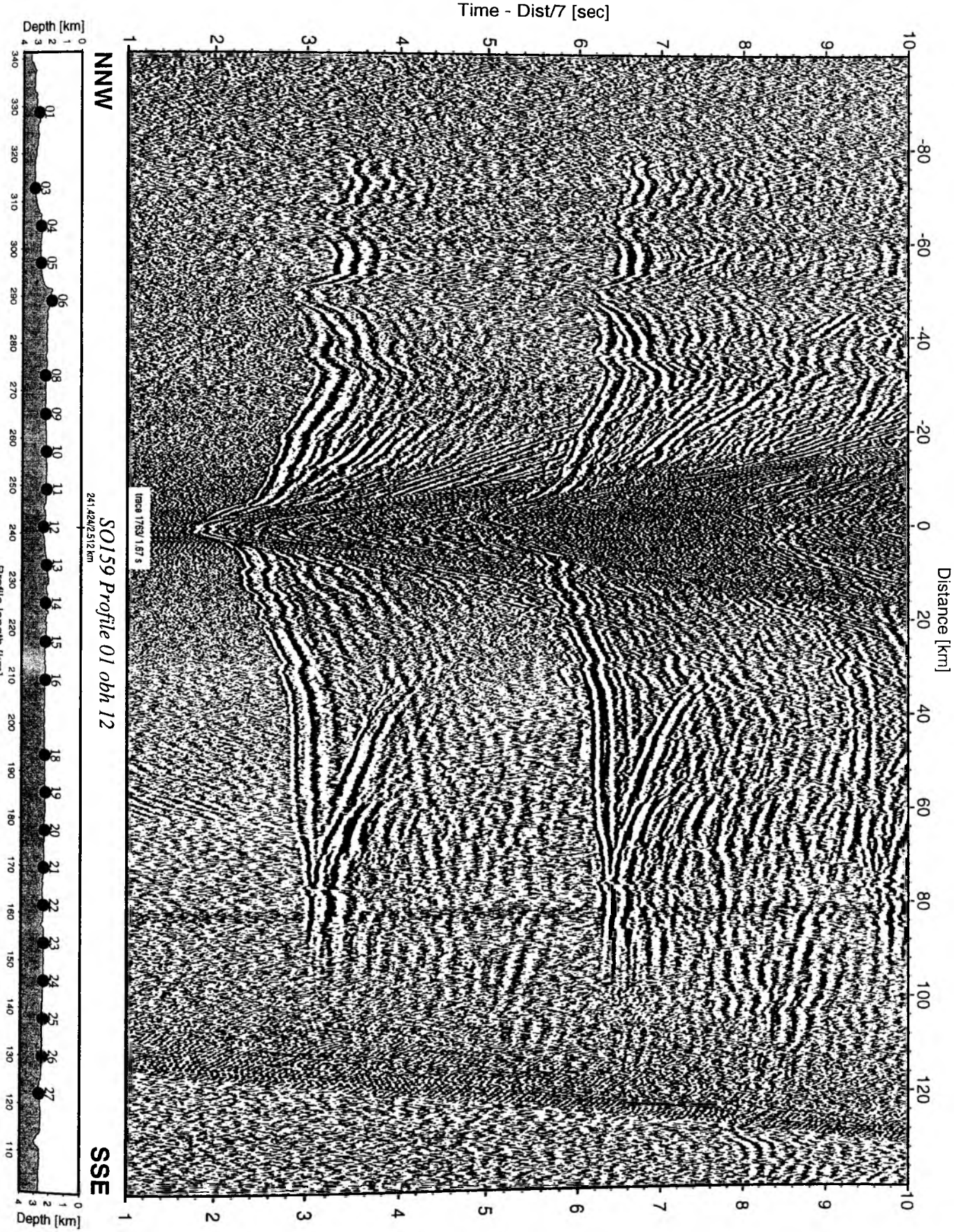

Figure 5.5.1.12: Record section from obh 12 , Profile 01.

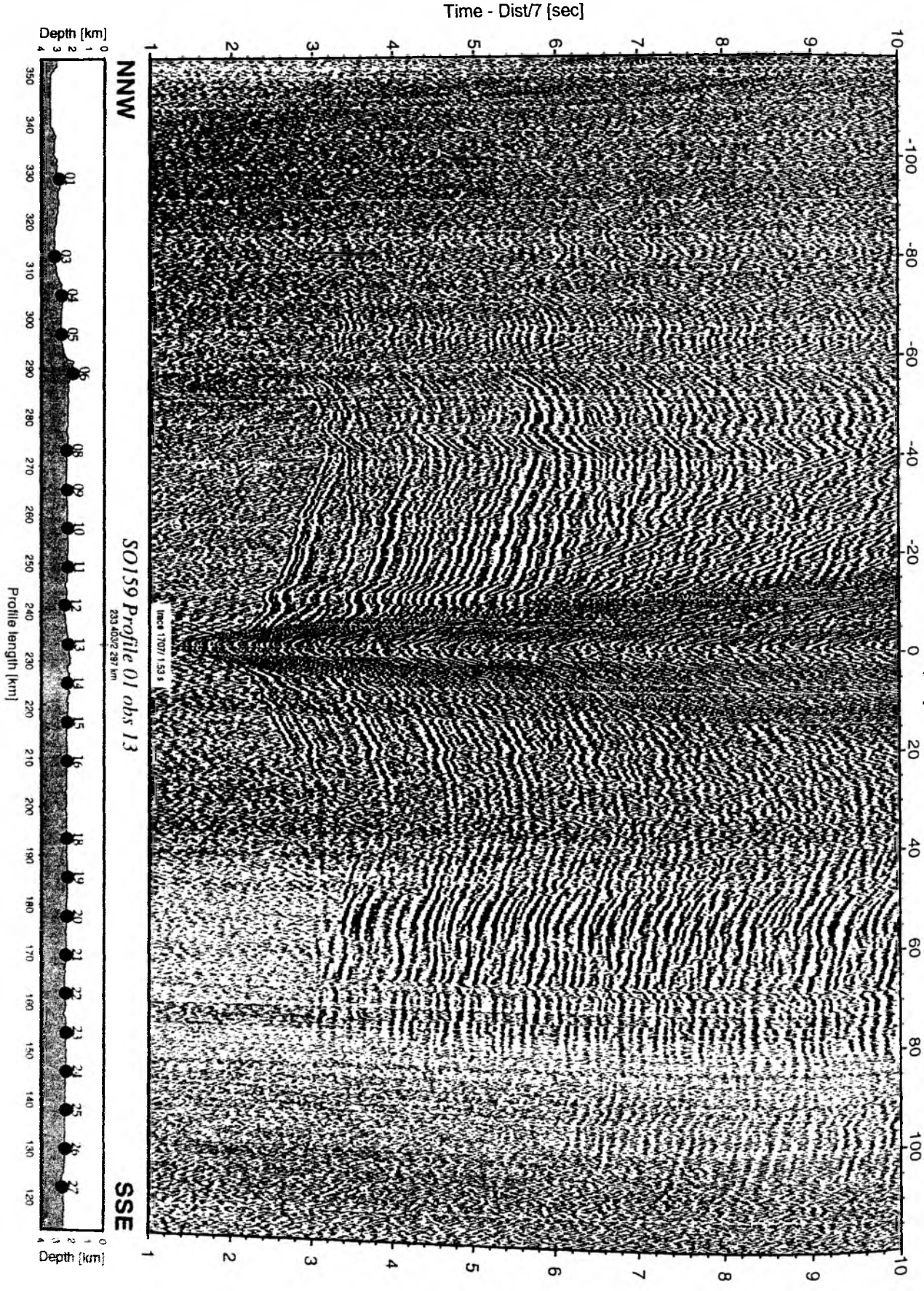

Figure 5.5.1.13: Record section from obs 13 vertical component, Profile 01.

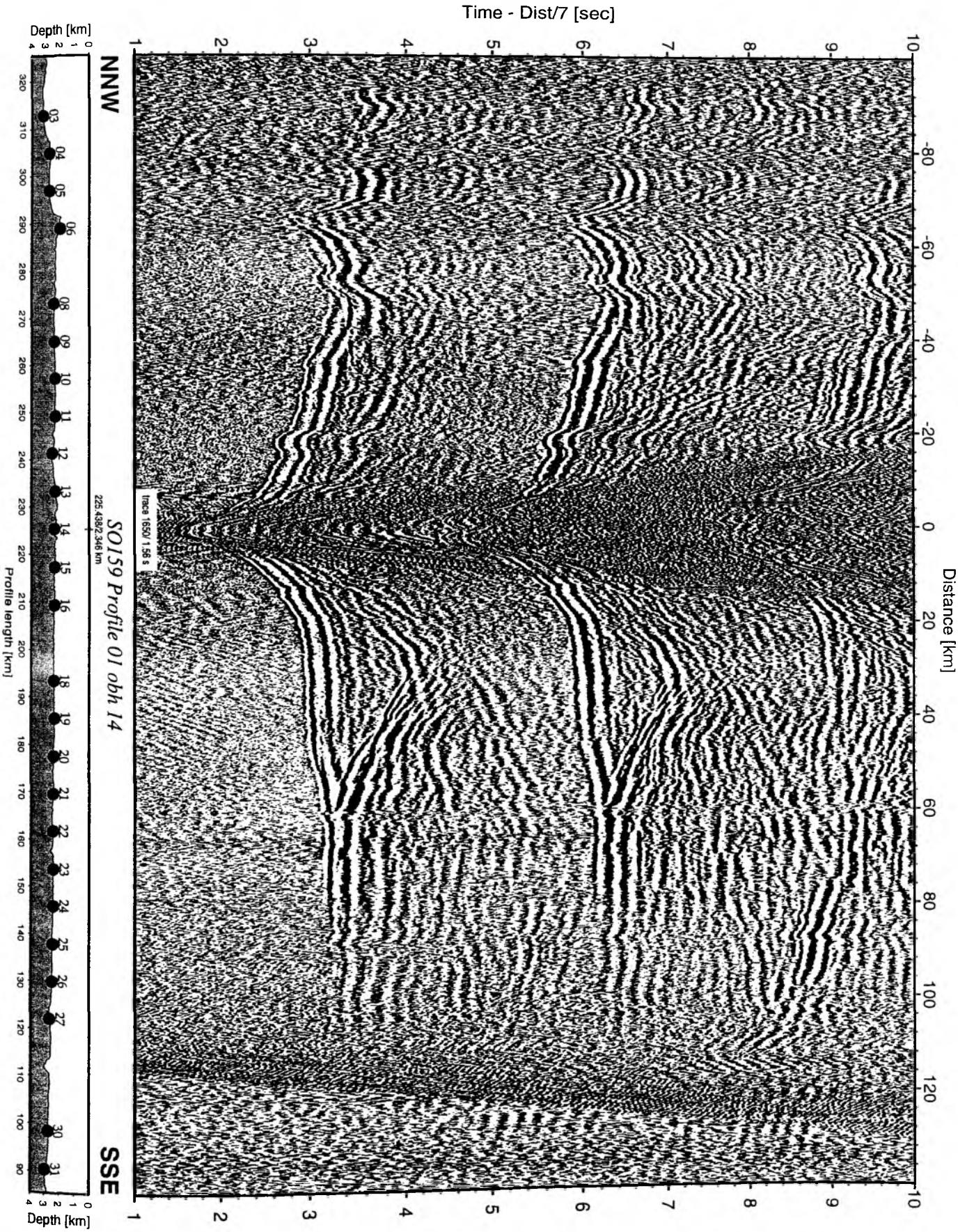

Figure 5.5.1.14: Record section from obh 14 , Profile 01.

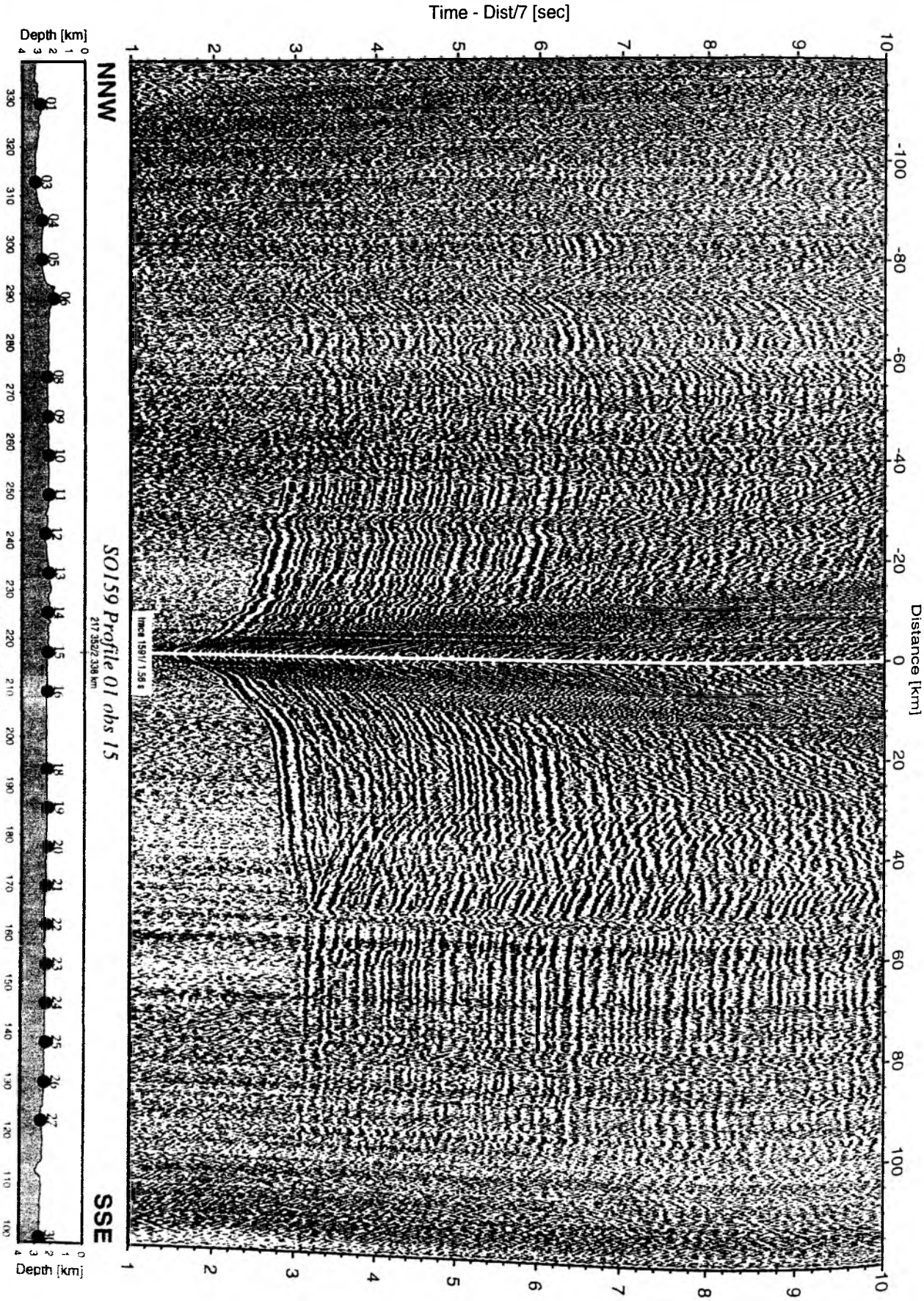

Figure 5.5.1.15: Record section from obs 15 vertical component, Profile 01.

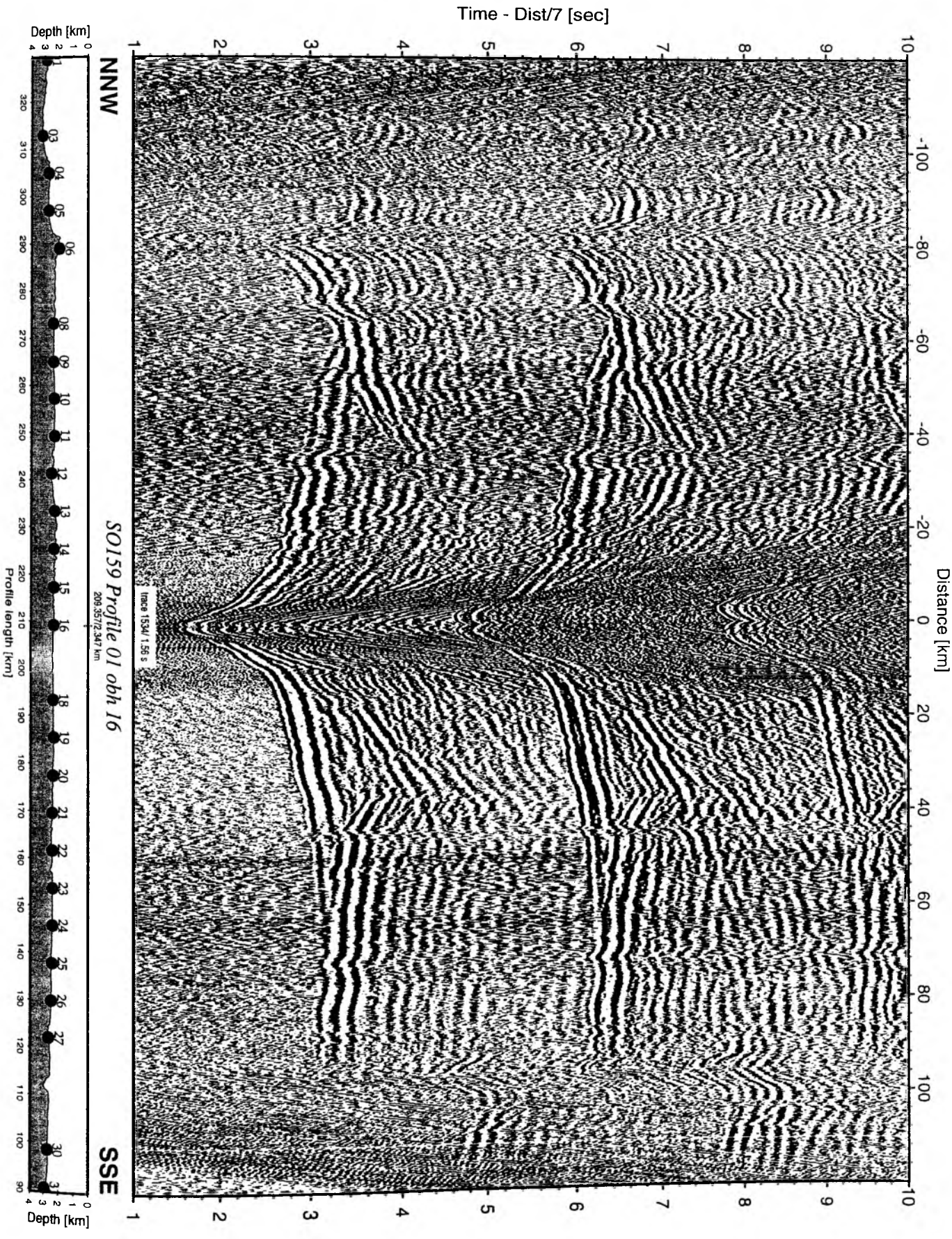

Figure 5.5.1.16: Record section from obh 16 , Profile 01.

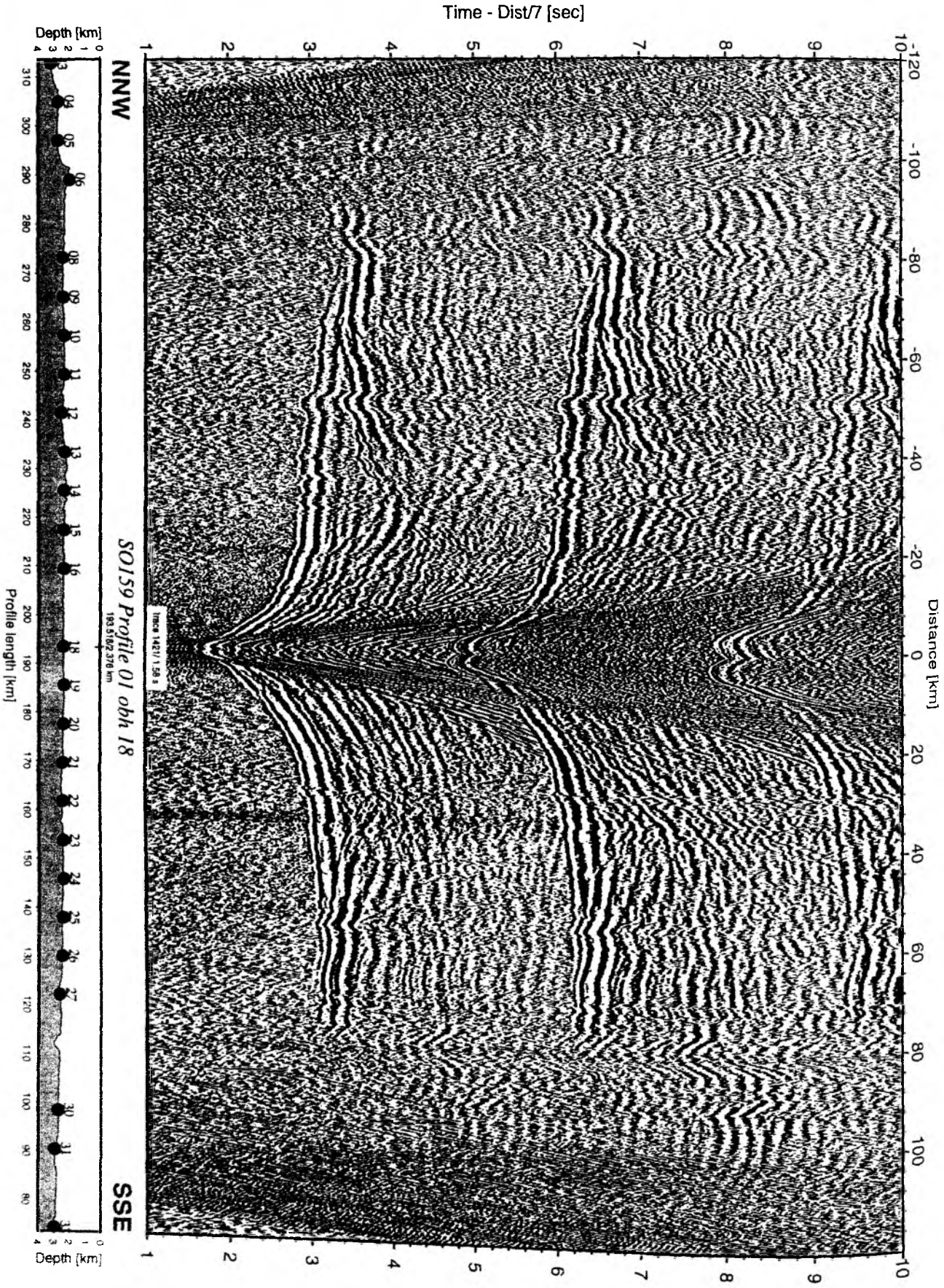

Figure 5.5.1.17: Record section from obh 18 , Profile 01.

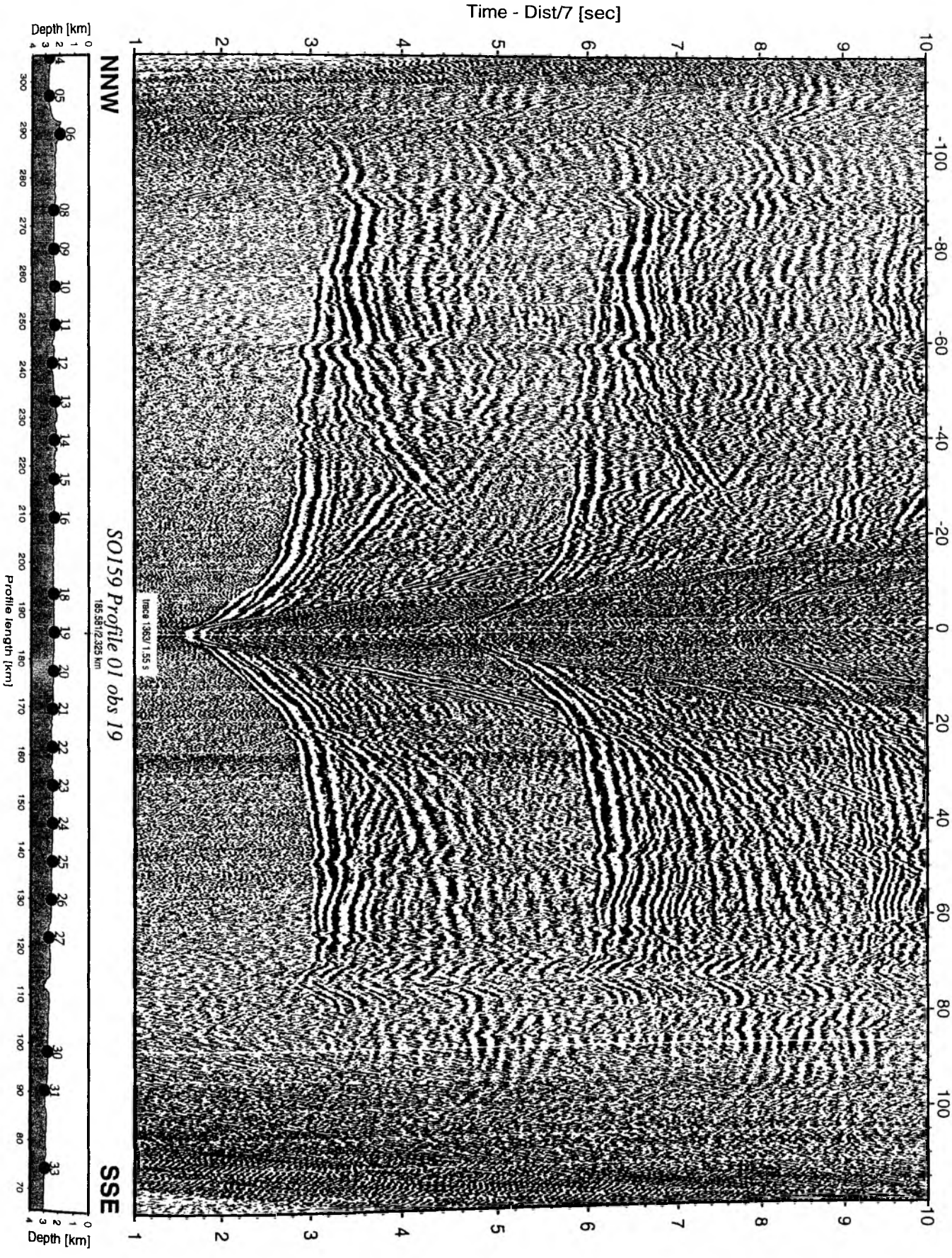

Figure 5.5.1.18: Record section from obs 19 hydrophone, Profile 01.

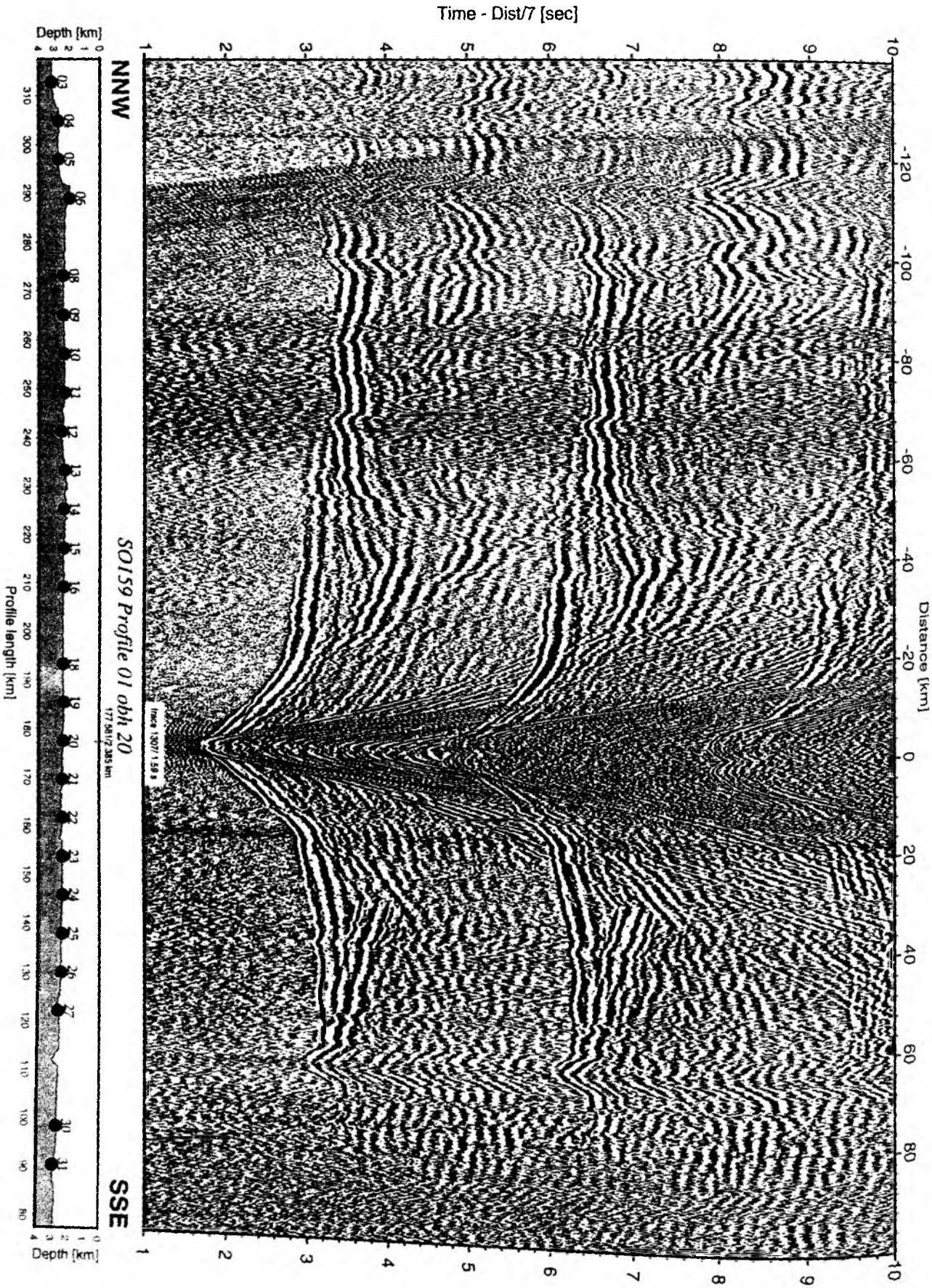

Figure 5.5.1.19: Record section from obh 20 , Profile 01.

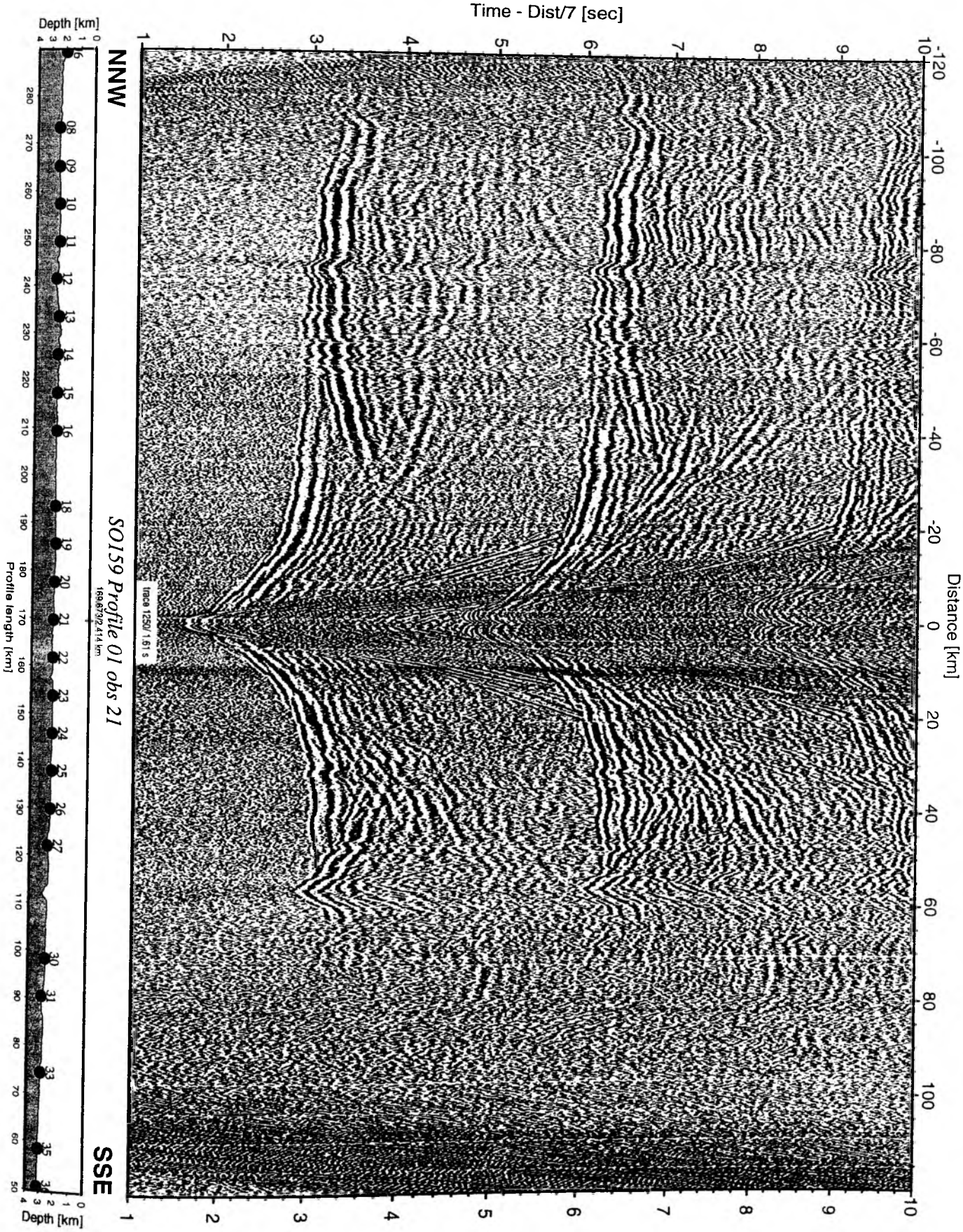

Figure 5.5.1.20: Record section from obs 21 hydrophone, Profile 01.

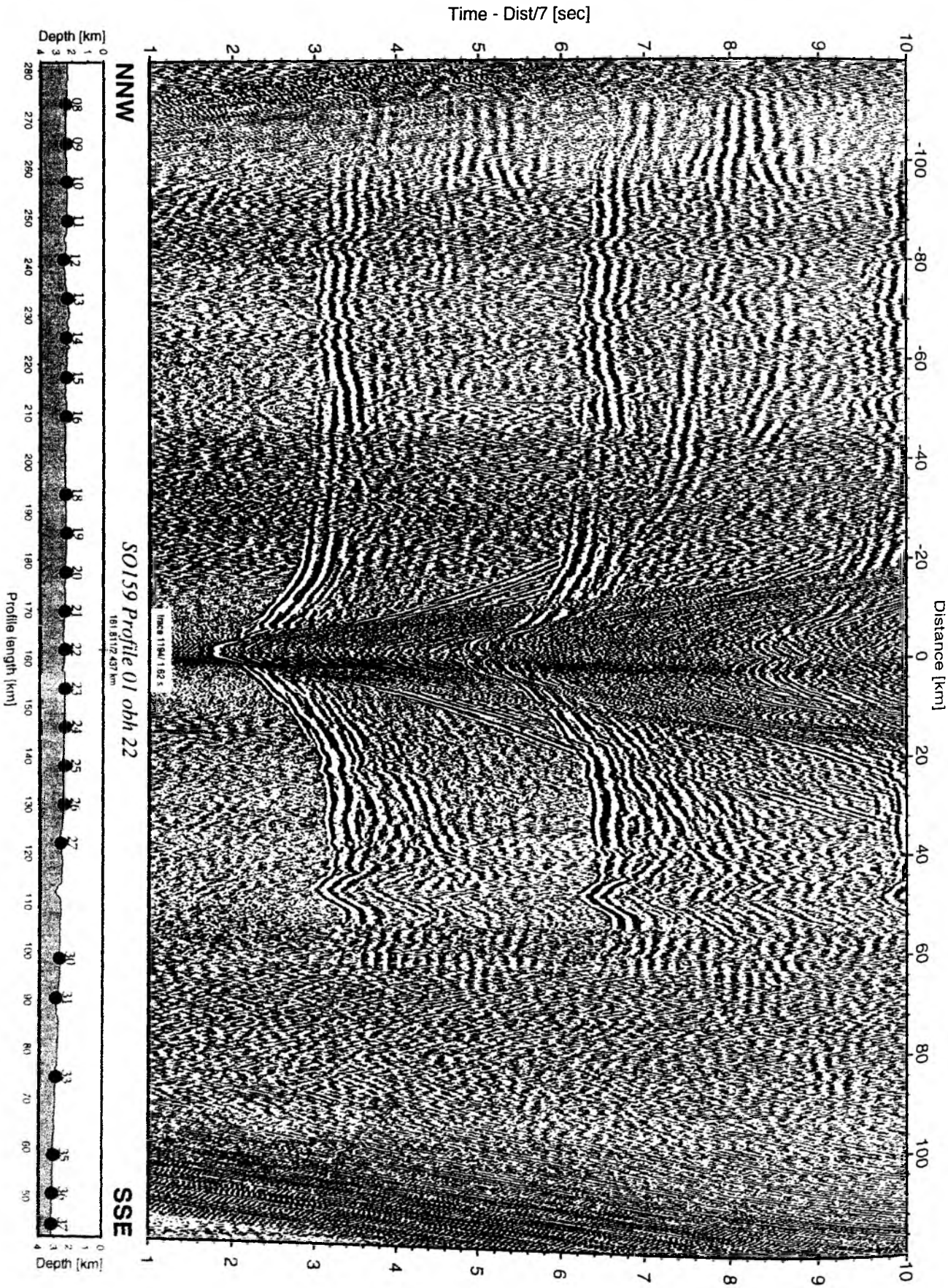

Figure 5.5.1.21: Record section from obh 22 , Profile 01.

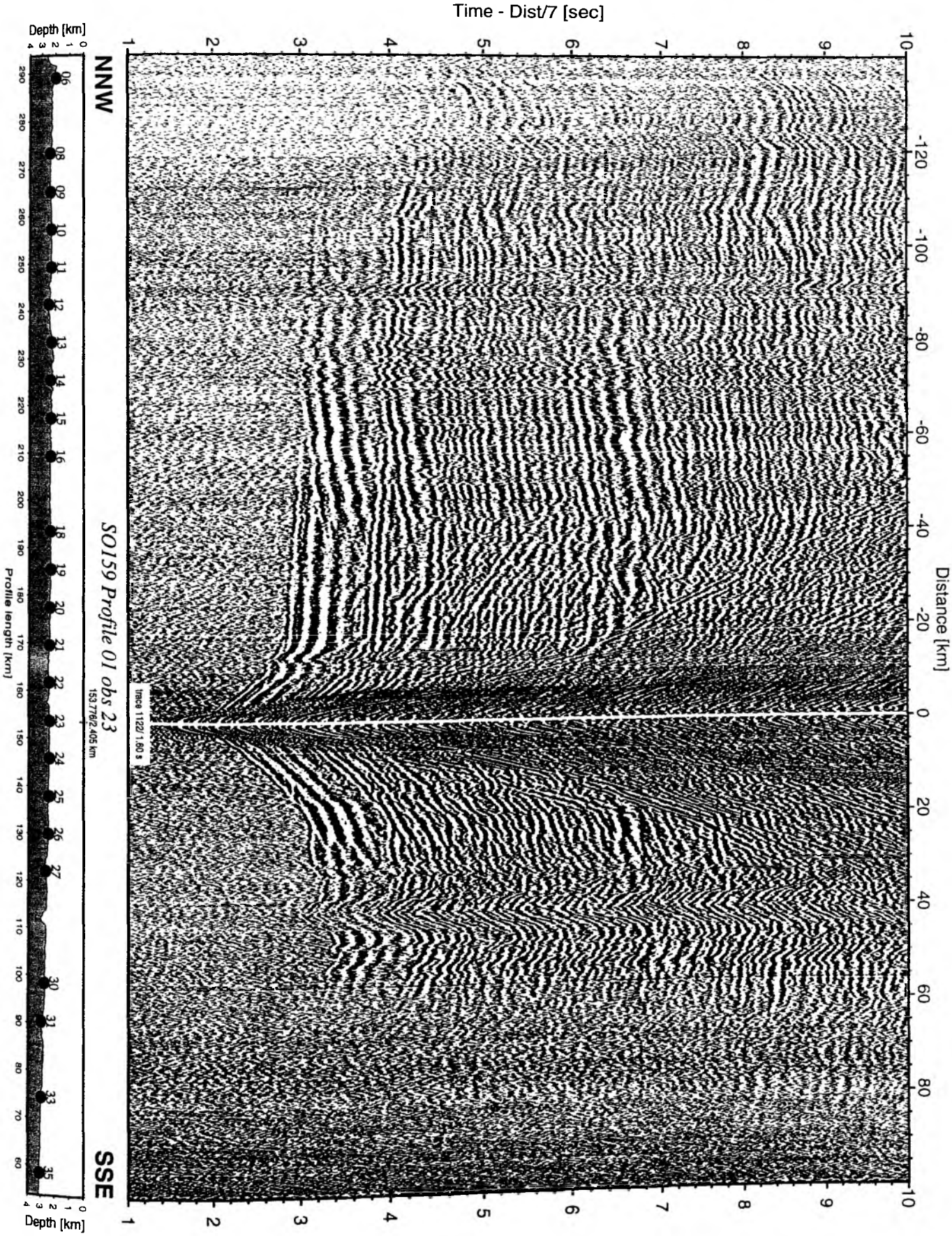

Figure 5.5.1.22: Record section from obs 23 vertical component, Profile 01.

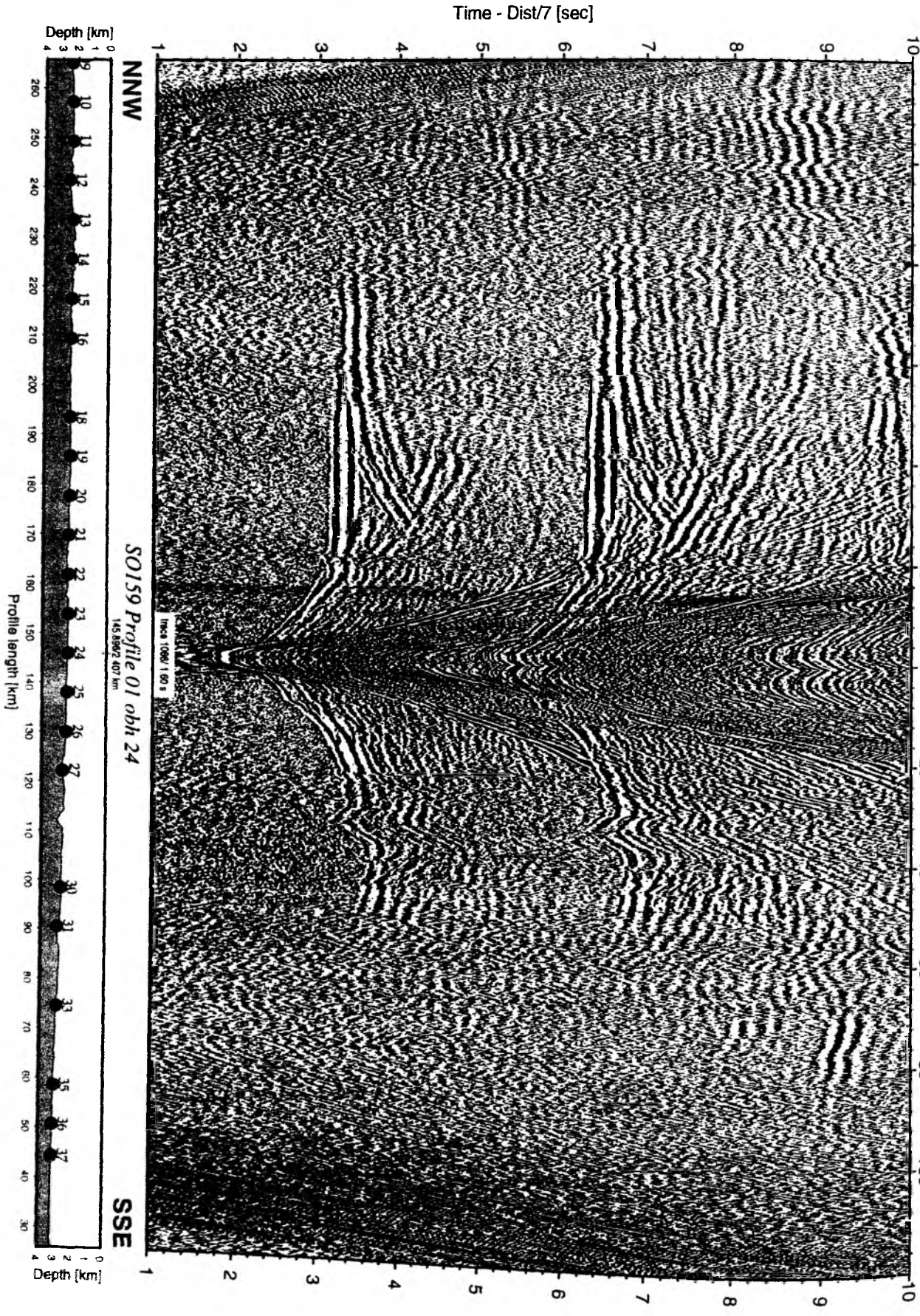

Figure 5.5.1.23: Record section from obh 24 , Profile 01.

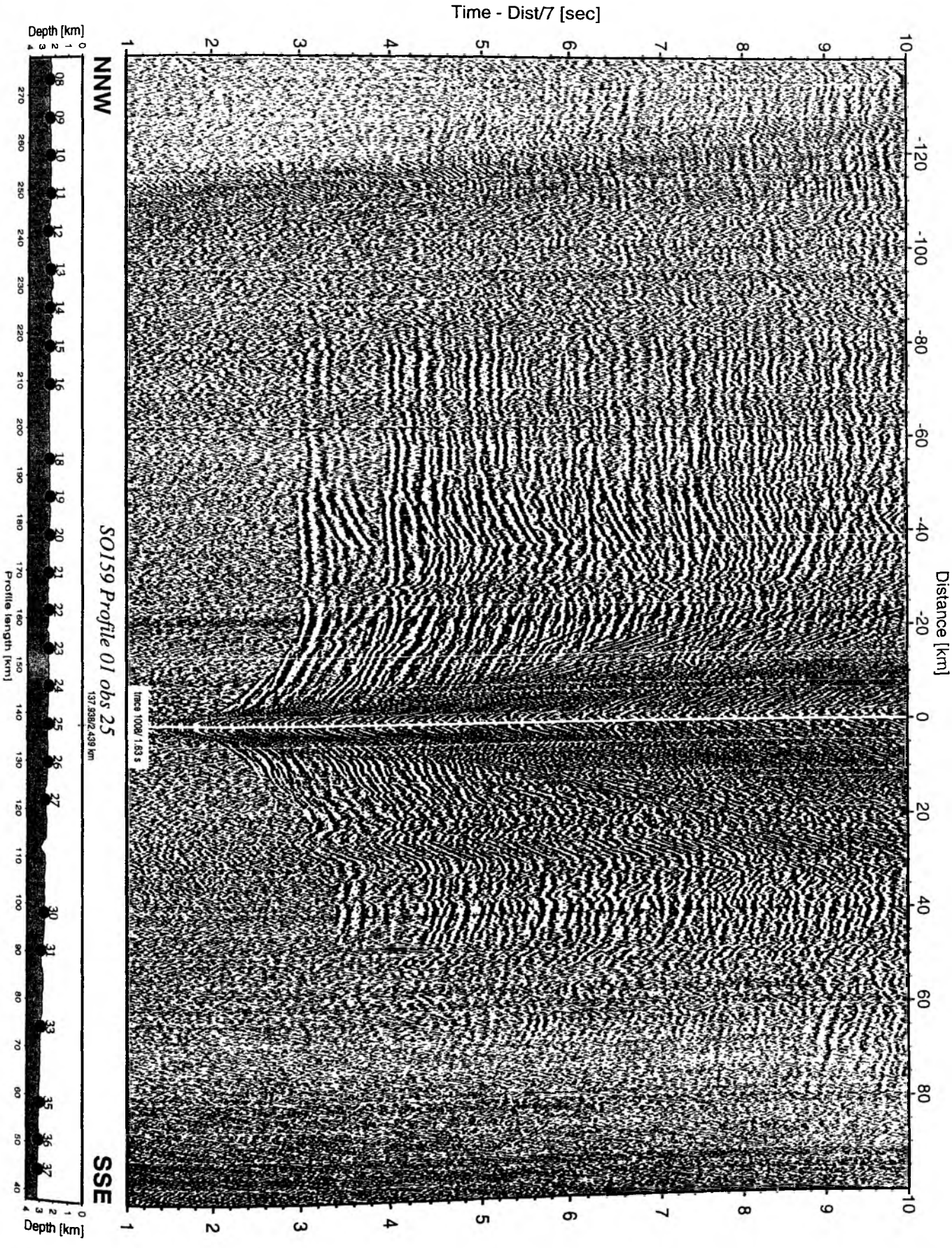

Figure 5.5.1.24: Record section from obs 25 vertical component, Profile 01.

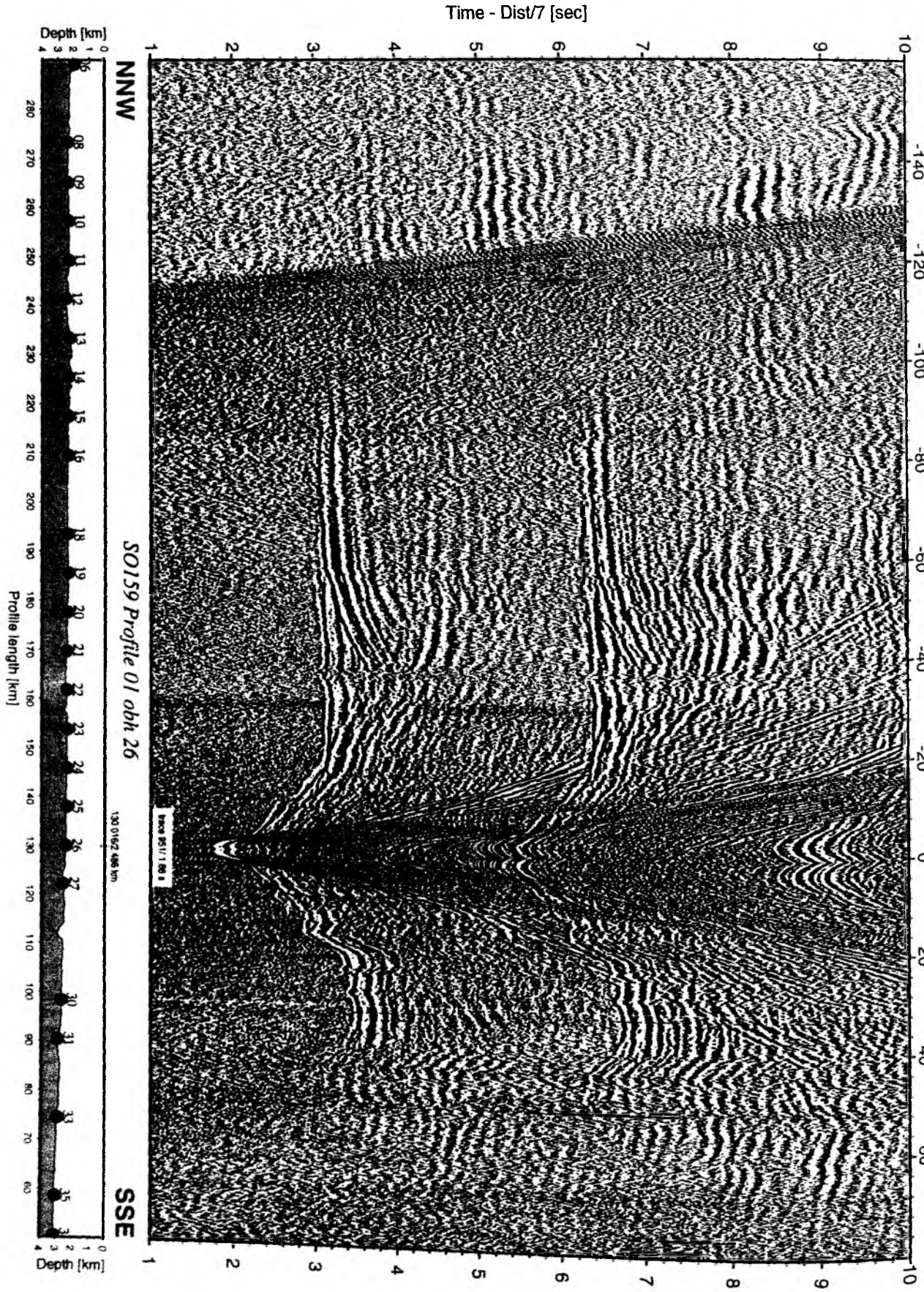

Figure 5.5.1.25: Record section from obh 26 , Profile 01.

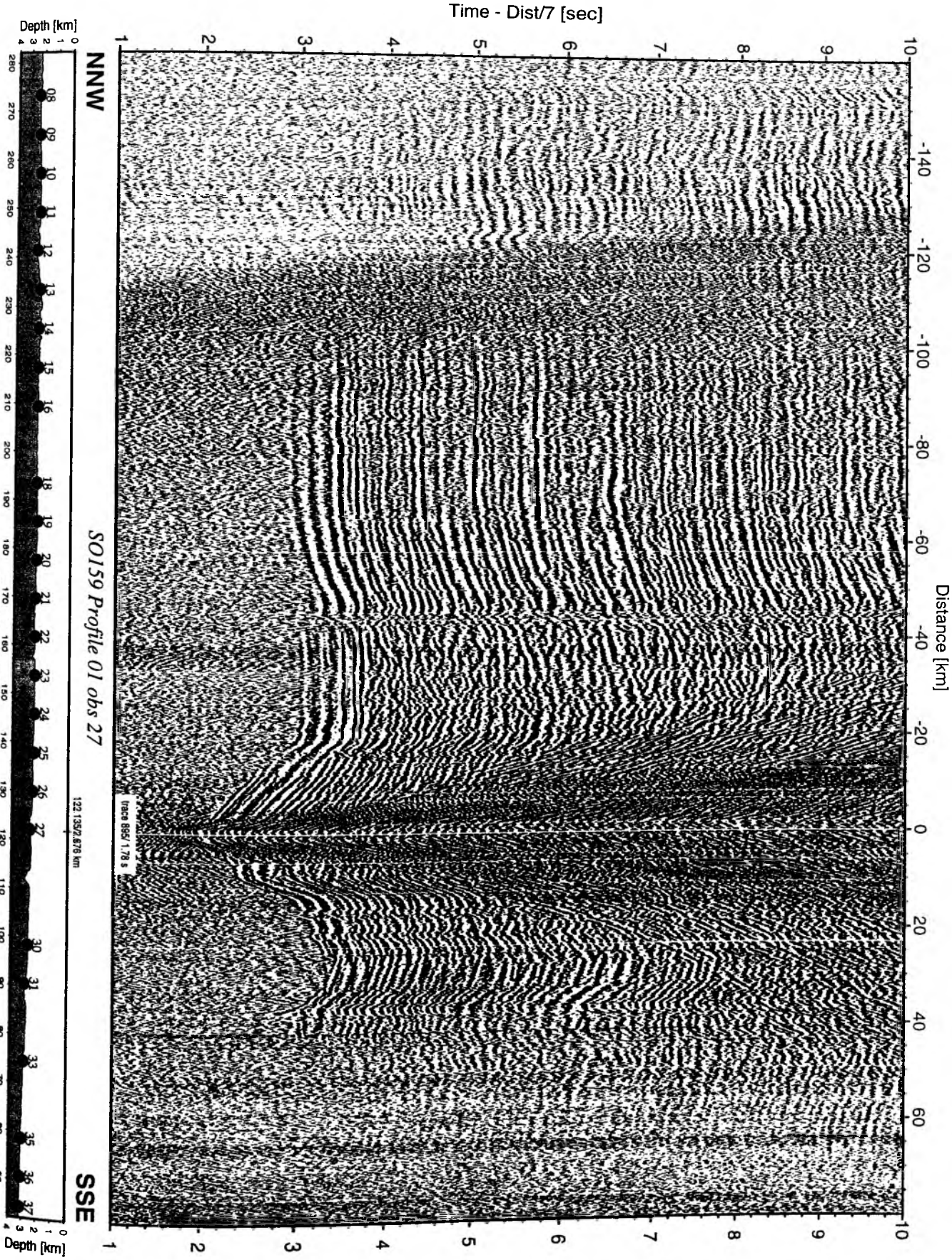

Figure 5.5.1.26: Record section from obs 27 vertical component, Profile 01.

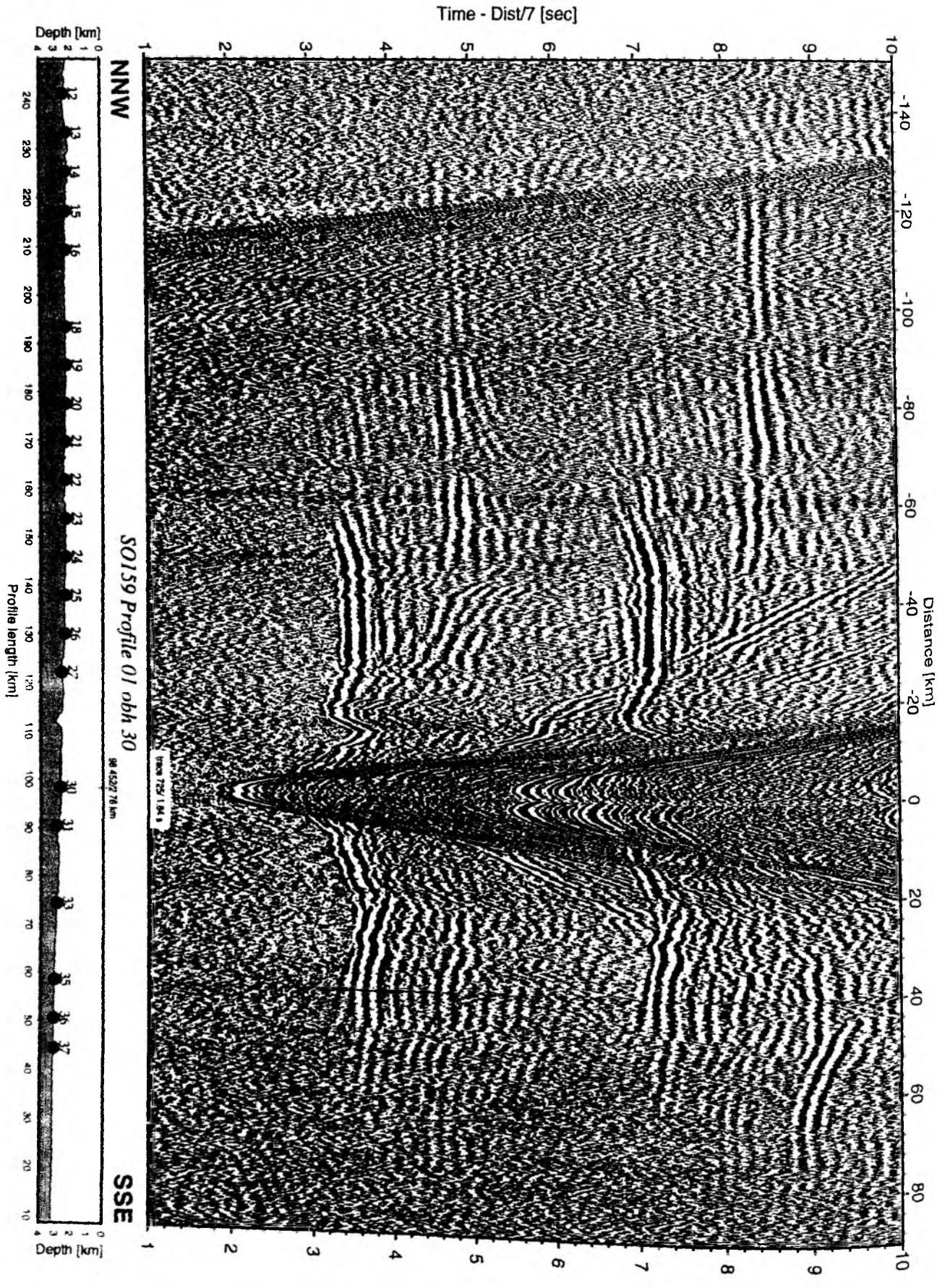

Figure 5.5.1.27: Record section from obh 30 , Profile 01.

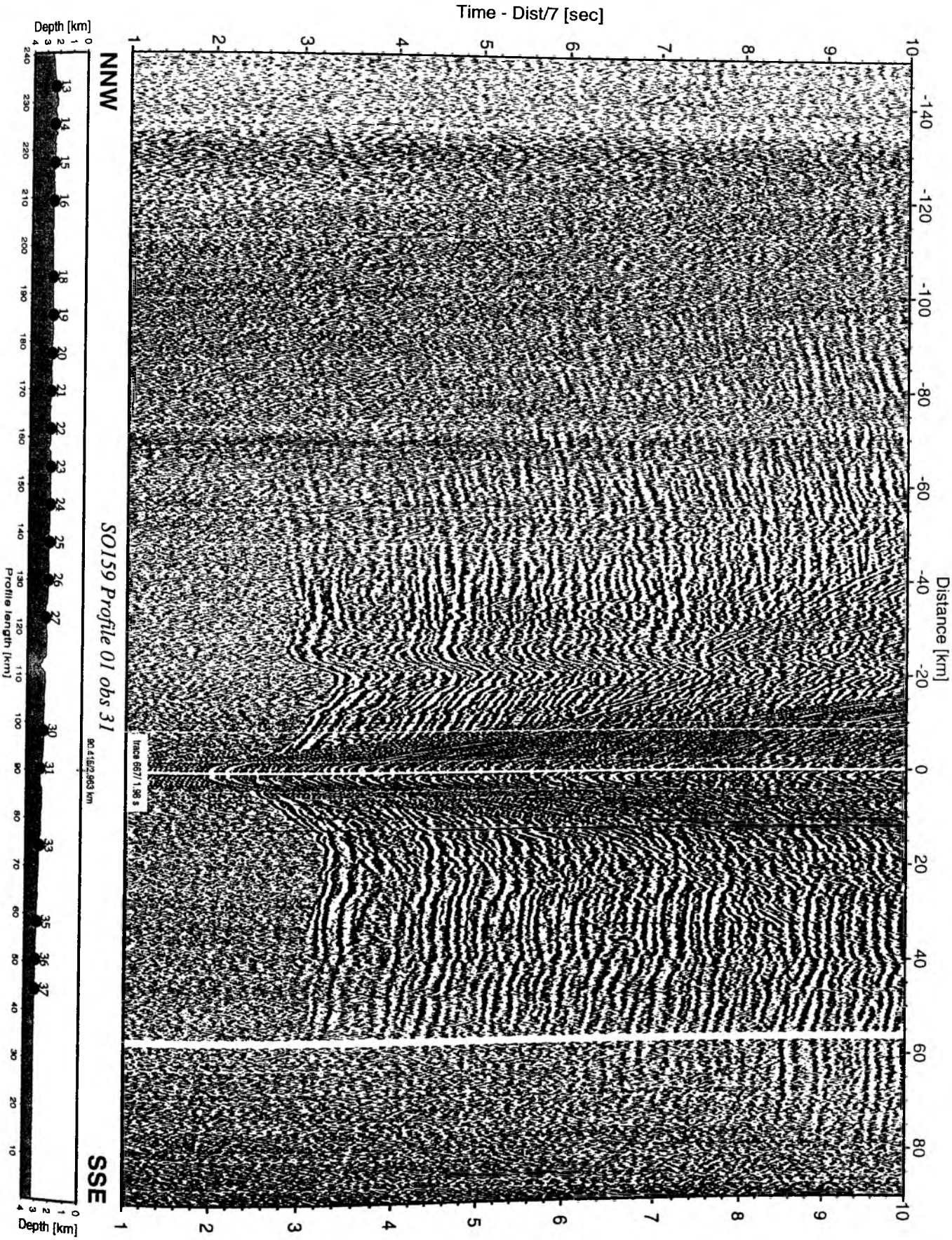

Figure 5.5.1.28: Record section from obs 31 vertical component, Profile 01.

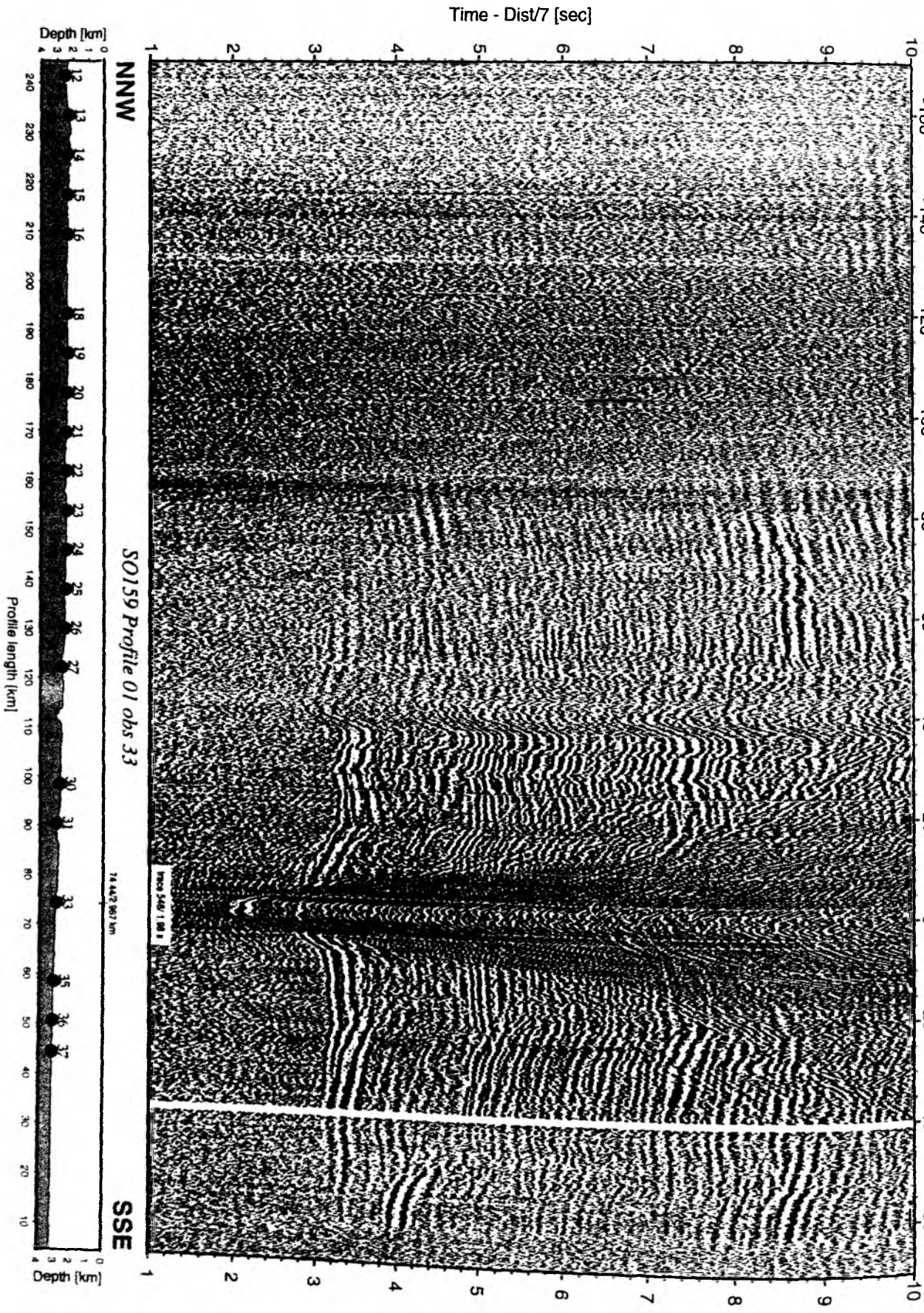

Figure 5.5.1.29: Record section from obs 33 vertical component, Profile 01.

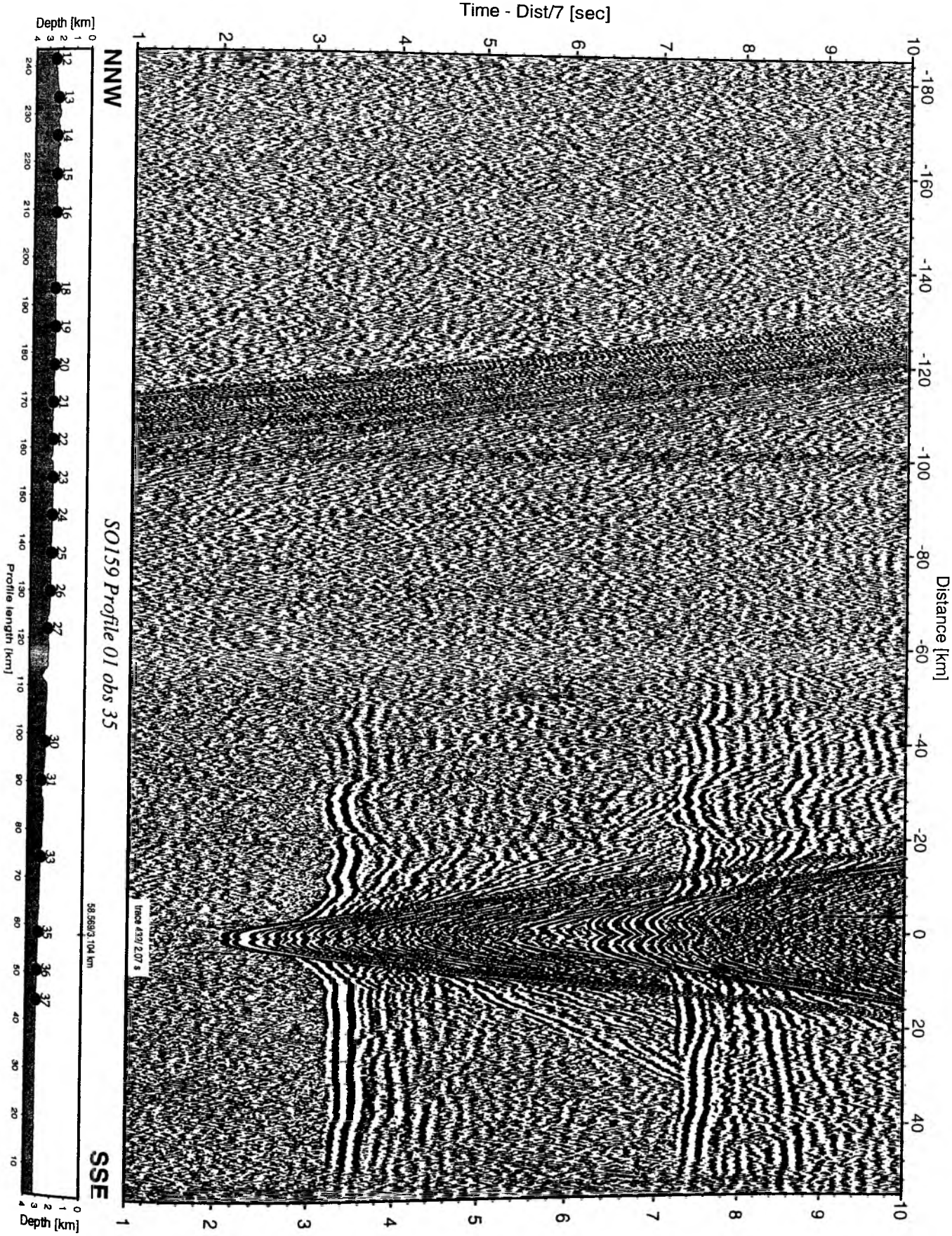

Figure 5.5.1.30: Record section from obs 35 hydrophone, Profile 01.

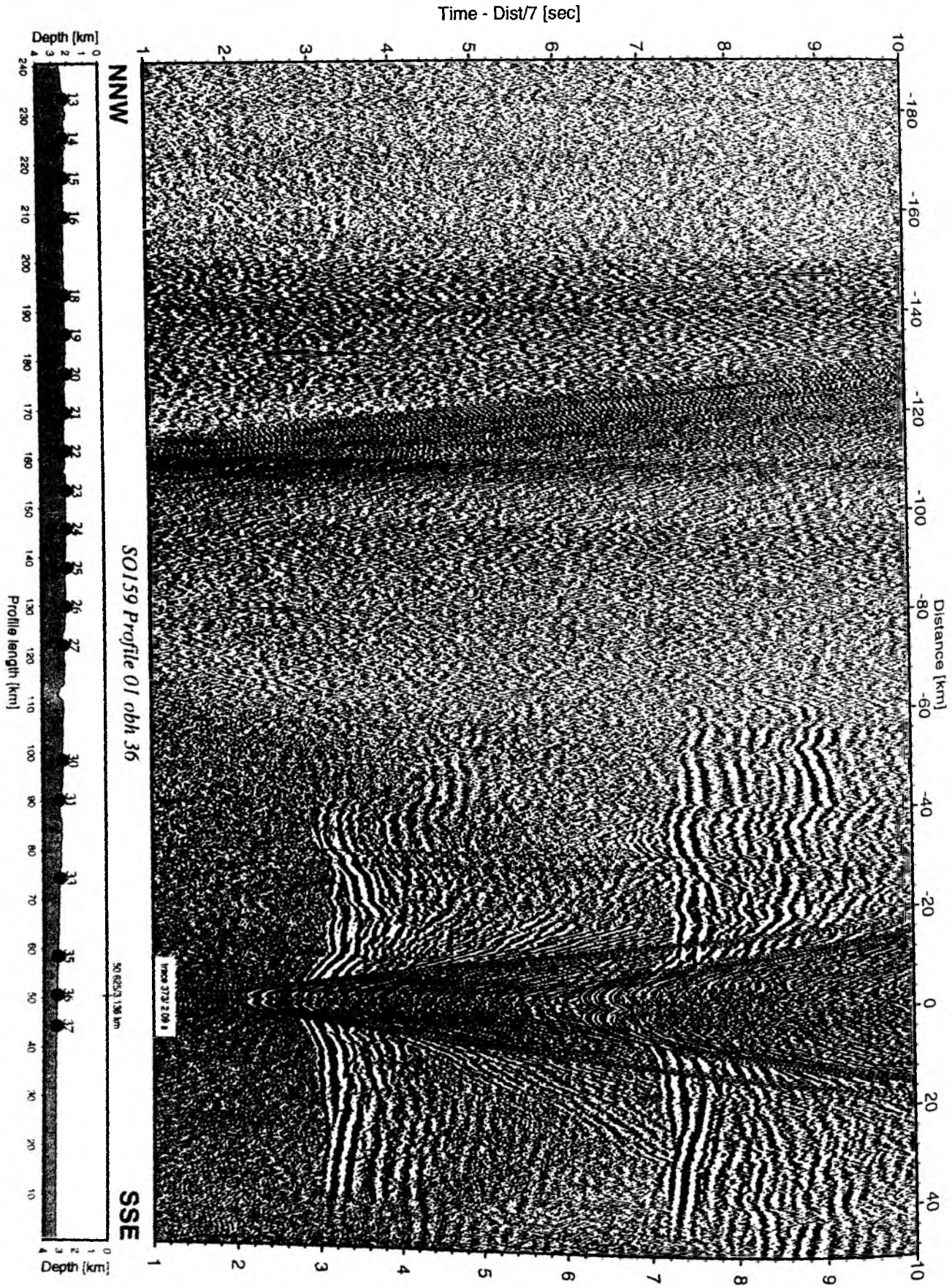

Figure 5.5.1.31: Record section from obh 36 , Profile 01.

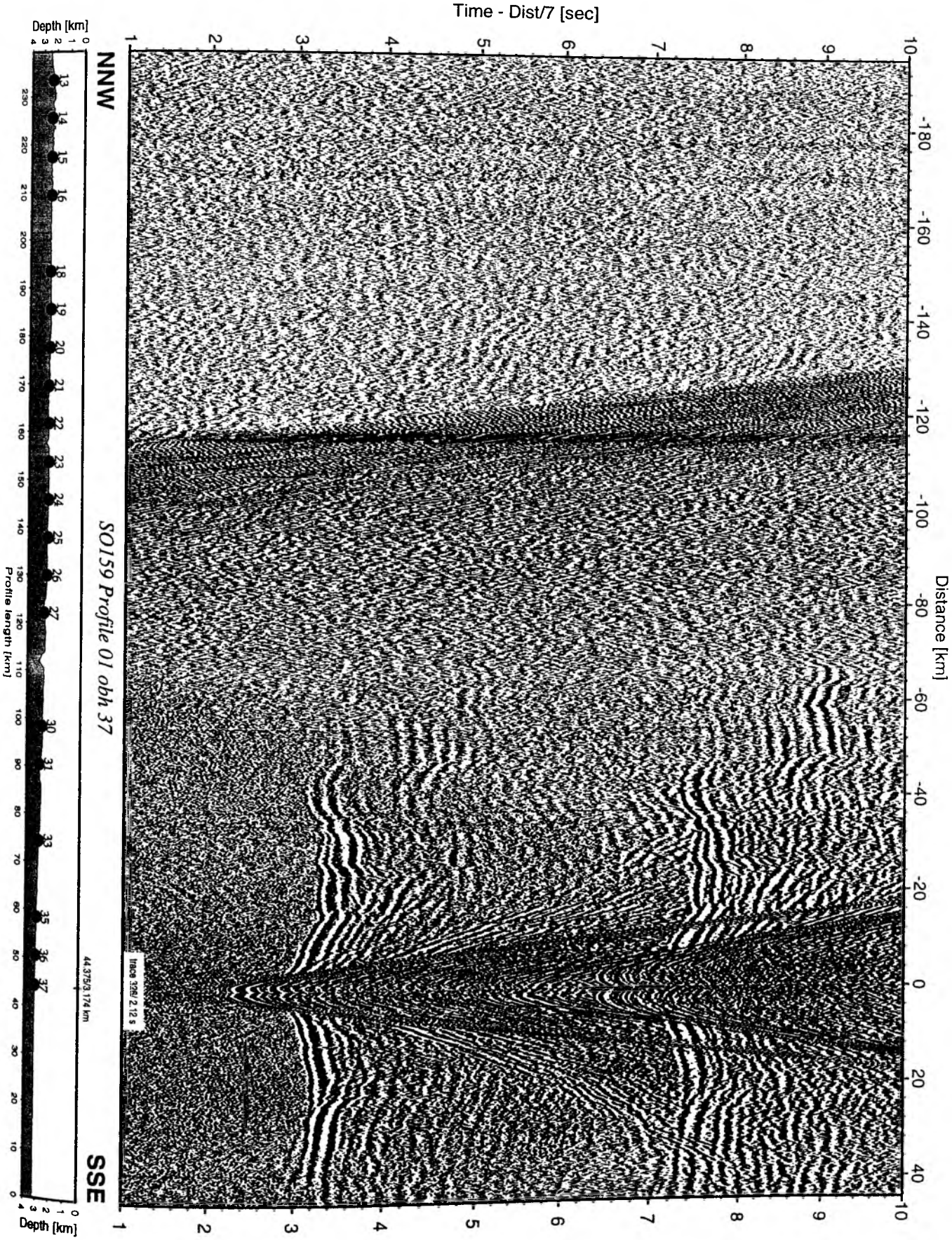

Figure 5.5.1.32: Record section from obh 37 , Profile 01.

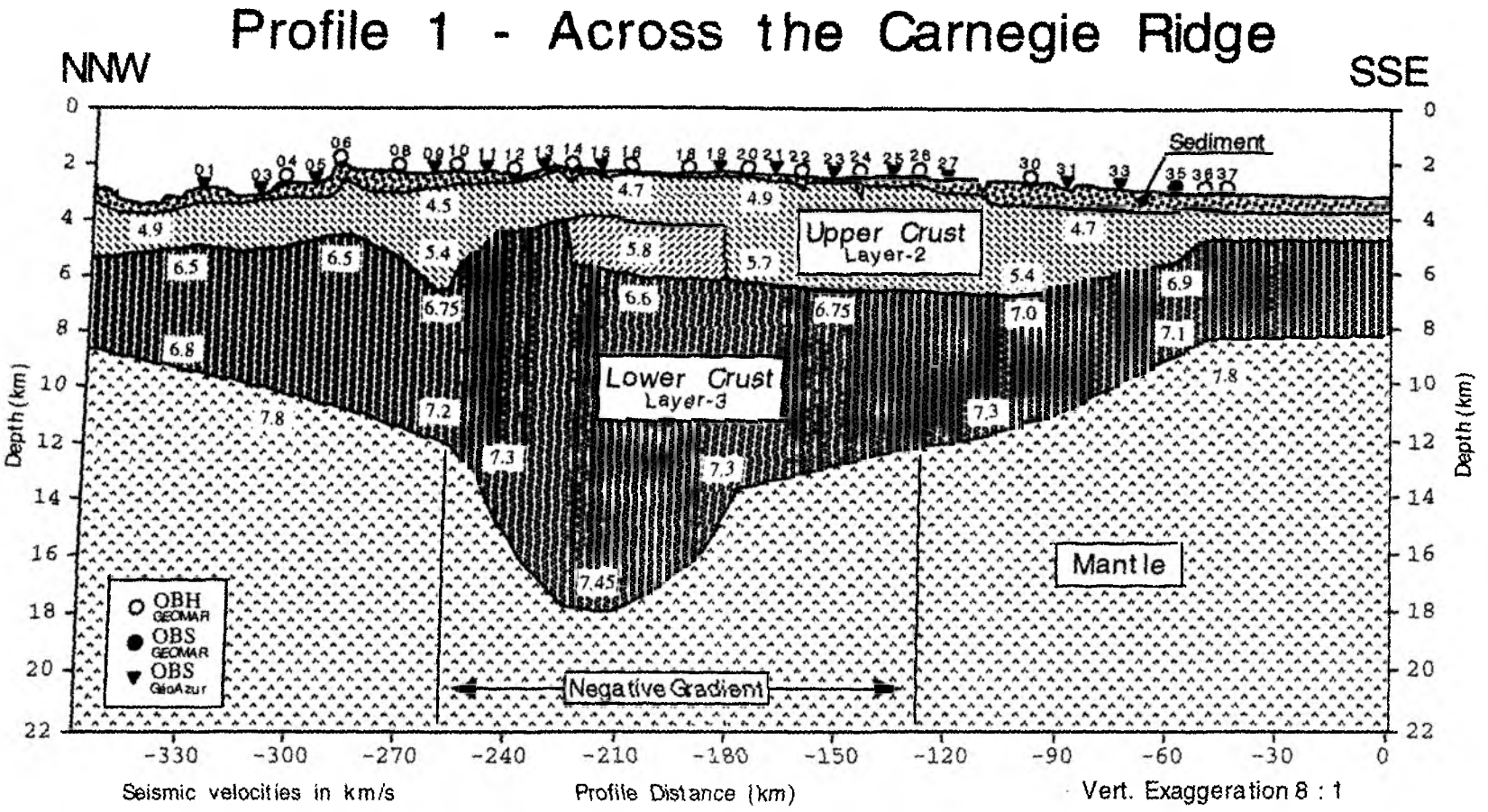

Figure 5.3.1.33

5.3.2 Profile SO 159-02

(Petra Liersch, Peter Thierer and Céline Ravaut)

Profile 02 is coincident with a multichannel seismic reflection line collected during the SISTEUR cruise in summer 2000. It reaches from the Carnegie Ridge towards the ESE across the trench into the bay of Guayaquil close to St. Clare island. The aim of the experiment was to investigate the velocity-depth distribution for the corresponding MCS profile in the subduction zone formed by the Nazca Plate and the South American Plate. We were especially interested in achieving more detailed information about the subducting sediment which is a very strong reflector.

Profile 2 intersects with two other profiles, which have been deployed at a right angle over this profile: profile 3 with OBH/S 60 to 66 intersected over OBS 48 and profile 4 with OBS 67 to 82, in order to see the lateral extension of the structure. In the morning of September 01 we deployed 20 OBS (OBS 39 to 58) in total for Profile 2. The spacing between the stations was 3 nm. The total coverage of the profile is 150,1 km at a strike of 290°. Station coordinates are listed within Appendix II. A location map of the profile including bathymetry is given in Figure 5.3.2.1. A line drawing of the MCS data is shown in Figure 5.3.2.2.

Shooting of the profile started on September 1st at 19:21 UTC and was carried out by all three airguns without any interruption at a speed of 4.5 kn with 60 sec shot interval for a total of 1172 shots, which form a shot spacing of approximately 135 m. During shooting the magnetometer was also deployed (see chapter 5.2). Shooting was completed on September 2nd at 14:59 UTC.

While most of the instruments were retrieved after shooting, OBS 48 was left in position for recording shots along strike line 3. Four instruments could not be recovered, and two instruments failed to record data, reducing the total number of usable seismic sections to 14 (see Appendix II-2). The quality of the record sections is generally quite good, with energy propagation in excess of 100 km. A preliminary interpretation of this data set was attempted at sea. These record sections which were processed as described in chapter 4.8.1 are shown in Figures 5.3.2.3 to 5.3.2.16. The reduction velocity of all seismic sections is V_{red} = 6 km/s.

Modeling and Interpretation

Due to the limited time on board, only the arrivals recorded by the GEOMAR Hydrophones were used for modeling profile SO159-02. Most prominent phases, first arrivals, plus the reflected and refracted phases were picked for every record section using Xzplot software (Zelt and Smith, 1992). Velocity-Depth Modeling was done using H. Luetgert's MacRay 2D, version 2.5.1, (Luetgert, 1992) modeling software.

First arrivals were fit to the uppermost sedimentary layer with velocities of 1.6 km/s to 1.8 km/s. The thickness of this sedimentary layer varies as shown in Figure 5.3.2.17. It ranges from about one hundred meters on the oceanic crust to more than six kilometers in the Guayaquil Basin. The thickness of the sedimentary cover deposited in the area of OBS 48 is about 900 meters, and compares directly to the modeled refraction seismic cross-section (SO159-03).
To the East of the trench, the continental crust is underlying the sediments deposited in the Guayaquil Basin. These crustal velocities range from 3,5 km/s right beneath the sediments to 4.6 km/s at the lower part of the crust. The continental Moho can not be resolved with the data, which leaves the continental structures below 18 km undefined.
The model suggests a total oceanic crust thickness of about seven kilometers seawards of the trench. The oceanic crust is divided into two layers. The upper oceanic crust (Layer 2) is about 2,5 km thick and has seismic velocities between 4,6 km/s in the oceanic domain to 5.6 km/s below the continent. The thickness of the lower oceanic crust (Layer 3) is about 4,5 km. Here we find velocities of 6,3 km/s in the upper part to 6,8 km/s close to the CMB.

The oceanic Nazca Plate subducts the South American Plate with an approximate slope inclination angle of 5° right underneath the trench. In a distance of about 40 km from the trench axis, the subduction angle changes to 2°. The average subduction angle of the "s-shaped" oceanic plate is 3°. In contrast to the landward side, the Moho can be well observed on the seaward side of the trench. In far westward distance to the trench, our model shows the Moho in a depth of 10.5 km. Underneath the trench it reaches down to 13 km, below the continent we estimate the CMB at a depth of 18 km. The layer between the subducting oceanic crust and the overlaying continental crust is about 800 meters thick next to the trench and is thinning with increasing distance to the trench. The thickness is however not constrained well by our data, although the strength of the reflections indicate a pronounced velocity inversion. This thin low velocity layer is interpreted as subducted sediment below the decollement.

Figure 5.3.2.1. Location map and OBS/OBH location for Profile SO 159 - P02

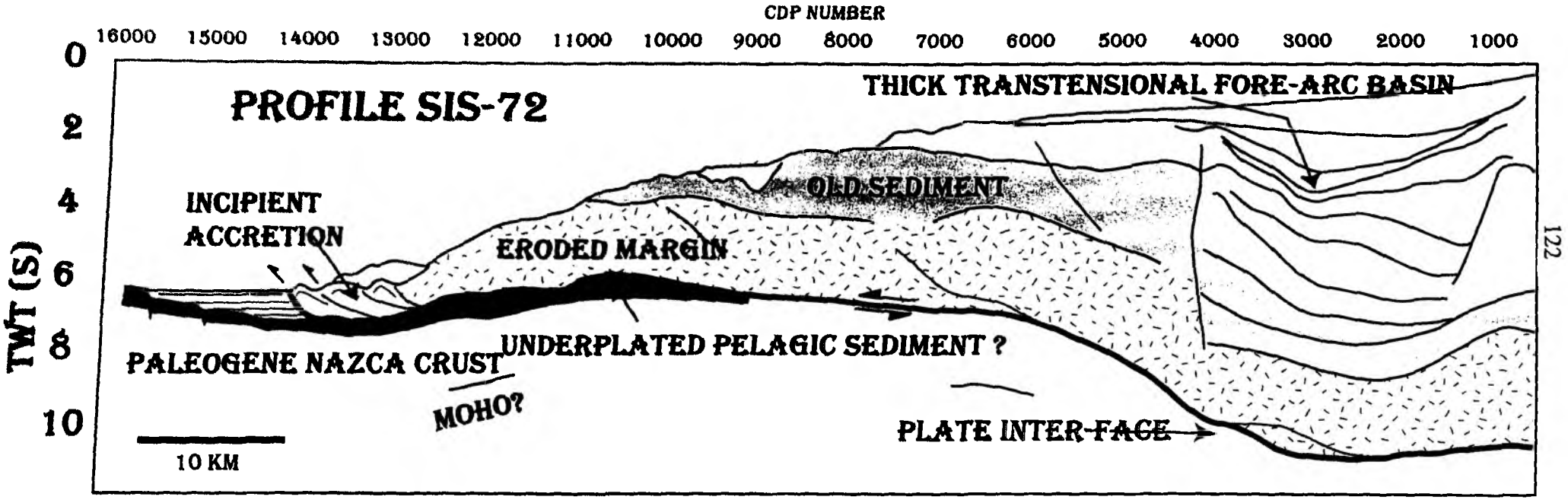
CDP NUMBER
16000
15000
14000
13000
12000
11000
10000
9000
8000
7000
6000
5000
4000
3000
2000
1000
0
2
4
6
8
10
TWT (S)
PROFILE SIS-72
THICK TRANSTENSIONAL FORE-ARC BASIN
OLD SEDIMENT
INCIPIENT
ACCRETION
ERODED MARGIN
UNDERPLATED PELAGIC SEDIMENT ?
PALEOGENE NAZCA CRUST
MOHO?
PLATE INTER-FACE
10 KM

Figure 5.3.2.2

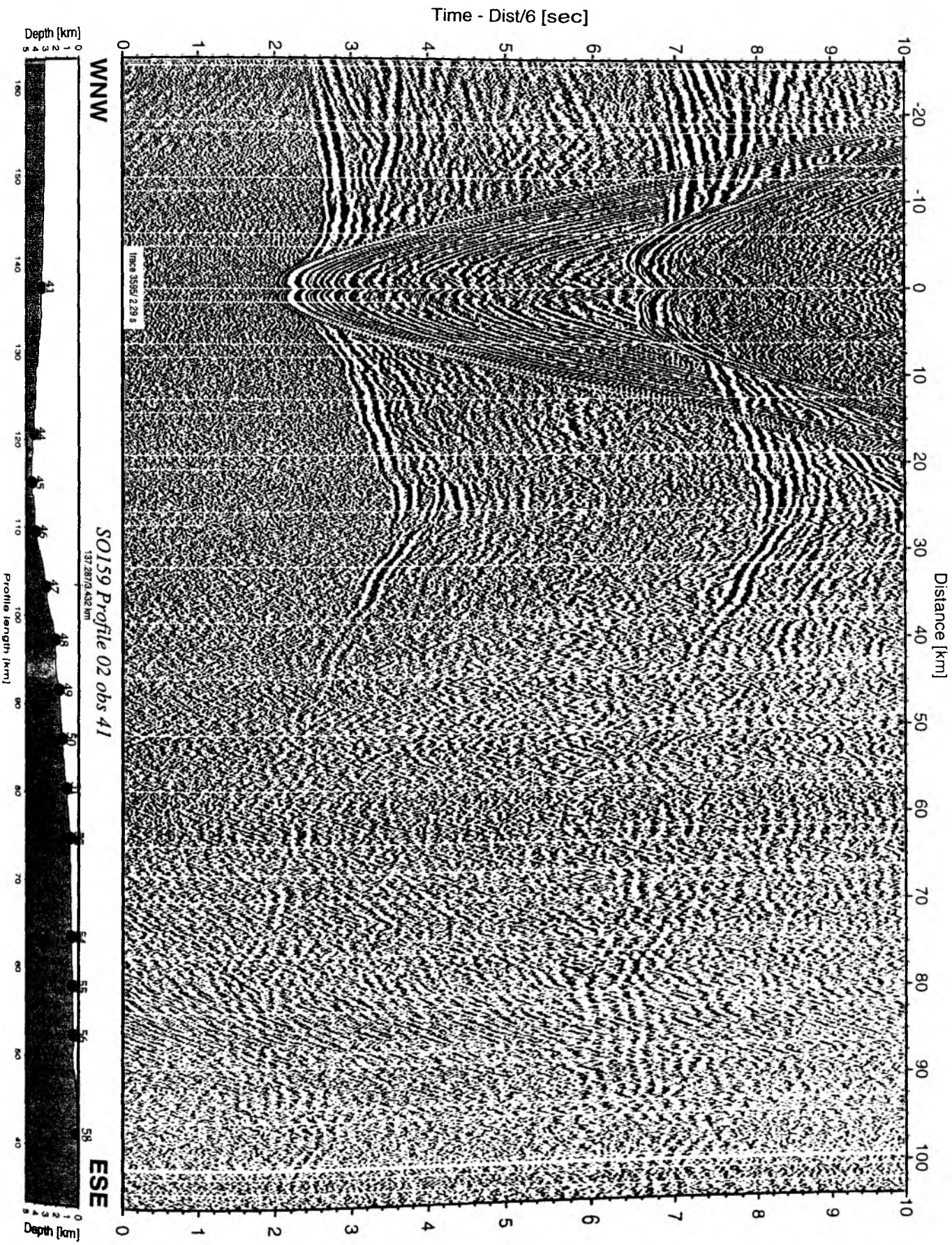

Figure 5.3.2.3: Record section from obs 41 hydrophone, Profile 02.

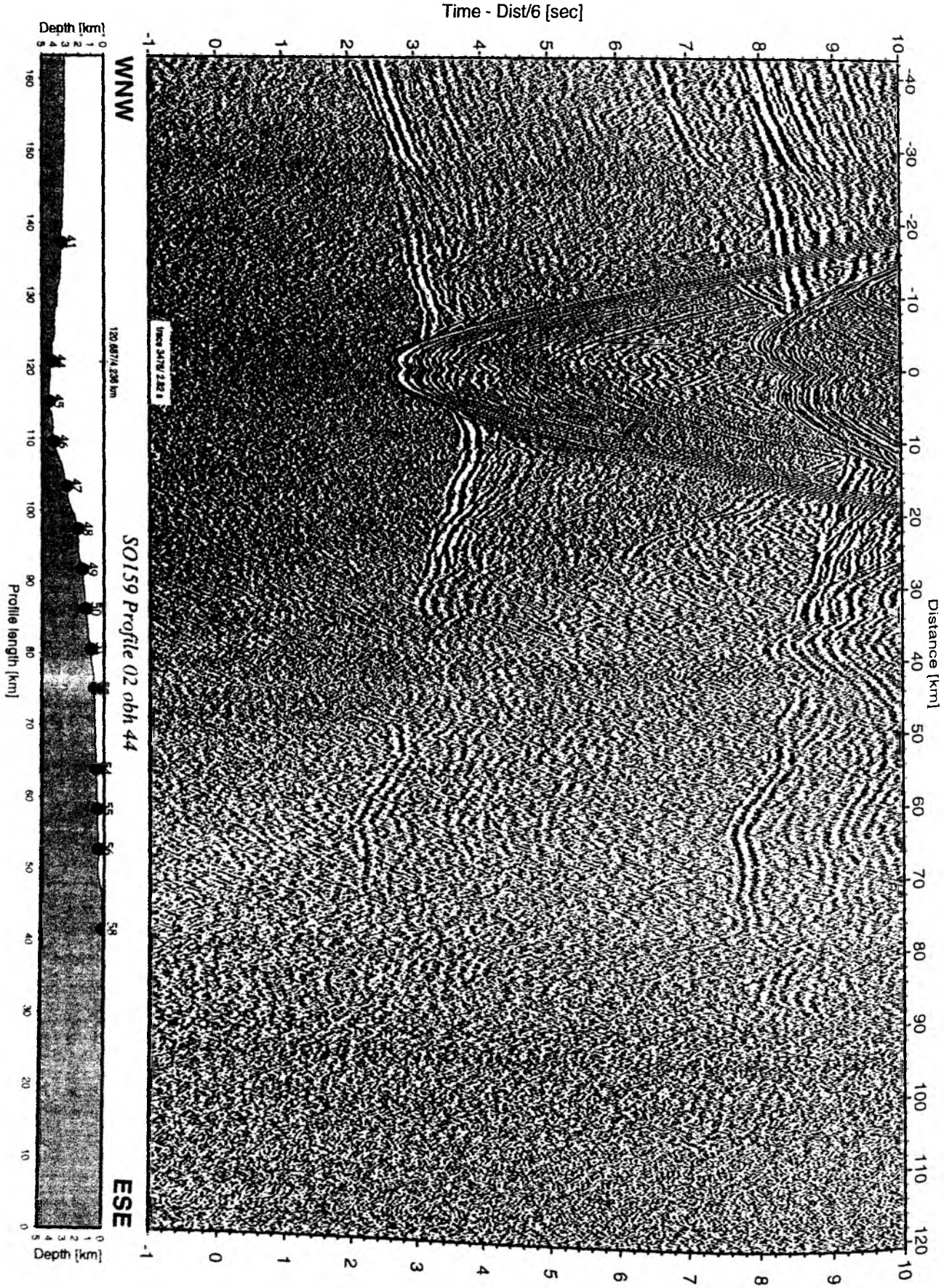

Figure 5.3.2.4: Record section from obh 44 , Profile 02.

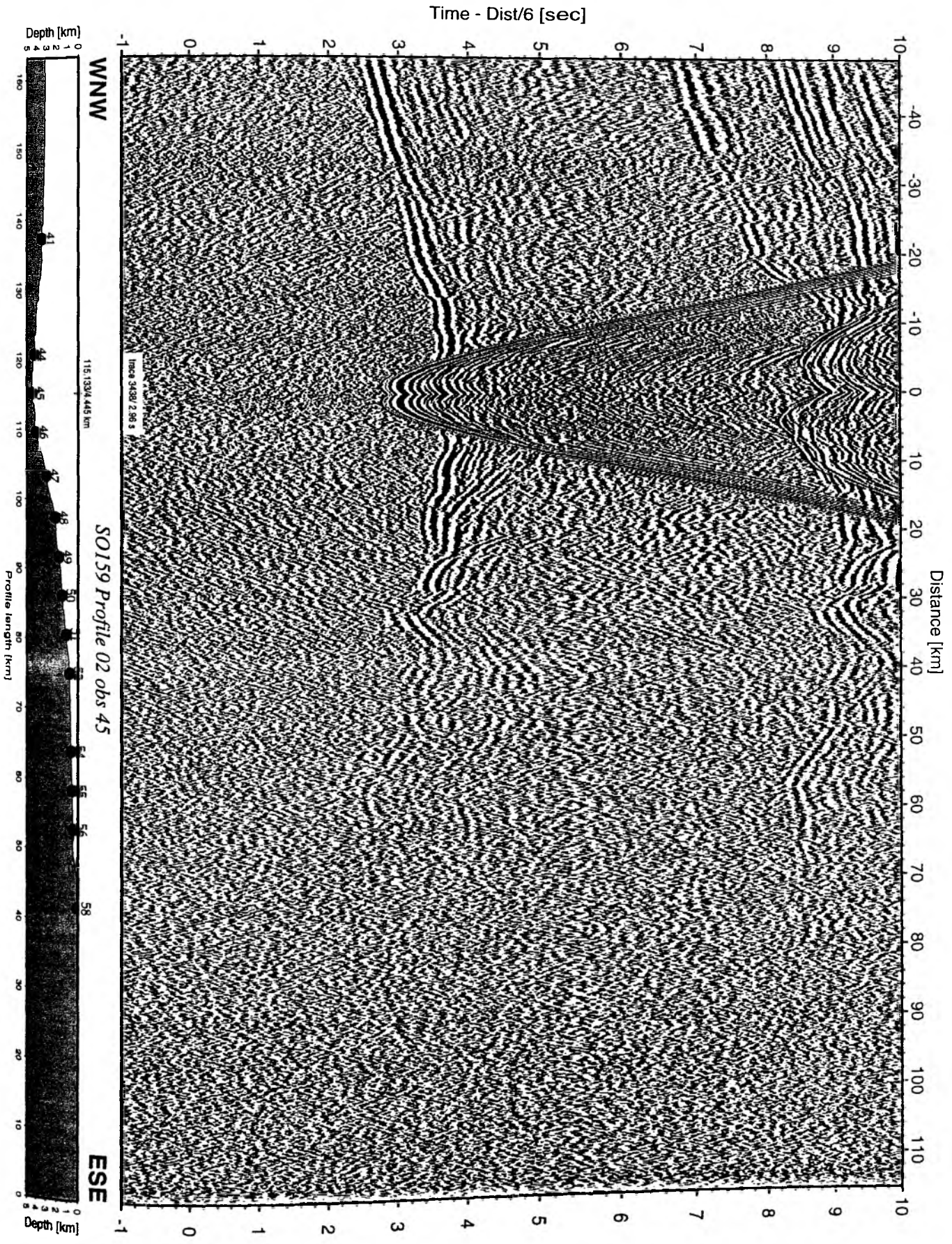

Figure 5.3.2.5: Record section from obs 45 hydrophone, Profile 02.

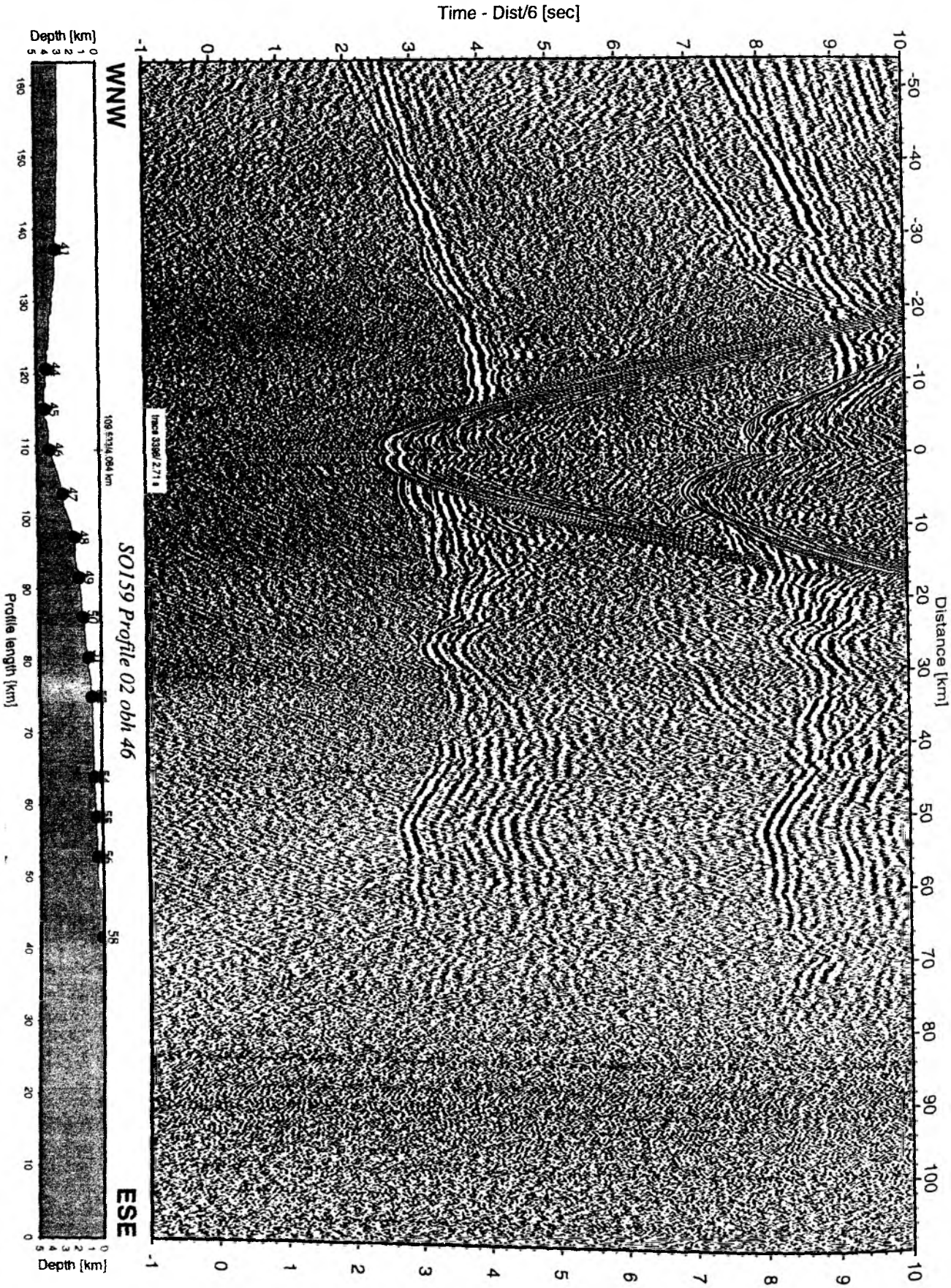

Figure 5.3.2.6: Record section from obh 46 , Profile 02.

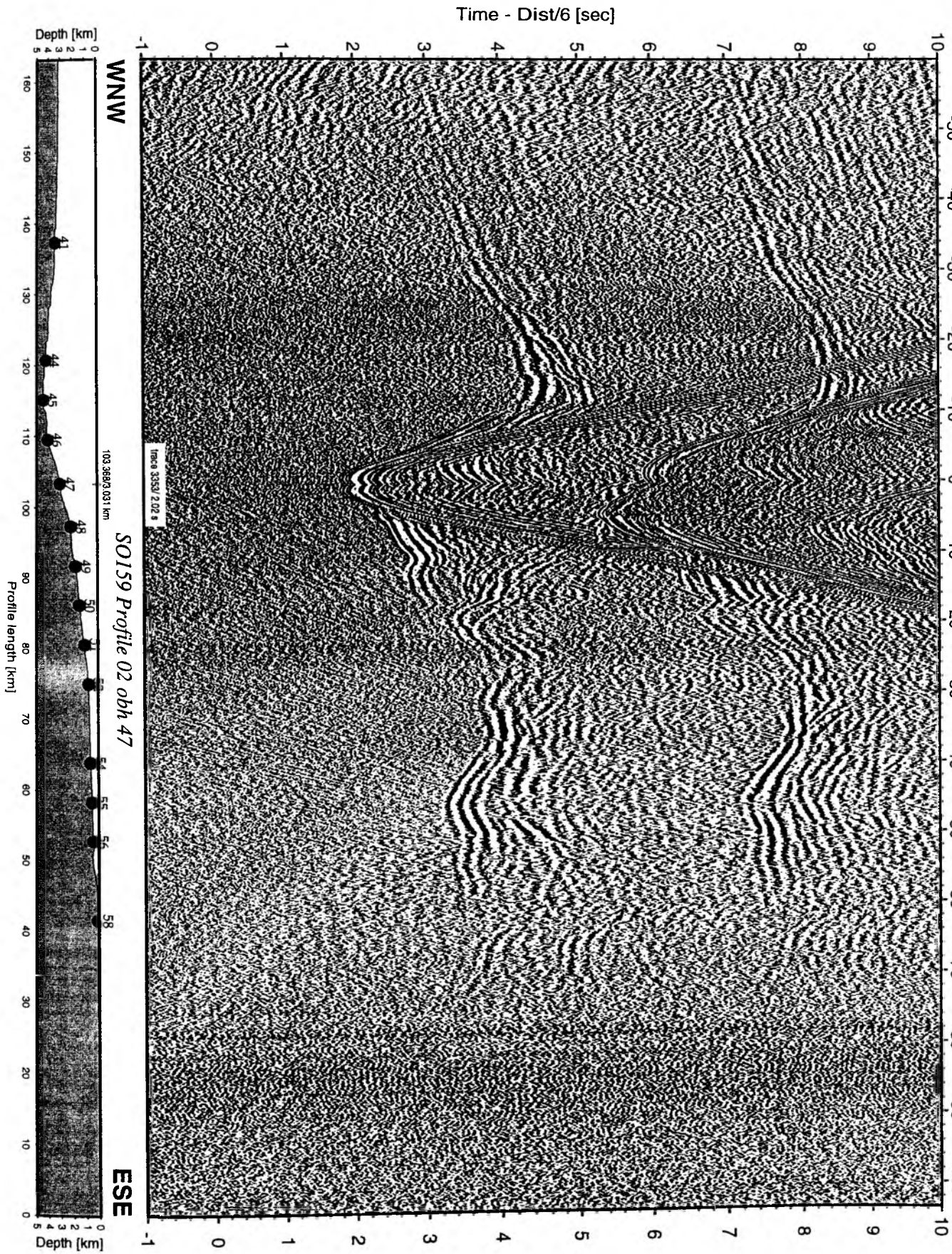

Figure 5.3.2.7: Record section from obh 47 , Profile 02.

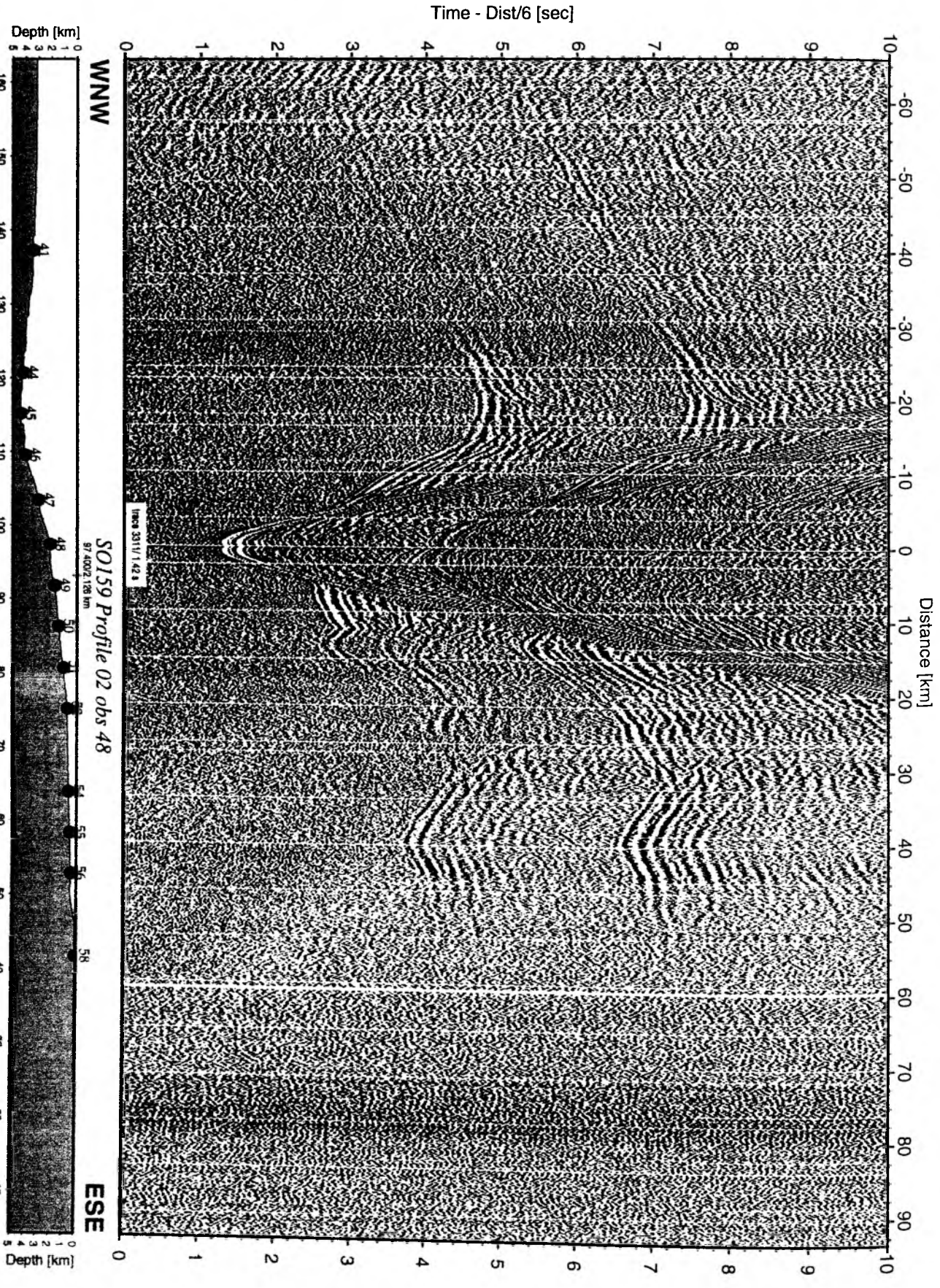

Figure 5.3.2.8: Record section from obs 48 hydrophone, Profile 02.

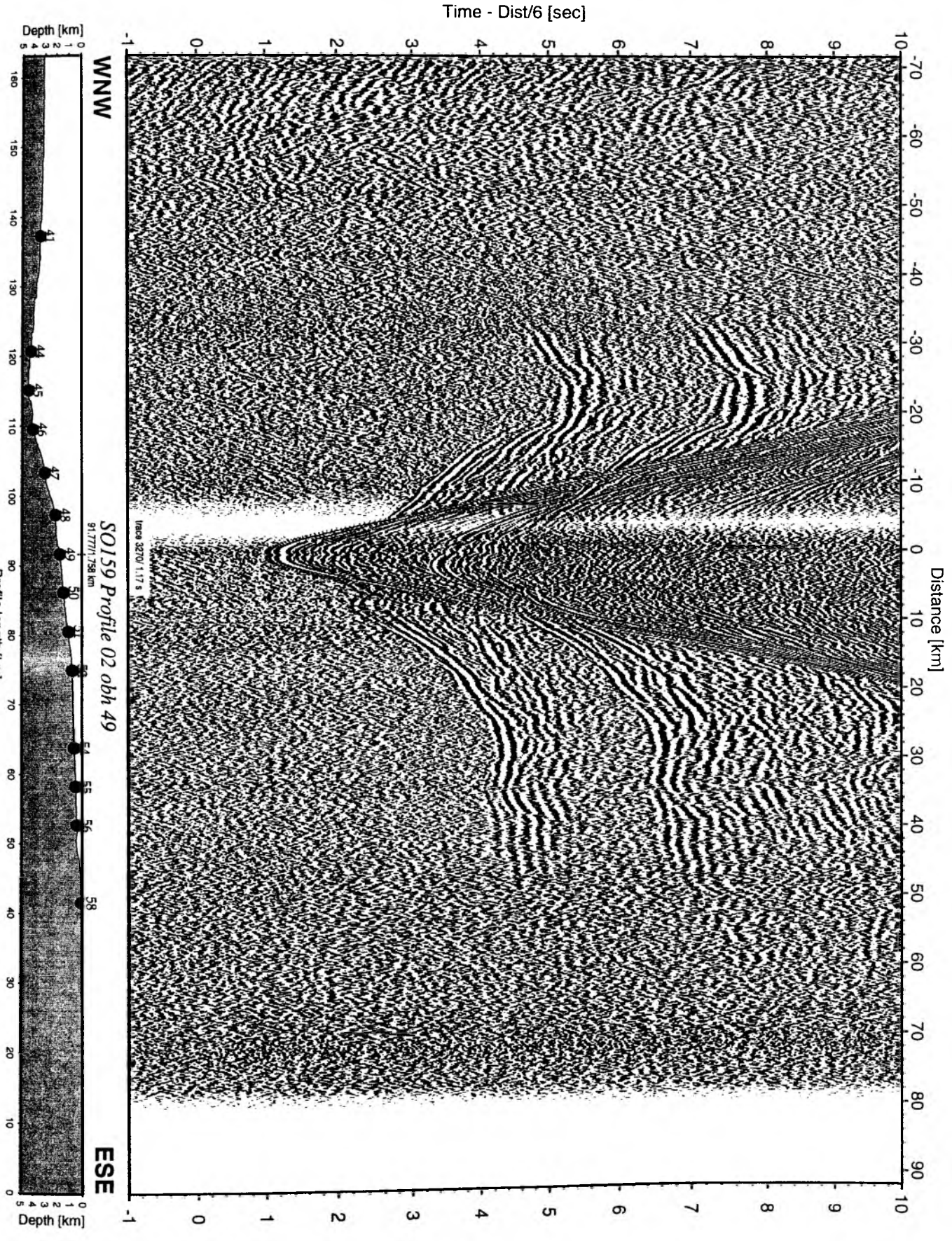

Figure 5.3.2.9: Record section from obh 49 , Profile 02.

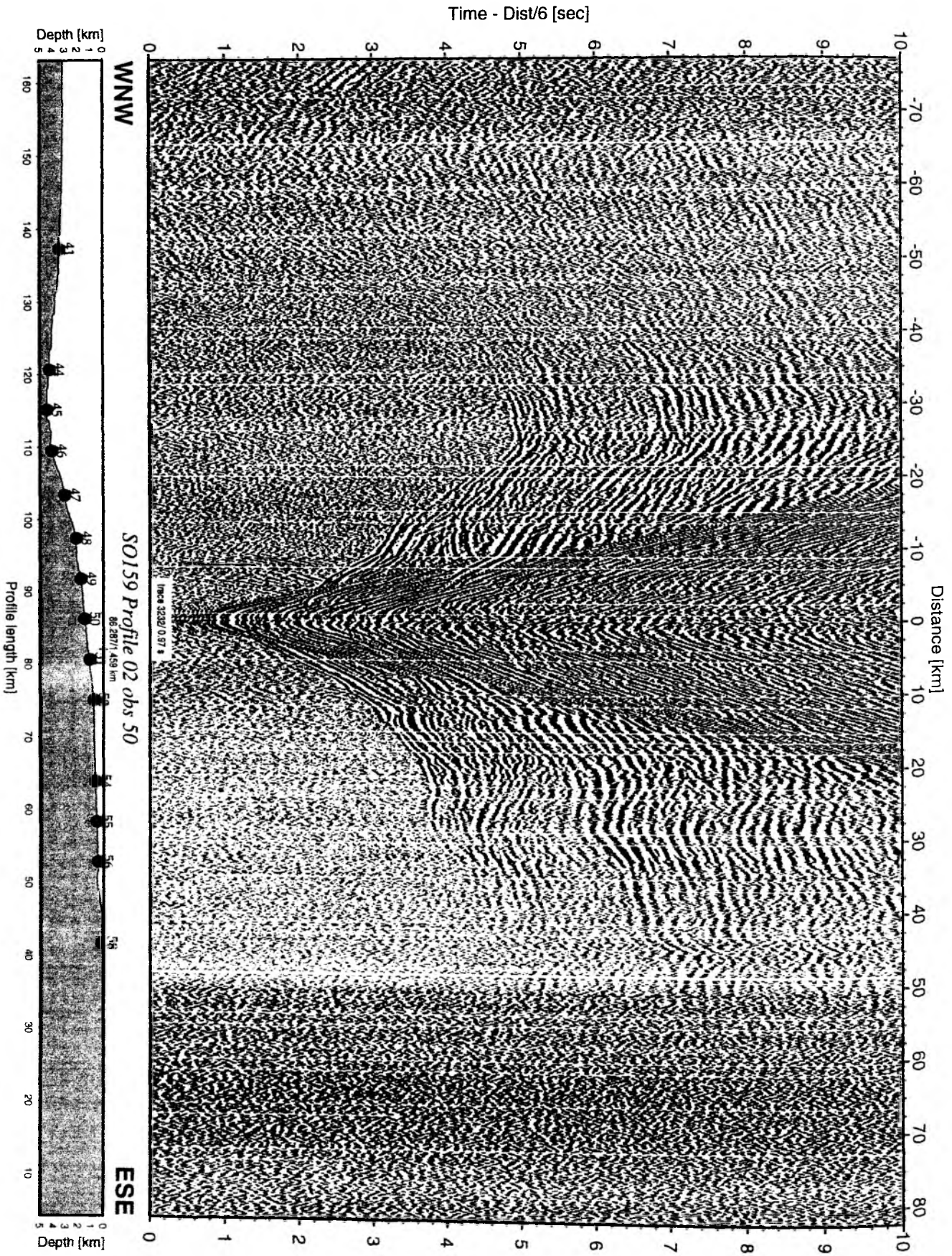

Figure 5.3.2.10: Record section from obs 50 vertical component, Profile 02.

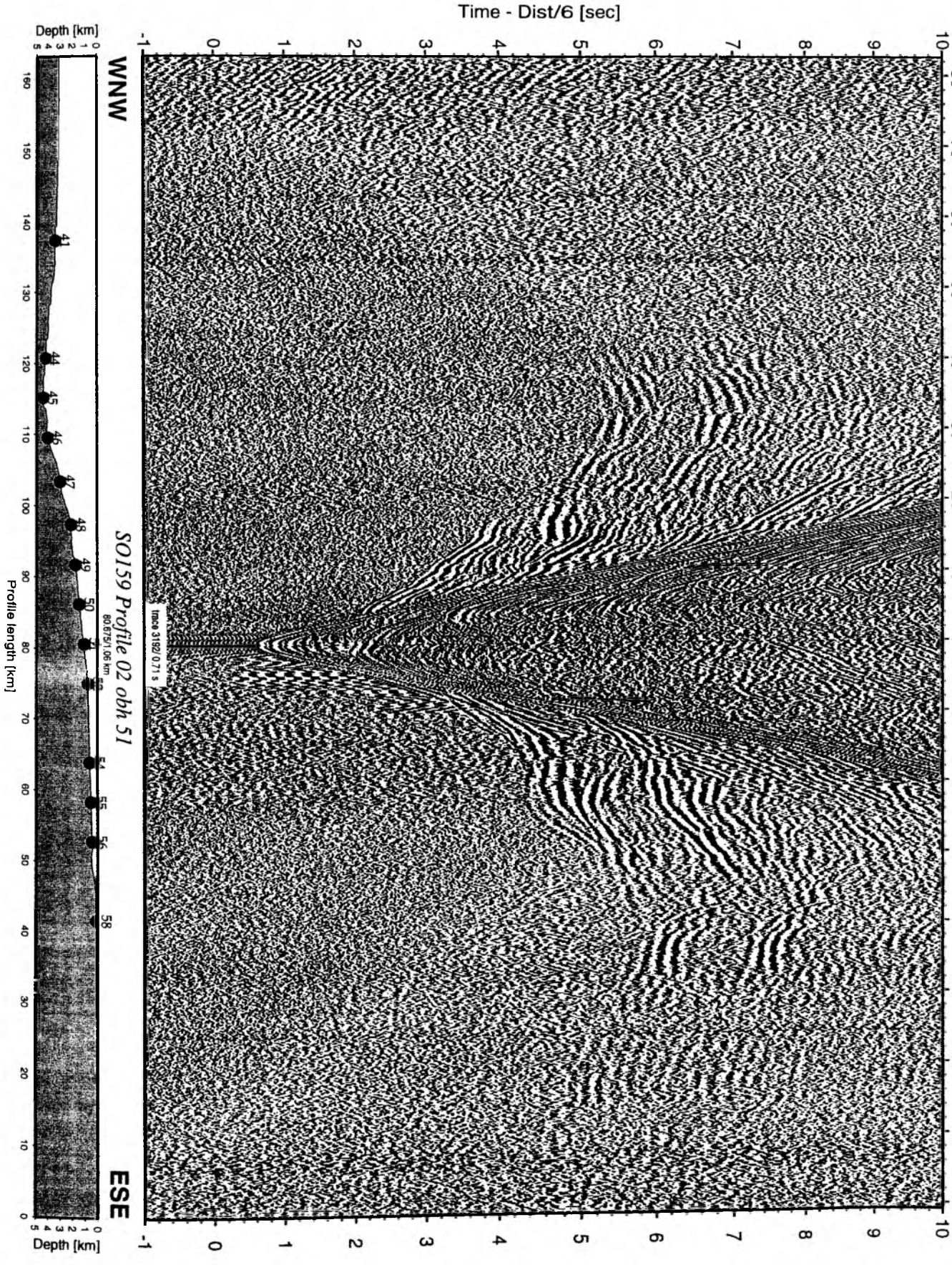

Figure 5.3.2.11: Record section from obh 51 , Profile 02.

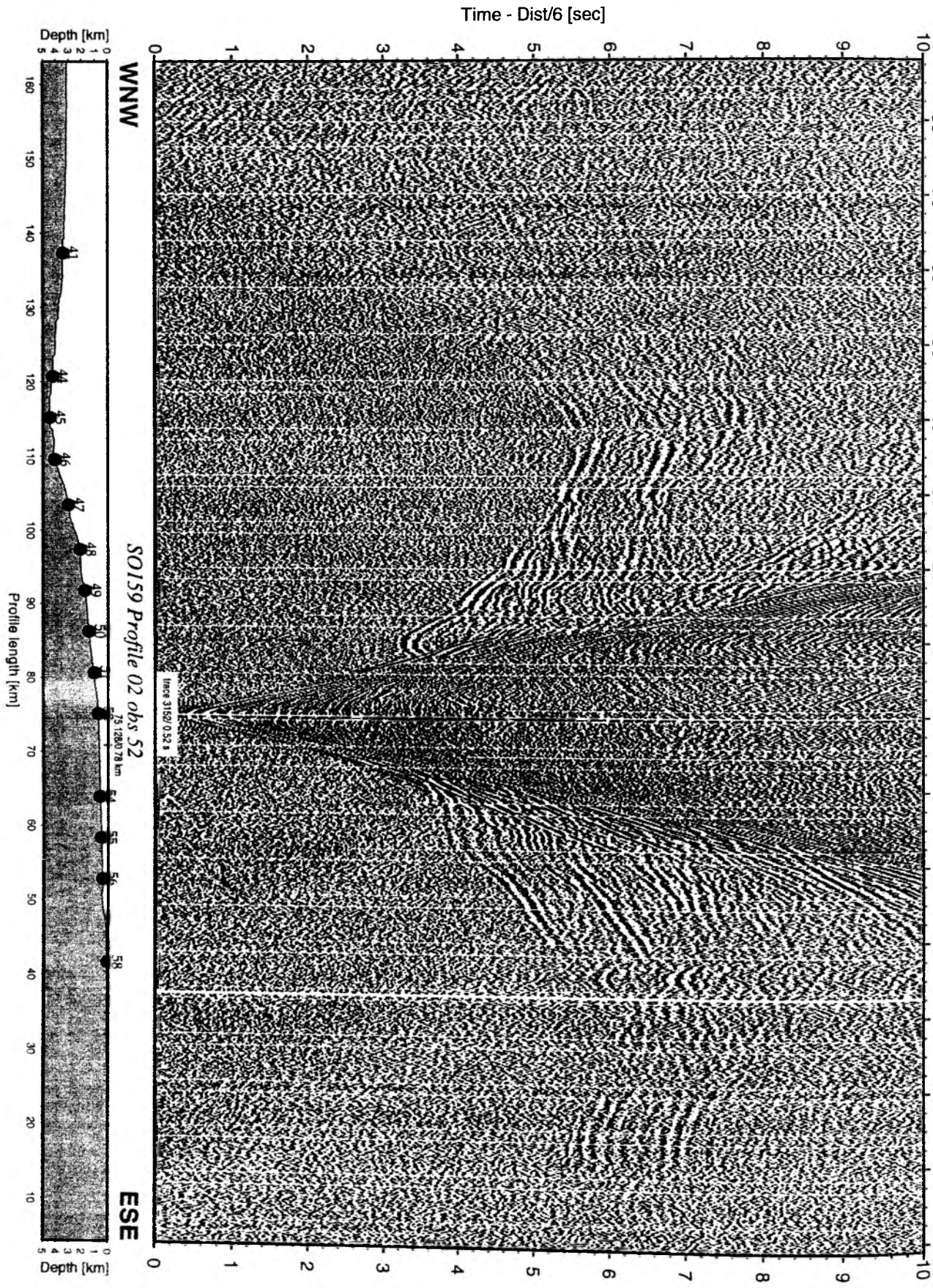

Figure 5.3.2.12: Record section from obs 52 hydrophone, Profile 02.

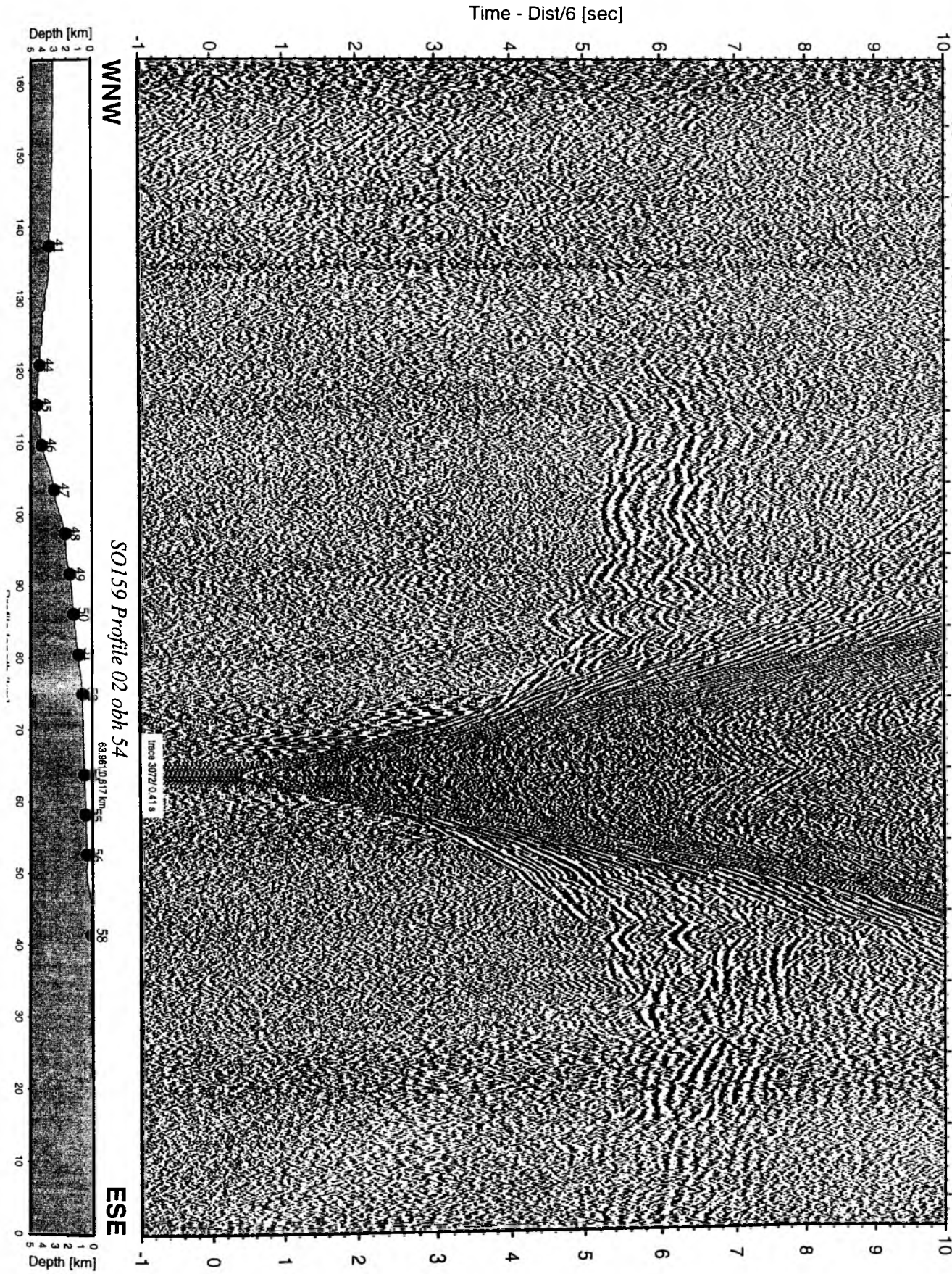

Figure 5.3.2.13: Record section from obh 54 , Profile 02.

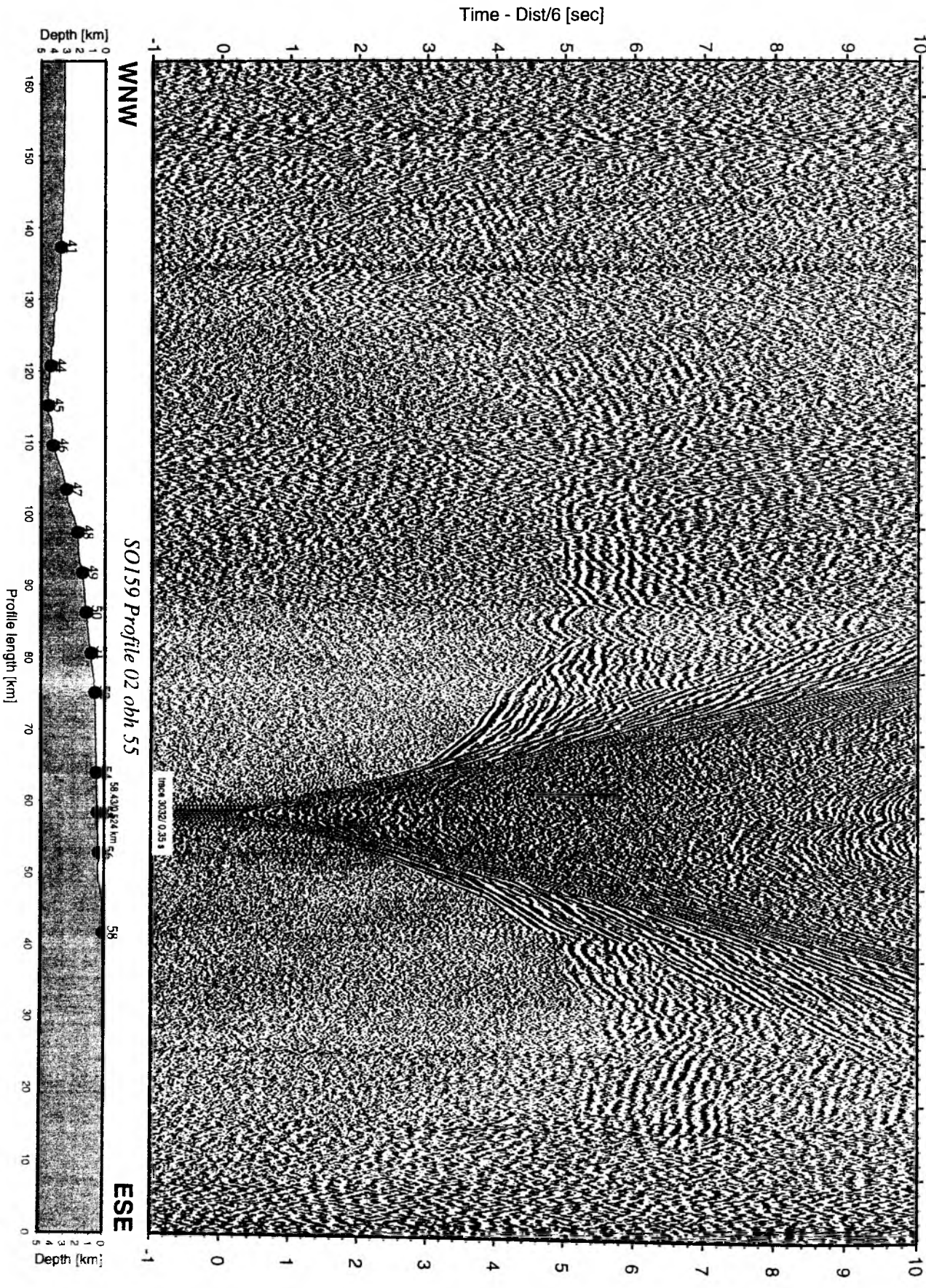

Figure 5.3.2.14: Record section from obh 55 , Profile 02.

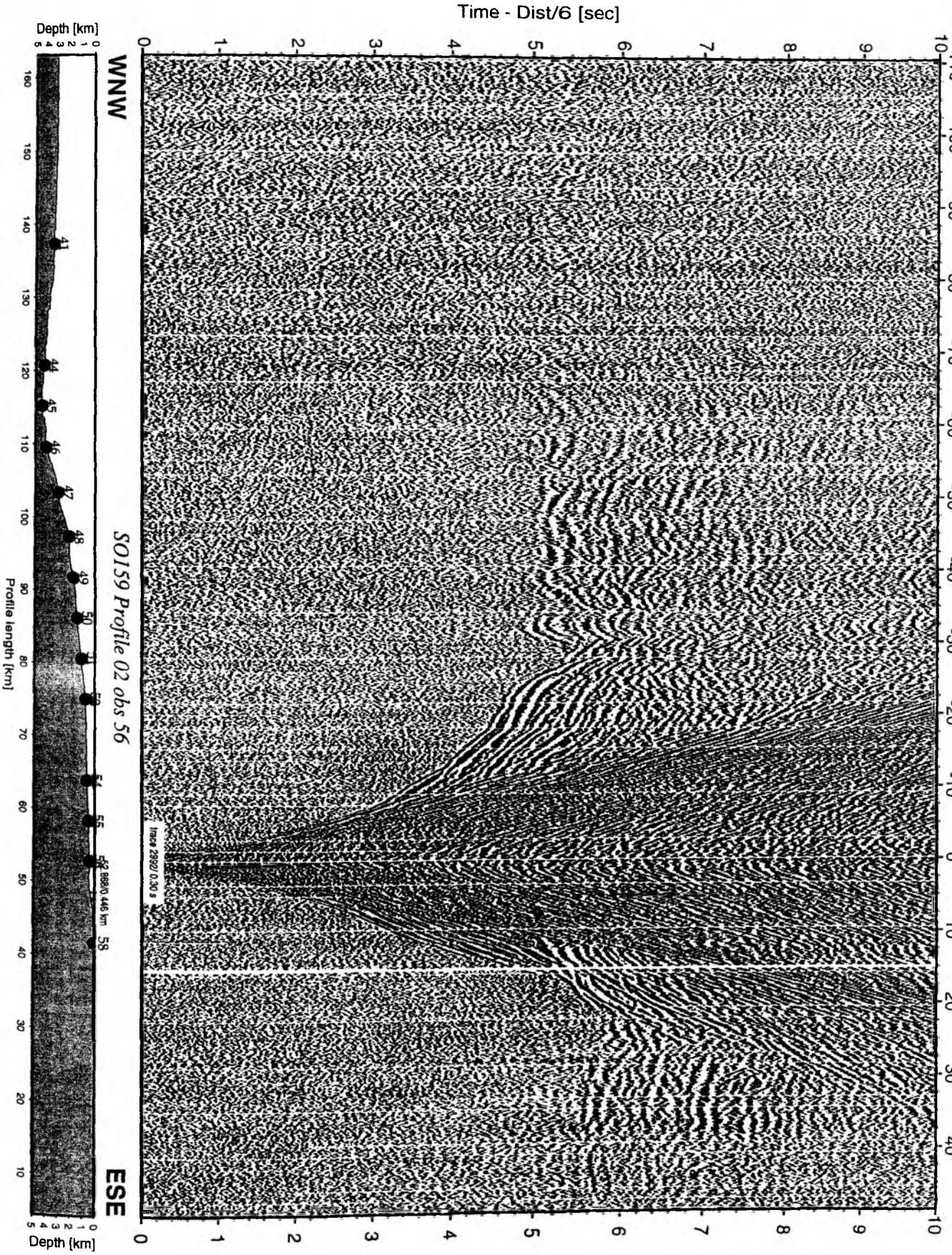

Figure 5.3.2.15: Record section from obs 56 vertical component, Profile 02.

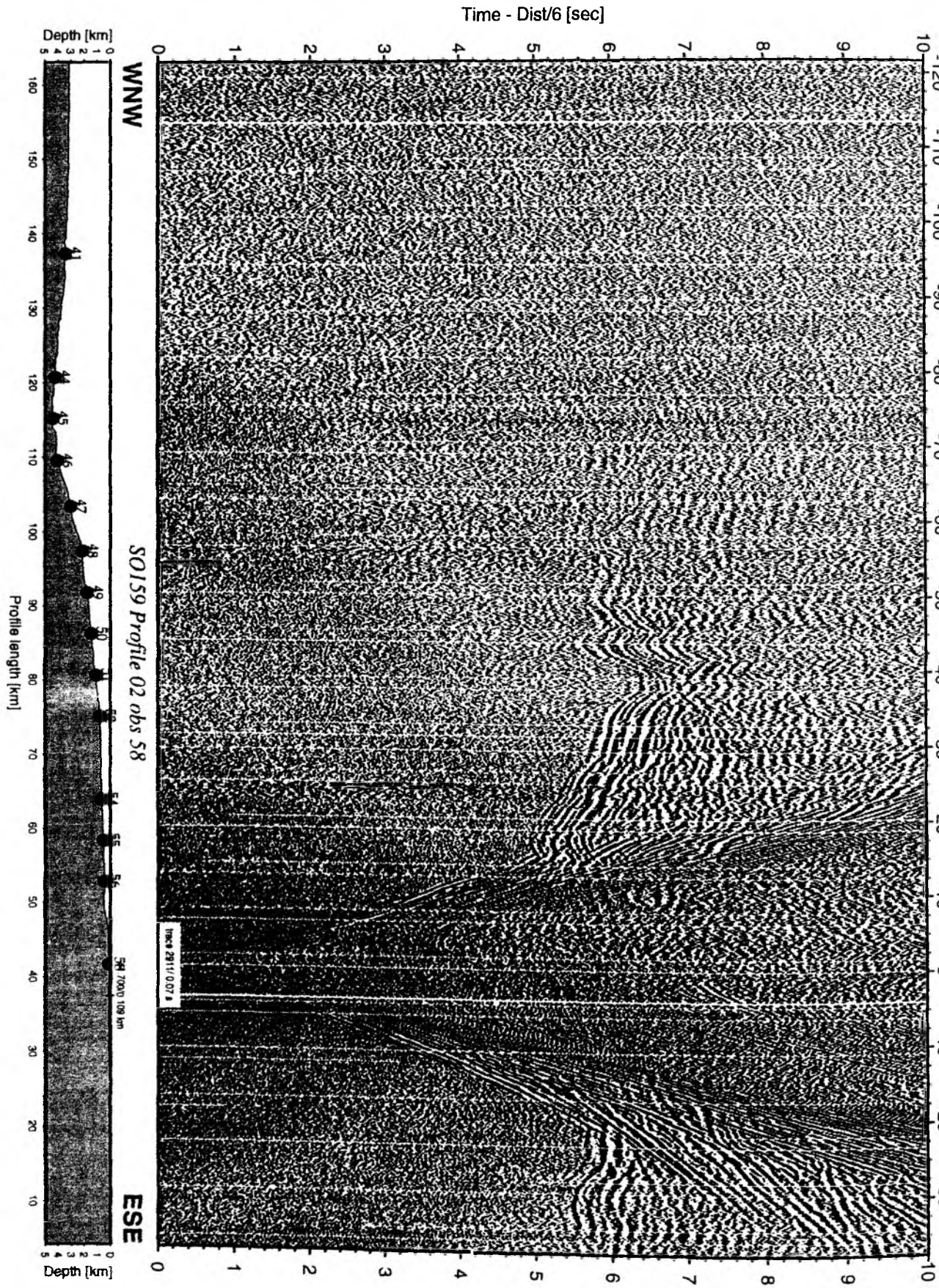

Figure 5.3.2.16: Record section from obs 58 hydrophone, Profile 02.

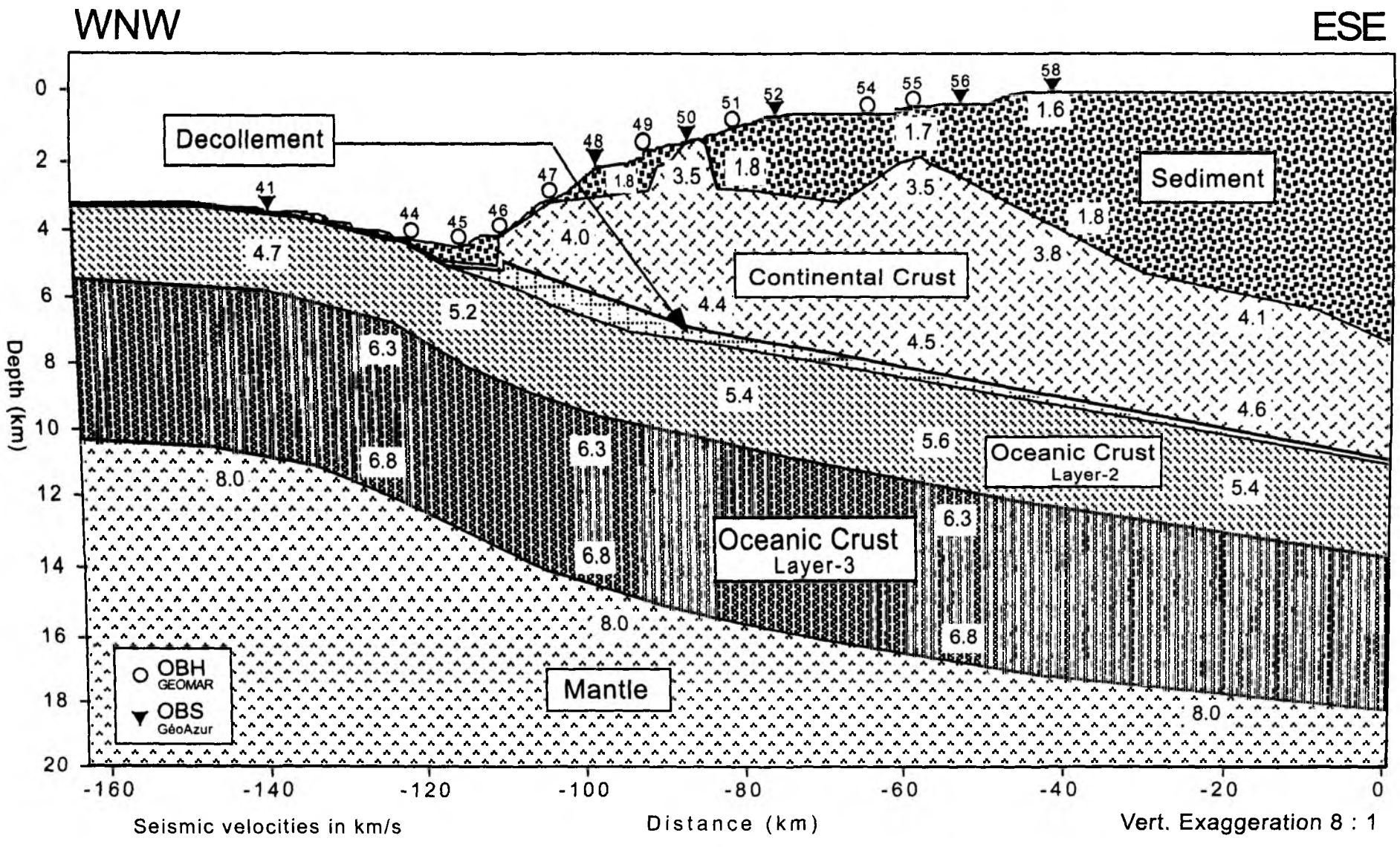

Figure 5.3.2.17

5.3.3 Profile SO 159-03

(C. Walther, E. Flüh)

Profile 03 was intended to study the subduction channel on the ecuadorian margin, that is so prominent on multichannel seismic reflection data collected in 2000 during the French SISTEUR cruise. The location of the line and the instruments is shown in Figure 5.3.3.1. An example of the subduction channel from the MCS data is shown in Figure 5.3.3.2.
In total 9 OBS (OBH/S59 to 66 and OBS48) were deployed at 3 nm intervals in the morning of September 03. Shooting was made using two airguns without any interruption at a speed of 4.5 kn with 60 sec shot interval at the far end, which was later decreased to 40s. Thus a shot spacing of apr. 135 m in the far offset and of 90 m for the main part of the line was achieved. During shooting the magnetometer was also deployed (see chapter 5.2). All instruments were recovered, with one instrument showing a disc failure (OBH 59), that could not be solved onboard (see Appendix II-2). These record sections are shown in Figures 5.3.3.3 to 5.3.3.??.

Model description from 2-D forward modeling

A preliminary interpretation of this dataset was done at sea.
From the location map it is evident (Figure 5.3.3.1), that the orientation of profile 3 is not parallel to the general strike direction, but somewhat oblique. The SSW profile part runs along the steeper part of the continental slope in about 3000 m waterdepth and close to the trench, the NNE part is located in a more shallow part of the slope in about 2000 m waterdepth and more distant to the trench.
At the beginning of the profile two deeper parts at 10 and 20 km are evident and belong to canyons running perpendicular to the profile as indicated in the location map (Figure 5.3.3.1). The seismic model clearly underlines the erosional character of these structures. The uppermost model layer has velocities below 2 km/s indicating sediment and an average thickness of 800 m. It completly vanishes in the center of the canyons. OBH 64 and 66 sit on top of the low velocity sediment and the arrivals in their record sections which first precede the waterwave have lower apparent velocities compared to OBH 63 and 65 located in the center of the outcarvings. These OBH show clear refractions from the layer below, which is modeled with 3.4 km/s at the top and 3.9 km/s at the bottom and makes up most of the continental margin wedge in the profile area. In the center of the profile from OBH 62 to 60 velocities within this layer increases to 3.7 km/s at the top and 4.3 km/s at the bottom, but are not well constraint further to the NNE. The pronounced velocity contrast between the upper two layers and the complete erosion of the upper one down to its base but not any deeper may point to much more consolidated sediment below or to a layer of completly different lithology, may be to ophiolites.
The subduction channel indicated in the MCS data is reflected in the seismic wide-angle model by a low velocity zone (LVZ) beneath the continental margin layer. Clear constraints for this LVZ come from OBH 60, 62, 63 and 66, all to the NNE, where a bright reflection is visible in the record sections at about 4 s reduced traveltime and 10 to 15 km offset. It has a 0.5 to 1 s time offset to the preceding refraction branch. However, the other OBH/S on the profile do not show this time offset and so the LVZ is postulated to be of variable thickness and velocity. The most obvious explanation for this layer that marks the plate boundary is subducted sediment.
In the near offset part of the bright reflection a refracted phase emerges with apparent velocities mostly > 6 km/s and is modeled to derive from a layer with 6.5 km/s at the top and 6.8 km/s at the base. It is interpreted as oceanic crust. The depth of this layer increases in the NNE, because of the oblique orientation of the profile, being close to the trench in the SSW where subduction just started and further inland to the NNE, where the subducting oceanic crust is already in greater depth.
In about 23 to 30 km offset the record sections show increasing amplitudes and indicate an additional seismic phase. It is interpreted as PmP, the reflection from the MOHO, and can be well matched in the model with the base of a 5 to 6 km thick oceanic crust.

Figure 5.3.3.1. Location map and OBS/OBH locations for Profile SO - P03

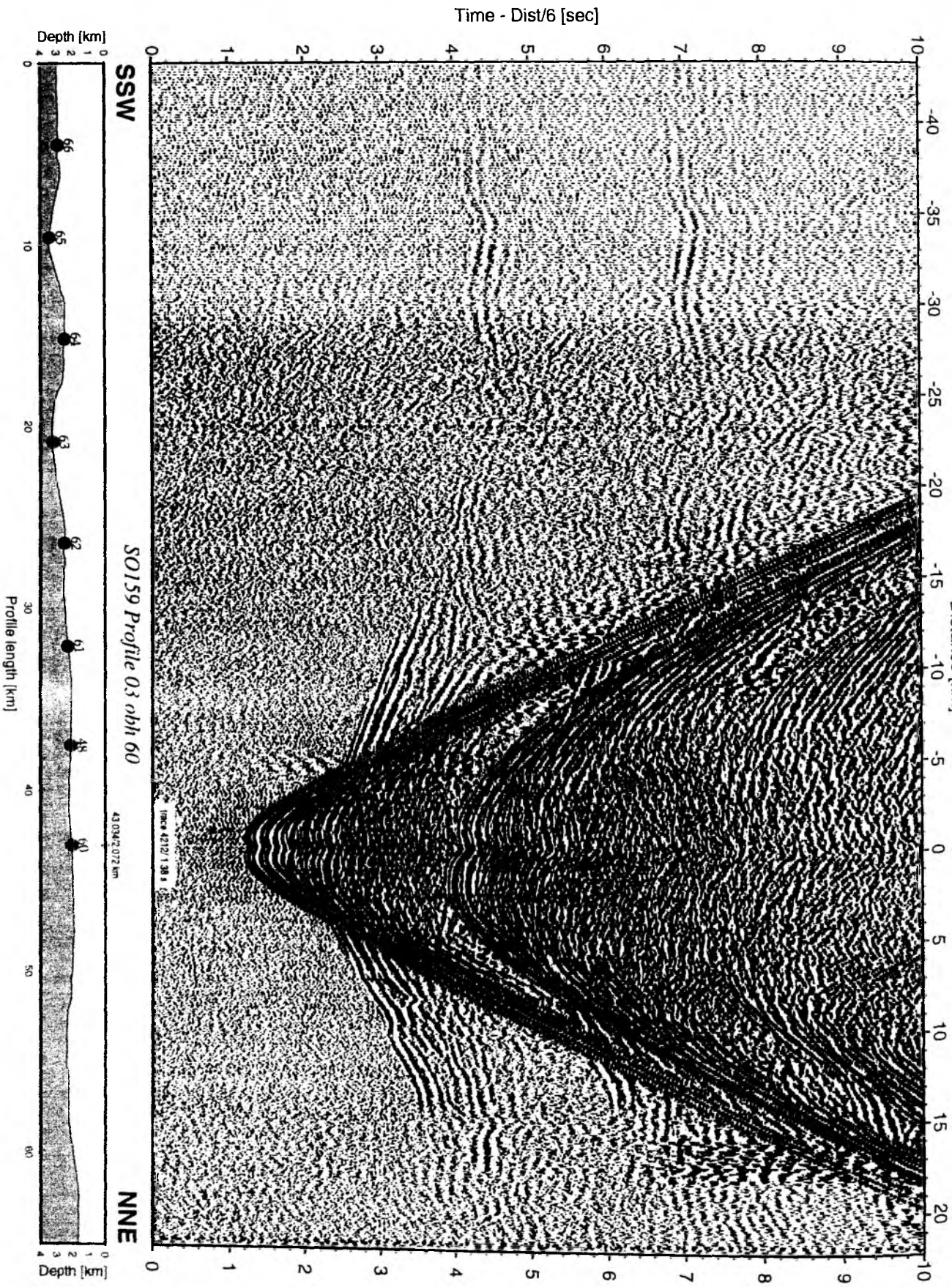

Figure 5.3.3.3: Record section from obh 60 , Profile 03.

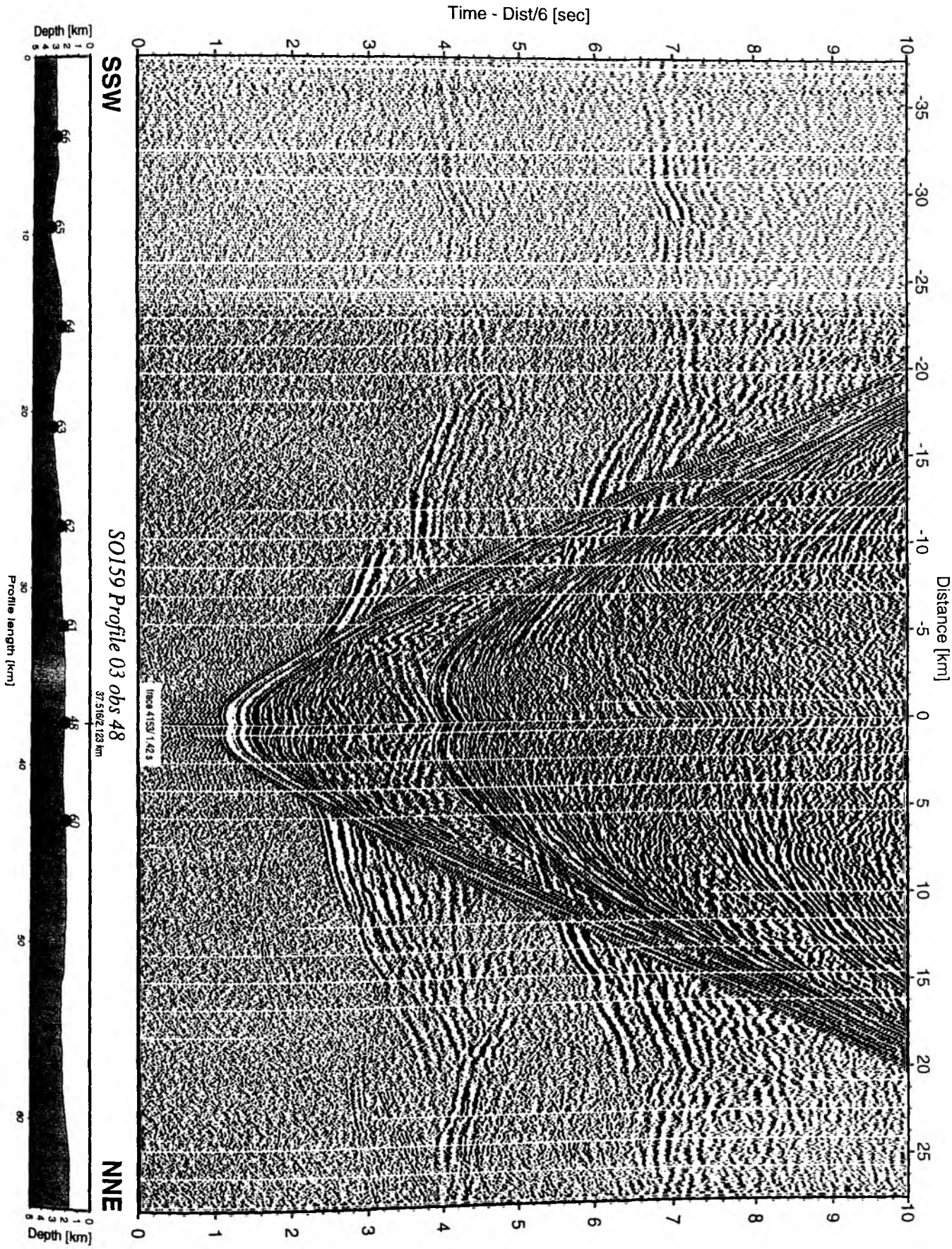

Figure 5.3.3.4: Record section from obs 48 hydrophone, Profile 03.

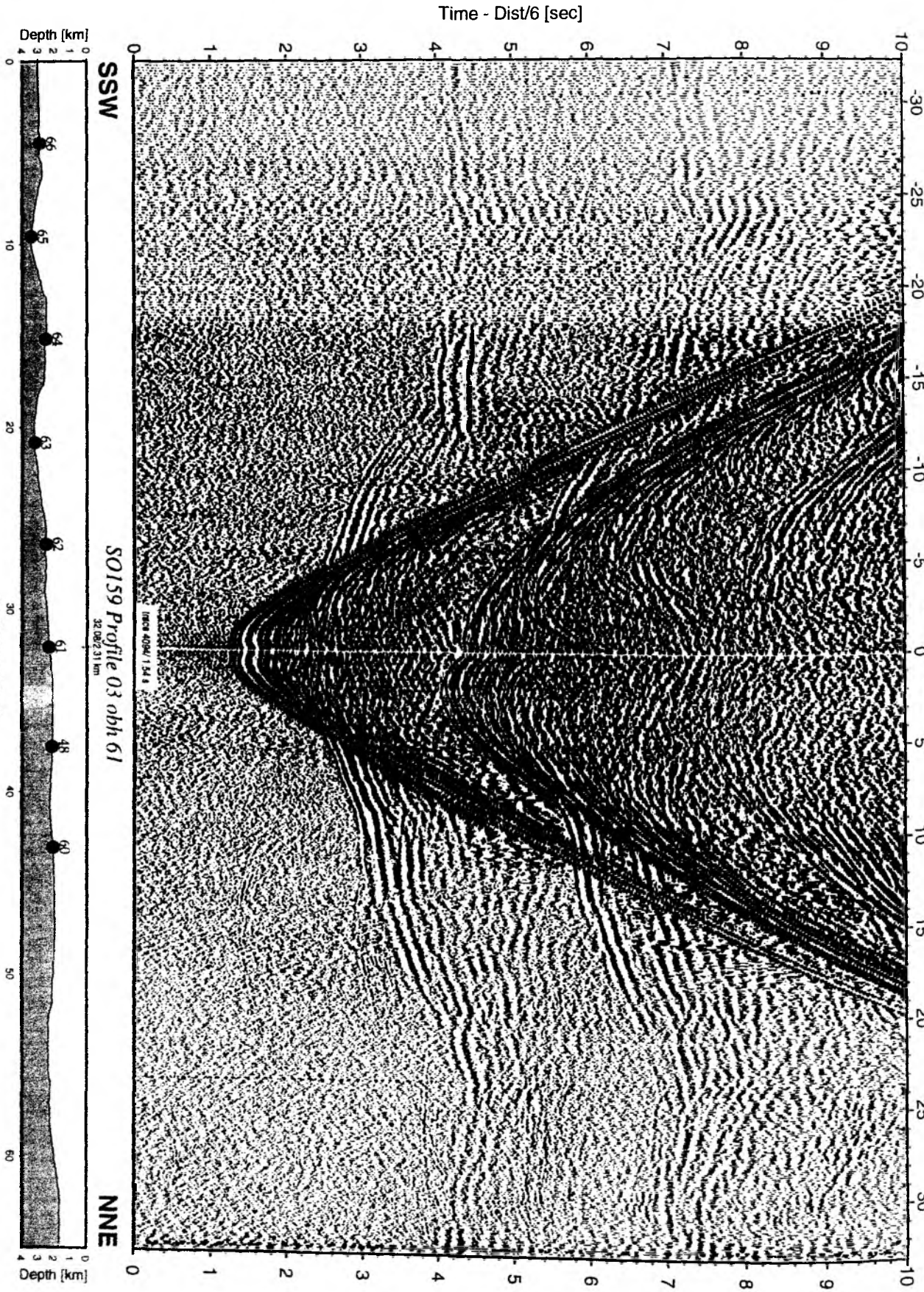

Figure 5.3.3.5: Record section from obh 61 , Profile 03.

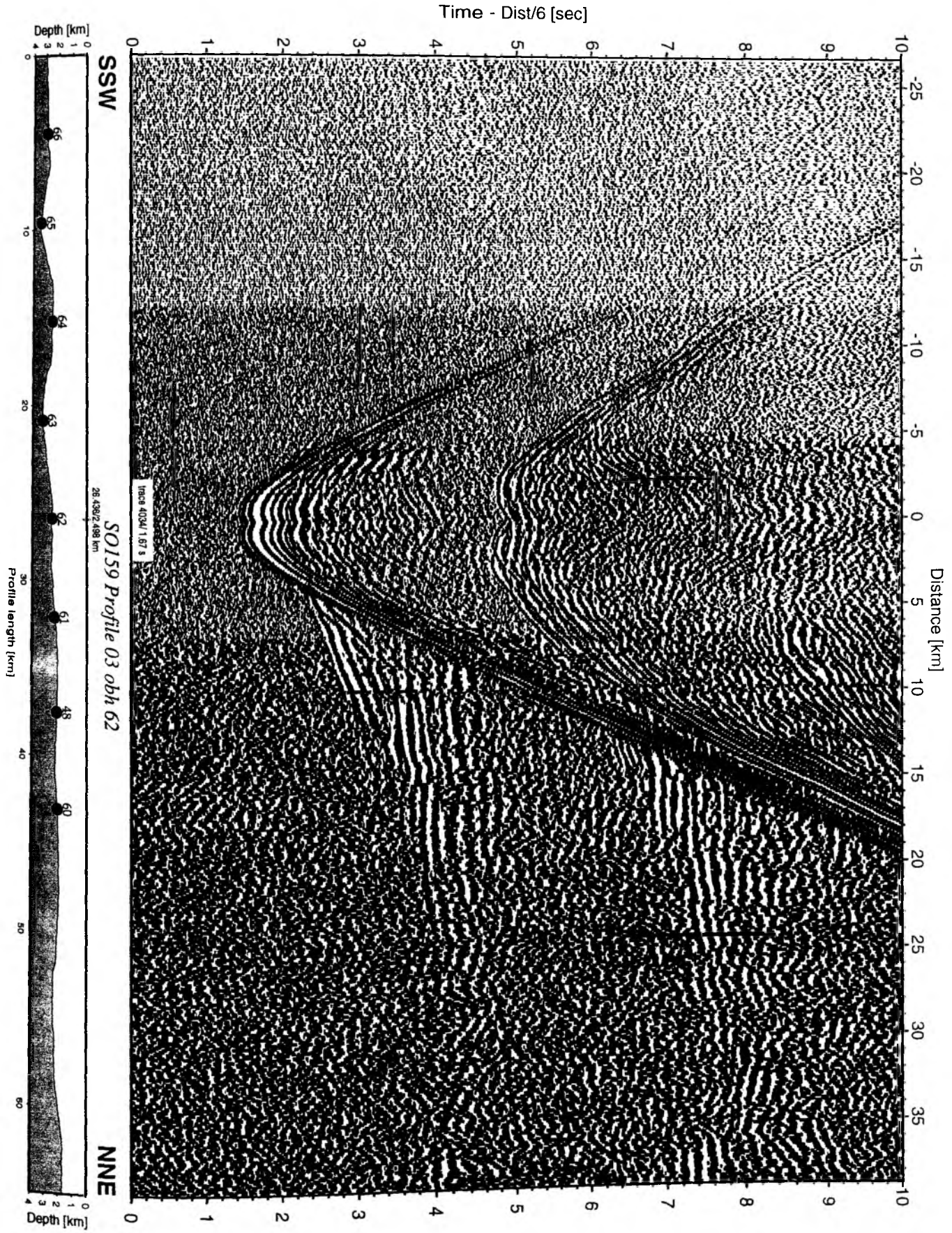

Figure 5.3.3.6: Record section from obh 62 , Profile 03.

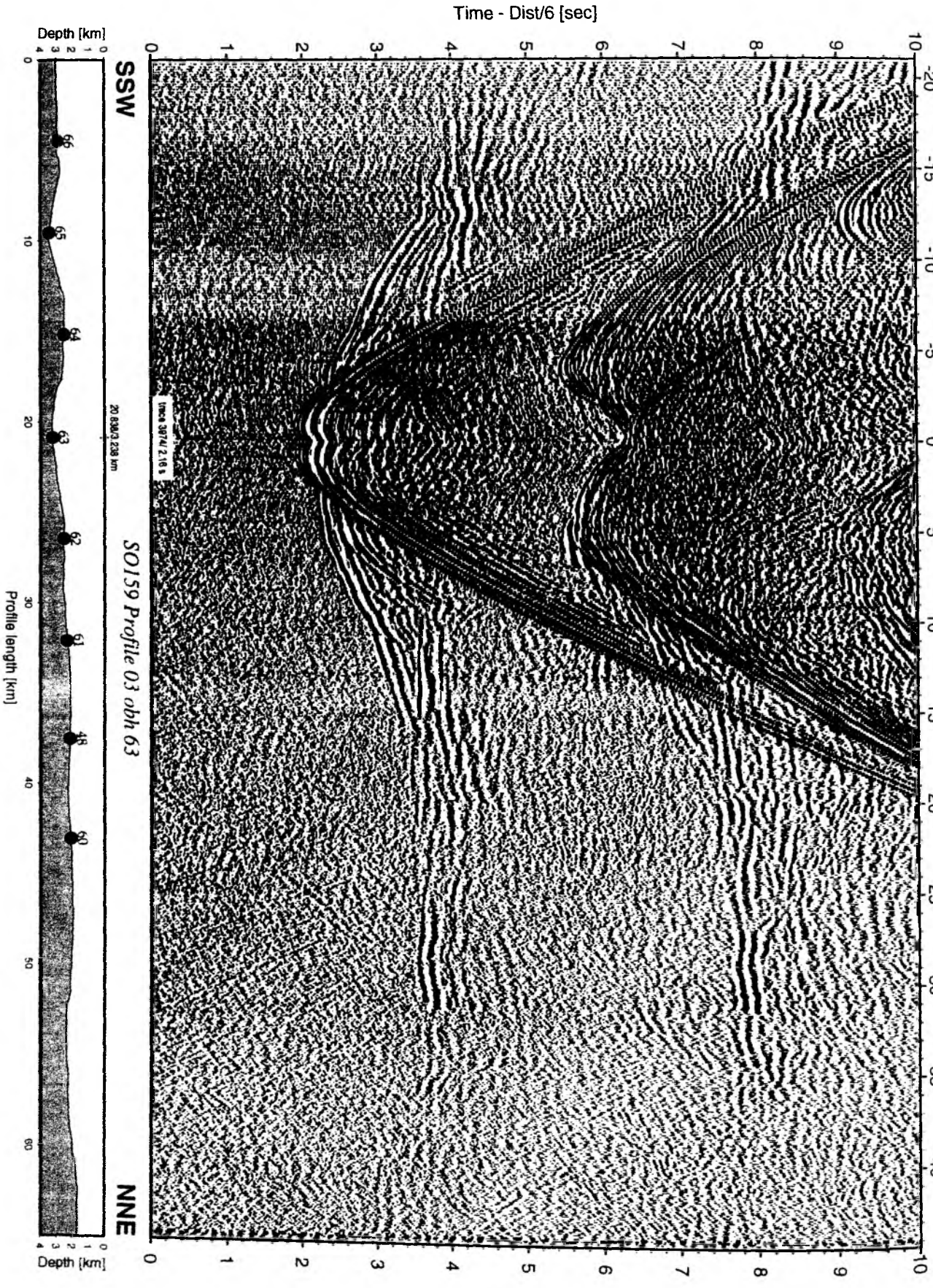

Figure 5.3.3.7: Record section from obh 63 , Profile 03.

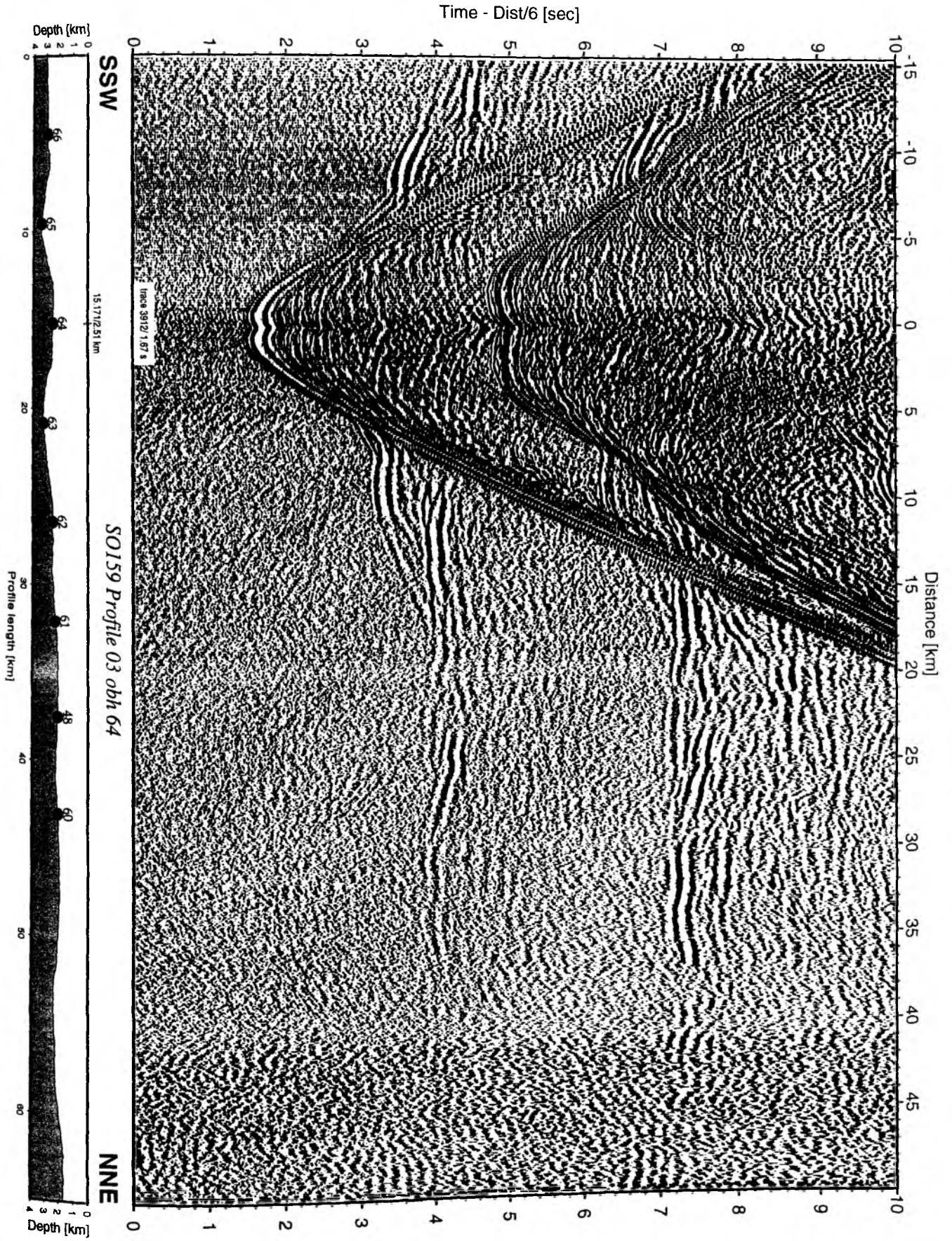

Figure 5.3.3.8: Record section from obh 64 , Profile 03.

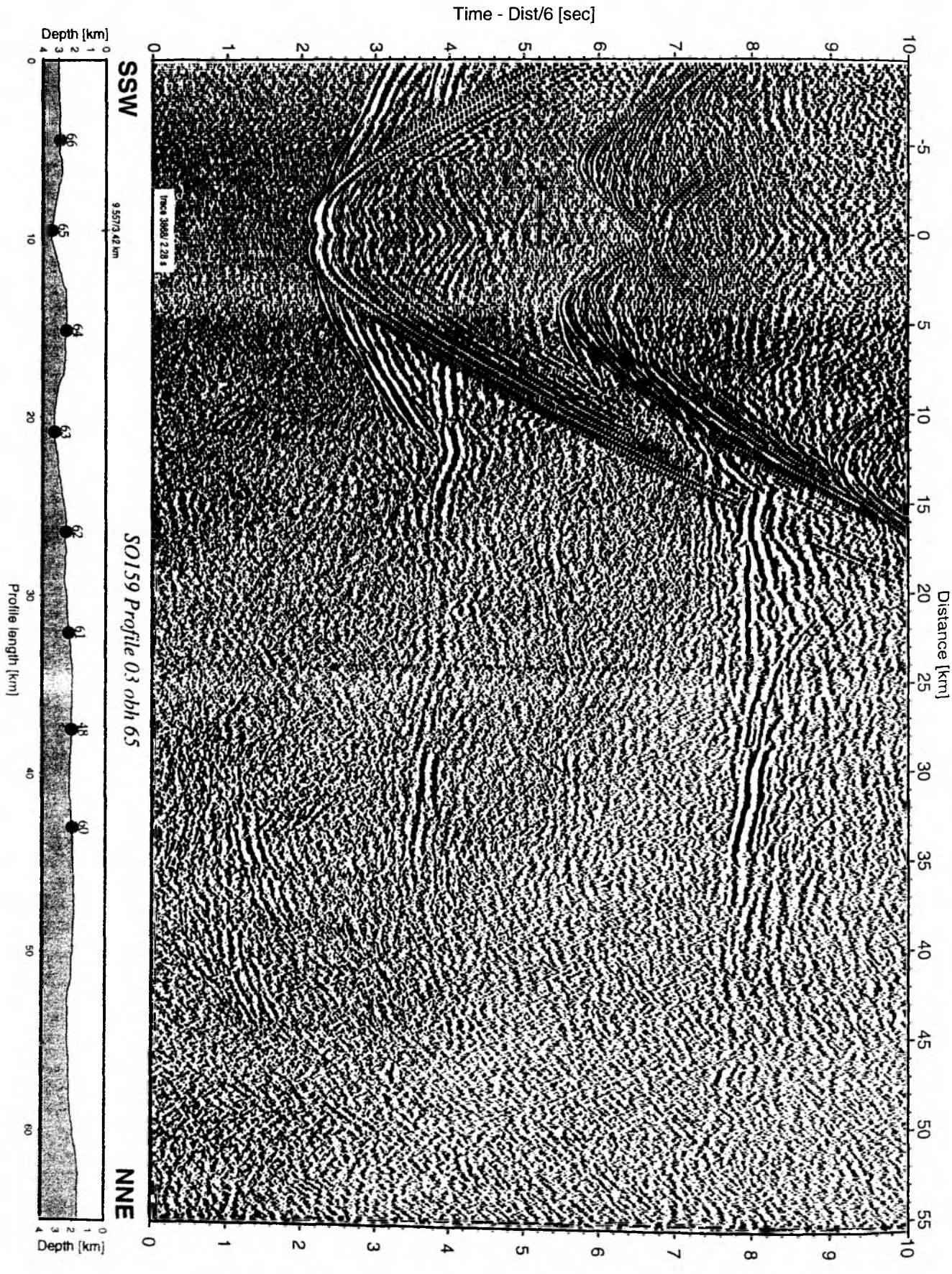

Figure 5.3.3.9: Record section from obh 65 , Profile 03.

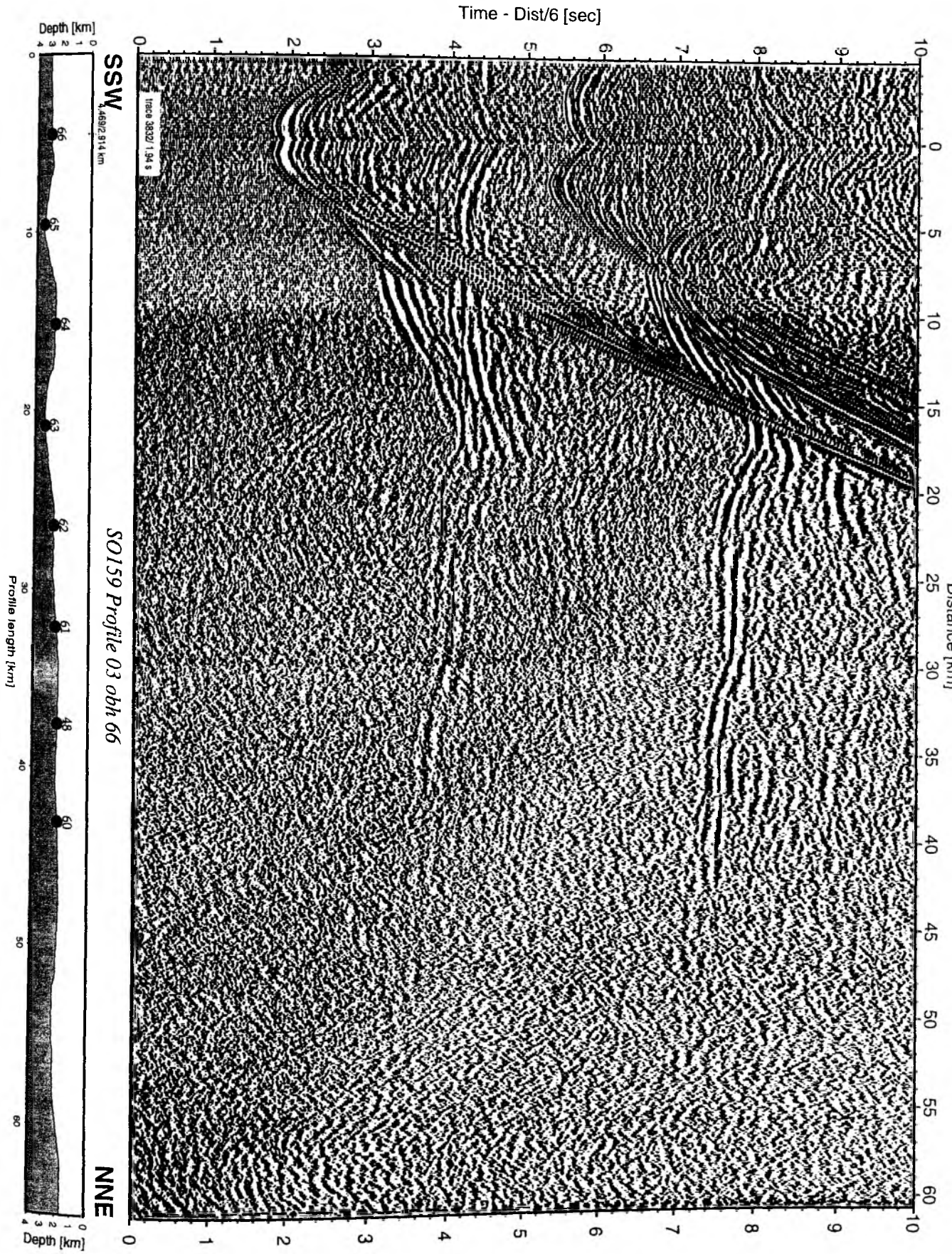

Figure 5.3.3.10: Record section from obh 66 , Profile 03.

5.3.4 Profile SO 159-04

(Noémi Fekete and Celine Ravaut)

Profile 04 is another dip line across the Guayaquil Basin, intersecting profile 2 and parallel to profile 3, further to the East. The aim was to find sedimentary velocities and identify the underlying basement and the plate boundary.

On September 04, 16 instruments (OBS67 to 82) were deployed with a spacing of 3.0 nm interval. The total profile length is 97.1 km and is oriented SSW-NNE. The location map of the profile and the stations including bathymetry is given in Figure 5.3.4.1 The station co-ordinates are listed in Appendix II.4.

Shooting started on the evening of September 4th at 23:28 UTC. During shooting (again at 60 s interval and a speed of 4.5 kn) several problems with the trigger cable occurred and the number of guns operational varied between one and three (see Appendix IV-4). The magnetometer was also deployed during shooting (see Chapter 5.2).

All but one instruments (OBS78) were recovered by acoustic release on September 05. Increased sea state and the shallow water increased the noise level considerably, and sometimes seismic energy could only be detected to distances of 20 to 30 km. All record sections are shown in Figures 5.3.4.2 to 5.3.4.14. These record sections were processed as described in Chapter 4.8.1. The velocity reduction used for all sections is Vred=6 km/s.

Modelling and Interpretation

On all recorded sections (GEOMAR and Geoazur), the arrivals were picked for modelling profile SO159-04. Most prominent phases, first arrivals, plus reflected and refracted phases were picked using Xzplot software (Zelt and Smith,1992) for GEOMAR record sections and Plotsegy software for Geoazur)ones. Due to low signal noise ratio, the picking was limited around 30 km away from the OBS/OBH. Depth Modelling was done using MacRay 2D, version 2.5.1, (Luetgert, 1992) modelling software.

The first arrivals were fit to the uppermost sedimentary layer with velocity of 1.8 to 2.9km/s. The highest velocity (2.9km/s) correspond to the thicker zone. The thickness of this layer varies from 1 km to 4 km as shown on Figure 5.3.4.15. This layer correspond to the Guayaquil basin's sediments with a bigger thickness than on profile3. From –60 to –80 km offset a well constrained geometrical variation can be seen in these sediments.
The second layer shows velocities of 2.7 to 4.2 km/s and can be interpreted as another layer of older sediments.
The third layer was not very well constrained. Due to the low signal-noise ratio, no refracted arrivals were picked in this layer, therefore velocity was fixed as a constant velocity of 4.6 km/s according to profile 2 and not inverted. The geometry of the lower interface was only constrained by some reflections and wide-angle refractions picked on the data.
The deeper part of the model can hardly be resolved by the data. The only constrained zones shown by dashed lines are derived from deep reflection waves and the fixed velocities vary between 5.5 to 6.5 km/s.
The picks from German instruments only yield results on the southern half of the profile, the northern end remains to be constrained – uncertainties are denoted with interrogation marks.
To improve this interpretation further work should be done, incorporating northern data from OBS, including data processing, etc...

Figure 5.3.4.1. Location map and OBS/OBH locations for Profile SO 159 - P04

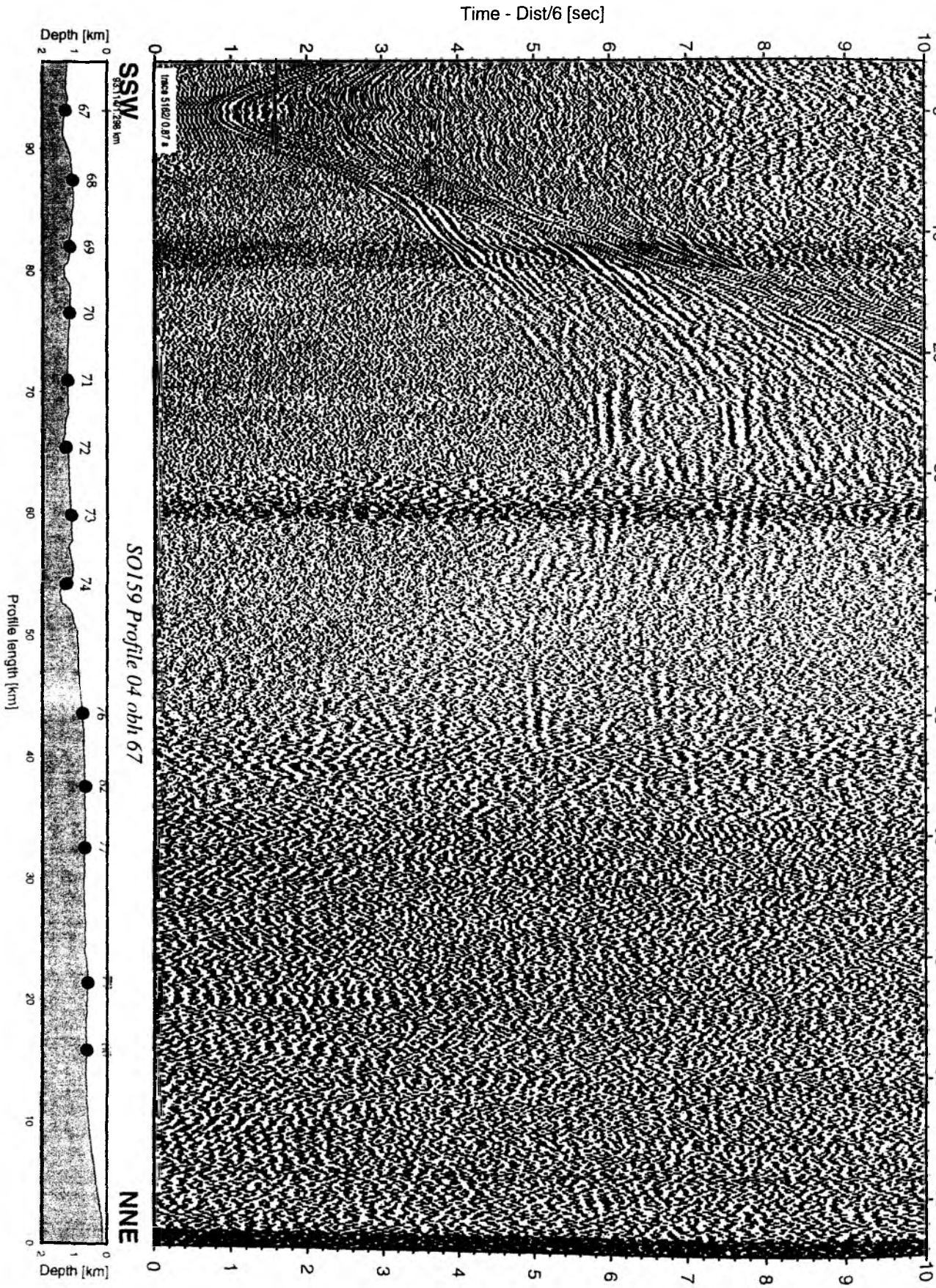

Figure 5.3.4.2: Record section from obh 67 , Profile 04.

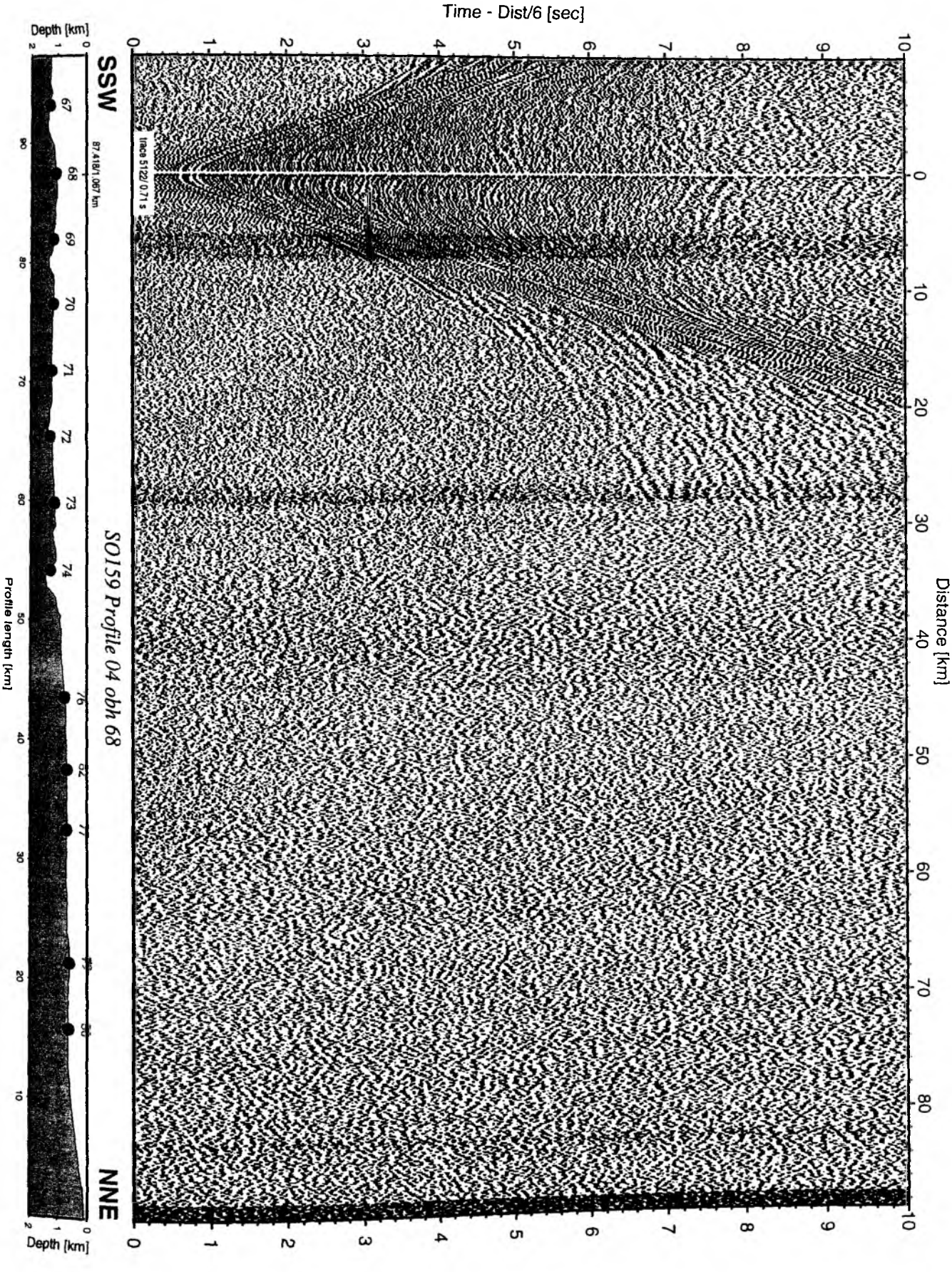

Figure 5.3.4.3: Record section from obh 68 , Profile 04.

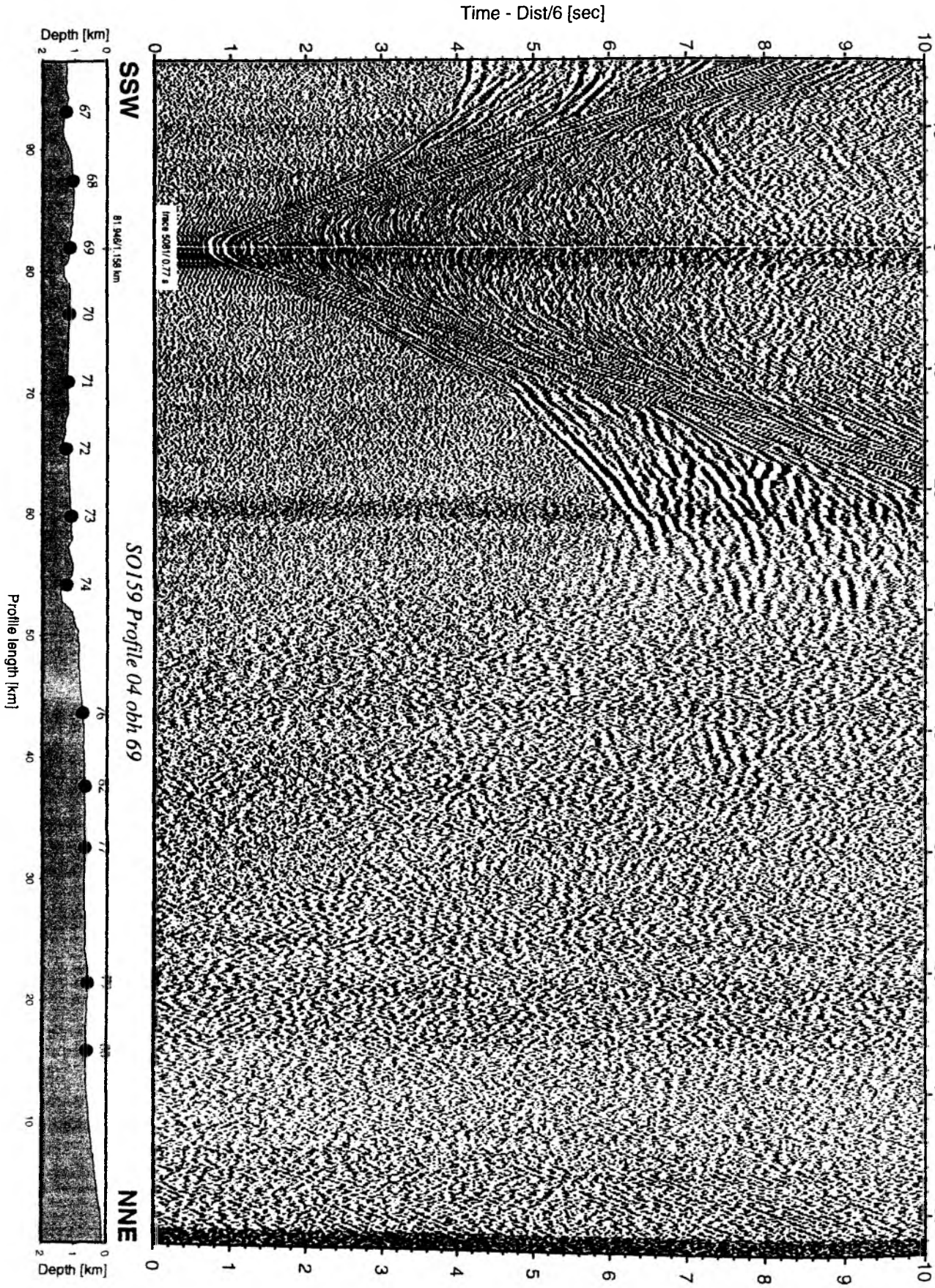

Figure 5.3.4.4: Record section from obh 69 , Profile 04.

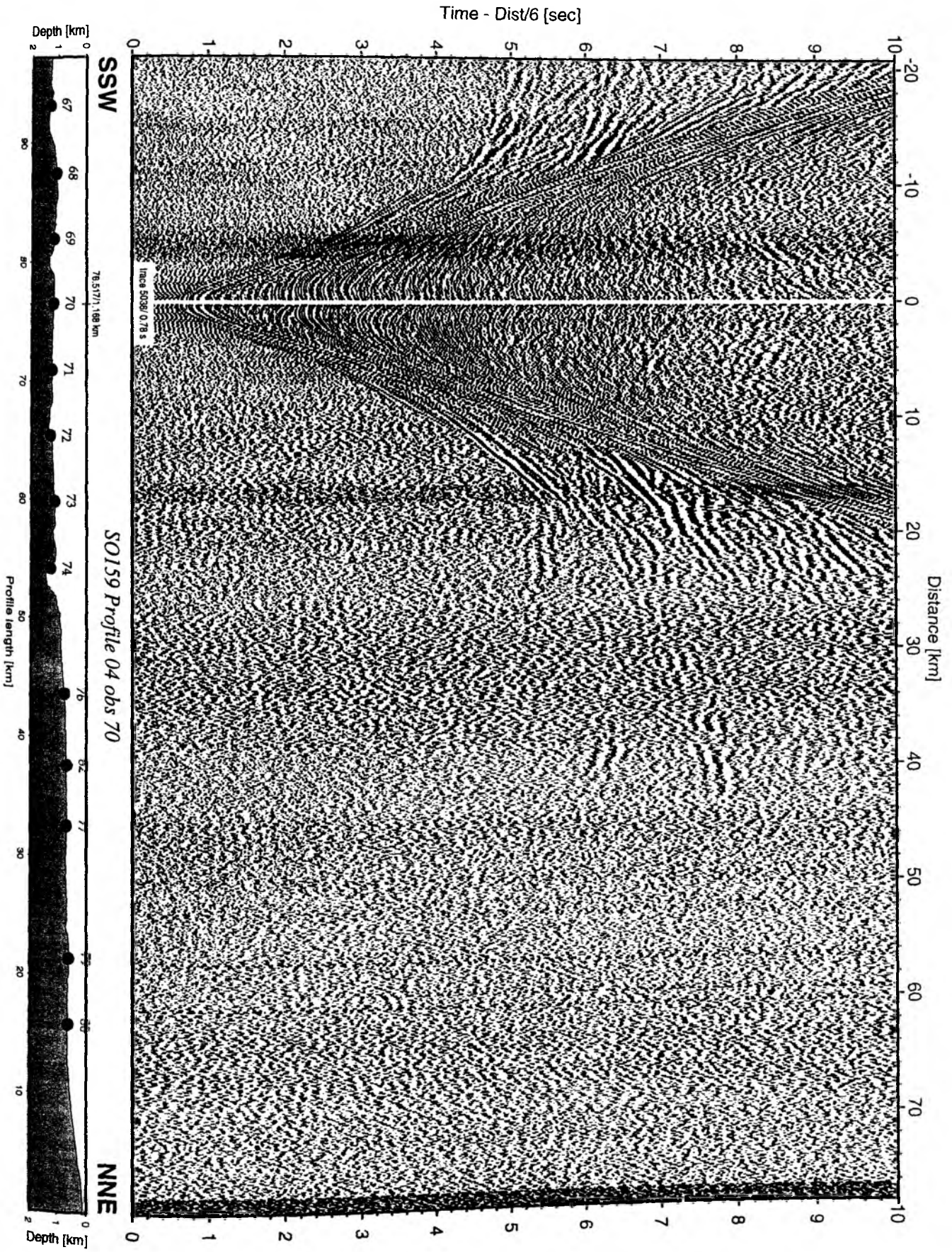

Figure 5.3.4.5: Record section from obs 70 hydrophone, Profile 04.

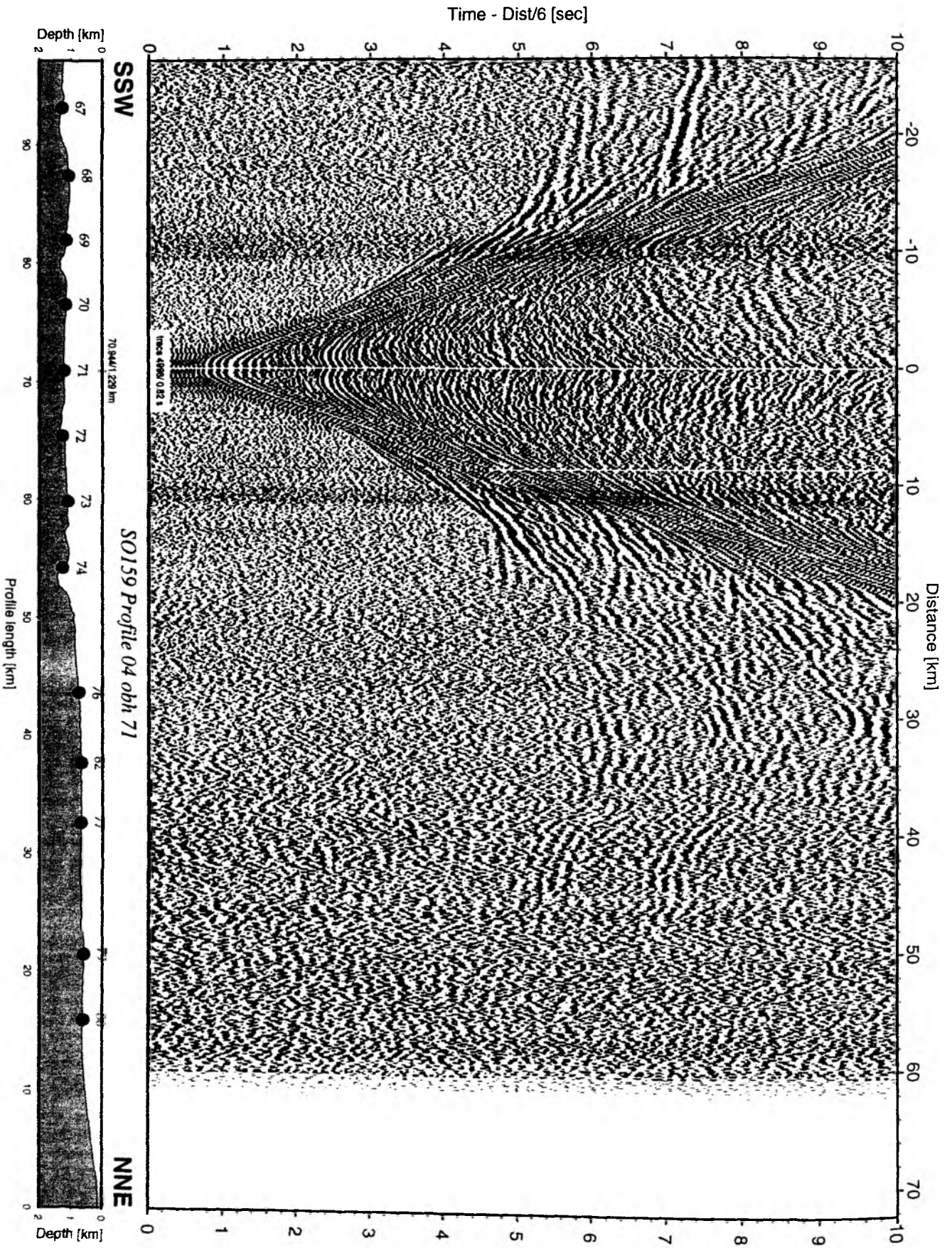

Figure 5.3.4.6: Record section from obh 71 , Profile 04.

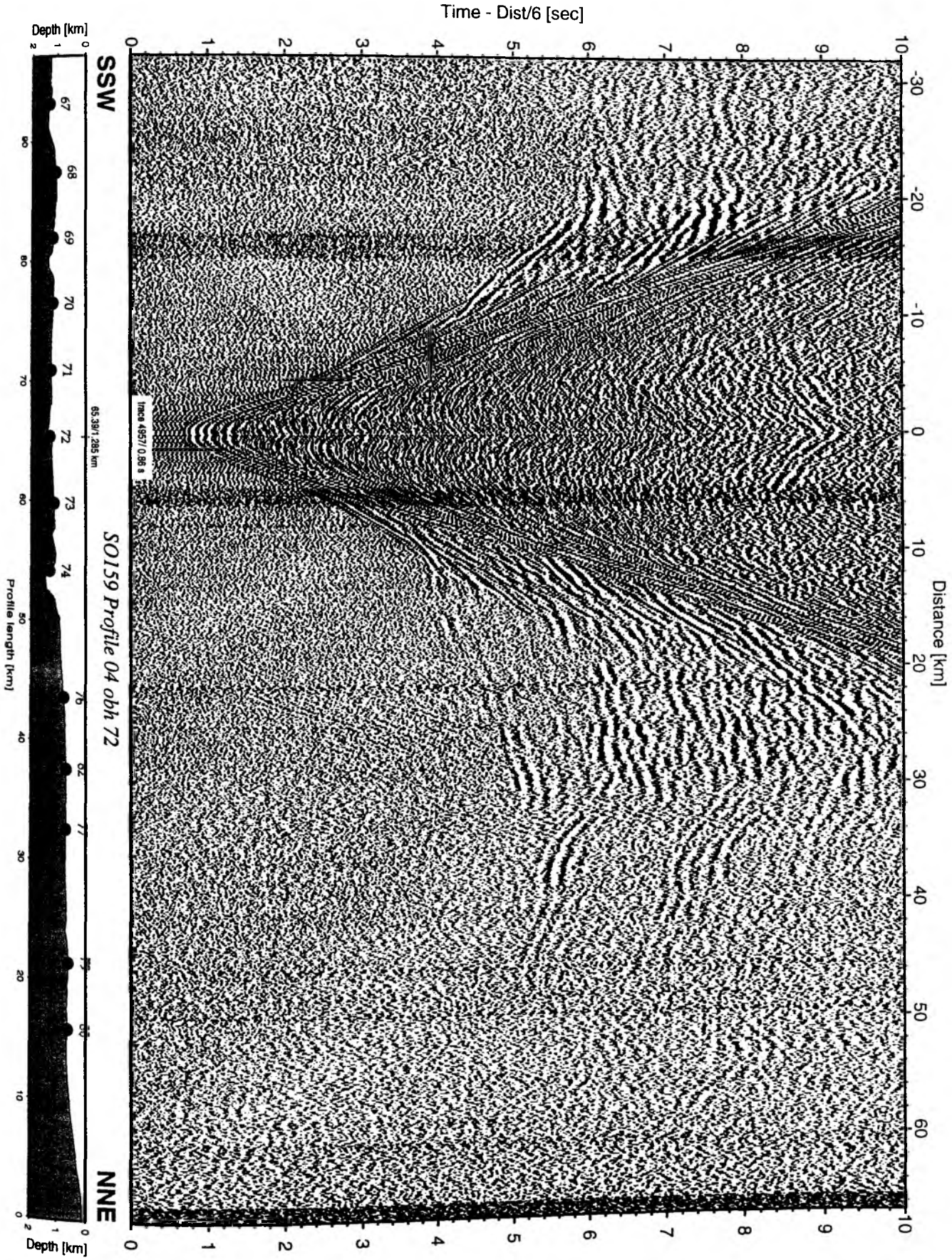

Figure 5.3.4.7: Record section from obh 72 , Profile 04.

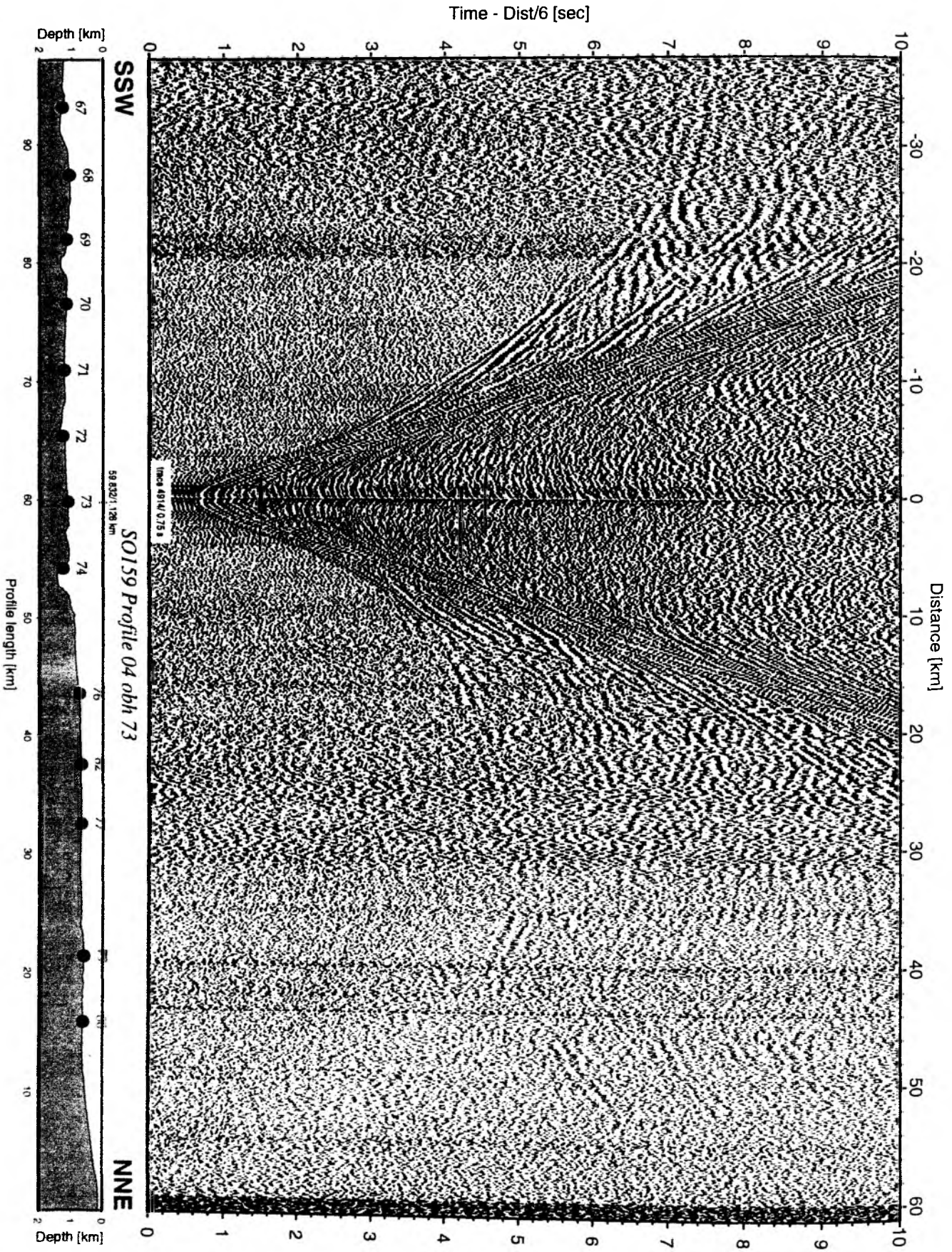

Figure 5.3.4.8: Record section from obh 73 , Profile 04.

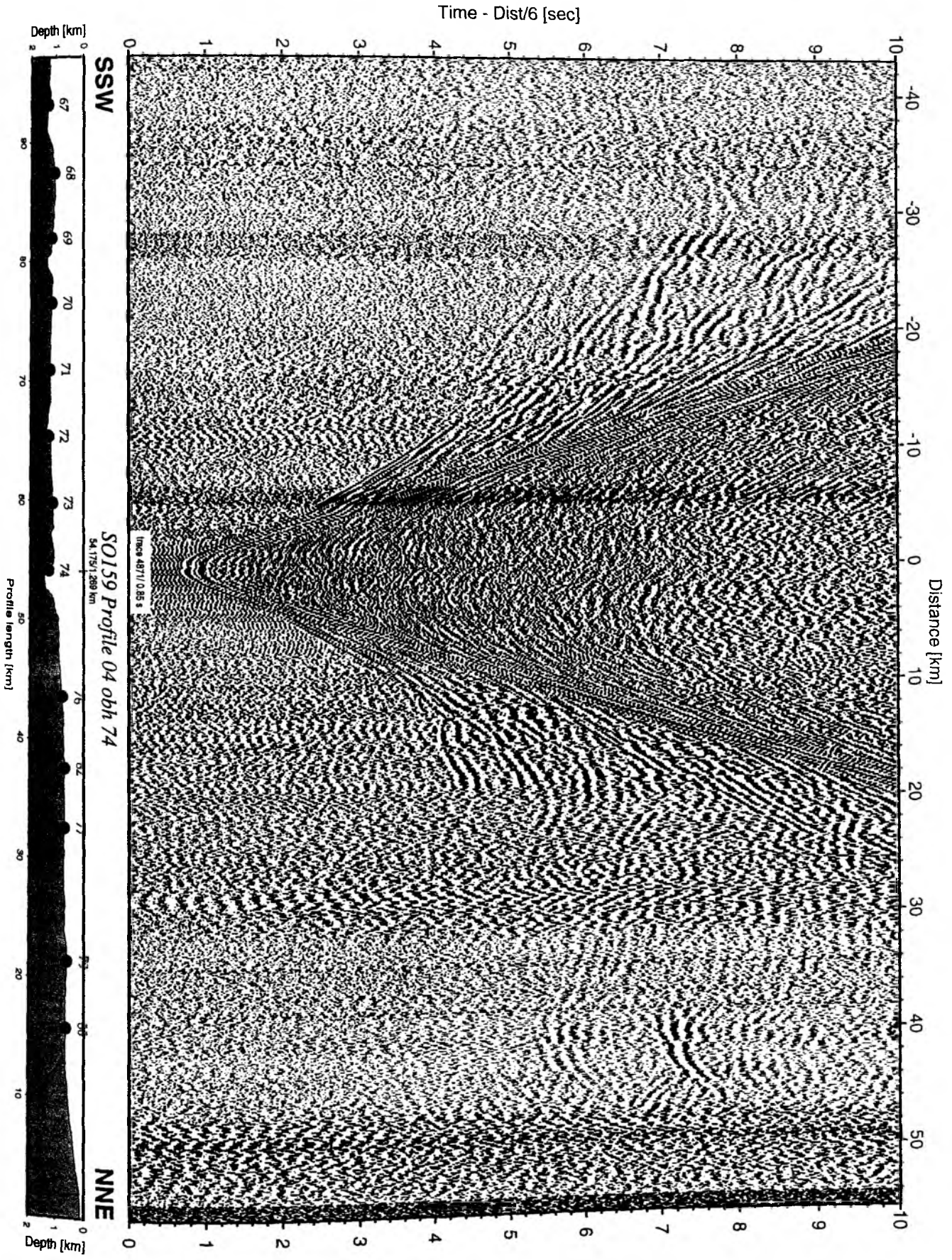

Figure 5.3.4.9: Record section from obh 74 , Profile 04.

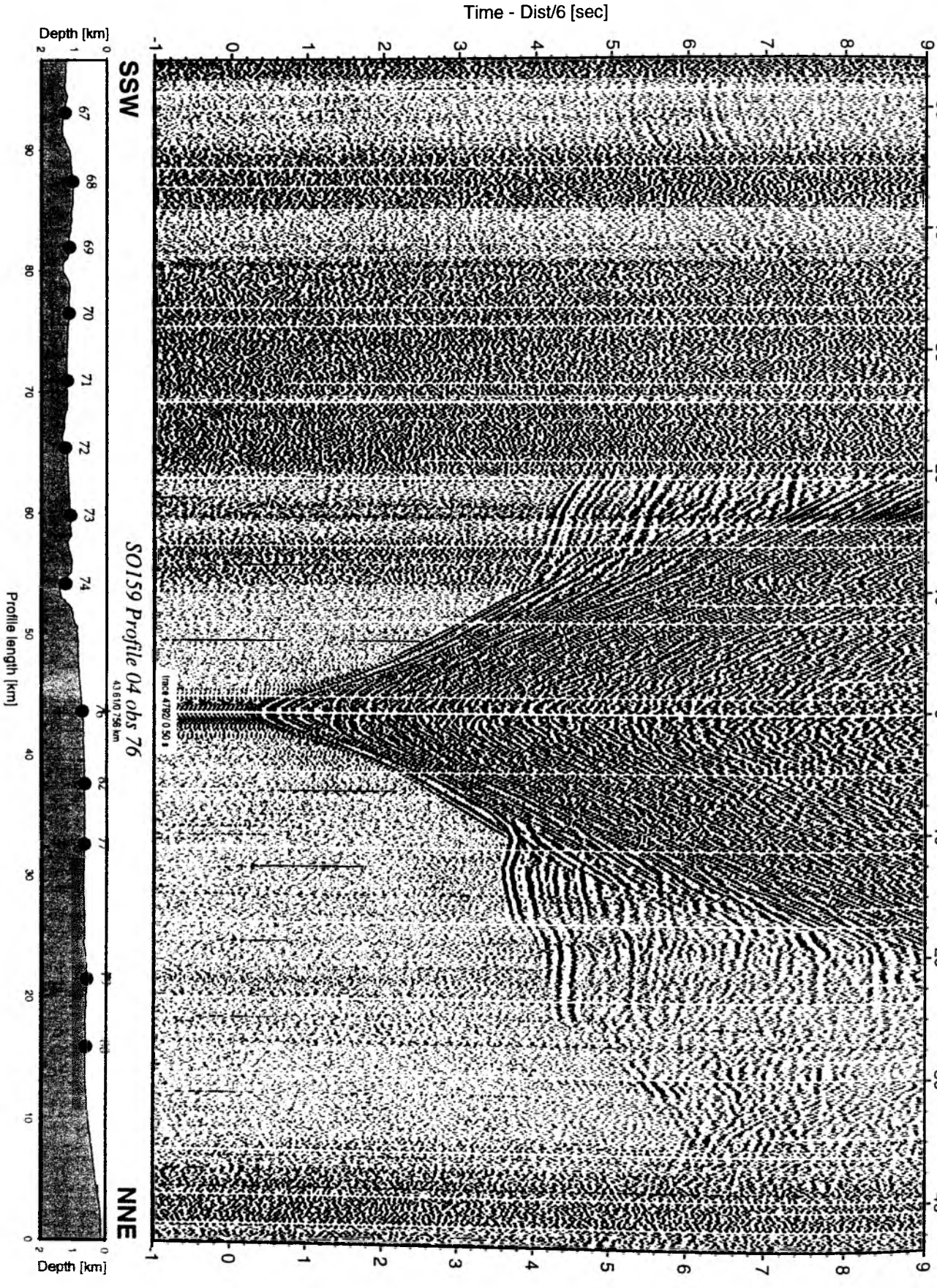

Figure 5.3.4.10: Record section from obs 76 vertical component, Profile 04.

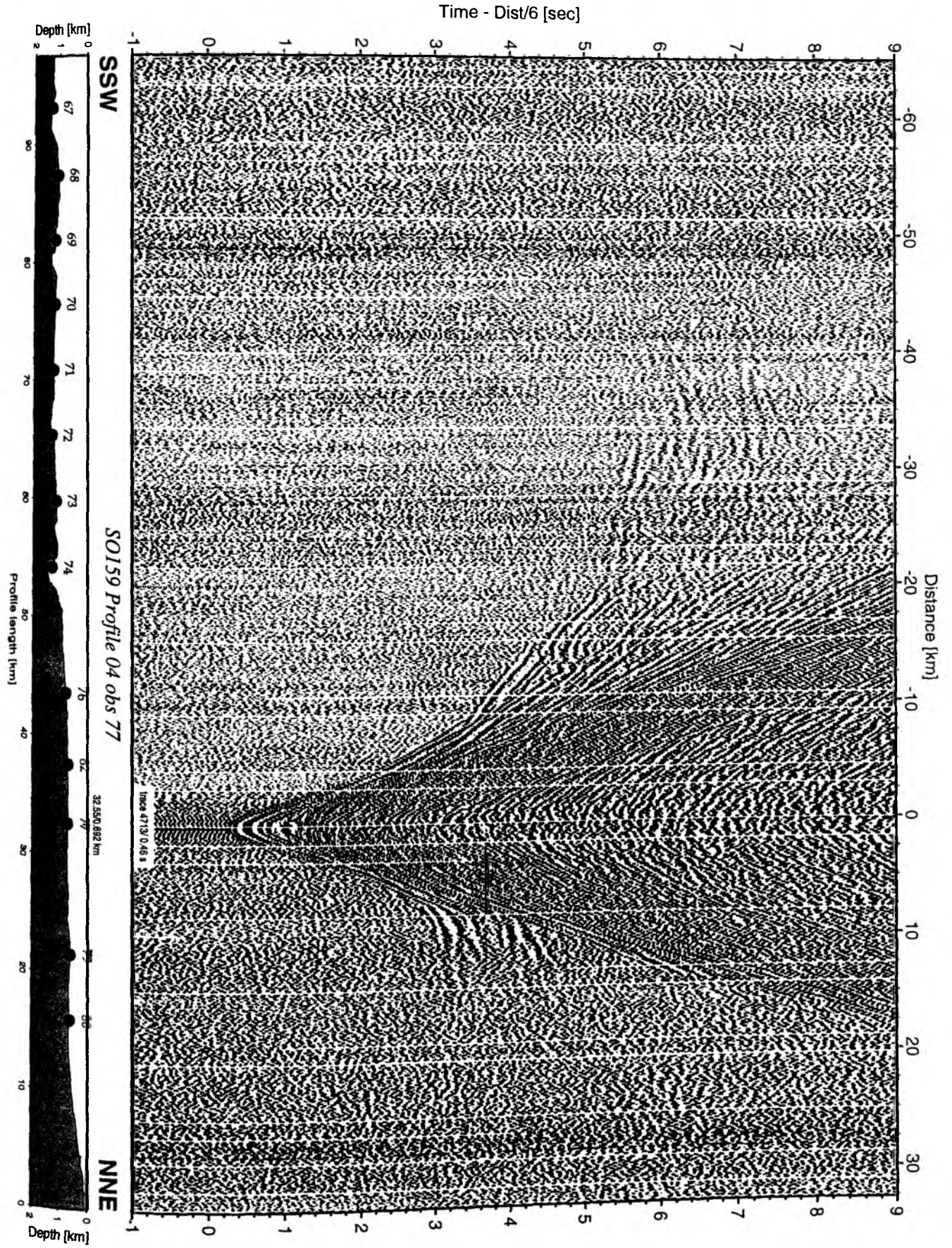

Figure 5.3.4.11: Record section from obs 77 vertical component, Profile 04.

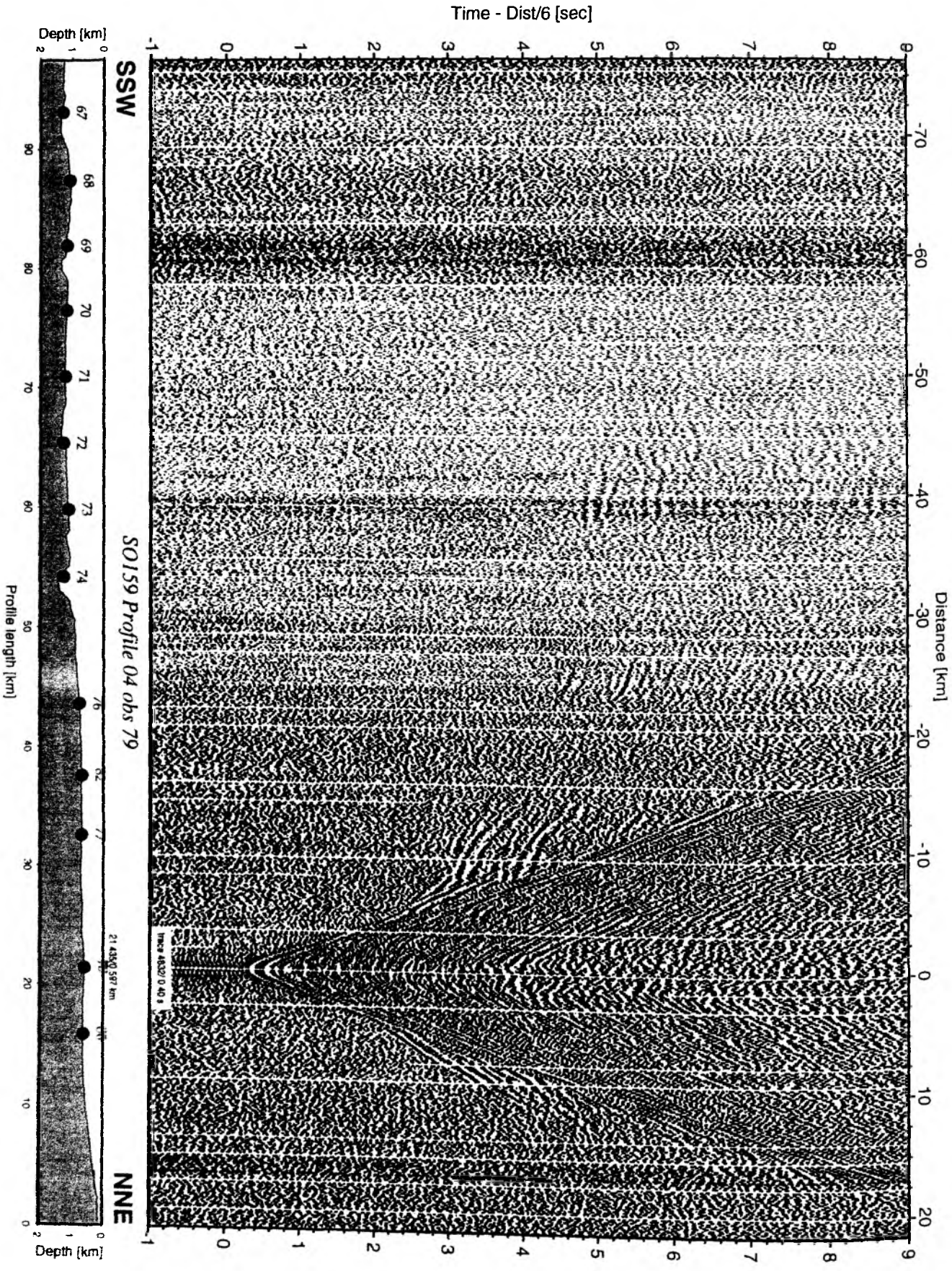

Figure 5.3.4.12: Record section from obs 79 vertical component, Profile 04.

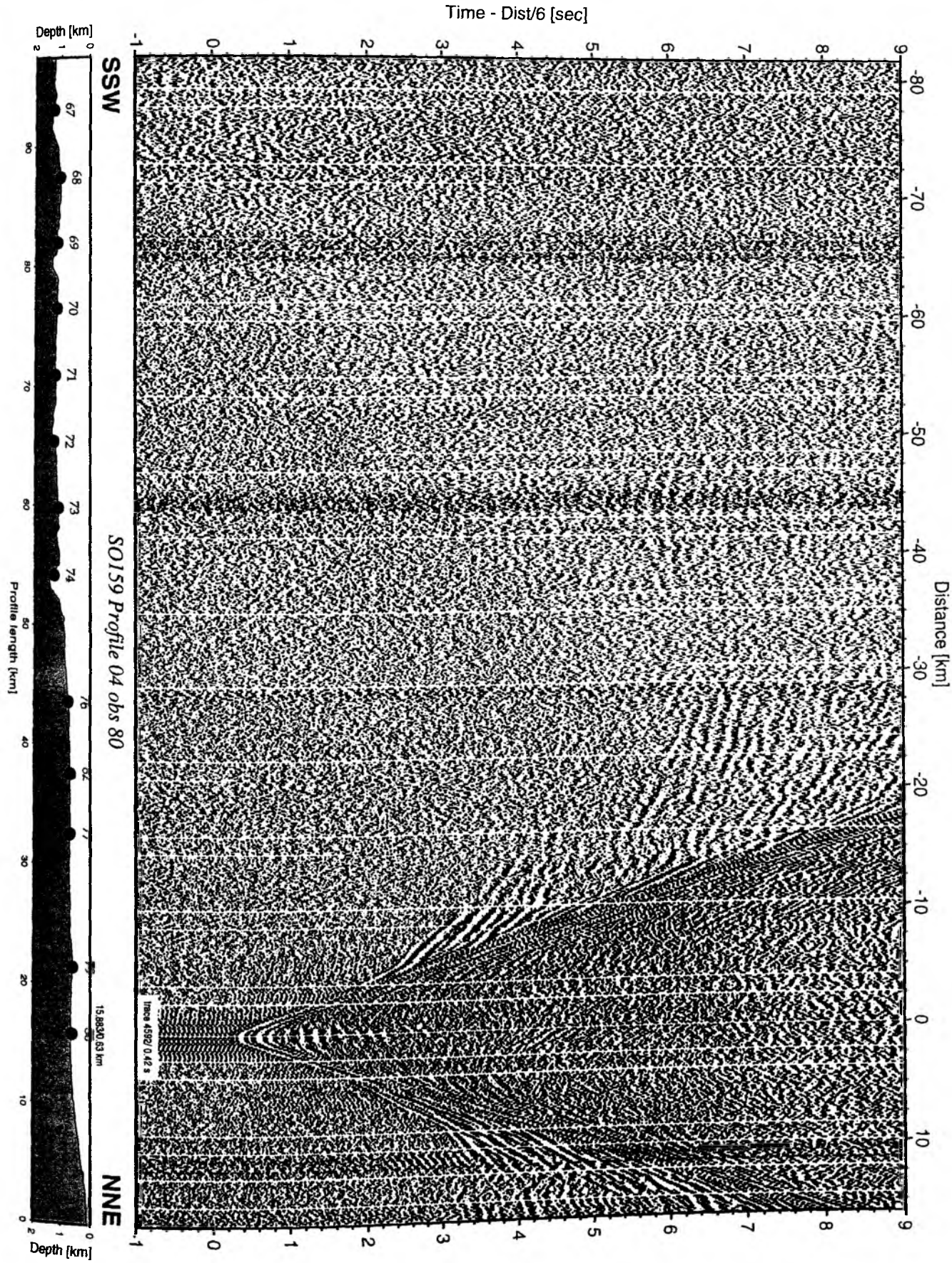

Figure 5.3.4.13: Record section from obs 80 hydrophone, Profile 04.

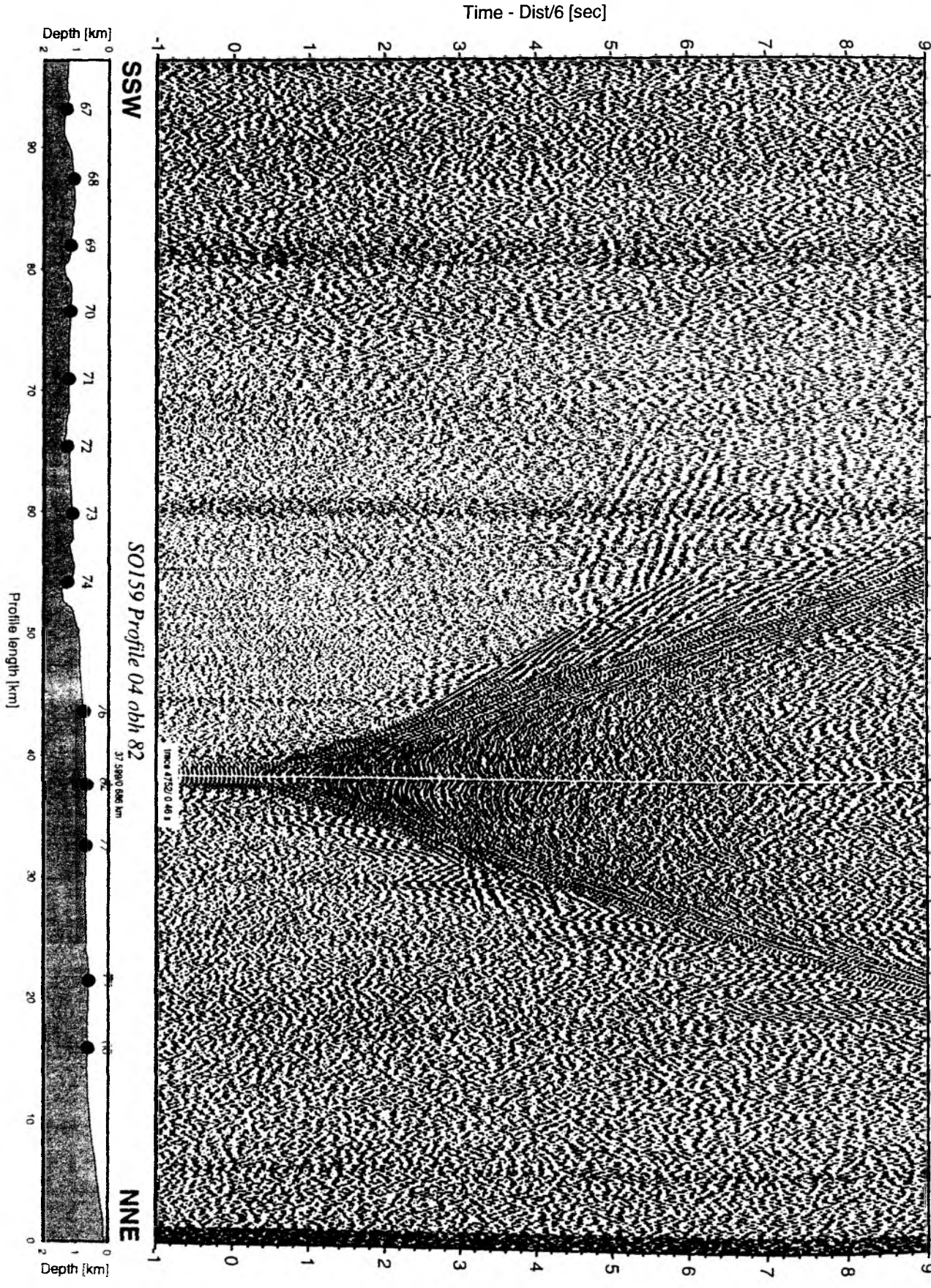

Figure 5.3.4.14: Record section from obh 82 , Profile 04.

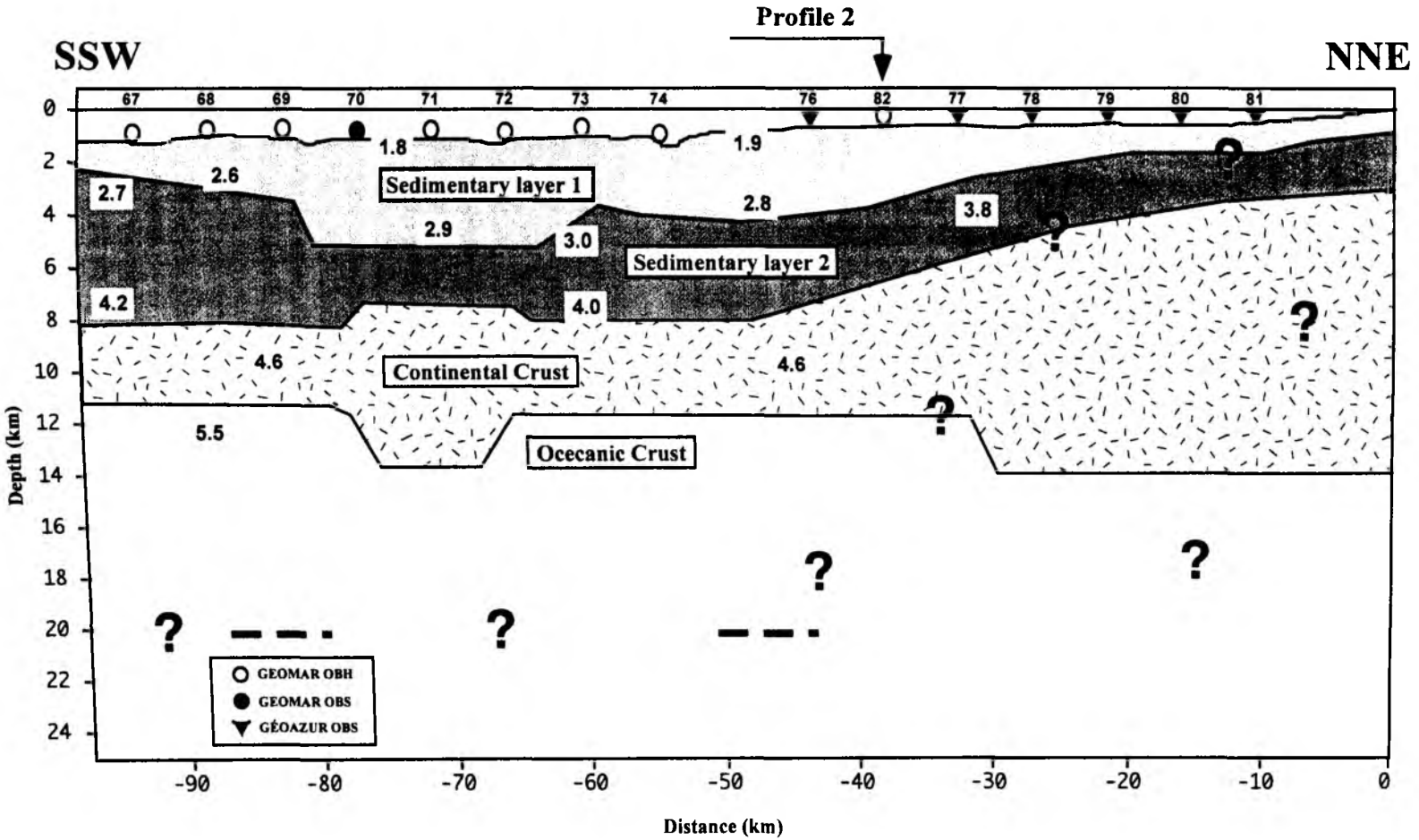

Figure 5.3.4.15

5.3.5 Profile SO 159-05

Profile 05 was made to investigate the crustal structure of Carnegie Ridge oposite the colombian/ ecuadorian Margin, where the seafloor depth is shallowest. On September 06 23 instruments were deployed (OBS83 to 106) along this 100 nm long profile at 4.5 nm interval. Shooting was not started before September 08 due to instrument recovery further south. A location map with deployment sites is shown in Figure 5.3.5.1. The shooting line extended for 120 nm and was made at usual speed of 4.5 kn. All three airguns were working, using 60 s trigger interval with a resulting shotspacing of 135 m.

Recorded data are of very good quality, showing clear first arrivals (Pg, Pn) and energetic Moho reflections (PmP) up to about 140 km from the sources (Figures 5.3.5.2 to 5.3.5.23). However, the appearence of the record sections varies notably along the profile, indicating important variations on the crustal structure across the ridge. A preliminary forward modelling and interpretation of those data was also attempted on board.

Model description from 2-D forward modeling

The most prominent seismic phases were picked for all OBH/S and are displayed in Figure 5.3.5.24 with no time reduction. The picking accuracy was better than 50 ms in the near offset range < 60 km, deteriorated to 100 ms in the far offset range > 60 km and may exceed 100 ms for PmP arrivals.

A starting model was set up with the morphology. Sediment coverage was modeled with the two-way-traveltime (TWT) information (top basement reflection) from the coincident MCS line of the SALIERI project and the appearance of the basement refraction in the wide-angle data. The preliminary model from 2-D forward modeling of the wide-angle data is presented in Figure 5.3.5.25 and shows the following:

- The Carnegie Ridge on this profile has only a thin blanket of sediment not exceeding 800 m thickness. In the most shallow part of the ridge, between OBS 99 and 96, almost no sediment is encountered. A very low velocity of 1.6 to 1.8 km/s was taken for sediment, because no precursors appear near the water wave phase.
- The upper crust starts with velocities of 4.7 km/s, slightly increasing to 5.0 km/s in the NNE. A constant velocity gradient of 0.35 s^{-1} gave a satisfying fit to this part of the Pg phase and yielded lower velocities of 5.6 km/s in the thin and up to 6.4 km/s in the thick parts of this crustal unit. In the NNE thickness is 1.5 to 2.0 km, increasing further SSW to 5 km in the most shallow ridge part and decreasing to 3 km in the SSW profile part.
- The lower crust can be devided in a layer-3A and -3B part. On the whole profile upper velocities begin with 6.6 km/s and together with the constant gradient of 0.08 s^{-1} outline the homogeneity of this crustal edifice. In 14 km to 20 km depth velocities reach 7.4 to 7.8 km/s and are well confirmed by the pronounced Pg. Below, the velocities are all 7.4 km/s. A velocity contrast between these parts is restricted to the profile range between OBH 94 and 91 and confirmed by the record sections of OBH/S 87 to 91, all to the SSW, showing secondary arrivals in a variable offset range concentrated in about 40 to 60 km offset.
- The crust-mantle boundary is well contraint through numerous PmP and Pn observations. These phases image the steep decent of the MOHO and transition from normal to thickened oceanic crust in the NNE. Strong PmP reflections on OBS 105 to 100 to the NNE from 60 km offset on, which increase in reduced time from 2.8 s on OBS105 to more than 4 s on OBS100 confirm the descent from the SSW to the center of the thickened crust beneath OBS 96.
- Uppermost mantle velocities of 8.0 km/s in 8 km depth and 8.3 km/s in 25 to 30 km depth are well constraint by various Pn observations. The gradient is 0.015 s^{-1} and normal for the effect of an increasing pressure with depth.

In summary the Carnegie Ridge is build up by a huge, almost 30 km thick, homogeneous crust with little lateral velocity variations. Normal oceanic crust in terms of velocities and thickness is found in the NNE. Approching the ridge the crust-mantle boundary dramatically deepens to more than 30 km depth and further to the SSW rises up to 21 km depth. The thickened crust may be easily divided in terms of velocities and gradient into a basaltic upper and a gabbroic lower crust. Crustal thickening is essentially achieved by lower crustal thickening. This crustal edifice makes up 80 % of the thickened crust

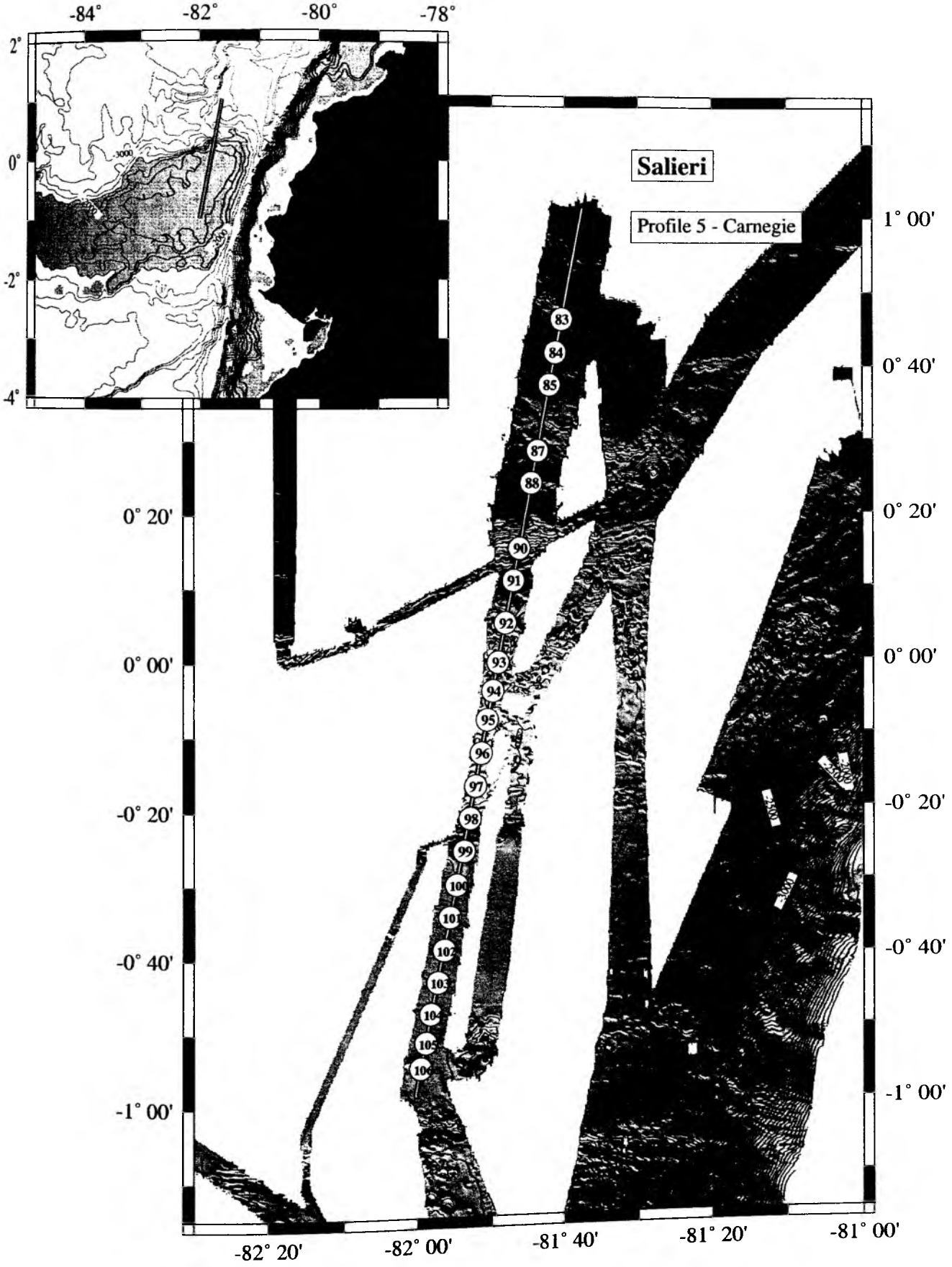

Figure 5.3.5.1. Location map and OBS/OBH location for profile SO 159 - P05

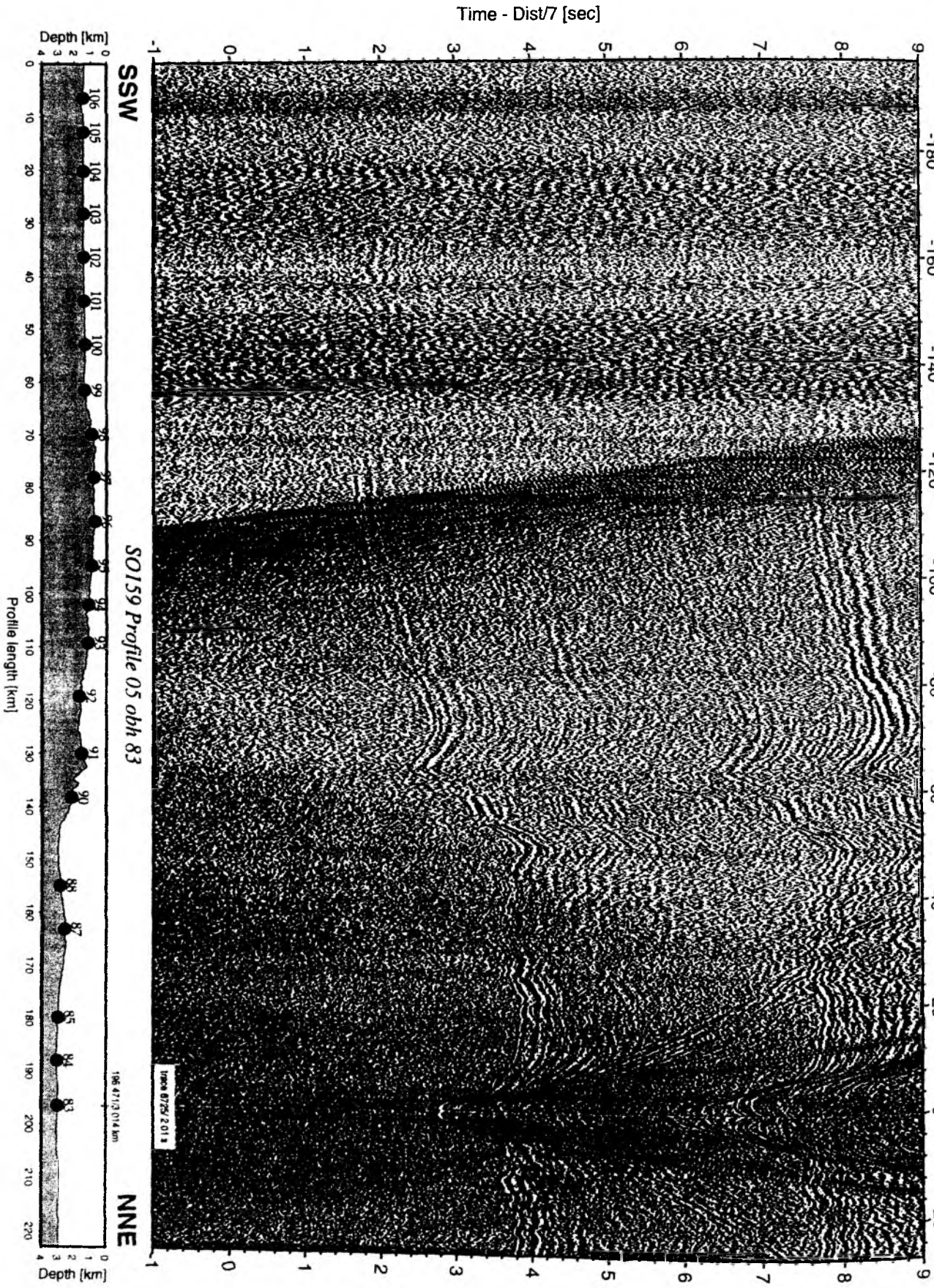

Figure 5.3.5.2: Record section from obh 83 , Profile 05.

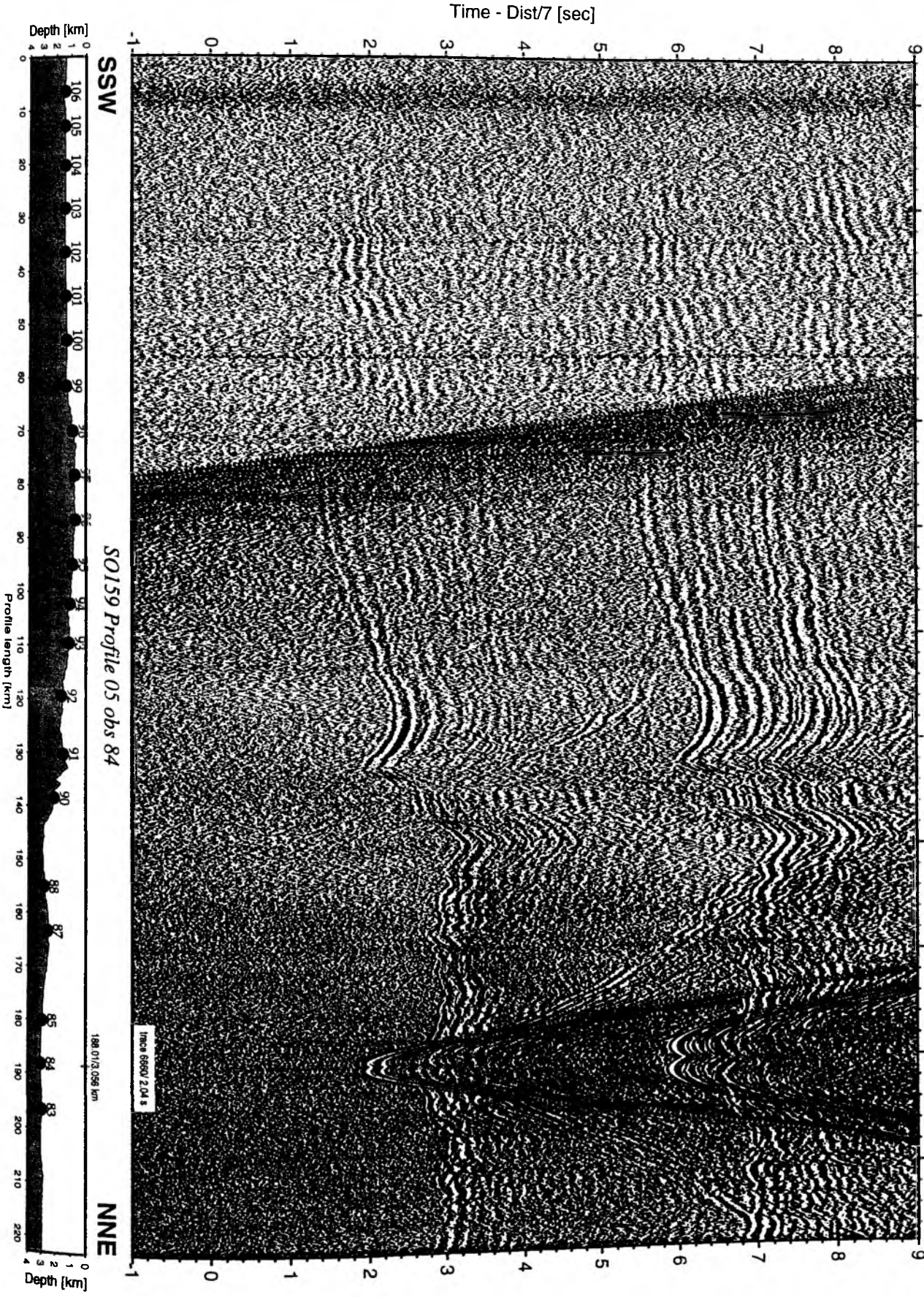

Figure 5.3.5.3: Record section from obs 84 hydrophone, Profile 05.

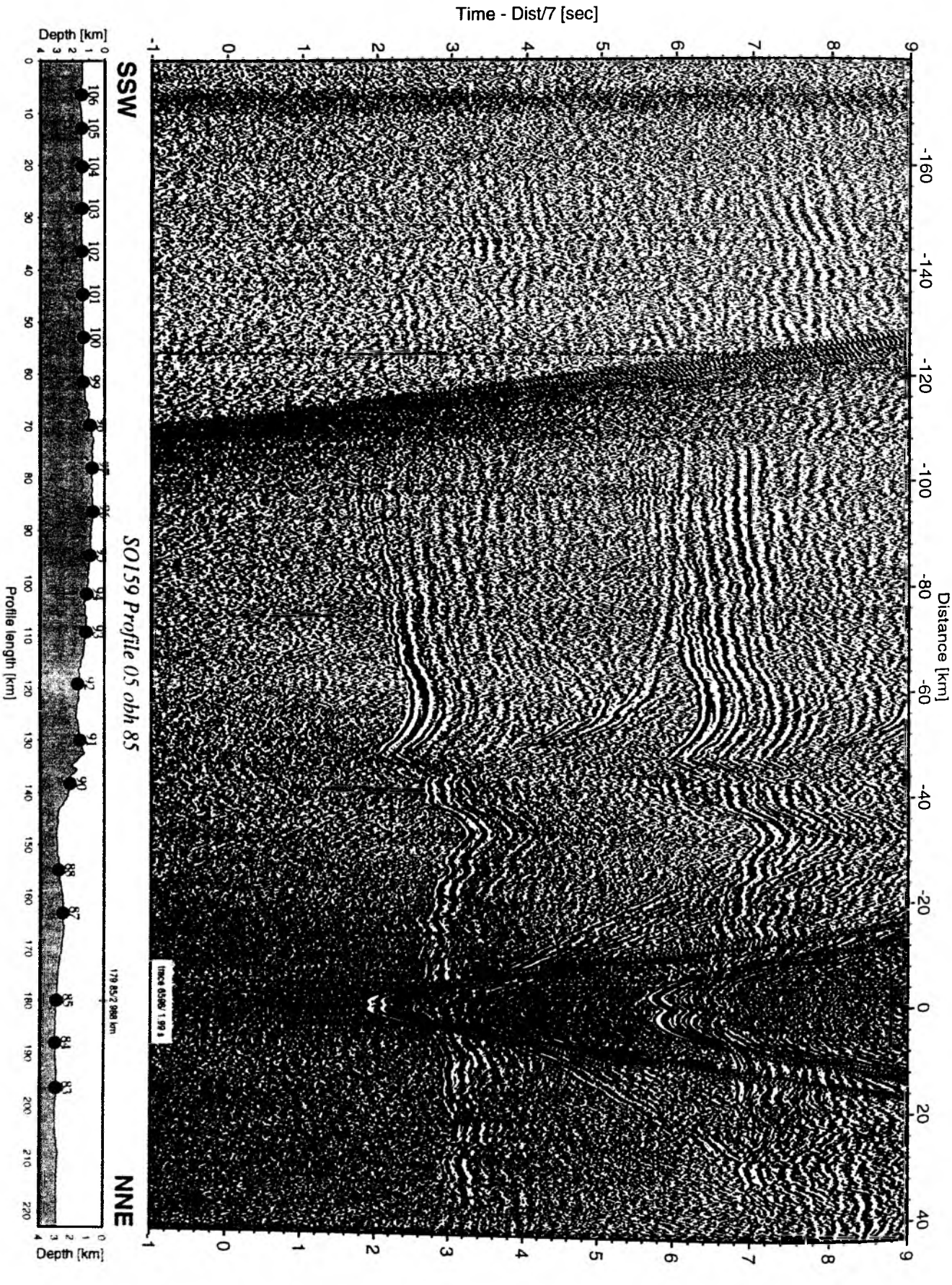

Figure 5.3.5.4: Record section from obh 85 , Profile 05.

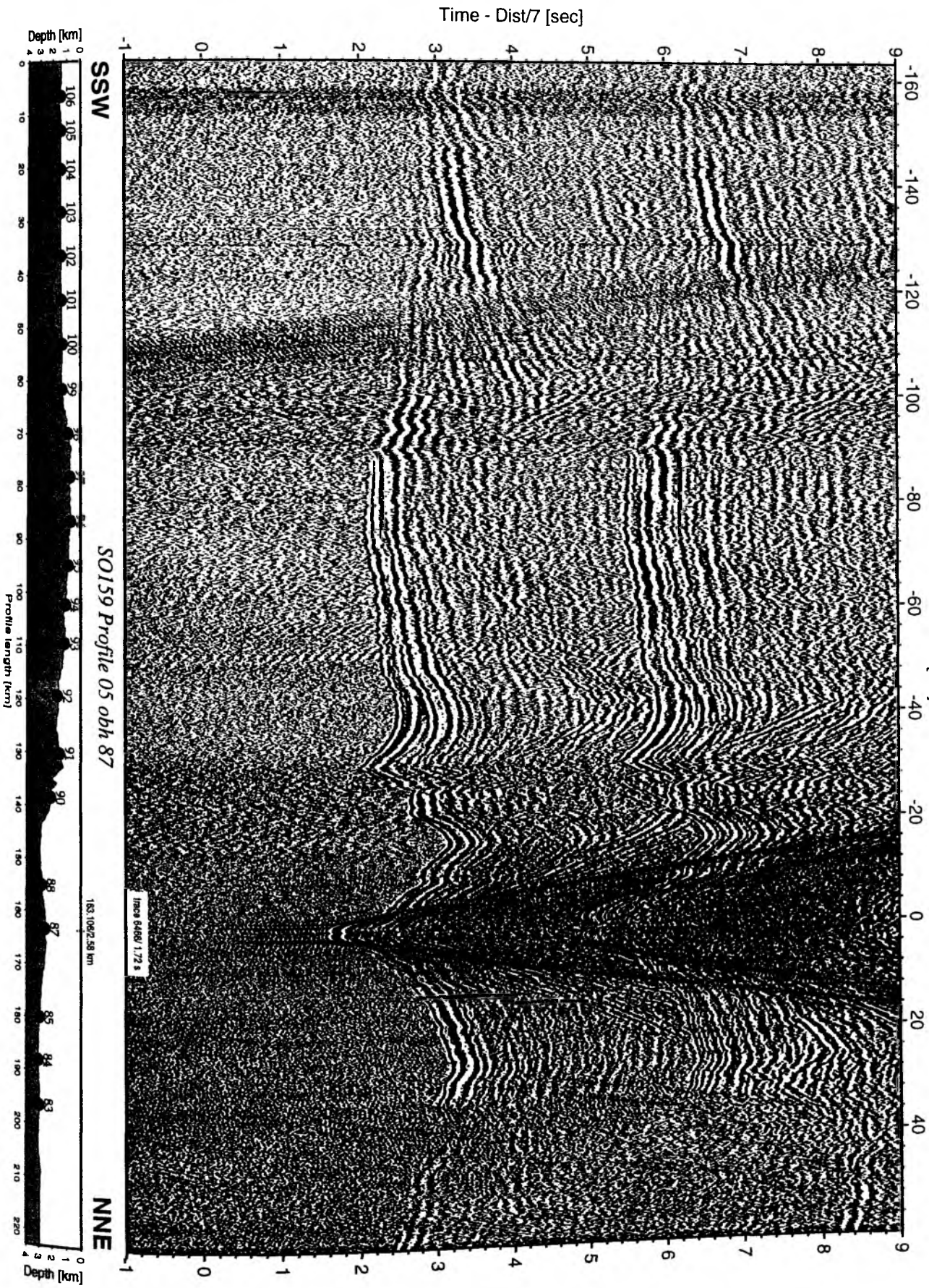

Figure 5.3.5.5: Record section from obh 87 , Profile 05.

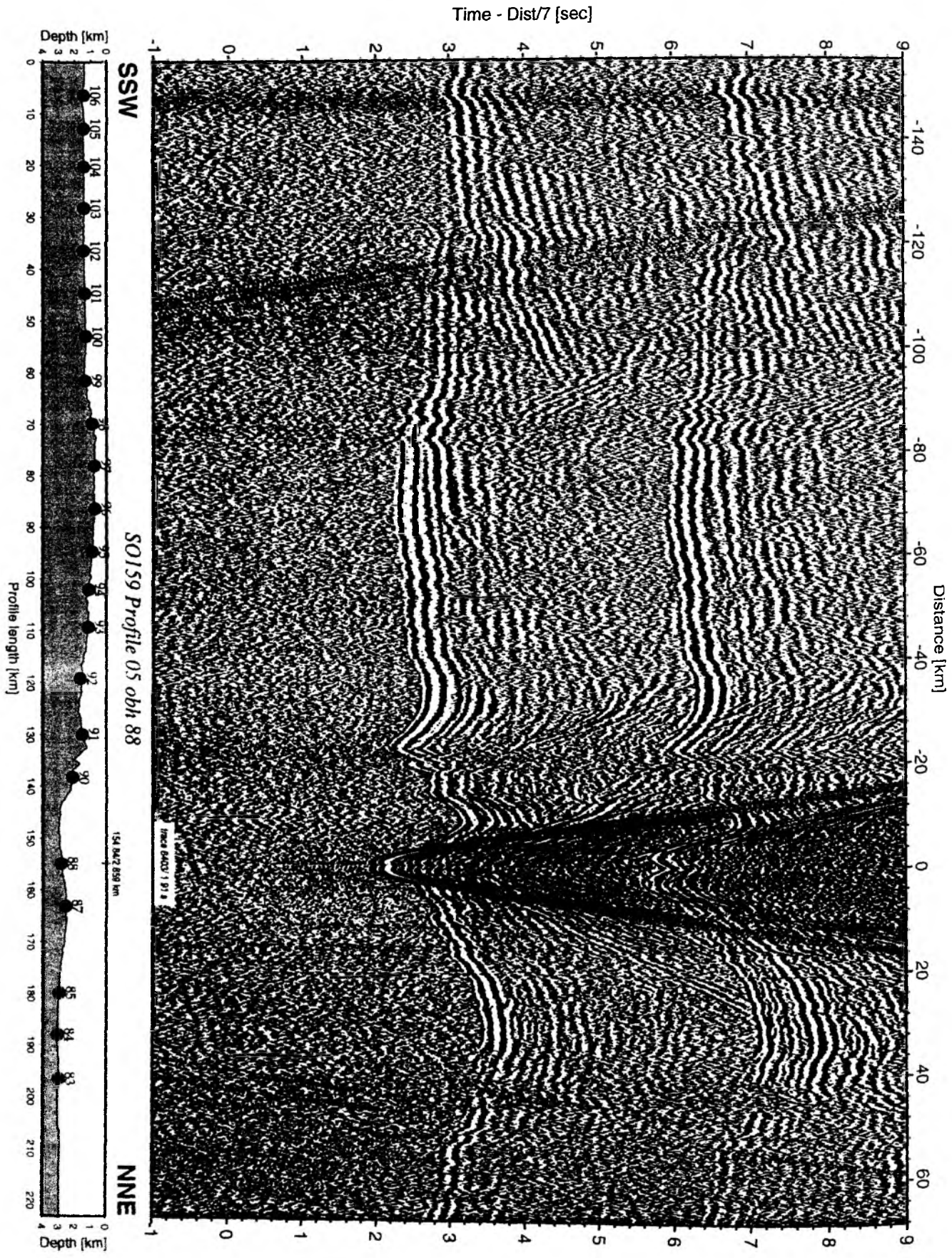

Figure 5.3.5.6: Record section from obh 88 , Profile 05.

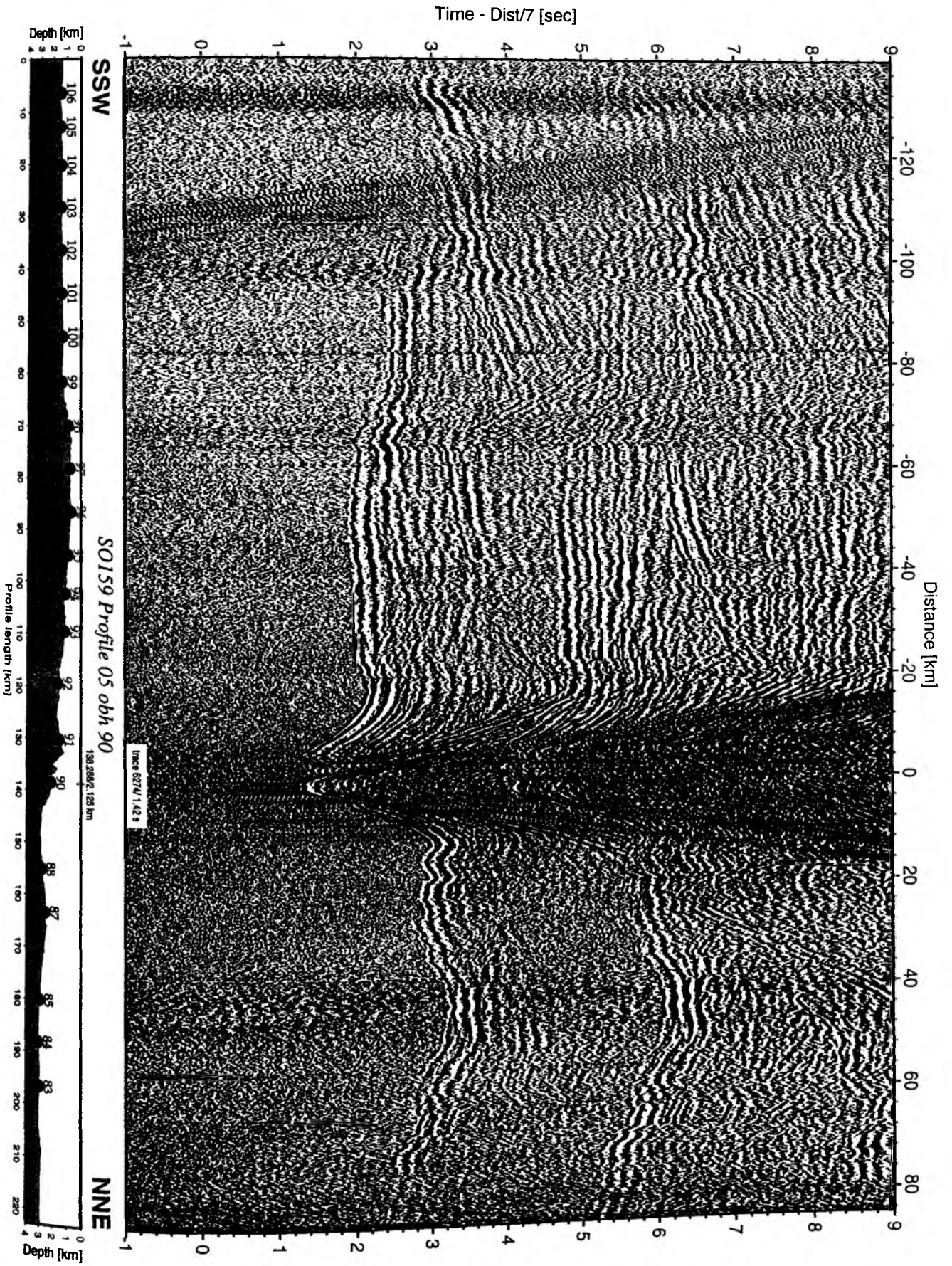

Figure 5.3.5.7: Record section from obh 90 , Profile 05.

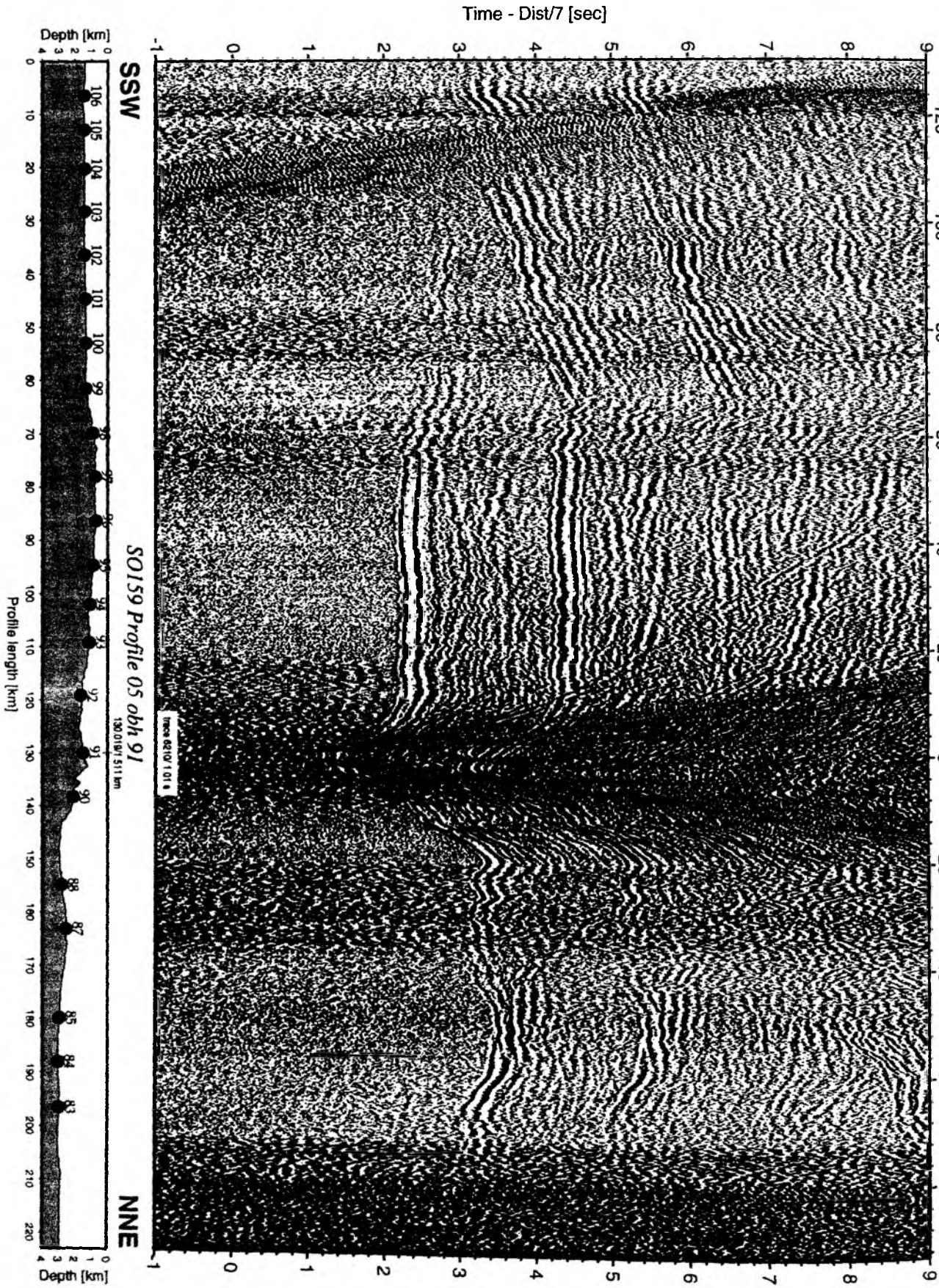

Figure 5.3.5.8: Record section from obh 91 , Profile 05.

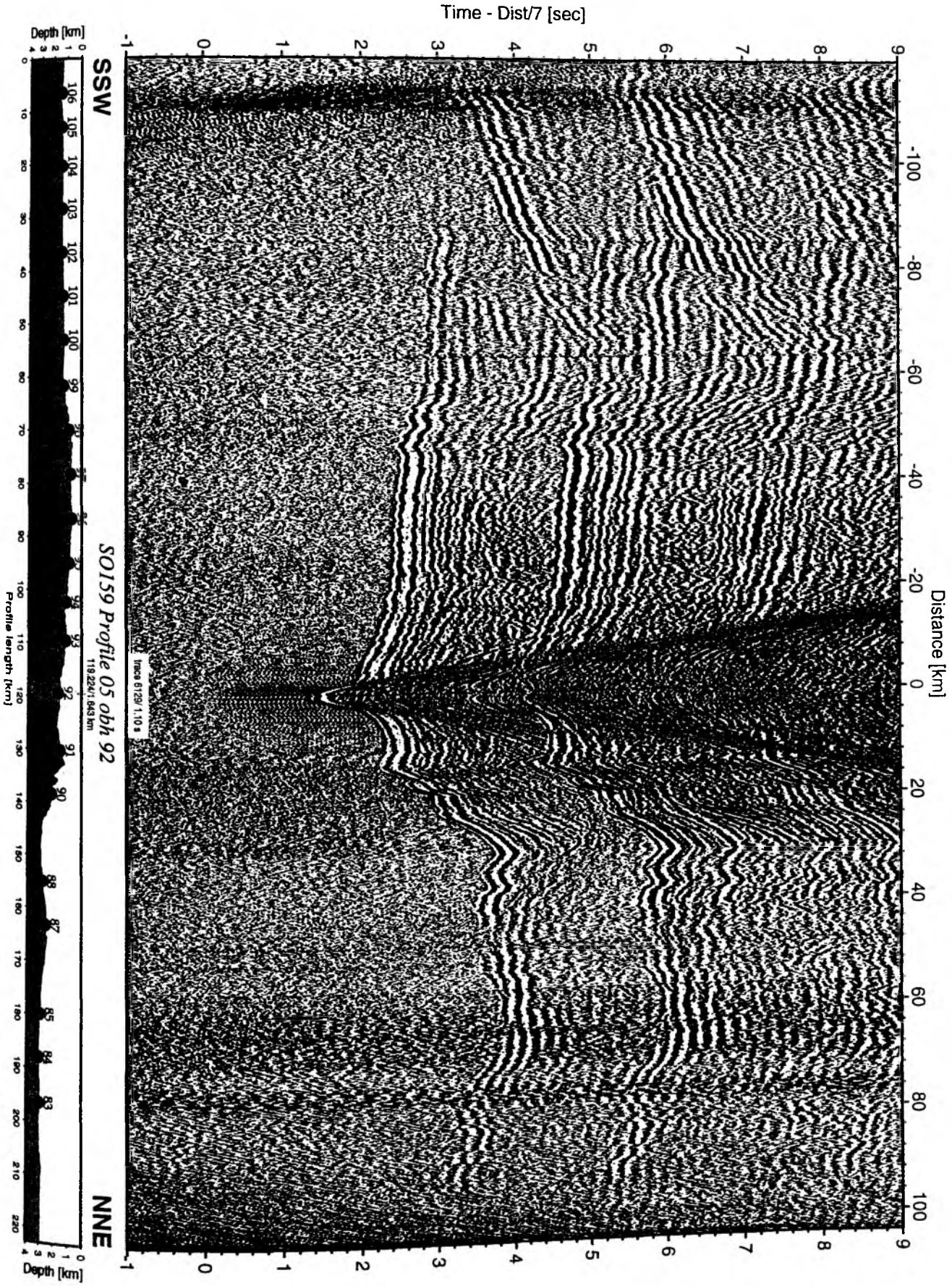

Figure 5.3.5.9: Record section from obh 92 , Profile 05.

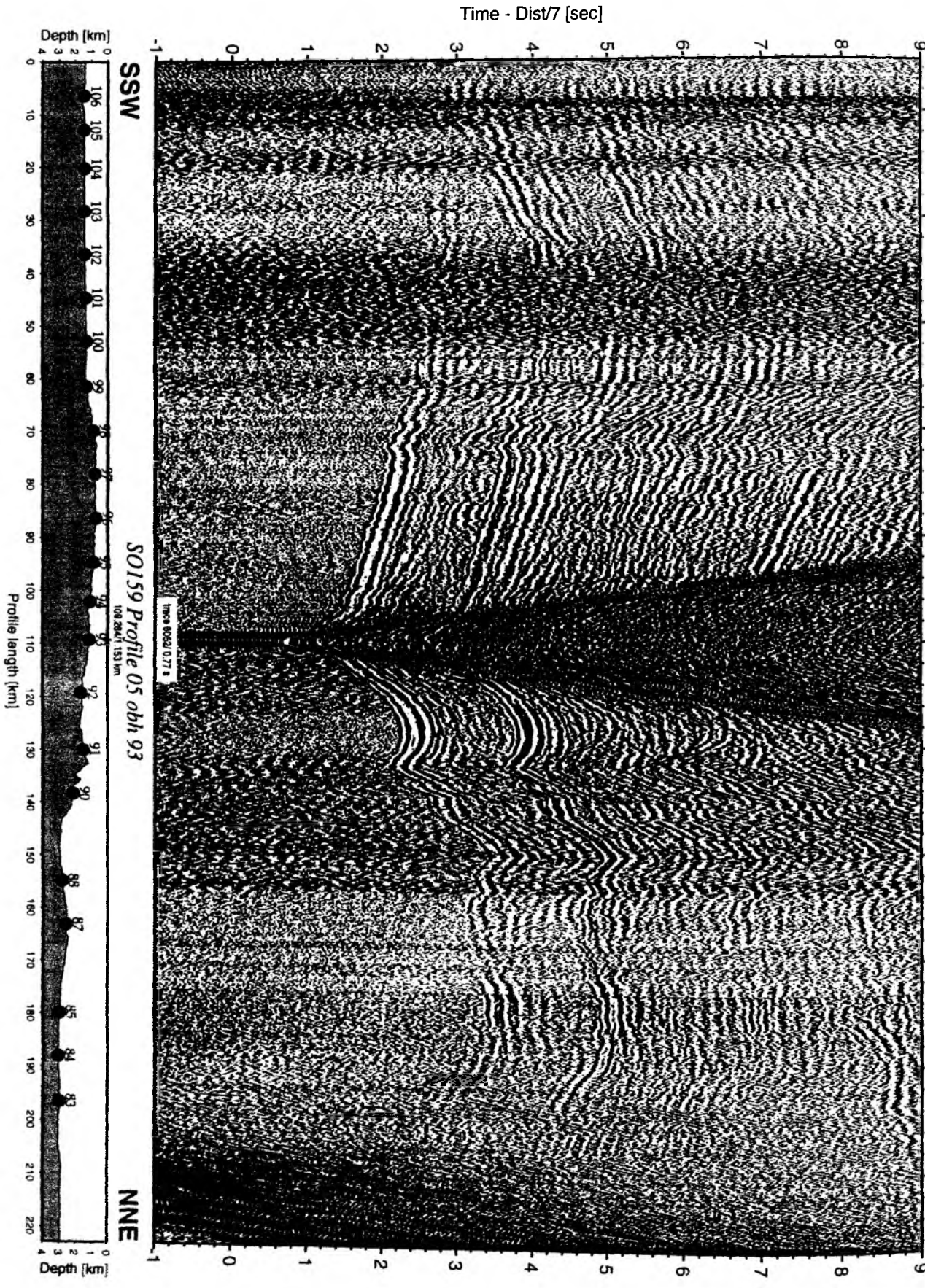

Figure 5.3.5.10: Record section from obh 93 , Profile 05.

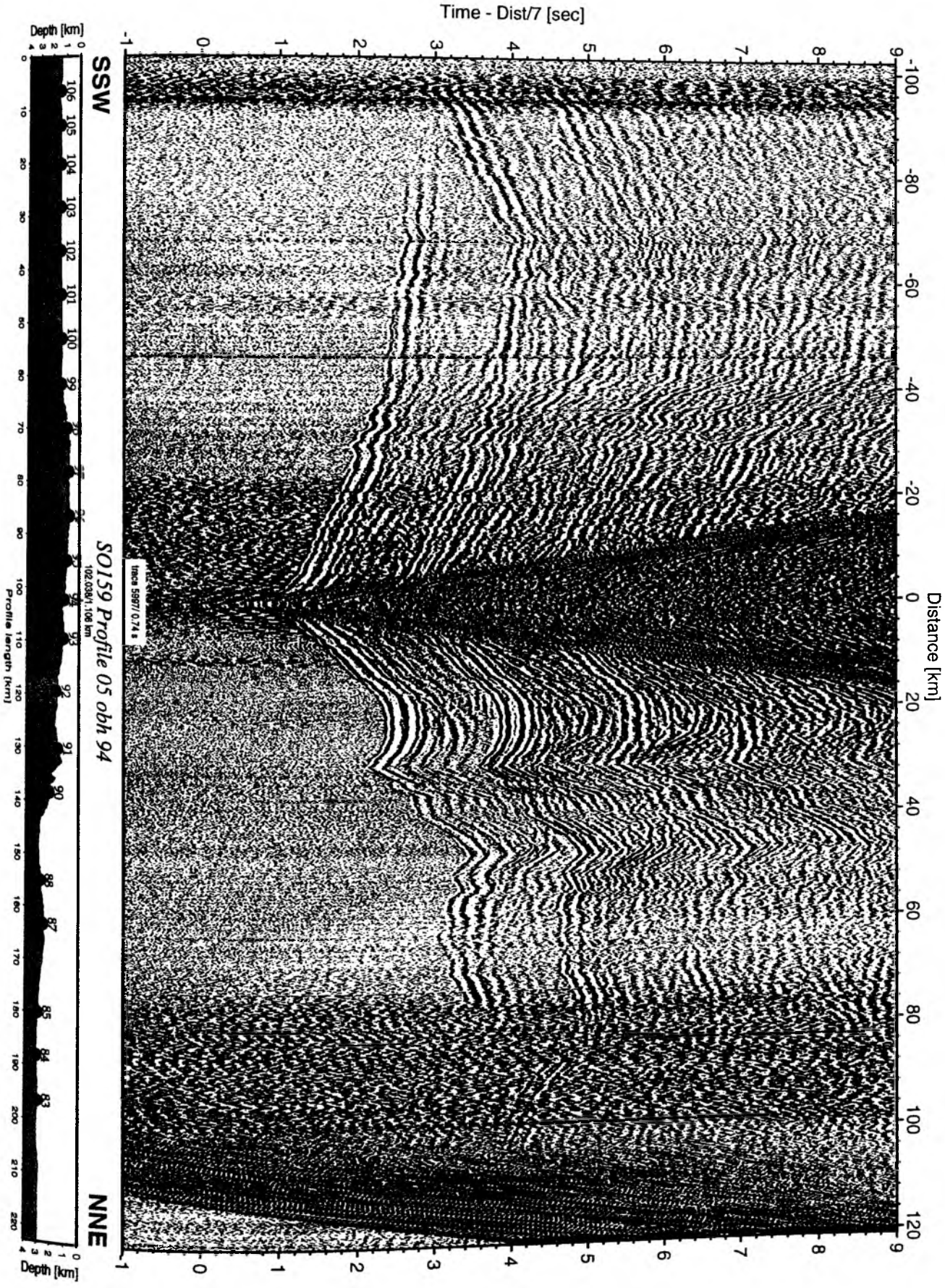

Figure 5.3.5.11: Record section from obh 94 , Profile 05.

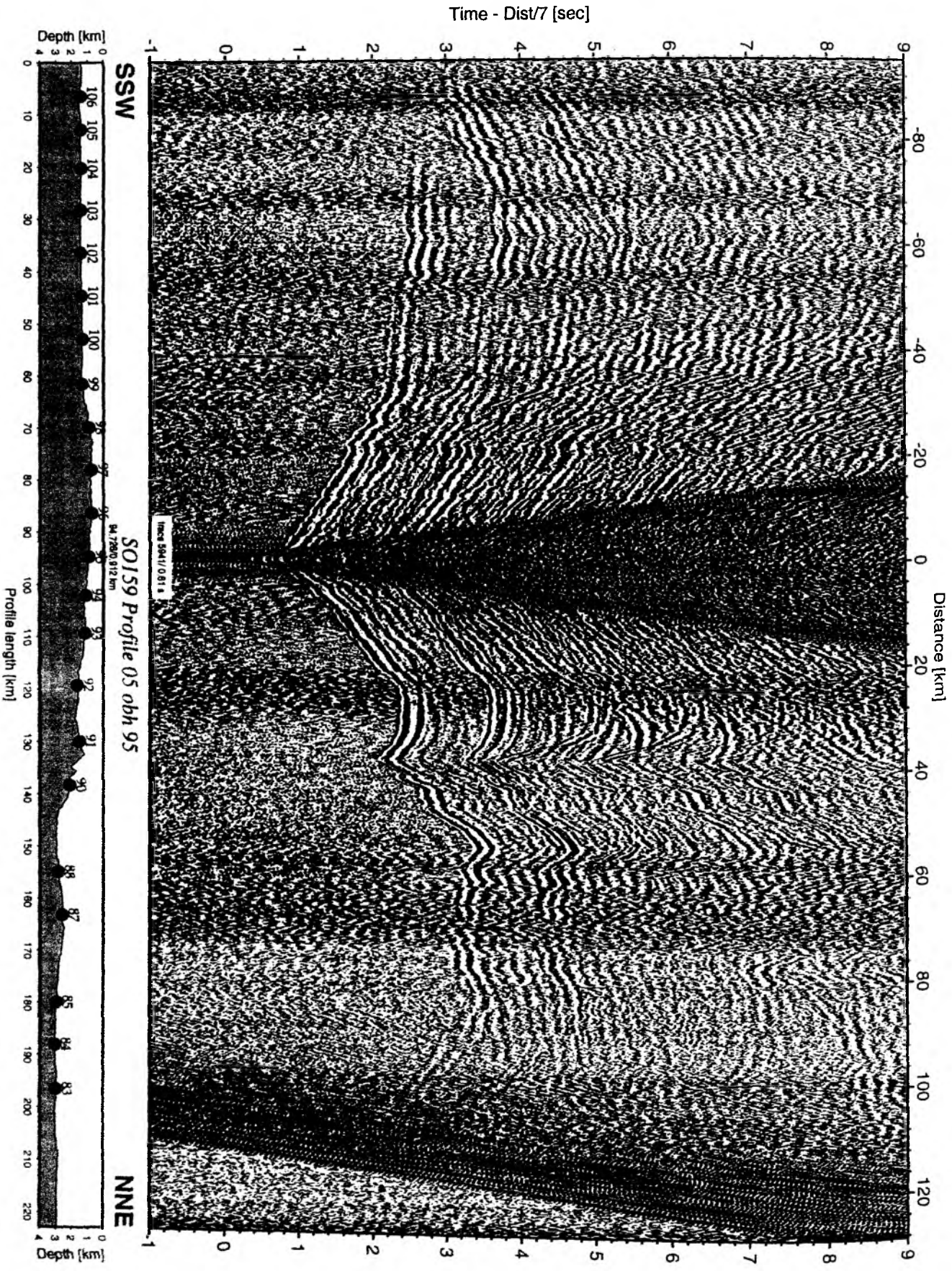

Figure 5.3.5.12: Record section from obh 95 , Profile 05.

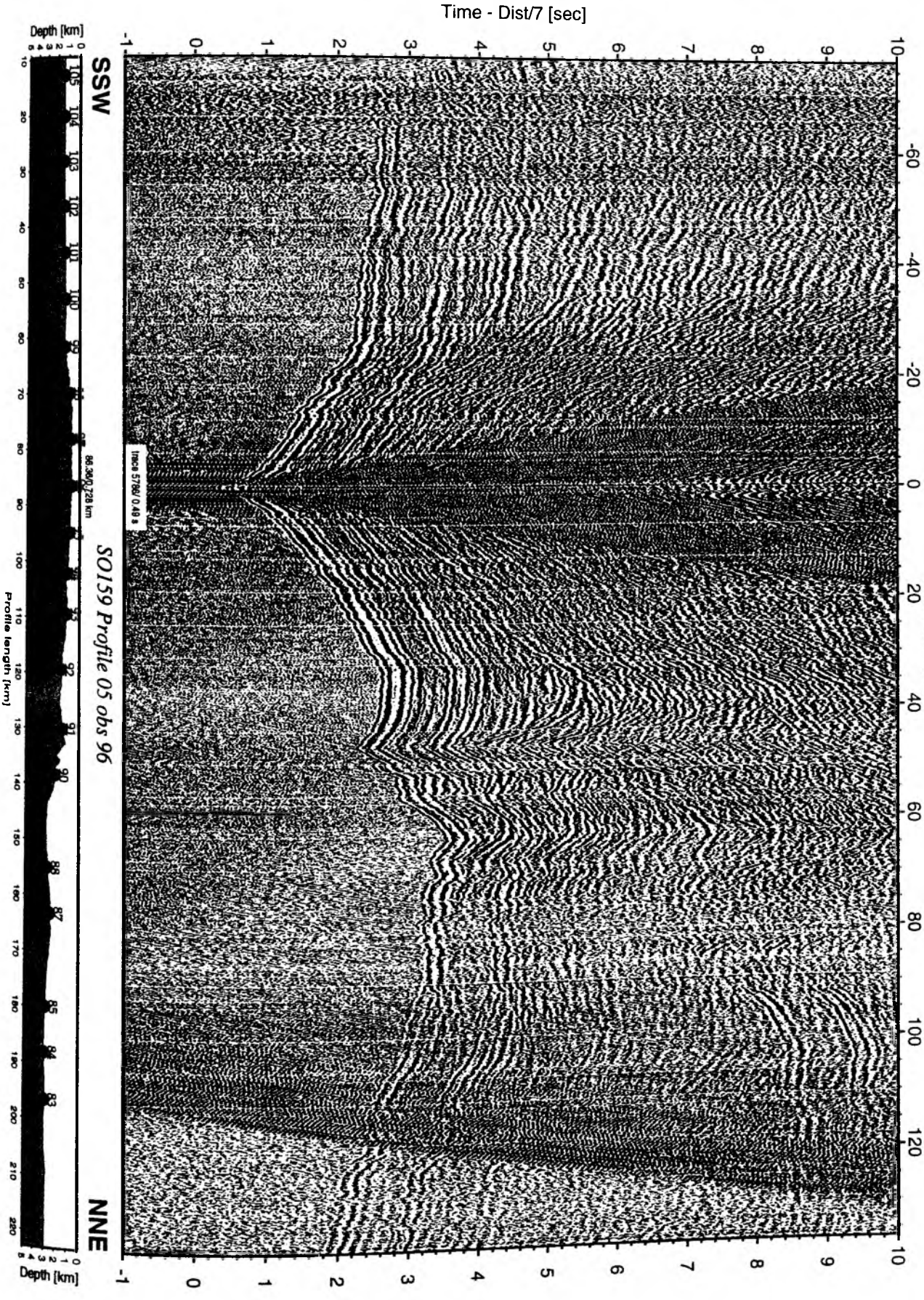

Figure 5.3.5.13: Record section from obs 96 vertical component, Profile 05.

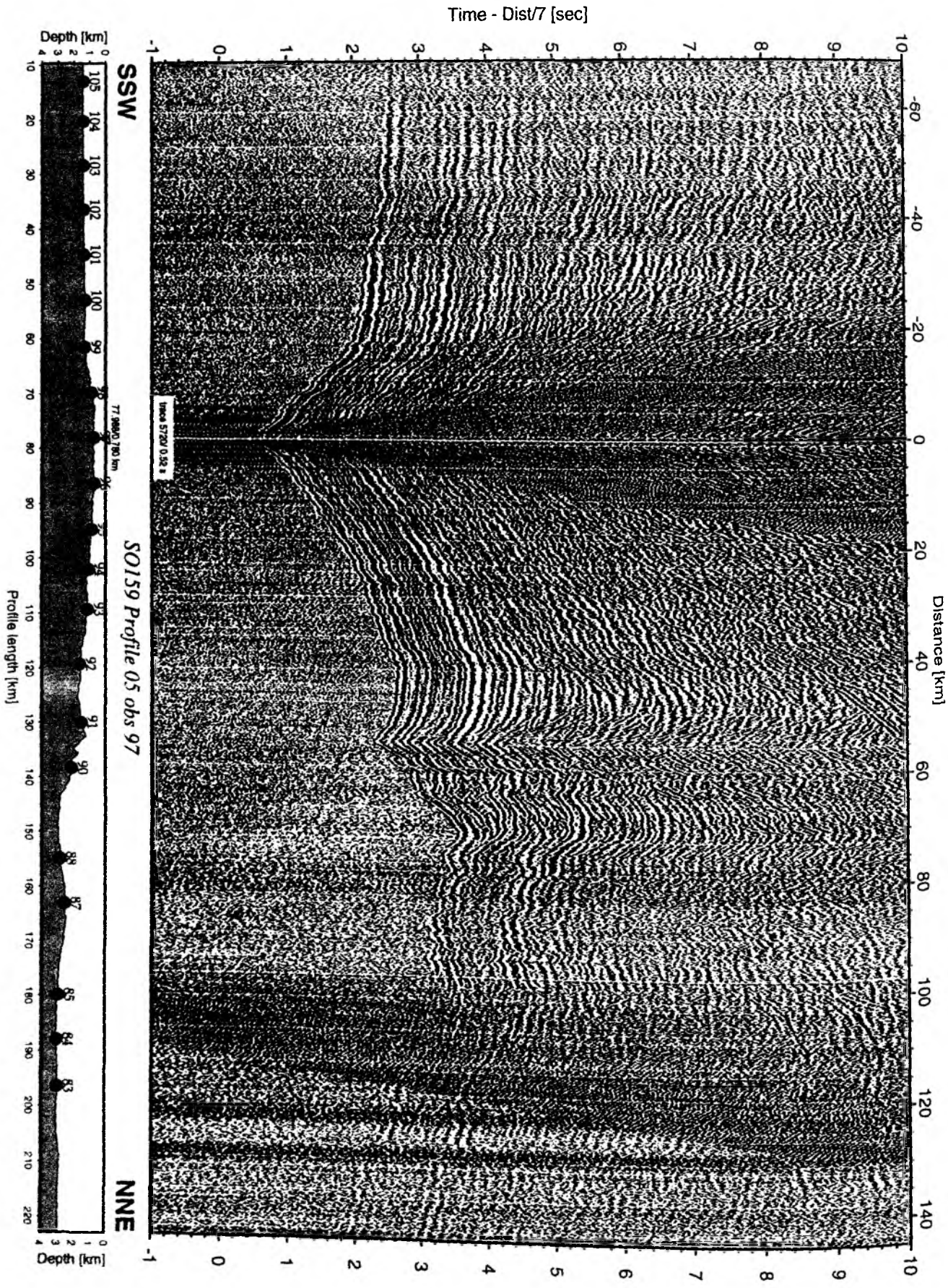

Figure 5.3.5.14: Record section from obs 97 vertical component, Profile 05.

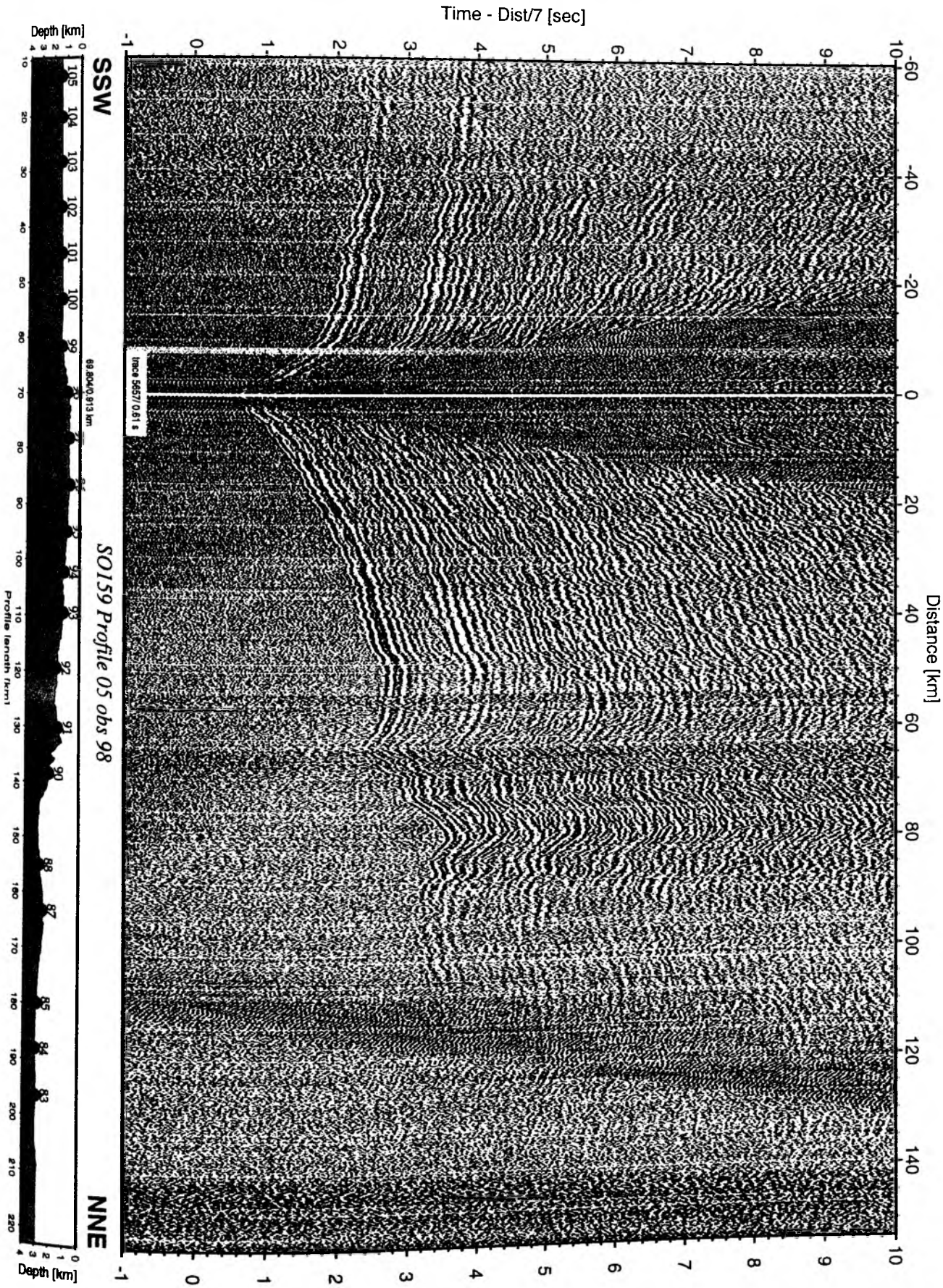

Figure 5.3.5.15: Record section from obs 98 hydrophone, Profile 05.

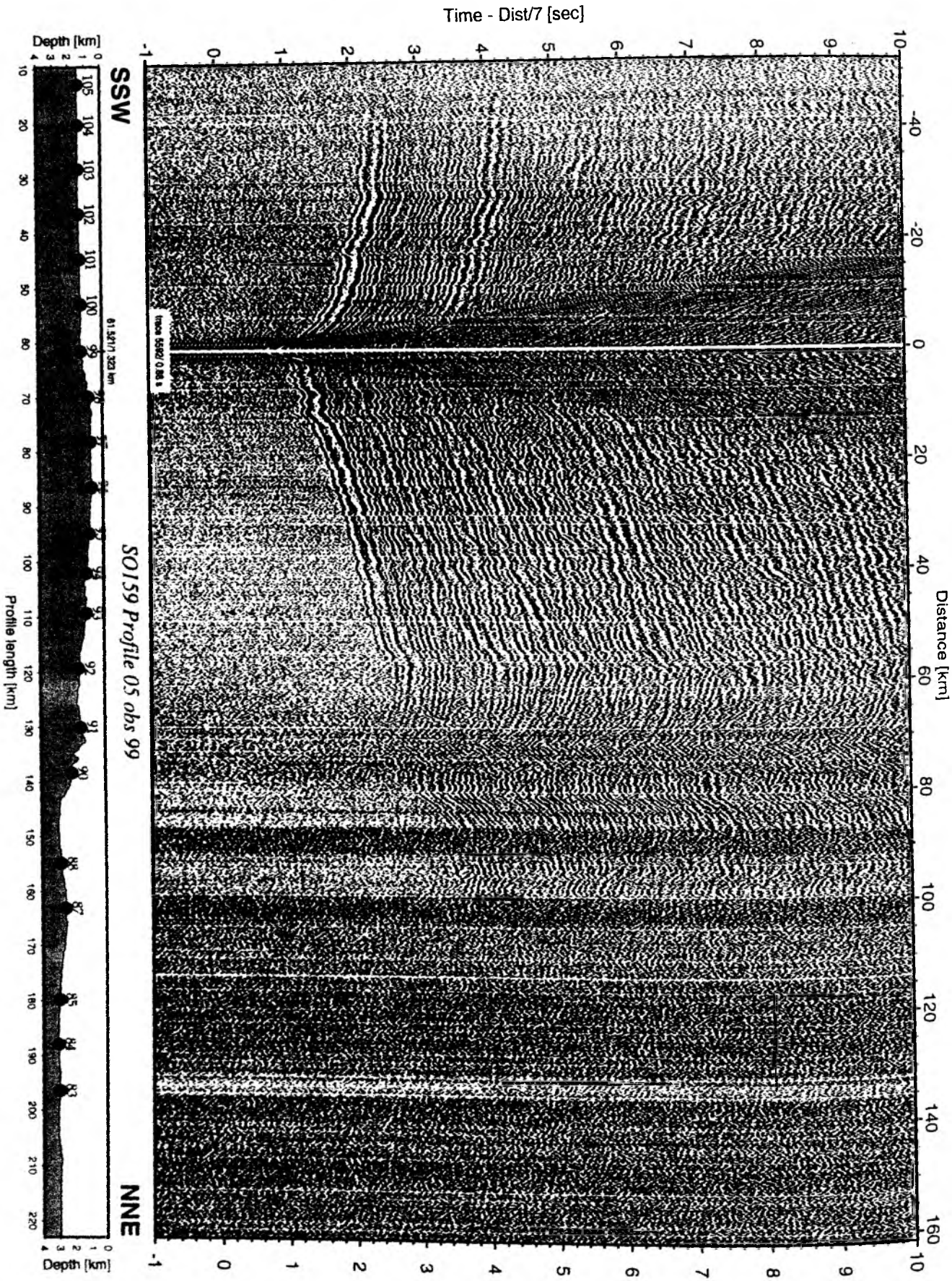

Figure 5.3.5.16: Record section from obs 99 vertical component, Profile 05.

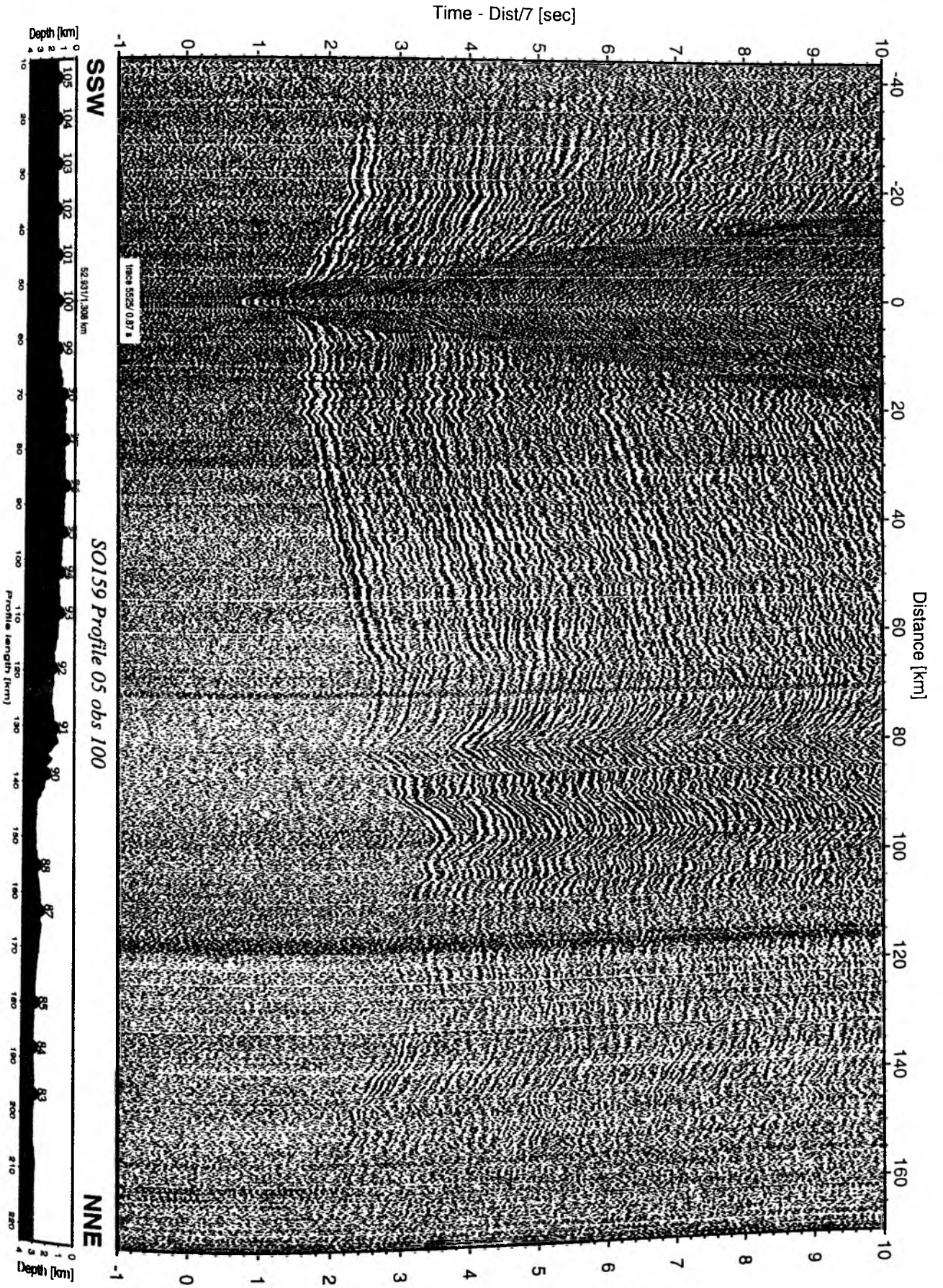

Figure 5.3.5.17: Record section from obs 100 vertical component, Profile 05.

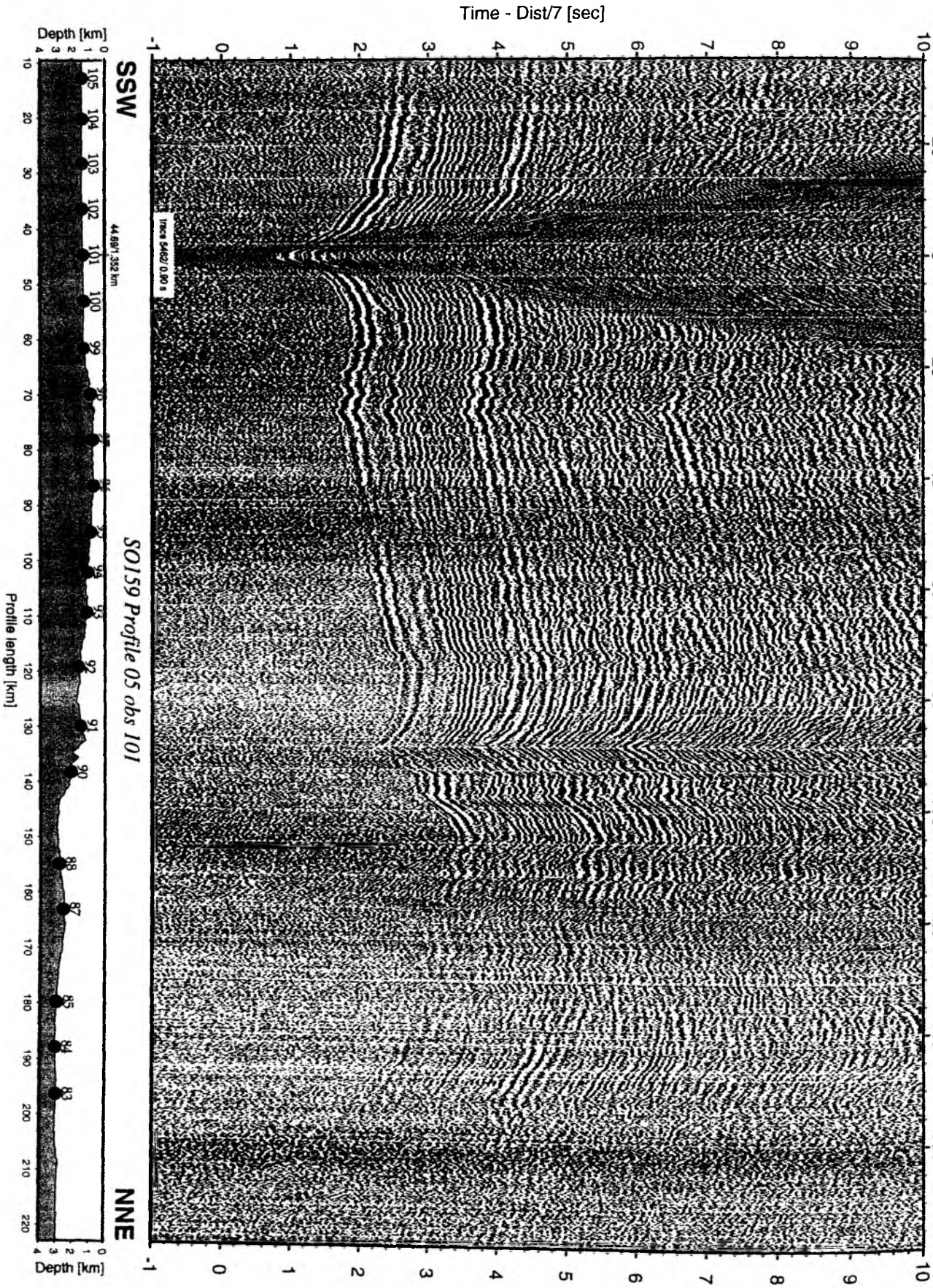

Figure 5.3.5.18: Record section from obs 101 vertical component, Profile 05.

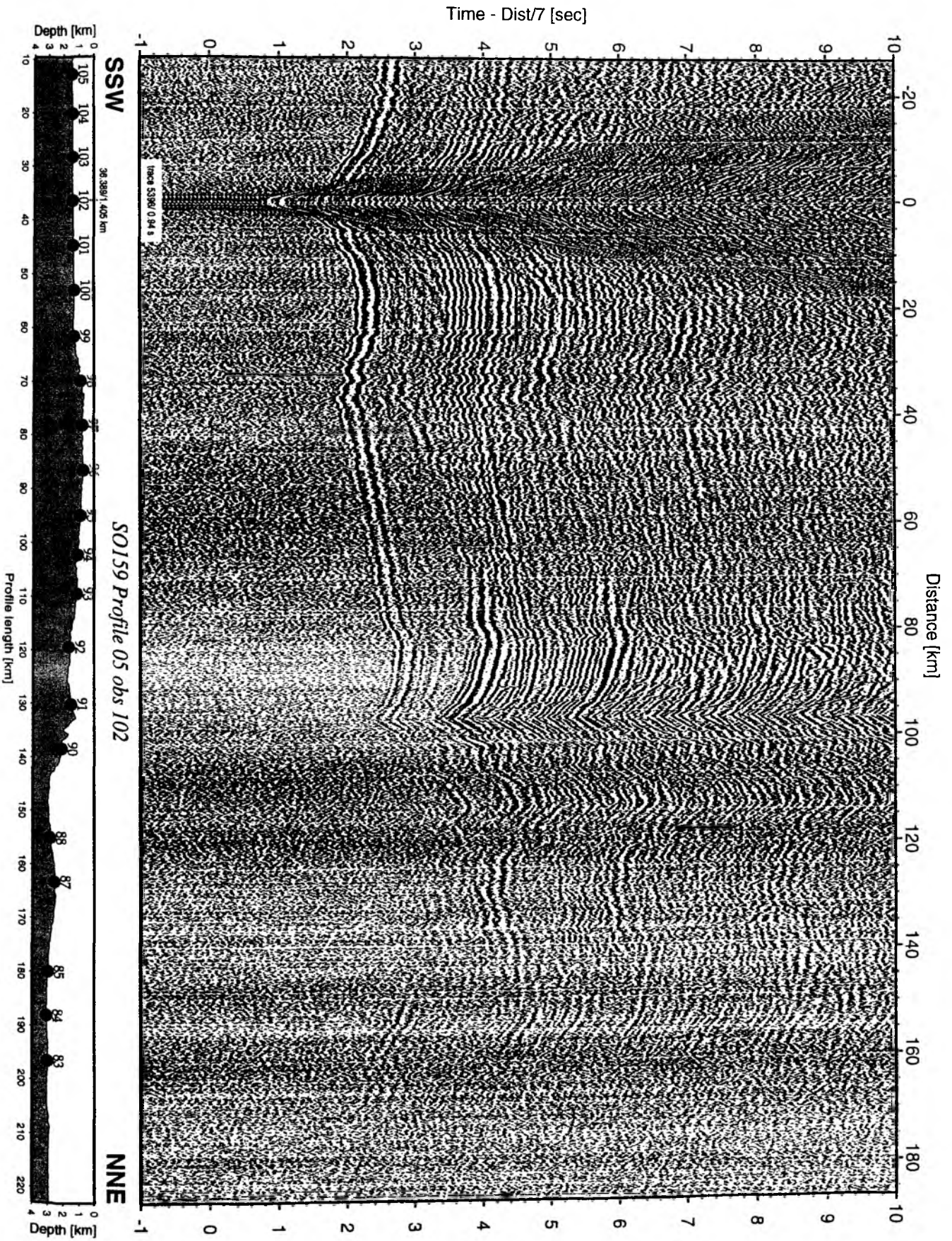

Figure 5.3.5.19: Record section from obs 102 vertical component, Profile 05.

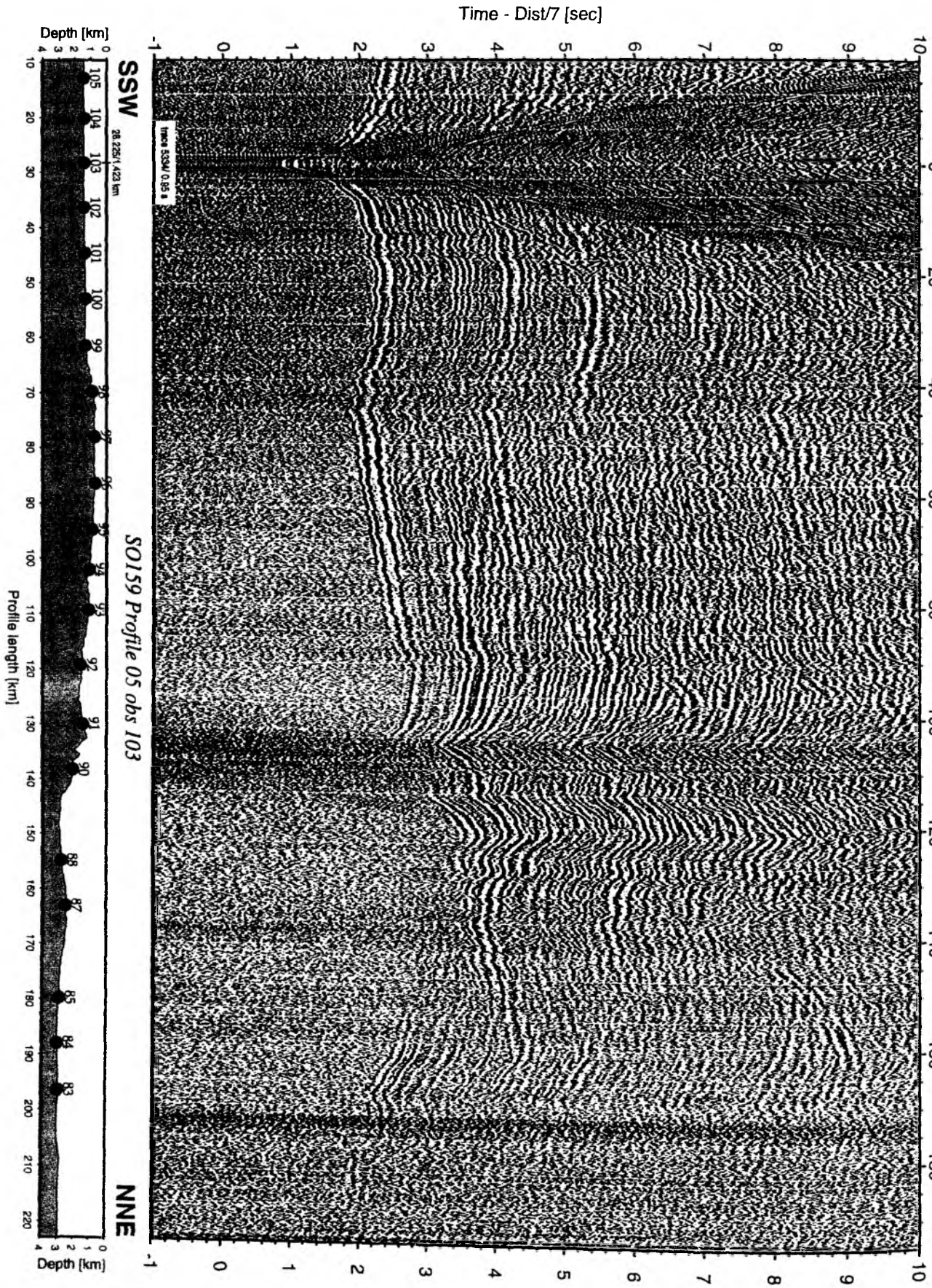

Figure 5.3.5.20: Record section from obs 103 vertical component, Profile 05.

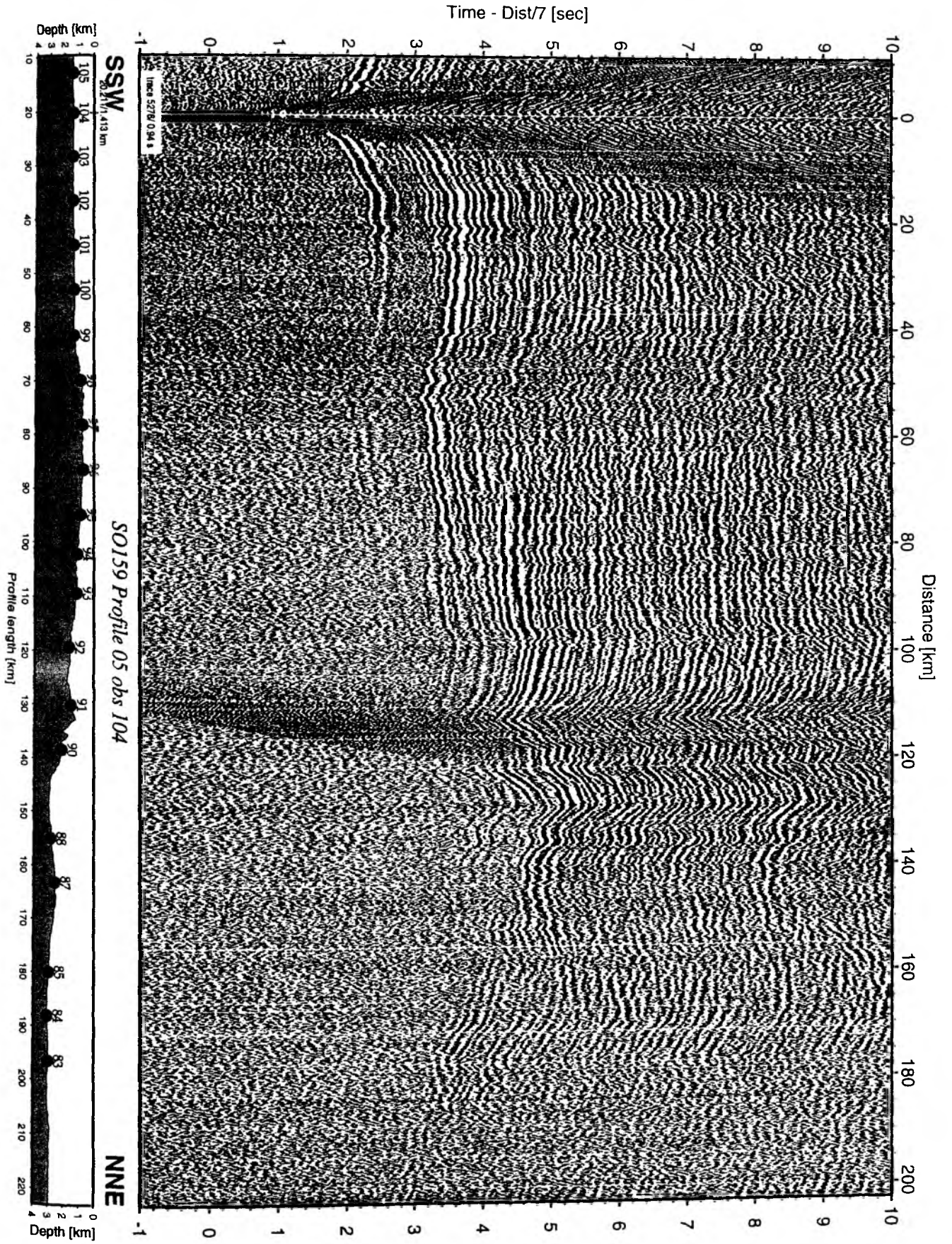

Figure 5.3.5.21: Record section from obs 104 vertical component, Profile 05.

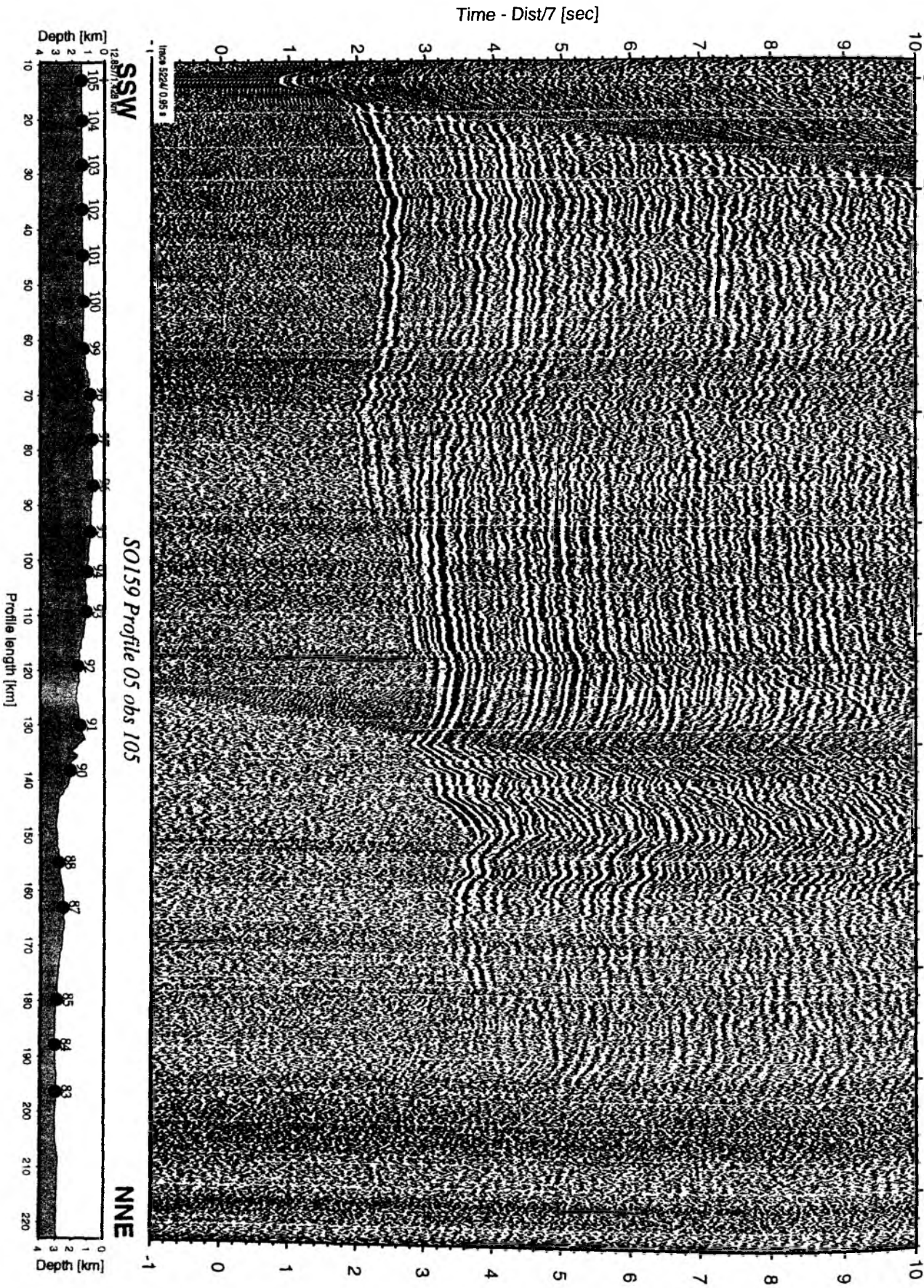

Figure 5.3.5.22: Record section from obs 105 vertical component, Profile 05.

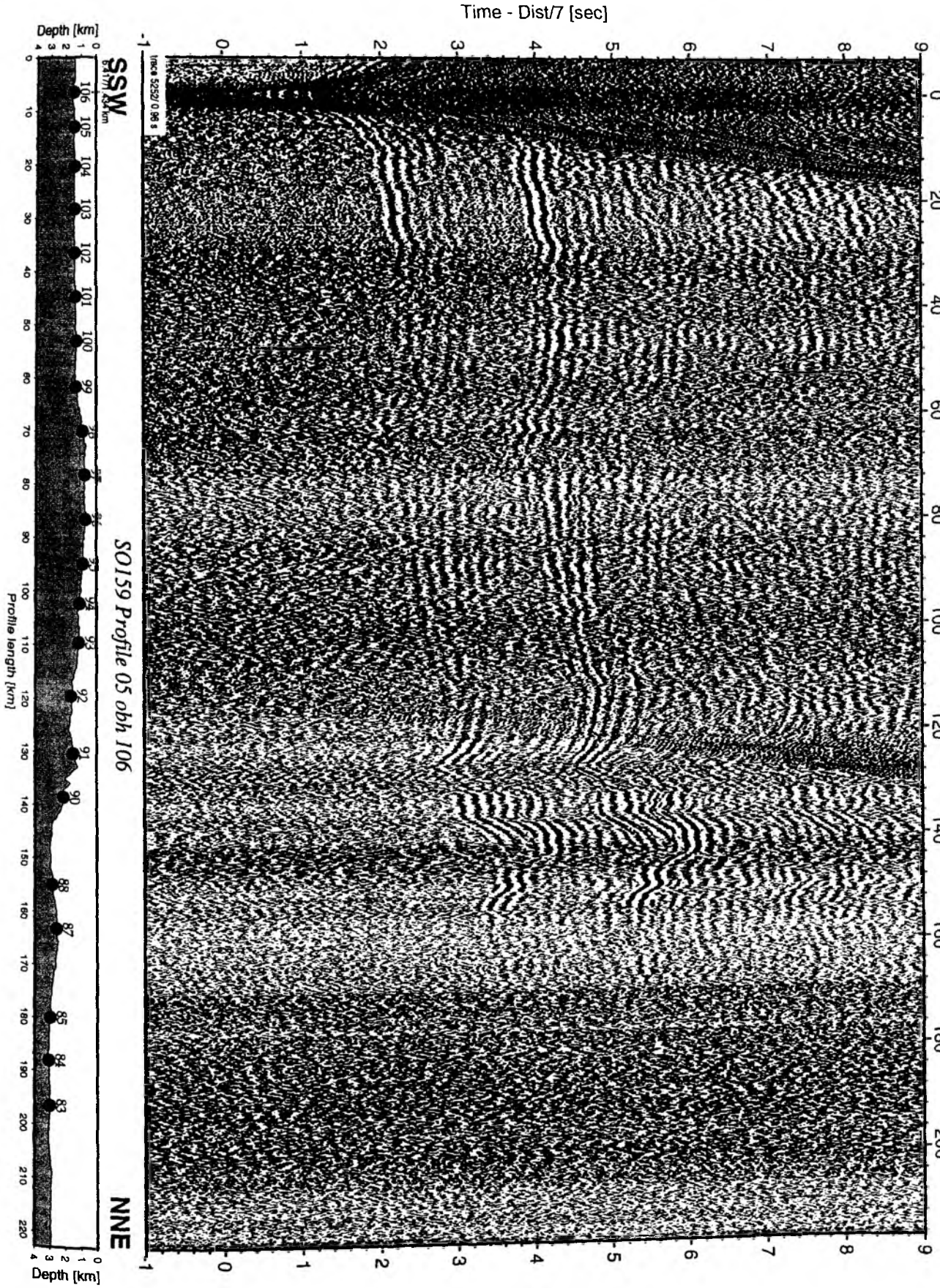

Figure 5.3.5.23: Record section from obh 106 , Profile 05.

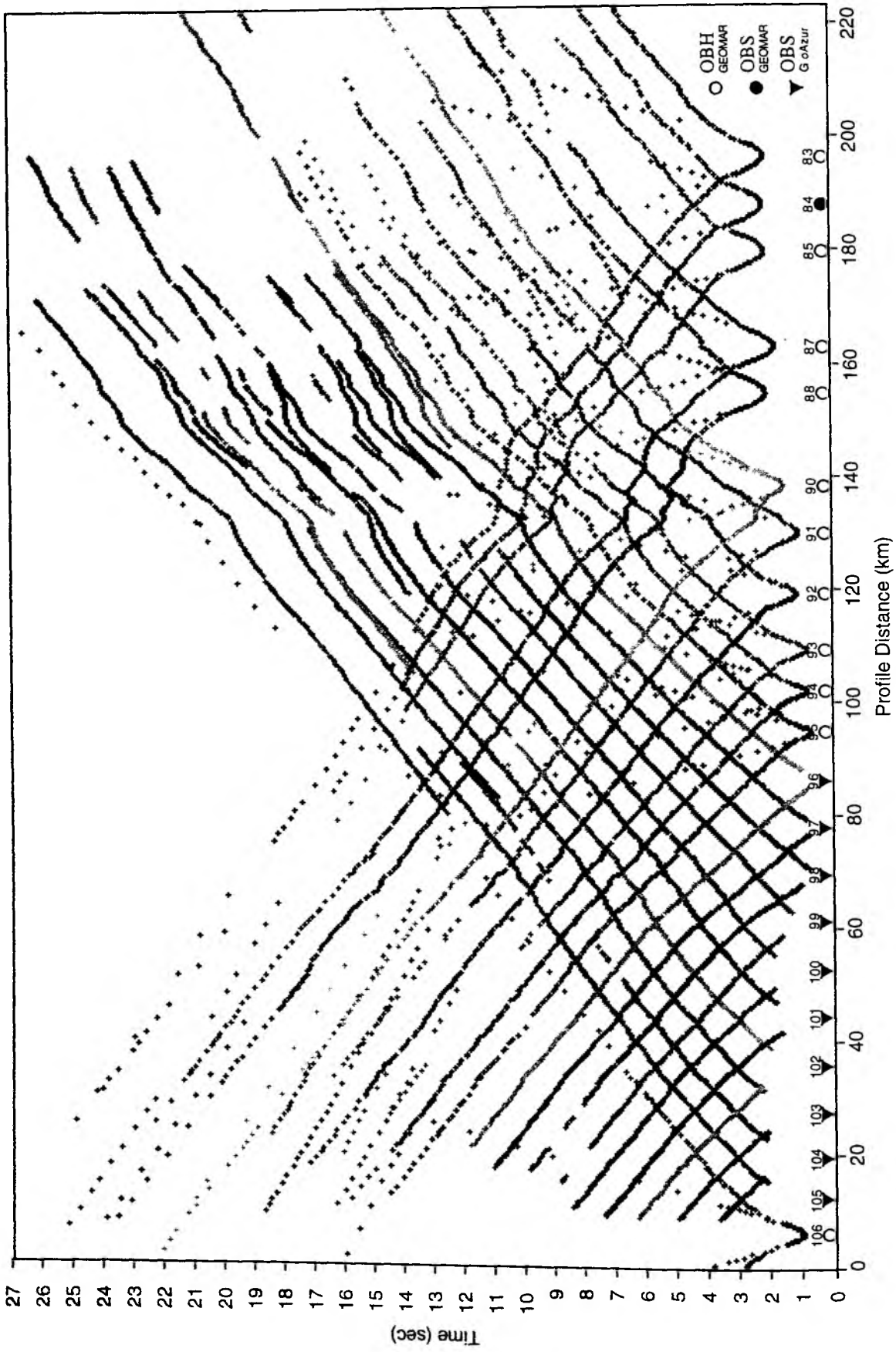

Figure 5.3.5.24

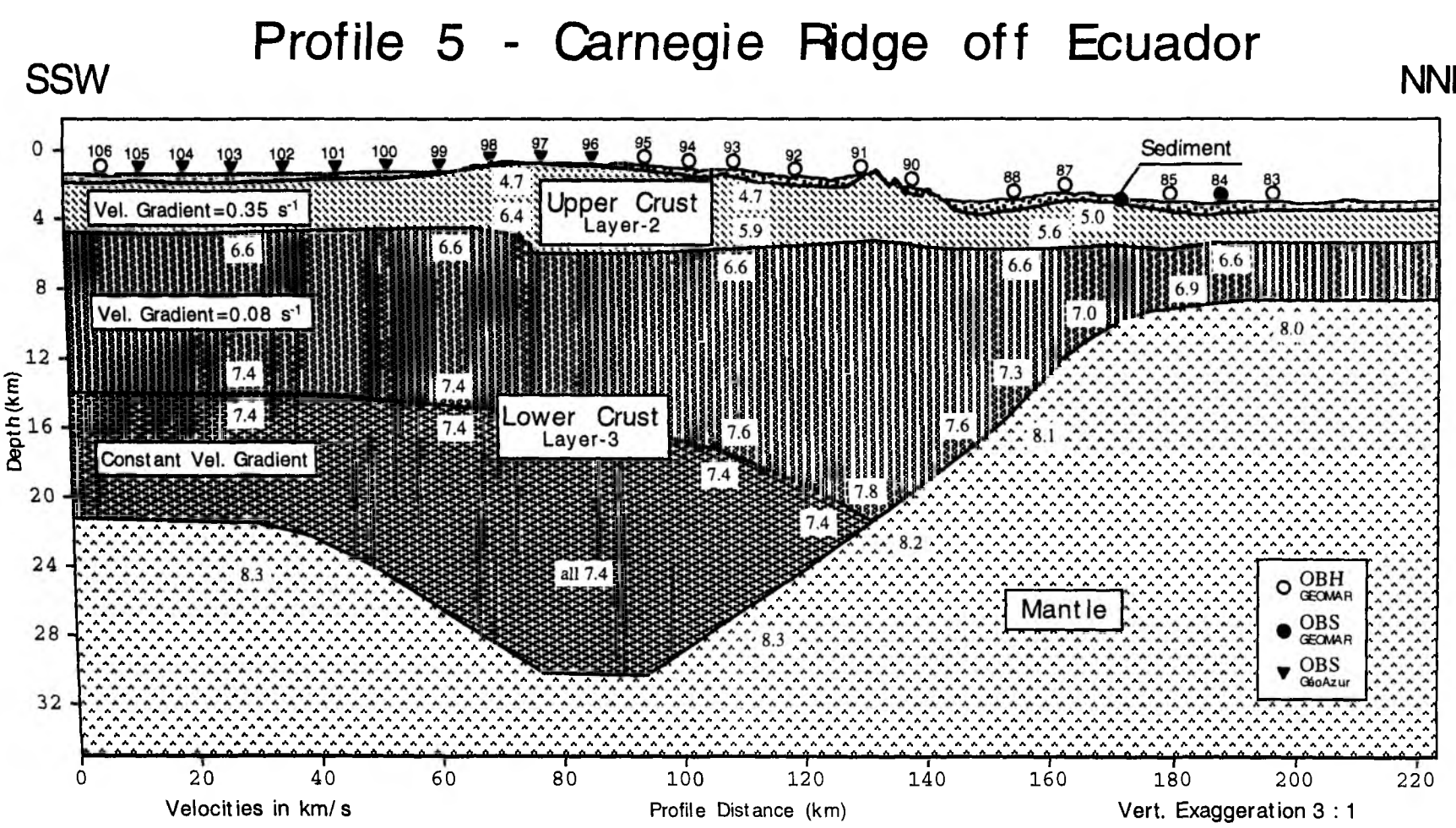

Figure 5.3.5.25

5.3.6 Profile SO 159-06

(W. Agudelo)

Profile 06 is a strike line across the margin in northern Ecuador, partly extending into Colombian waters. It was chosen coincident with a MCS line 42 of the SISTEUR project from summer 2000. On September 11 a total of 24 instruments were deployed (OBS107 to 130) along this 75 nm long profile at about 3.0 nm interval. Shooting was started at 17:00 and lasted to 10:00 the next day. As for previous lines shots were fired at 60 sec intervals and the gun were towed at 4.5 kn. The magnetometer was also deployed. All three airguns worked without interruption throughout the profile. A location map is shown in Figure 5.3.6.1. All but one instrument were recovered (see Appendix II-6) by 07:00 September 13. The expected structure is evident from a line drawing of a neighbouring profile (SISTEUR-35) collected during the SISTEUR cruise, which is shown in Figure 5.3.6.2. This profile is interesting because it is a good example of the transition from active accretion in the North to non or incipient accretion in the South. Pelagic sediments upon the oceanic crust are covered by thicker turbidites deposited in the trench which reach ~2.5 s (TWTT). These sediments form the upper layer of the oceanic crust and lay on a oceanic basement affected by normal faults. Some of this faults are extending into the sediments. No direct evidence of recent accretion was found on this profile. Some thrusts could be identified in the margin toe, sole out to a common reflector, interpreted as a décollement level. It follows the top of the sedimentary layer that therefore is being completely underthrusted, forming a thick subduction channel. An outer high arc shows a gentle slope that shows evidences for active deformation. It marks the eastern boundary of a forearc basin that reach 3.0 s in depth.

Record sections description

The profile SO159-06 was the last one collected during the cruise and its data were gathered and processed a few days before the cruise end. Unfortunately, the reduced time available prevents the construction of a model with acceptable quality. This model will be made in the laboratories later. Records sections of OBH along the profile are shown in the figures 5.6.3 to 5.6.20. In most of the records, the data quality is good and some arrivals can be clearly follow throughout the profile.

The OBH 107-110, were deployed on the oceanic crust. No low velocity arrival was observed, indicating that sediment are absent or very thin. The record sections show strong arrivals within an offset of 40 Km, with high velocities (4.5 – 6.0 Km/s). A sharp PmP phase can be identified, extending to 40 Km offset. The oceanic crust thickness could be estimated to ~7 Km. Specially interesting are the records of OBH 108 and OBH 109 which show a clear Pn eastern arrival which can be followed until an offset of 100 Km, with apparent velocities more than 7.5 Km/s.

The OBH 111-113, were located near to the oceanic trench. Some low velocity (~2.5 Km/s) arrivals of short length are observed, indicating the presence of a thin layer of sediments. These arrivals became longer towards the trench, possibly because of thickening of this layer (i.e. compare figures 5.3.6.7. and 5.3.6.9). In the western side of the record section the arrivals are clearer, as a result of a less complex bathymetry. On the contrary, it is more difficult to interpret the eastern side, where two striking features disturbing the data: the trench and a main diffraction at 30 Km East of the deformation front. This side shows also prominent Pn arrivals, but the PmP phase is less clear, partly due to the interference of diffractions.

The OBH 115-120 display clearly some subsurface features of the margin. A very prominent low velocity arrival is observed next to the direct wave, possibly resulting from a thick layer of unconsolidated sediments. A second arrival, possibly a layer of low velocity (3.0- 4.0 Km/s) is seen over all this set of OBH. This layer is clearly thicker eastwards (compare the western and eastern offsets for this arrival in OBH 116, figure 5.3.6.11). Particularly clear are data in the figure 5.3.6.13. (OBH 117) where the structure of the margin is revealed. Two very strong reflections are observed in the eastern side of the record section, marking the top of the continental basement and the PmP phase. Between them, there is an arrival with a velocity close to 6 Km/s. Also clear is the Pn phase which starts in at offset of 55 Km.

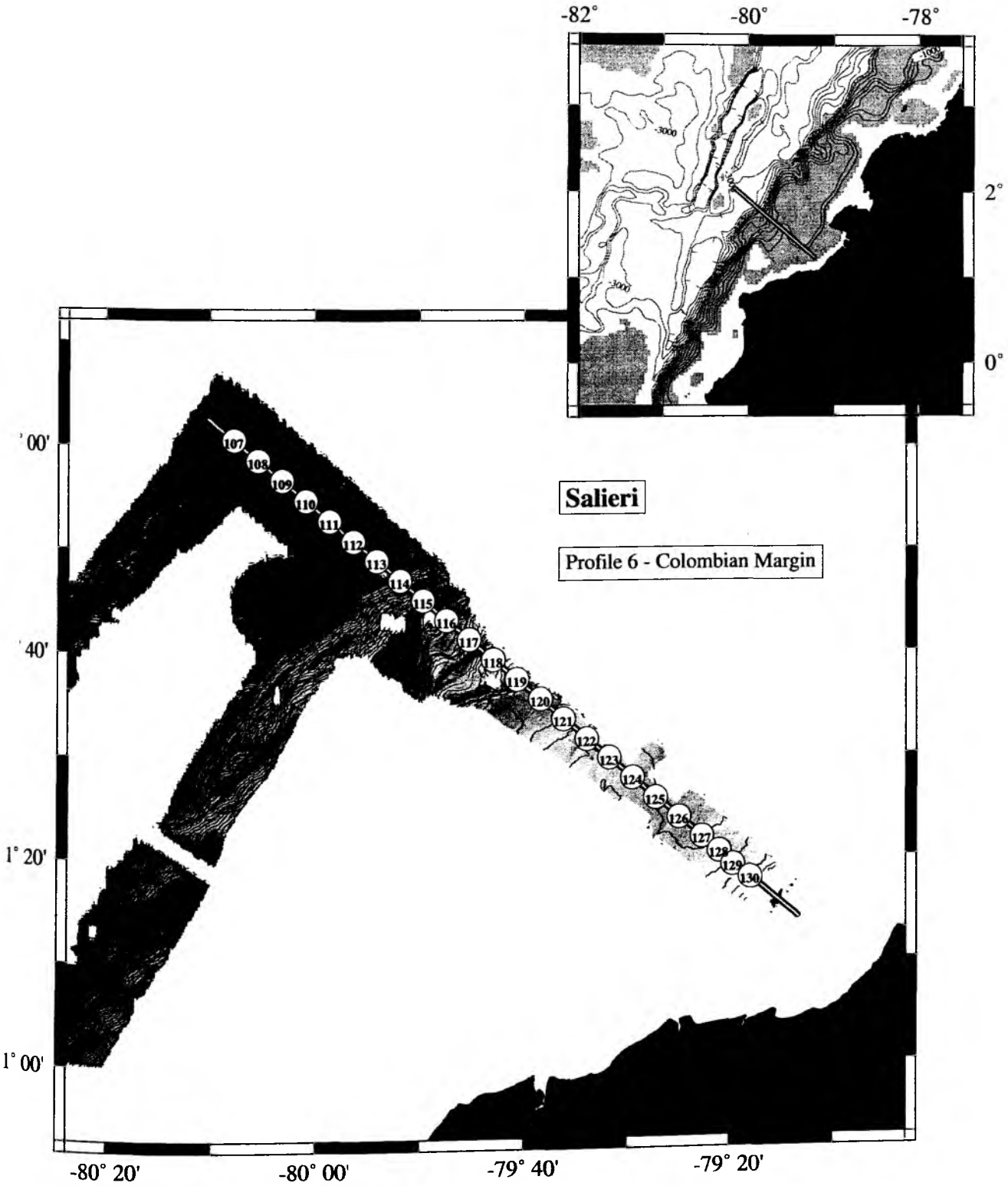

Figure 5.3.6.1. Location map and OBS/OBH location for profile SO 159 - P06

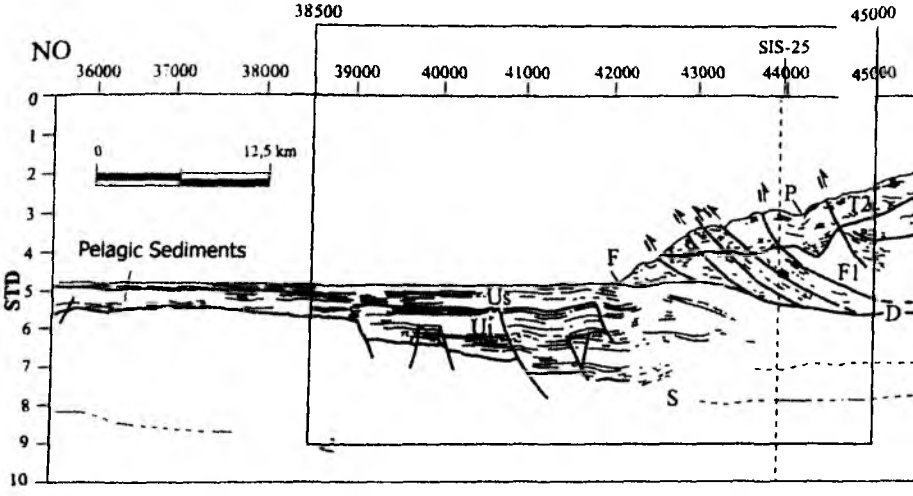
38500
45000
NO
SIS-25
36000
37000
38000
39000
40000
41000
42000
43000
44000
45000
0
12,5 km
Pelagic Sediments
STD
F
P
T
Fl
D
Us
Ui
S

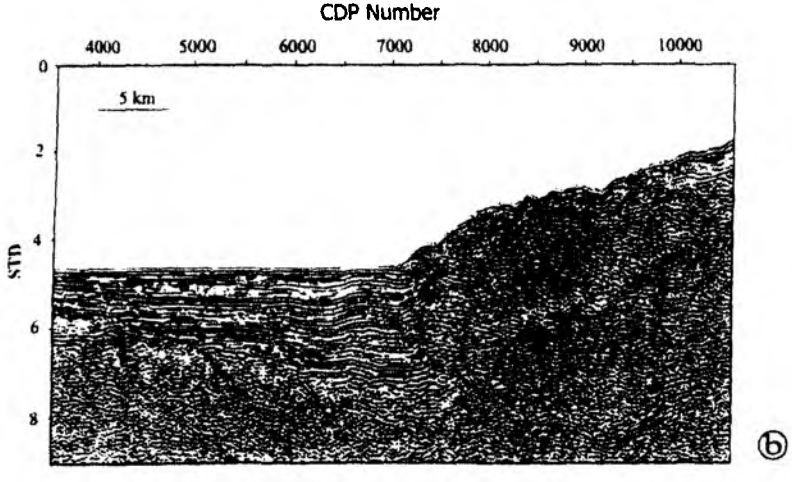
CDP Number
4000
5000
6000
7000
8000
9000
10000
5 km
STD
b

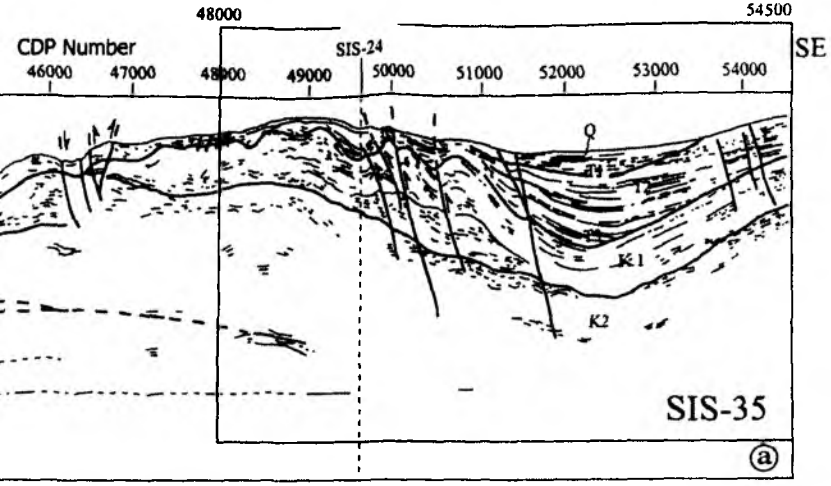

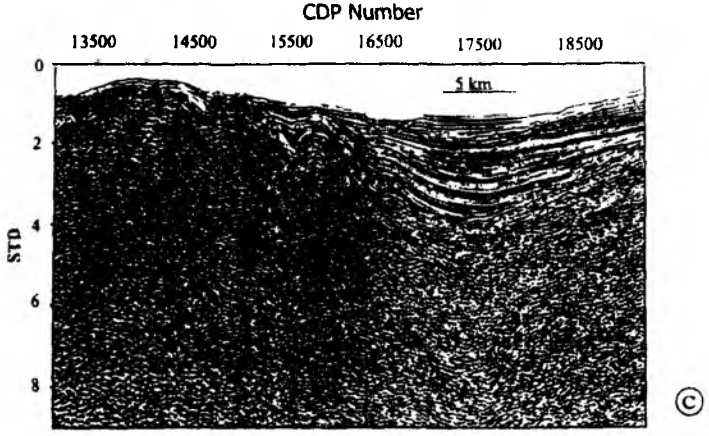

Figure 5.3.6.2. Profile SIS-35
a. Profile line drawing
b. Zoom on the deformation front
c. Zoom on the forearc basin and the eastern deformation zone in the outer high arc

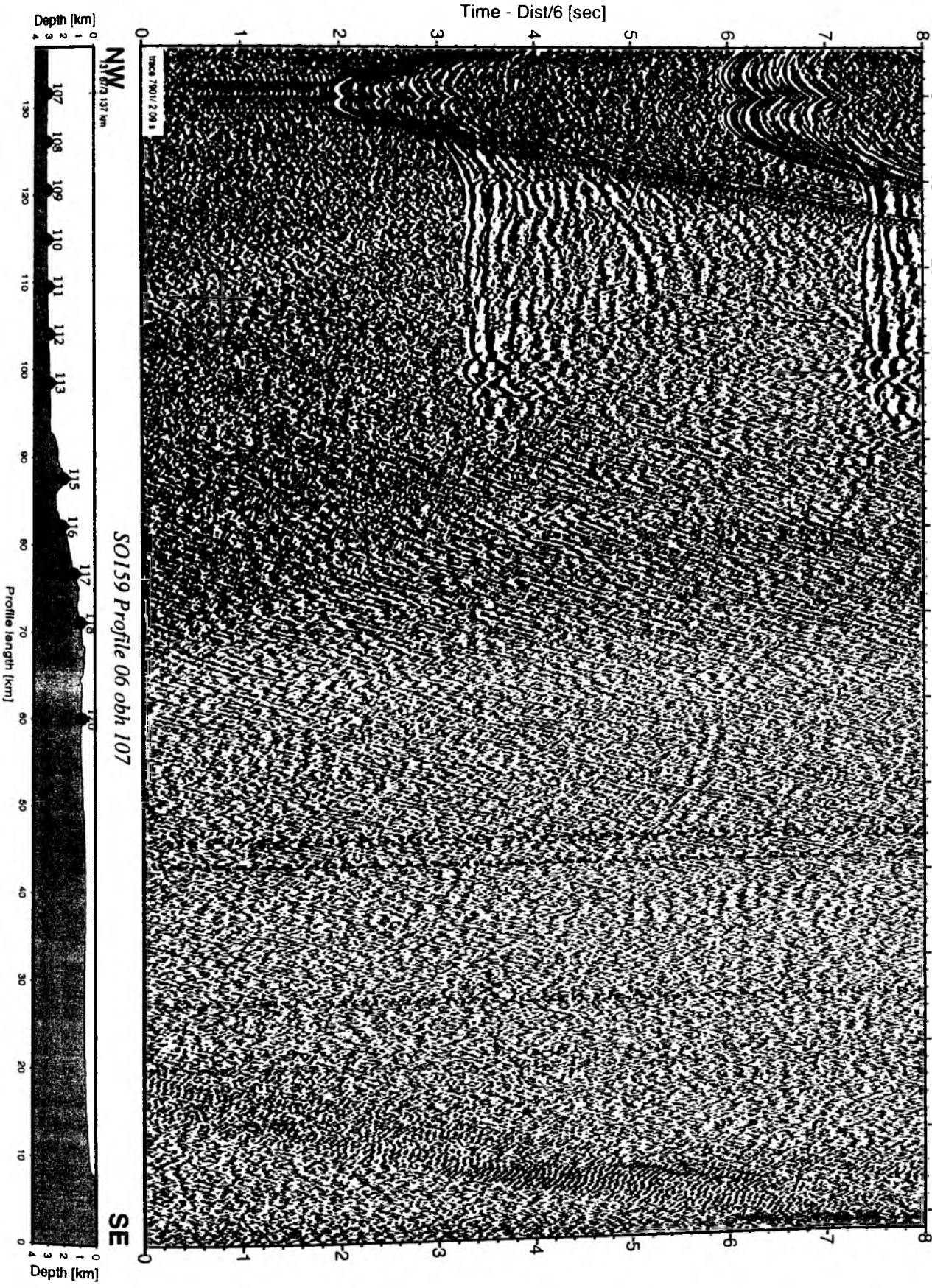

Figure 5.3.6.3: Record section from obh 107 , Profile 06.

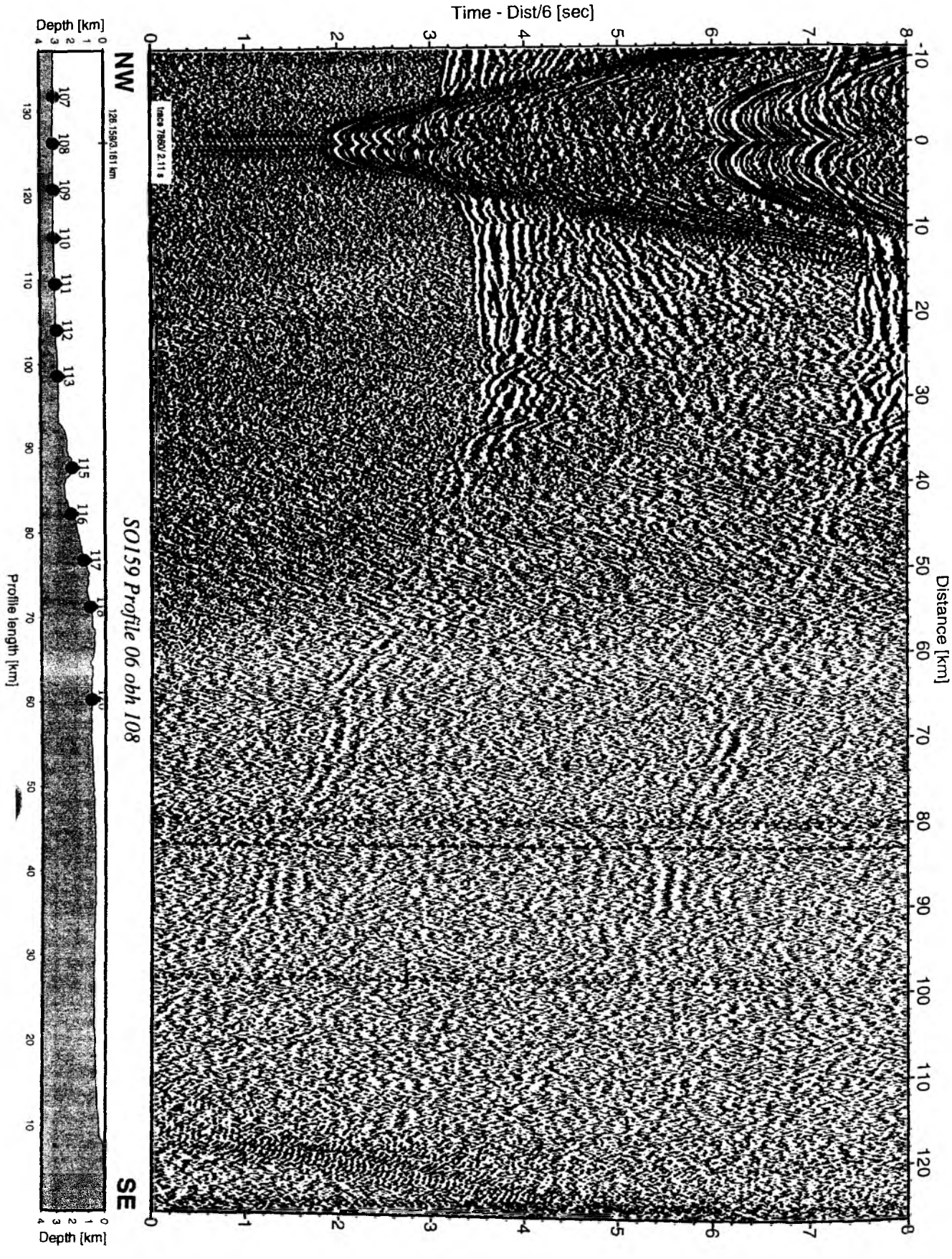

Figure 5.3.6.4: Record section from obh 108 , Profile 06.

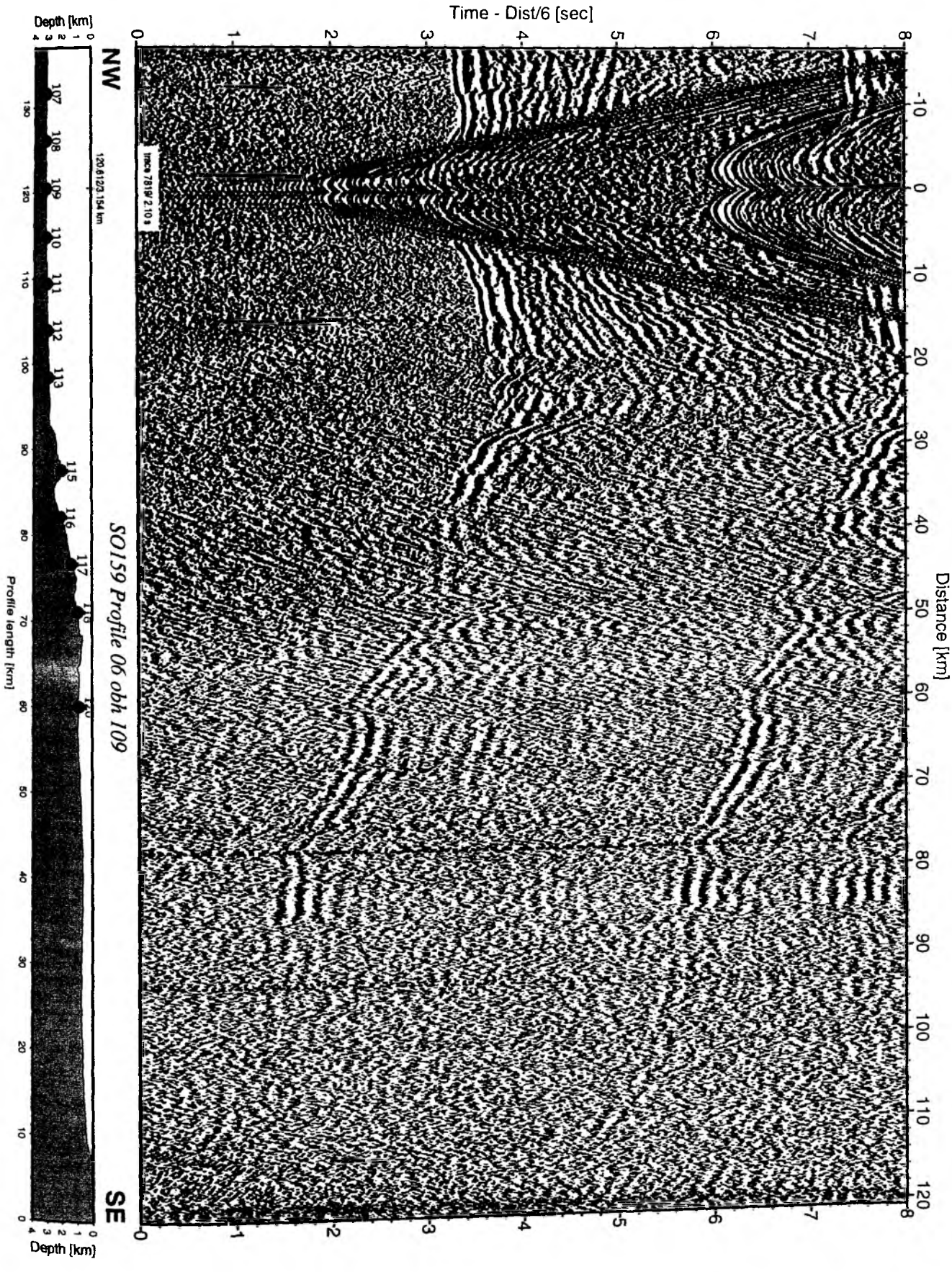

Figure 5.3.6.5: Record section from obh 109 , Profile 06.

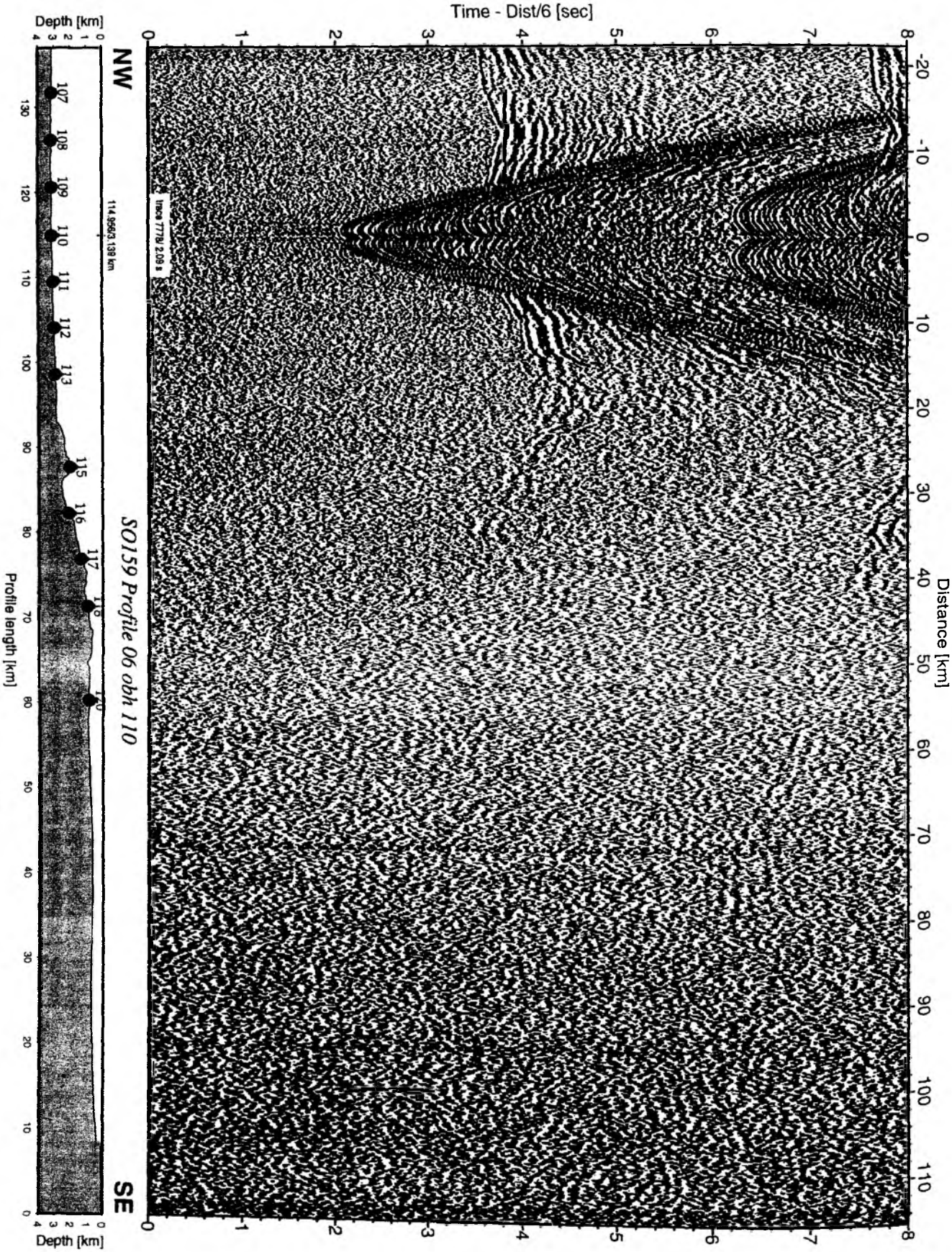

Figure 5.3.6.6: Record section from obh 110 , Profile 06.

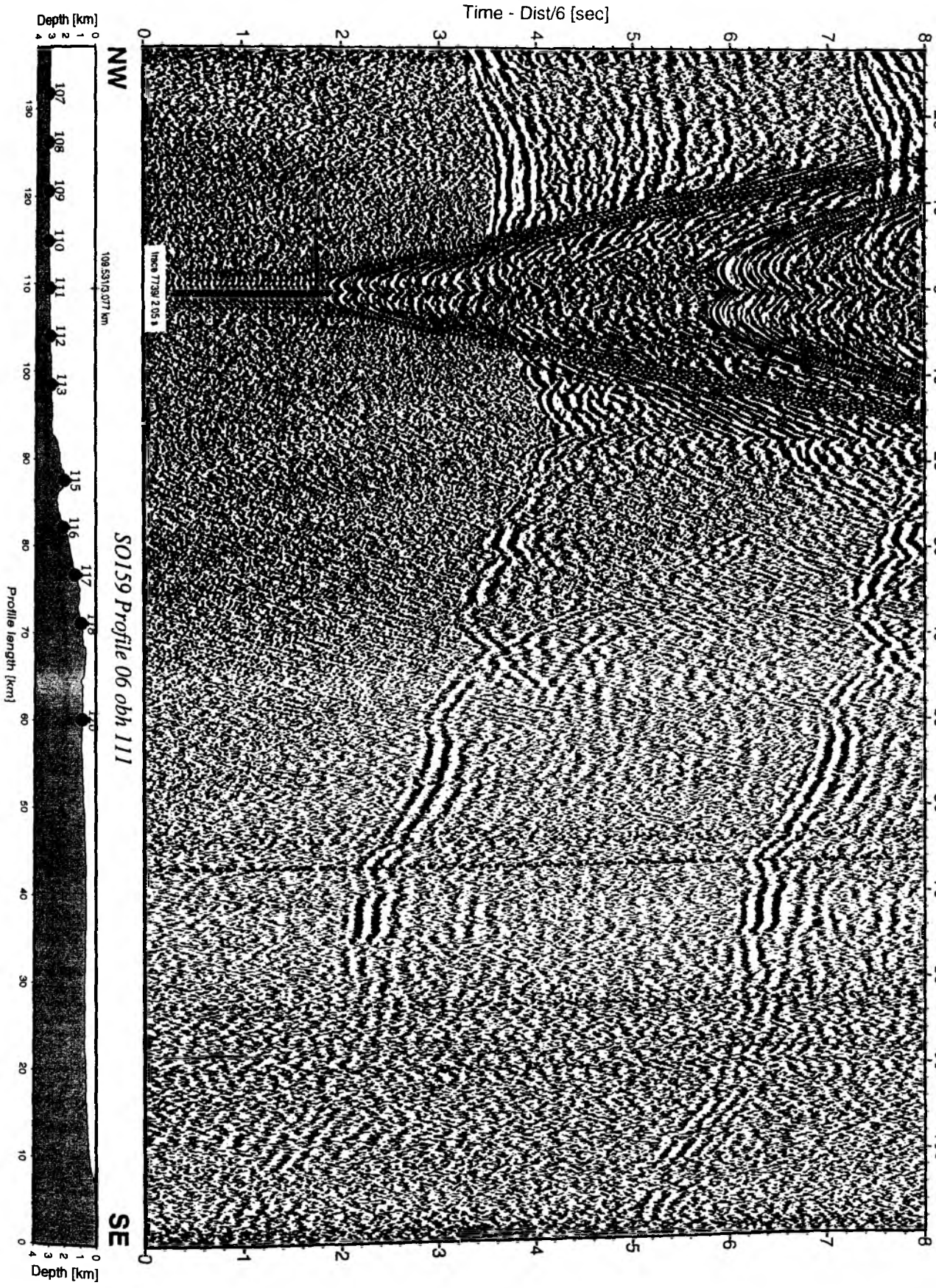

Figure 5.3.6.7: Record section from obh 111 , *Profile 06.*

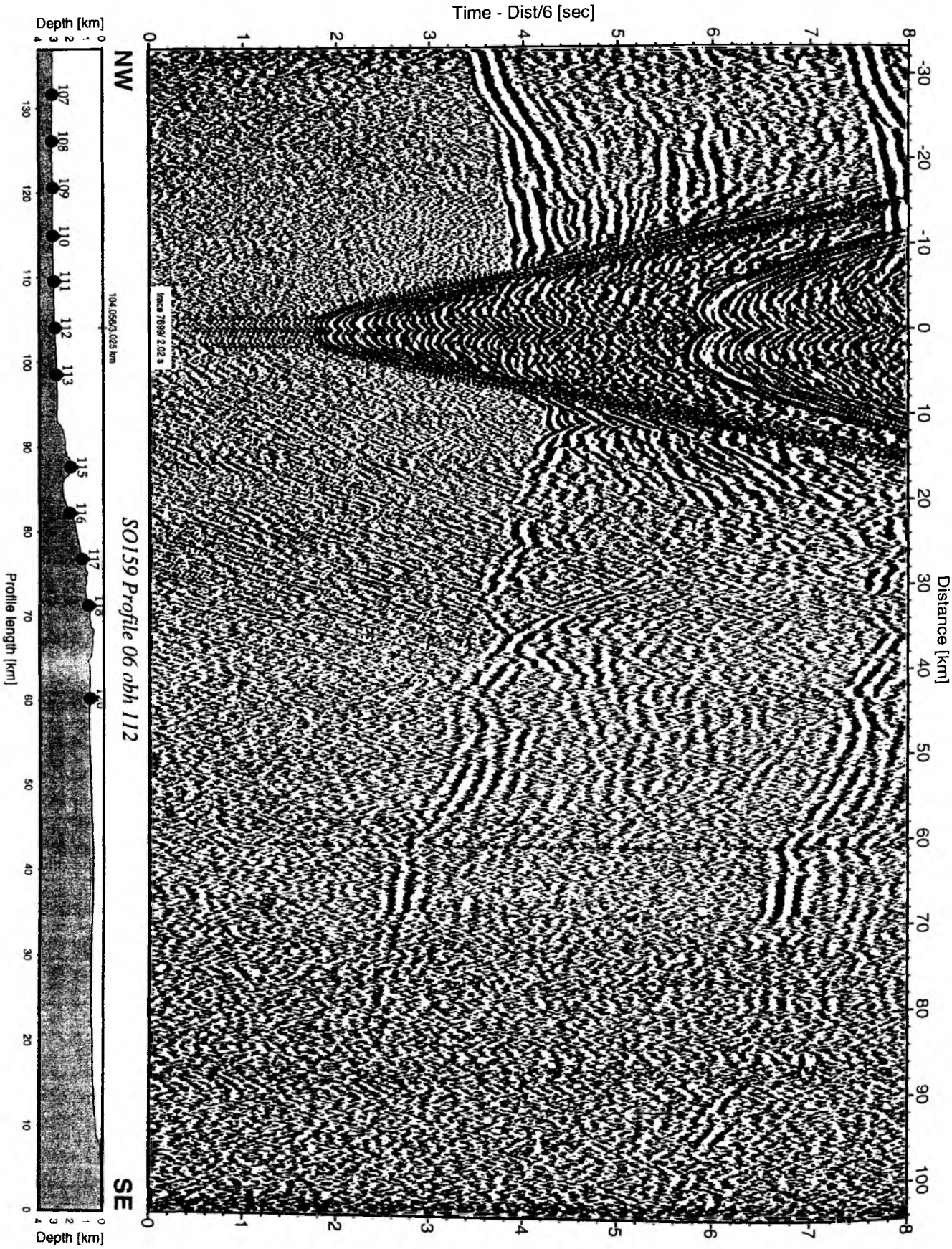

Figure 5.3.6.8: Record section from obh 112 , Profile 06.

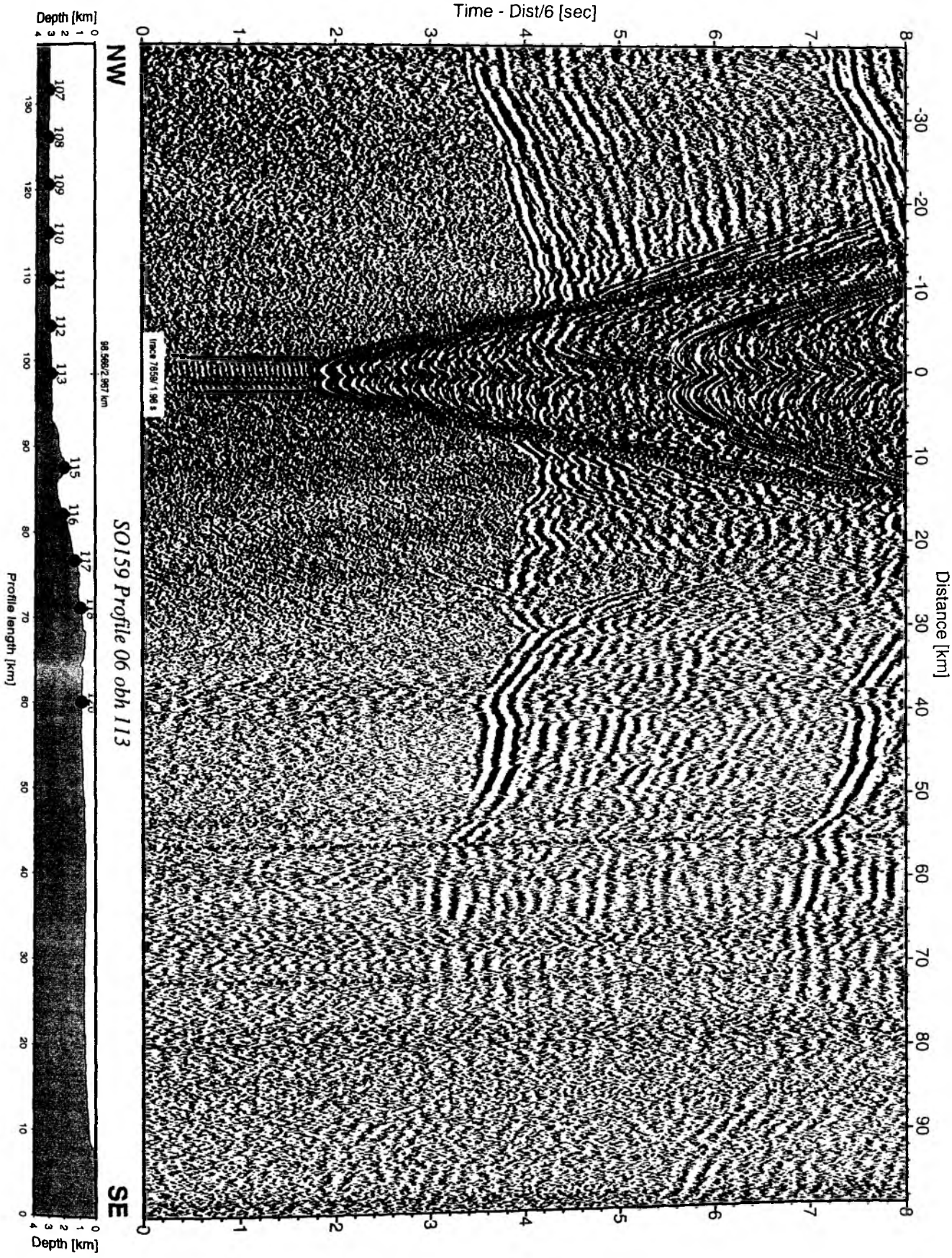

Figure 5.3.6.9: Record section from obh 113 , Profile 06.

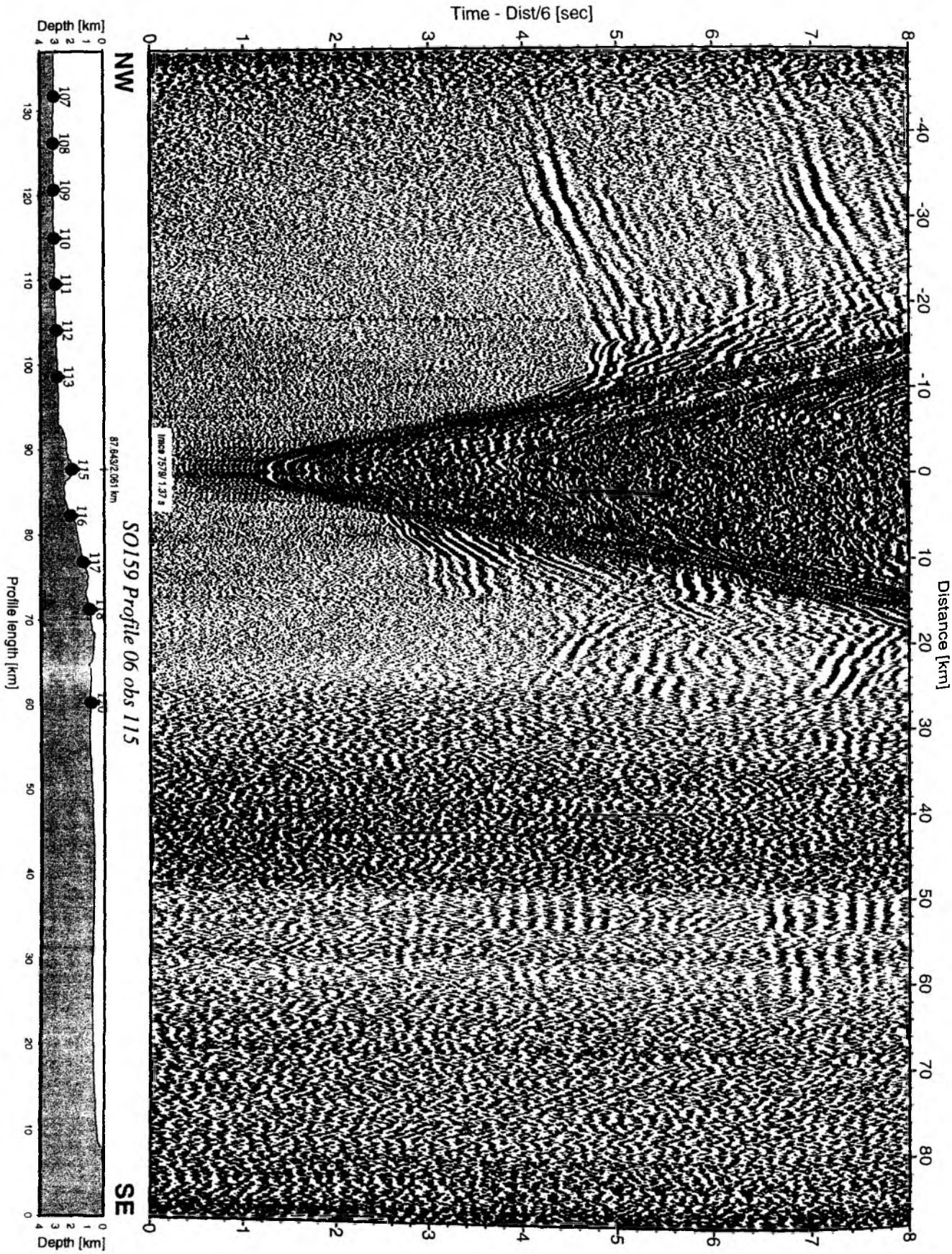

Figure 5.3.6.10: Record section from obs 115 hydrophone, Profile 06.

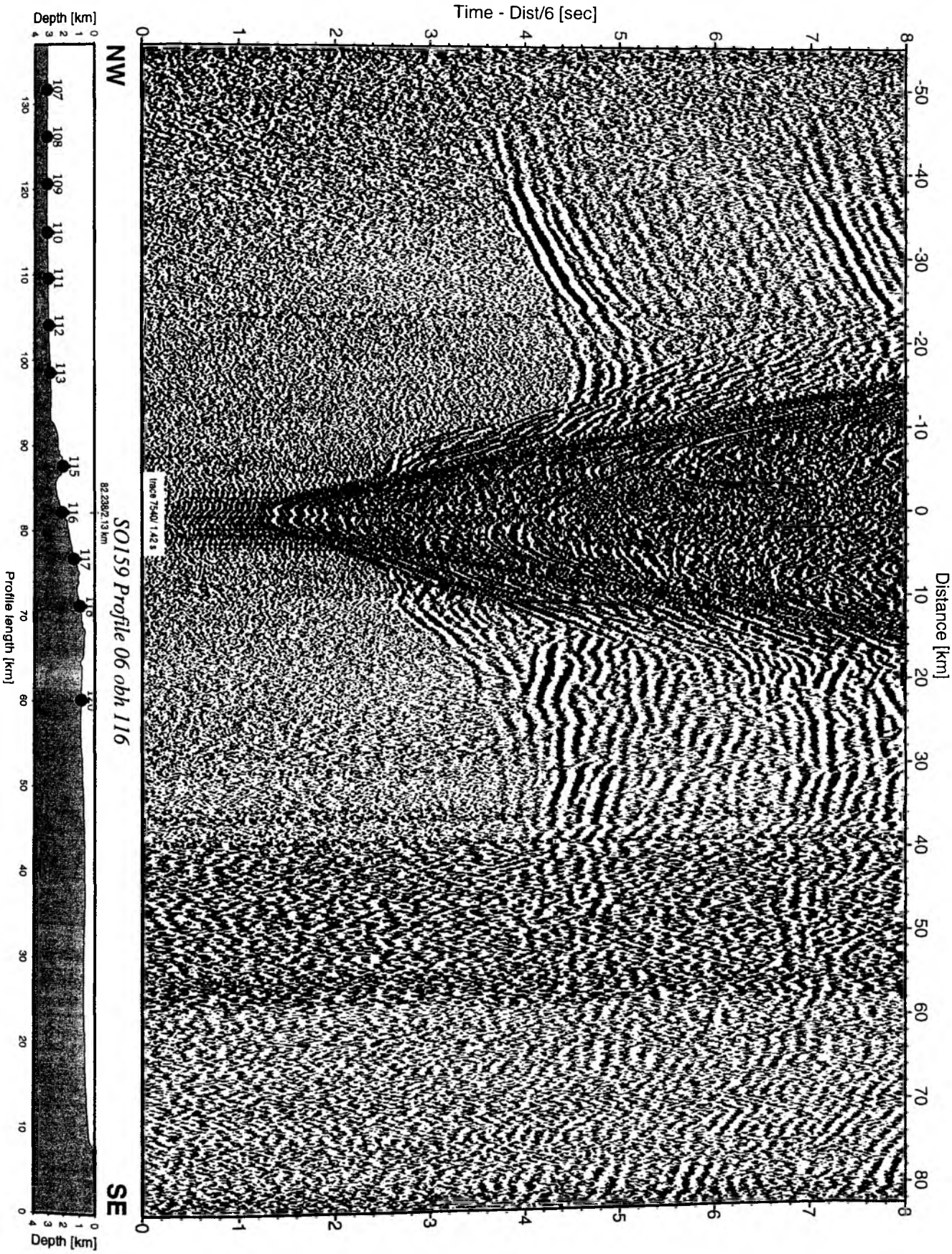

Figure 5.3.6.11: Record section from obh 116 , Profile 06.

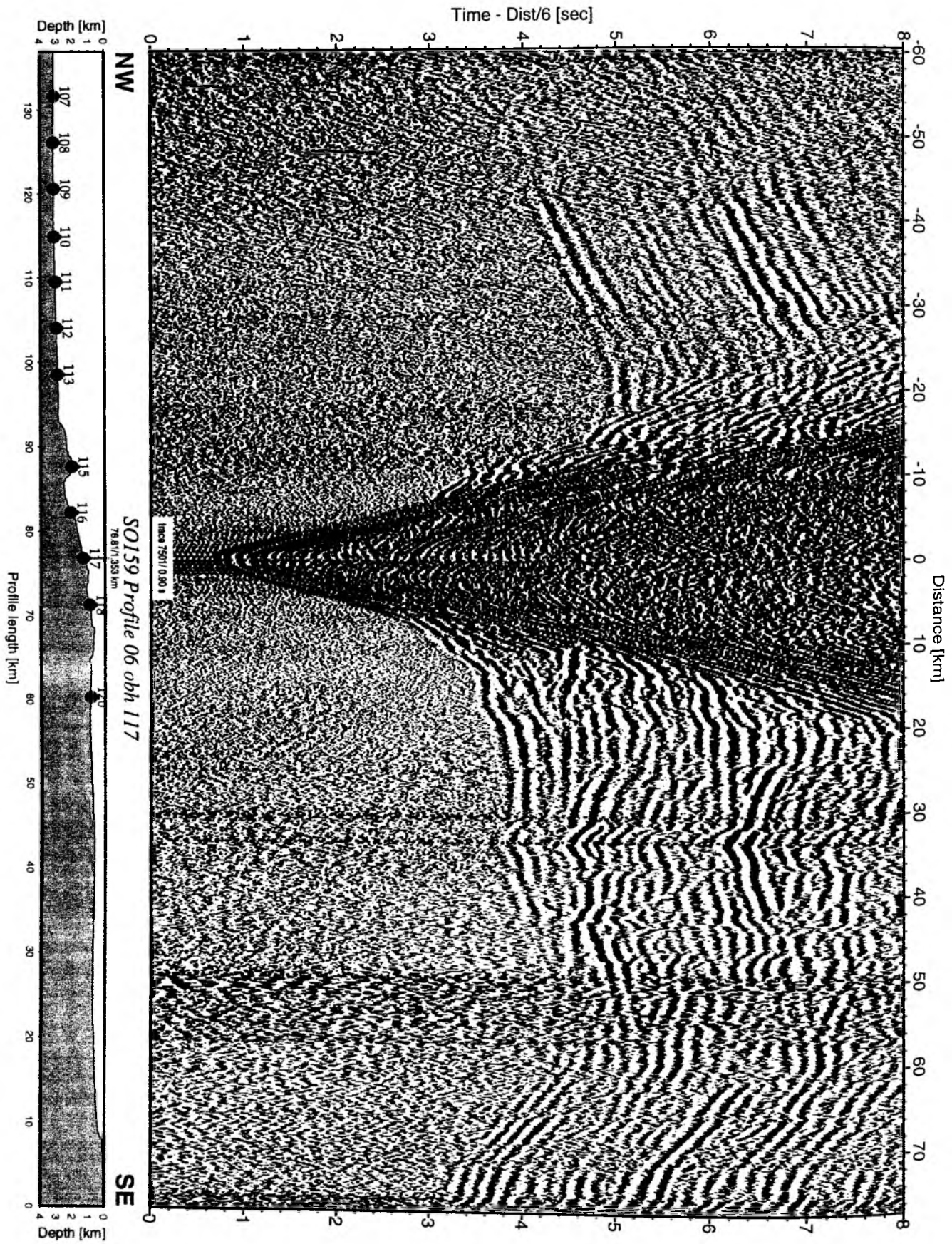

Figure 5.3.6.12: Record section from obh 117 , Profile 06.

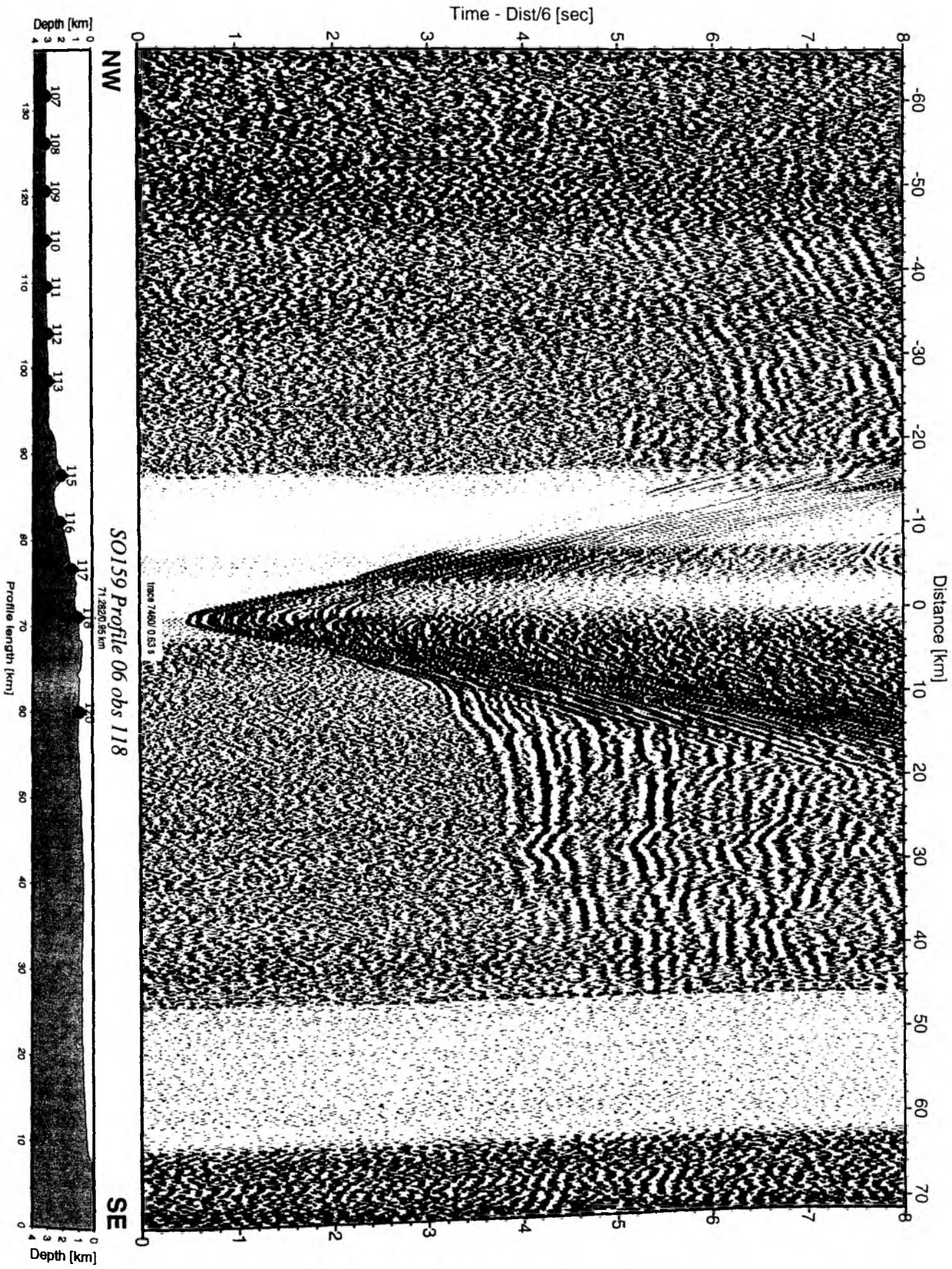

Figure 5.3.6.13: Record section from obs 118 hydrophone, Profile 06.

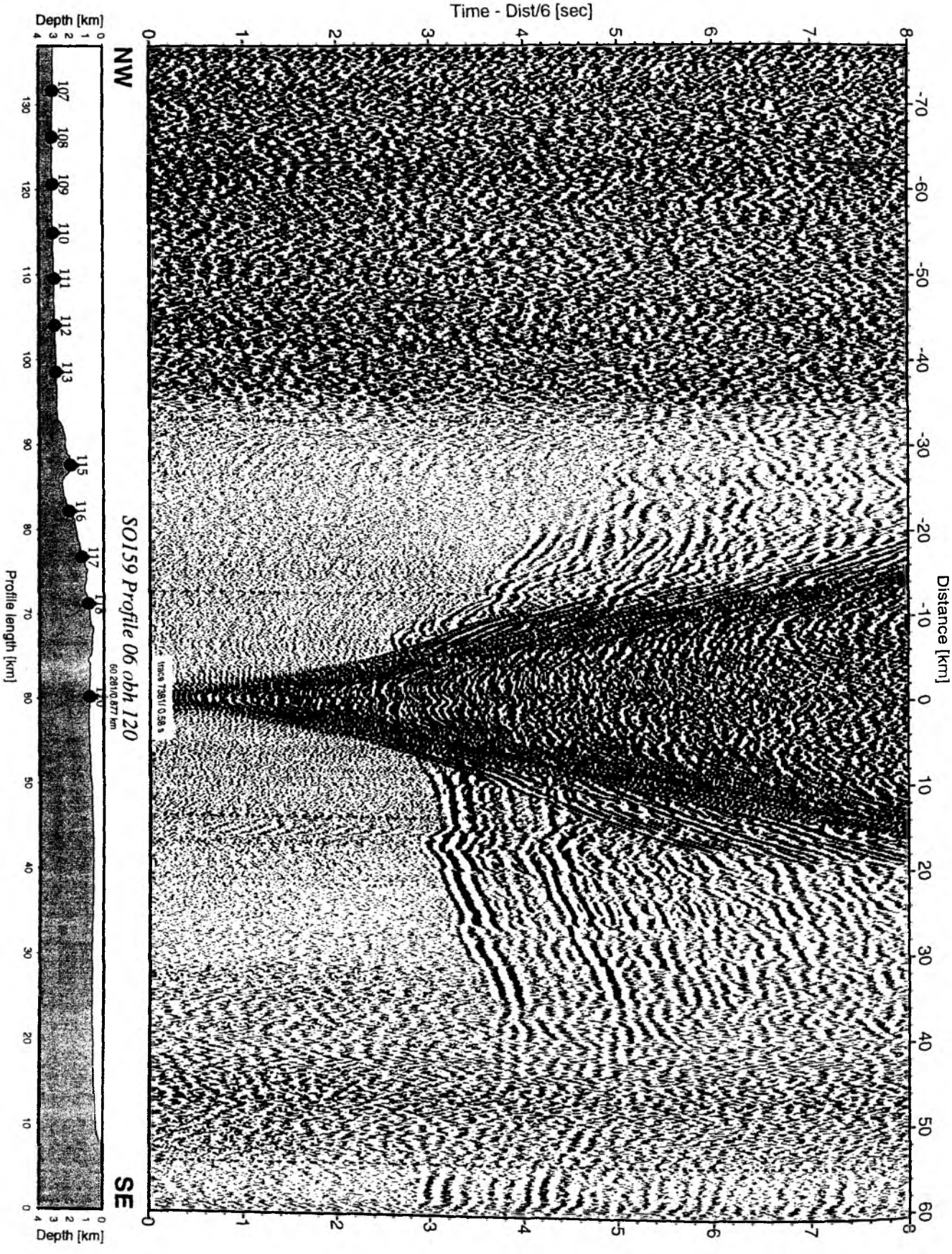

Figure 5.3.6.14: Record section from obh 120 , Profile 06.

5.3.7 – Earthquakes

(M. Müller)

The Ocean Bottom Seismic Recorders deployed are operated in a continuous recording mode. Thus besides the signals from the airgun shots (active seismics), they also record all earthquakes that occur during deployment times (passive seismics or seismological observations). Thus the data can be scanned for local earthquakes (teleseismic events will not be detected because of the 4.5 Hz high-pass filter). If the earthquakes occur during airgun profiling, they are apparent on the record sections.

Two examples that occurred during acquisition along Profile 01 and were further analyzed. The first one was recorded at 26. Aug. 17.13 UTC and the second one at 28. Aug. 00.32 UTC. Only the northern OBH-Stations 04, 06, 08 and 10 of the north-south oriented profile across the Carnegie-Ridge recorded these events. At the stations in the middle and in the south (OBH12 to 36) the signals are too weak to be detected, either due to attenuation or an increased noise level. The seismograms are shown in Figures 5.3.7.1 and 5.3.7.2. The starting time and the ending time are identical for all traces. The amplitudes are normalized to median trace values for display. Both figures show increasing start times to the south, thus a northernly location of the epicenter can be inferred. With ball instruments located on one line and poor constraints on the s-wave arrivals, any attempt to precisely locate the earthquake is strongly biased.

Also evident on some traces are the airgun shots, that were fired at 60 sec intervals. They are most pronounced on the trace of OBH36 in Figure 5.3.7.1 and OBH04,06,08, and 10 in Figure 5.3.7.2.

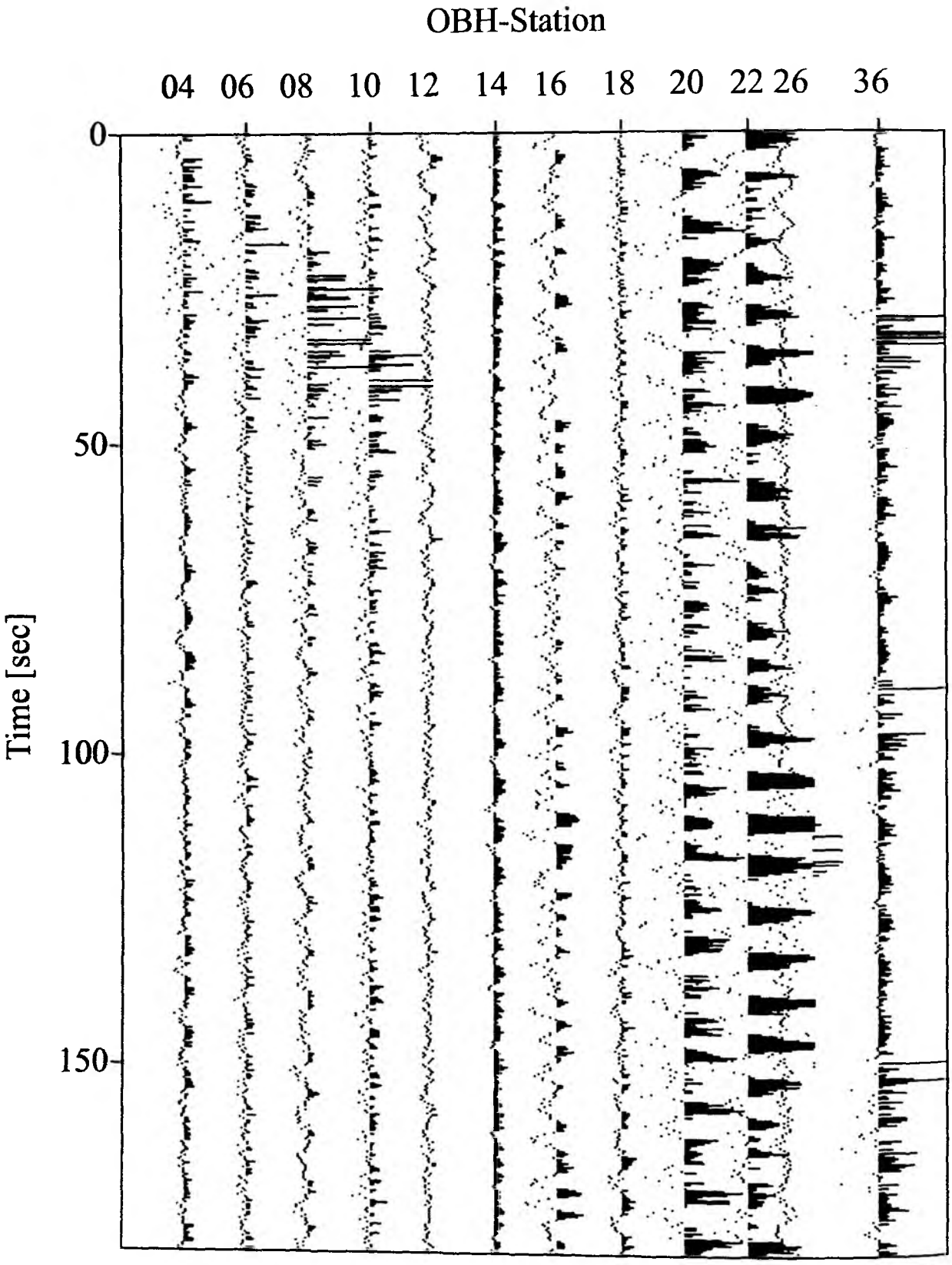

Figure 5.3.7.1: Recordings of the 26. Aug. 2001, 17:13 UTC earthquake event
Observations along the N-S trending profile1 across the Carnegie Ridge

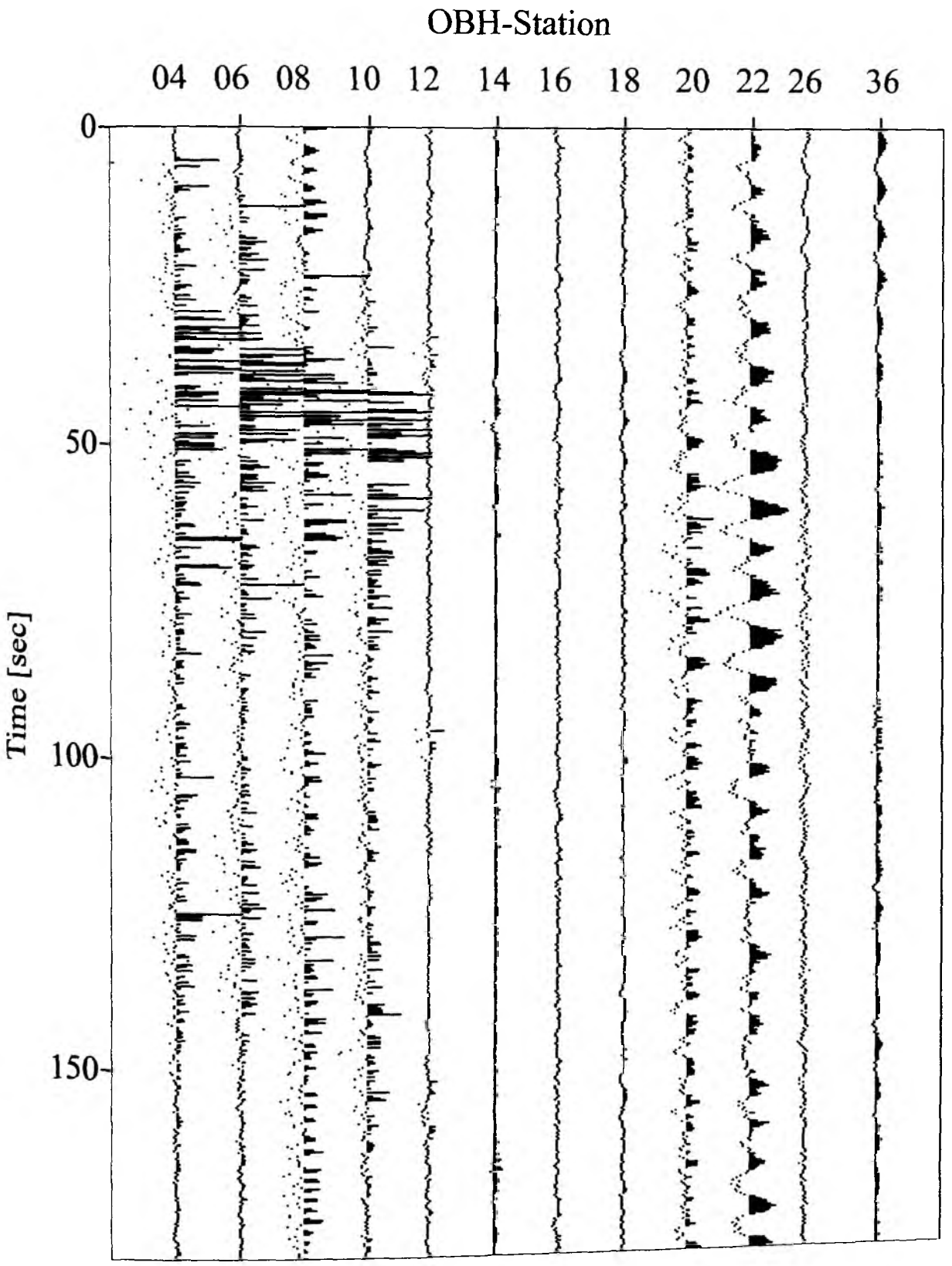

Figure 5.3.7.2: Recordings of the 28. Aug. 2001, 00:32 UTC earthquake event
Observations along the N-S trending profile1 across the Carnegie Ridge

ACKNOWLEDGEMENTS

Cruise SO 159 was funded by the German Ministry of Education, Research, Science, and Technology (BMBF) under project No. 03G0159A to GEOMAR within the continued and generous most commendable support for marine sciences with an outstanding research vessel such as SONNE.

The French scientific party was supported by IRD (Institut de Recherche pour le Développement), INSU (Institut National des Sciences de l'Univers) and IFREMER through ship-time exchange. We acknowledge the French embassies in Bogota and Quito for support to Colombian and Ecuadorian students attending the cruise. We also thank INOCAR (Guayaquil) for their help in the initial preparation of the instruments on-shore

We warmly thank master H. Andresen and his crew for their professional support and for the positive working atmosphere throughout the entire cruise.

References

Beck, S. L. and Ruff, L. J., 1984. The Rupture Process of the Great 1979 Colombia Earthquake: Evidence for the Asperity Model. Journal of Geophysical Research, 89, 9281-9291.

Barry, K.M., Cavers, D.A. & Kneale, W., 1975. Recommended standarts for digital tape fomats, Geophysics, 40, 344-352.

Bialas, J., Flueh, E., and Bohrmann, G., 1999. SO-144/1&2 Cruise Report R/V Sonne, PAGANINI (Panama Basin and Galapagos "Plume" - New Investigations of Intraplate Magmatism). San Diego - Caldera September 7 - November 7, 1999. GEOMAR Report #94, Kiel, Germany.

Bialas, J., and E. R. Flueh, 1999: Ocean Bottom Seismometers; Sea Technology, 40, 4, 41-46.

Blondel, P., and B.J. Murton, 1997: Handbook of Seafloor Sonar Imagery, John Wiley and Sons, Chichester, 314.

Christeson, G., OBSTOOL: Software for processing UTIG OBS data, 27 pp., Tech Rept. 134, Institute for Geophysics, Austin, June 1995.

Cloos, M., 1996. Lithospheric buoyancy and collisional orogenesis: Subduction of oceanic plateaus, continental margins, island arcs, spreading ridges, and seamounts. Geological Society of America Bulletin, 105, 715-737.

Cloos, M. and Shreve, R. L., 1996. Shear-zone thickness and the seismicity of Chilean and Marianas-type subduction zones. Geology, 24, 107-110.

Collot, J.-Y., Charvis, Ph. and the SISTEUR Scientific Party, (subm.) Exploring the Ecuador-Colombia margin and the seismogenic zone. EOS, (subm.).

DeMets C., Gordon R.G., Argus D.F. and Stein S., 1990. Current plate motions., Geophys. J. Int., 101, 425-478.

De Vries, T., 1988. The geology of late Cenozoic marine terraces (tablazos) in northwestern Peru. Journal of South American Earth Sciences, 1, 121-136.

Deniaud, J., 1999. Neogene evolution of sedimentary basins in Ecuador. Ph. D. Thesis, Univ. Grenoble

Dumont, J.-F., Benitez, S., et al., Neotectonics of the coastal region of Ecuador: A new pluridisciplinary research project, Third International Symposium on Andean Geodynamics (ISAG), edited by Dumont, J.-F., Benitez, S., et al., 175-178, ORSTOM, France, St. Malo, 1996.

Ego, S., Sebrier, M., Lavenu, A., Yepes, H. and Eques, A., 1996. Quaternary State of Stress in the Northern Andes and the Restraining Bend Model for the Ecuadorian Andes. Tectonophysics, 259, 101-116.

Engdahl, E. R., van der Hilst, R. D. and Buland, R., 1998. Global teleseismic earthquake relocation with improved travel times and procedures for depth relocation. Bulletin of the Seismological Society of America, in press.

Flueh, E. R., and J. Bialas, 1996: A digital, high data capacity ocean bottom recorder for seismic investigations; Int. Underwater Sytems Design, 18(3), 18-20.

Gardner, T. W., Verdonck, D., Pinter, N. M., Slingerland, R., Furlong, K. P., Bullard, T. F. and Wells, S. G., 1992. Quaternary uplift astride the aseismic Cocos Ridge, Pacific coast, Costa Rica. Geological Society of America Bulletin, 104, 219-232.

Guillier, B., Chatelain, J.-L., Jaillard, E., Yepes, H., Poupinet, G., Fels, J.-F., (2001). Seismological evidence of the geometry of the orogenic system in Central-Northern Ecuador (South America). Geophys. Res. Lett., (in press).

Gutscher, M.-A., Malavieille, J., Lallemand, S. and Collot, J.-Y., 1999. Tectonic segmentation of the North Andean margin: Impact of the Carnegie Ridge collision. Earth and Planetary Science Letters, 168, 255-270.

Gutscher, M.-A., Maury, R., Eissen, J.-P. and Bourdon, E., 2000. Can slab melting be caused by flat subduction? Geology, v. 28, p. 535-538.

Hardy, N. C., 1991. Tectonic evolution of the easternmost Panama Basin: Some new data and inferences. Journal of South American Earth Sciences, 4, 261-269.

Hello, Y., and P. Charvis, Les stations sismiques sous-marines (OBS): utilisation et perspectives, in 17e réunion des Sciences de la Terre, pp. 128, Société Géologique de France, Brest, 1998.

Hello, Y., P. Charvis, B. Pontoise, Y. Nakamura, and A.T. Chen, Long-range seismic refraction using digital OBS, in European Geophysical Society General Assembly, pp. C51, Annales Geophysicae, Edinburg, 1992.

Hoernle, K.A., Werner, R., Phipps-Morgan, J., Bryce, J., and Mrazek, J., 2000. Existence of complex spatial zonation in the Galapagos plume for at least 14.5 Ma. Geology, 28, 435-438.

Jaillard E.et al., 1995. Basin development in an accretionary, oceanic-floored fore-arc setting: southern coastal Ecuador during late cretaceous-late eocene time, in *Petroleum basins of South America*, Tankard A., Suarez R. and Welsink H., Eds, 615-631.

Kellogg, J. N. and Vega, V., Tectonic development of Panama, Costa Rica and the Colombian Andes: Constraints from Global Positioning System geodetic studies and gravity, Geologic and Tectonic Development of the Caribbean Plate Boundary in Southern Central America, Special Paper 295, edited by Kellogg, J. N. and Vega, V., 75-90, Boulder, Colorodo, Boulder, Colorodo, 1995.

Kellogg, J. N. and Trenkamp, R.., Kinematics of the Northwestern Andes and southern Central America based Global Positioning System (GPS) data from the CASA Network. EOS special number, AGU Fall Meeting, Dec. 1998.

Knickmeyer, E.T., 1996: Hochgenaues Differential-GPS, Proc. 11th Annual Meeting of the German Hydrographic Society, Glücksburg, 3.-5.6.

Kolarsky, R.A., Mann, P., and Montero, W., 1995. Island arc response to shallow subduction of the Cocos Ridge, Costa Rica,) in: P. Mann (Ed) *Geologic and Tectonic Development of the Caribbean Plate Boundary in Southern Central America*, Geol. Soc. Am. Special Paper 295, 235-262.

Korenaga, J., W.S. Holbrook, G.M. Kent, P.B. Kelemen, R.S. Detrick, H.-C. Larsen, J.R. Hooper, and T. Dahl-Jensen, Crustal structure of the southeast Greenland margin from joint refraction and reflection seismic tomography, J. Geophys. Res., 105, 21591-21614, 2000.

Lavenu, A., Winter, T. and Davilla, F. A , 1995. Pliocene-Quaternary compressional basin in the Interandean Depression, Central Ecuador, Geophys. J. Int. 121, 279-300.

Lonsdale, P. and Klitgord, K. D., 1978. Structure and tectonic history of the eastern Panama Basin. Geological Society of America Bulletin, 89, 981-999.

Luetgert, J., 1992: Interactive two-dimensional seismic raytracing for the Macintosh, USGS Open File Report, 43.

McGeary, S., Nur, A. and Ben-Avraham, Z., 1985. Spatial gaps in arc volcanism: The effect of collision or subduction of oceanic plateaus. Tectonophysics, 119, 195-221.

Mountney, N. P. and Westbrook, G. K., 1997. Quantitative analysis of Miocene to Recent forearc basin evolution along the Colombian margin. Basin Research, 9, 177-196.

Nakamura, Y. and J. Garmany, Development of upgraded ocean-bottom seismograph, 45 pp., Tech. Rept. 111, Institute for Geophysics, Austin, March 7, 1991.

Nakamura, Y., P. L. Donoho, P. H. Roper and P. M. McPherson, Large-offset seismic surveying using ocean-bottom seismographs and air guns: Instrumentation and field technique, Geophysics, 52, 1601-1611, 1987.

Pennington, W. D., 1981. Subduction of the Eastern Panama Basin and seismotectonics of Northwestern South America. Journal of Geophysical Research, 86, 10753-10770.

Pilger, R. H., 1981. Plate reconstructions, aseismic ridges, and low-angle subduction beneath the Andes. Geological Society of America Bulletin, 92, 448-456.

Reynaud C., Lapierre H., Jaillard E., Benitez S., Berrones G. and Mascle G., 1996. Mineralogical and geochemical characterisation of middle Cretaceous to Paleocene oceanic and continental volcanic rocks from southwestern Ecuador, in: *ISAG 1996, Andean Geodynamics*, Extended Abstract, pp. 633.

Ruff, L. J., 1992. Asperity distributions and large earthquake occurence in subduction zones. Tectonophysics, 211, 61-83.

Ruff, L. J. and Tichelaar, B. W., 1996. What controls the seismogenic plate interface in subduction zones?, Subduction: Top to Bottom, edited by Ruff, L. J. and Tichelaar, B. W., 105-111, American Geophysical Union, Washington, D.C.

Sallarès, V. Charvis, Ph., Flueh, E. R., Walther, C. H., and Bialas, J., 2001. Seismic structure of Malpelo and Cocos Volcanic Ridges and implications for Hotspot-Mid Oceanic Ridge interaction. Proceedings AGU Fall Meeting, San Francisco, EOS Special Number .

Scholz, C. H. and Small, C., 1997. The effect of seamount subduction on seismic coupling. Geology, 25, 487-490.

Seeber, G., 1996: Stand und Einsatzmöglichkeiten von GPS - ein Überblick, Proc. 11th Annual Meeting of the German Hydrographic Society, Glücksburg, 3.-5.6.

Shepherd, G. L. and Moberly, R., Coastal structure of the continental margin, northwest Peru and southwest Ecuador, Nazca Plate: Crustal Formation and Andean Convergence, edited by Shepherd, G. L. and Moberly, R., 351-391, Geological Society of America, Boulder, 1981.

Smith, W. H. F. and Sandwell, D. T., 1997. Global seafloor topography from satellite altimetry and ship depth soundings. Science, 277, 1956-1962.

Swenson, J. L. and Beck, S. L., 1996. Historical 1942 Ecuador and 1942 Peru Subduction Earthquakes, and Earthquake Cycles along Colombia-Ecuador and Peru Subduction Segments. Pure and Applied Geophysics, 146, 67-101.

Taboada, A., et al., 2000. Deformation and kinematics in the Colombian Andes, Tectonics, 19, 701-716.

Villamar R., Subduction de la Ride de Carnégie sous la marge d'équateur : structure et déformation à partir des données de sismique réflexion multitrace de la campagne SISTEUR, Rapport de DEA, 100 p., UMR Geosciences Azur, Villefranche s/mer, 2001

von Huene, R., Pecher, I. and Gutscher, M.-A., 1996. Development of the accretionary prism along Peru and material flux after subduction of Nazca Ridge. Tectonics, 15, 19-33.

Walther, C.H.E., (subm.). The crustal structure of the Cocos Ridge off Costa Rica. subm. to J. Geophys.Res.

Wessel, P. and Smith, W. H., 1991. Free software helps map and display data. Eos Transactions AGU, 72, 445-446.

Westbrook, G. K., Hardy, N. C. and Heath, R. P., Structure and tectonics of the Panama-Nazca plate boundary, Geologic and Tectonic Development of the Caribbean Plate Boundary in Southern Central America, Special Paper 295, edited by Westbrook, G. K., Hardy, N. C. and Heath, R. P., 91-109, Geological Society of America, Boulder, Colorodo, 1995.

Winter, T., Avouac, J.-P. and Lavenu, A., 1993. Late Quaternary kinematics of the Pallatanga strike-slip fault (central Ecuador) from topographic measurements of displaced morphological features. Geophysical Journal International, 115, 905-920.

Zelt, C. A. and P. J. Barton, Three-dimensional seismic refraction tomography: A comparison of two methods applied to data from the Faeroe Basin, J. Geophys. Res., 103, 7187-7210, 1998.

Zelt, C. A. and R. B. Smith, Seismic travel time inversion for 2-D crustal velocity structure, Geophys. J. Int., 108, 16-34, 1992.

Zelt, C.A., and R.B. Smith, 1992: Seismic traveltime inversion for 2-D crustal velocity structure. Geophys. J. Int. 108, 16-34.

Zelt, C. A., Lateral velocity resolution from three-dimensional seismic refraction data, Geophys. J. Int., 135, 1101-1112, 1998.

Appendices

I - Captains Report

II - OBH/S Deployments

III - Airgun Protocols

VI - Magnetic Profiles

RF Reedereigemeinschaft
Forschungsschiffahrt GmbH

F.S. "S O N N E" Reise SO 159

Eingesetzte Geräte		Einsätze
MAG	Magnetometer Profile	: 1419 sm
CTD	CTD Sonde	: 4
OBS	Ocean Bottom Seismometer (Ausgesetzt)	: 143
OBS	Ocean Bottom Seismometer (Aufgenom.)	: 135
SM	Seizmik Profile(3 x 32Ltr Airguns, Streamer)	: 568 sm
SIM	Simrad Profile	: 1752 sm
Releaser Test		: 2

Eingesetzte Winden :

Winde	*D/M*	*Typ*	*RF-Nr*	*SO 159 Einsatz*	*Gesamt Einsatz*	*SO 159 S`länge*	*Gesamt S`länge*	*Zust.*
W 1	18,2	LWL	816233	0000 h	1922 h	000000 m	1241262 m	5
W 2	18,2	LWL	810001	0000	0239	000000	0082684	2
W 4	11,0	NSW	817141	0009	0234	010770	0154653	3
W 5	11,0	NSW	817164	0000	0209	000000	0184173	3
W 6	18,2	DRAKO	814150	0007	1900	006851	1609451	3

Winde	*SO 159 gefierte max.Länge*	*jemals gefierte max.Länge*
W 1	0000 m	6474 m (nur noch 5340 m lang)
W 2	0000	3000
W 4	4120	6100
W 5	0000	5200
W 6	4201	7900 (nur noch 6589 m lang)

Geräteverluste :
8 OBH's (Franzosen)

Abkürzungen im Stationsprotokoll:

z.W.	zu Wasser
a.D.	an Deck
Boko	Bodenkontakt
Bosi	Bodensicht
SL(max.)	(maximale)Seillänge
LT	Lottiefe nach Hydrosweep
W x	eingesetzte Winde
SM	Simrad- Multibeam-Lot
PS	Parasound
XPNDR	Transponder

FS SONNE Stationsprotokoll SO 159

Zeit : UTC – 05 Stunden

23.08.01

Profil MAG 101 :

0150	Beginn Profil, Magnetometer z/W	LT = 45 m	02-52.10S 80-40.20W
0200	Magnetometer ausgesteckt, SL 180m, V = 10Kn		
0315	Ende Profil 12 sm		02-57.50S 80-51.00W

Profil MAG 102

0315	Beginn Profil		02-57.50S 80-51.00W
0735	Ende Profil 44 sm		02-54.00S 81-34.50W
0745	Magnetometer a/D		

Station Releaser Test W6

0820	Beginn Station	LT = 4342 m	02-54.29S 81-35.15W
0822	Dreibein m. 8 Releaser z/W		
0834	Windenausfall (SL 100 m)		
1000	Winde oK, Hieven Dreibein bis Wasseroberfläche		
1005	Fieren		
1126	Slmax 4201 m	LT = 4358 m	02-55.02S 81-35.12W
1316	Dreibein m. Releaser a/D		
1318	Ende Station		

Station CTD 01 W4

1330	Beginn Station	LT = 4370 m	02-55.14S 81-35.17W
1333	CTD z/W		
1455	Slmax 4120 m	LT = 4367 m	02-55.05S 81-35.07W
1651	CTD a/D		
1653	Ende Station		
1800	OBS # 1 z/W	LT = 4431 m	02-42.99S 81-31.51W

Profil MAG 103

1807	Beginn Profil, Magnetometer z/W	LT = 1453m	02-43.00S 81-31.50W
1810	Magnetometer ausgesteckt, SL 180 m, V = 10Kn		

24.08.01

1255	Ende Profil 188 sm		00-56.45S 84-05.85W
1312	Magnetometer a/D		

Station Releaser Test W6

1318	Beginn Station	LT = 1715 m	00-85.70S 84-07.04W
1320	Dreibein mit 8 Relaeser z/W		
1357	Slmax 1650 m	LT = 1750 m	00-55.83S 84-07.23W
1415	Dreibein m. Releaser a/D		
1417	Ende Station		

Während des Releaser Tests wurden gleichzeitig ein Test mit den 3 x 32 Ltr Airguns durchgeführt.

Profil MAG 104

1515	Beginn Profil, Magnetometer z/W	LT = 1686m	00-57.79S 84-04.26W
1525	Magnetometer ausgesteckt, SL 180 m, V = 10Kn		

25.08.01

0033	Ende Profil 90 sm		00-05.51S 85-19.65W
0047	Magnetometer a/D		
0107	OBS #02 z/W	LT = 2912 m	00-05.59S 85-19.55W
0145	OBS #03 z/W	LT = 3091 m	00-10.01S 85-18.96W
0218	OBS #04 z/W	LT = 3208 m	00-14.21S 85-18.39W
0247	OBS #05 z/W	LT = 2735 m	00-18.50S 85-17.84W
0316	OBS #06 z/W	LT = 2752 m	00-22.78S 85-17.28W
0345	OBS #07 z/W	LT = 1990 m	00-27.05S 85-16.75W
0414	OBS #08 z/W	LT = 2316 m	00-31.32S 85-16.25W
0444	OBS #09 z/W	LT = 2405 m	00-35.58S 85-15.67W
0513	OBS #10 z/W	LT = 2411 m	00-39.93S 85-15.14W
0542	OBS #11 z/W	LT = 2338 m	00-44.16S 85-14.54W
0613	OBS #12 z/W	LT = 2316 m	00-48.45S 85-14.03W
0642	OBS #13 z/W	LT = 2542 m	00-52.68S 85-13.50W
0712	OBS #14 z/W	LT = 2314 m	00-56.94S 85-12.96W
0744	OBS #15 z/W	LT = 2347 m	01-01-24S 85-1241W
0811	OBS #16 z/W	LT = 2356 m	01-05.53S 85-11.88W
0848	OBS #17 z/W	LT = 2369 m	01-09.83S 85-11.33W
0919	OBS #18 z/W	LT = 2443 m	01-14.12S 85-10.80W
0951	OBS #19 z/W	LT = 2397 m	01-18.32S 85-10.24W
1021	OBS #20 z/W	LT = 2357 m	01-22.57S 85-09.70W
1051	OBS #21 z/W	LT = 2401 m	01-26.88S 85-09.15W
1212	OBS #22 z/W	LT = 2435 m	01-31.13S 85-08.59W
1241	OBS #23 z/W	LT = 2473 m	01-35.40S 85-08.03W
1309	OBS #24 z/W	LT = 2427 m	01-39.79S 85-07.50W
1337	OBS #25 z/W	LT = 2405 m	01-44.00S 85-06.97W
1405	OBS #26 z/W	LT = 2434 m	01-48.27S 85-06.40W
1433	OBS #27 z/W	LT = 2483 m	01-52.57S 85-05.87W

Station CTD 02 W4

1433	Beginn Station	LT = 2493 m	01-52.57S 85-05.87W
1442	CTD z/W		
1522	Slmax 2000 m	LT = 2484 m	01-52.73S 85-05.88W
1632	CTD a/D		
1635	Ende Station		
1716	OBS #28 z/W	LT = 2659 m	01-56.88S 85-05.30W
1746	OBS #29 z/W	LT = 2573 m	02-01.13S 85-04.79W
1825	OBS #30 z/W	LT = 2676 m	02-05.33S 85-04.26W
1855	OBS #31 z/W	LT = 2767 m	02-09.64S 85-03.70W
1925	OBS #32 z/W	LT = 2965 m	02-13.92S 85-03.16W
1956	OBS #33 z/W	LT = 2796 m	02-18.23S 85-02.62W
2027	OBS #34 z/W	LT = 2974 m	02-22.49S 85-02.07W

2057	OBS #35 z/W	LT = 3024 m	02-26.77S	85-01.53W
2131	OBS #36 z/W	LT = 3102 m	02-31.01S	85-00.99W
2202	OBS #37 z/W	LT = 3139 m	02-35.32S	85-00.44W
2227	OBS #38 z/W	LT = 3178 m	02-38.66S	85-00.01W

Profil MAG 105

2233	Beginn Profil, Magnetometer z/W	LT = 3165m	02-38.61S	84-59.95W
2241	Magnetometer ausgesteckt, SL 180 m, V = 10Kn			

26.08.01

0002	Ende Profil	14 sm	02-26.79S	84-52.02W

Profil MAG 106

0006	Beginn Profil	LT = 2958m	02-26.54S	84-51.53W
0207	Ende Profil	17 sm	02-26.81S	84-34.78W

Profil MAG 107

0215	Beginn Profil	LT = 2970m	02-27.49S	84-34.99W
0634	Ende Profil	37 sm	03-03.43S	84-56.86W
0643	Magnetometer a/D			

Profil SM 01

0645	Bb-Airgun z/W			
0656	Stb-Airgun z/W			
0710	Mitte-Airgun z/W			
0720	Beginn Profil SM 01 Magnetometer z/W	LT = 2289m	03-01.05S	84-57.17W
0759	Streamer ausgesteckt, SL 150 m (Während Profilfahrt div. Einholen/Aussetzen der Airguns)			

28.08.01

0012	Streamer a/D		00-01.12N	85-20.35W
0200	Ende Profil	197 sm	00-09.38N	85-21.40W
0211	Bb-Airgun a/D			
0227	Stb-Airgun a/D			

Profil MAG 108

0235	Beginn Profil	LT = 2824m	00-10.45N	85-21.93W
0415	Ende Profil	15 sm	00-04.79S	85-19.59W
0426	Magnetometer a/D			

OBS #02

0400	Release Command			
0500	OBS gesichtet			
0505	Schlauchboot z/W			
0512	Schlauchboot mit OBS a/D		00-05.49S	85-19.73W

OBS #03

0512	Release Command			

FS SONNE Stationsprotokoll SO 159

0538	OBS gesichtet	
0606	OBS a/D	00-10.08S 85-19.34W
OBS #04		
0620	Release Command	
0735	OBS gesichtet	
0746	Schlauchboot z/W	
0750	Schlauchboot mit OBS a/D	00-13.90S 85-18.64W
OBS #05		
0752	Release Command	
0814	OBS gesichtet	
0825	OBS a/D	00-18.37S 85-18.02W
OBS #06		
0846	Release Command	
0940	OBS gesichtet	
0945	Schlauchboot z/W	
0950	Schlauchboot mit OBS a/D	00-22.70S 85-17.17W
OBS #07		
0953	Release Command	
1022	OBS gesichtet	
1029	OBS a/D	00-27.04S 85-16.87W
OBS #08		
1043	Release Command	
1205	Erneutes Release Command; Schiff auf Stand By nahe Aussetzpos. Kein Signalempfang	
1300	OBS nicht aufgetaucht	
1627	Hydrophon z/W; Erneutes Release Command; Schiff auf Stand by	
1700	Hydrophon z/W; Erneutes Release Command; Schiff auf Stand by	
1750	OBS nicht aufgetaucht	
OBS #09		
1300	Release Command	
1326	OBS gesichtet	
1347	OBS a/D	00-35.65S 85-15.92W
OBS #10		
1404	Release Command	
1455	Hydrophon z/W; Erneutes Release Command	
1521	OBS gesicht; Hydrophon a/D	
1529	Schlauchboot z/W	
1534	Schlauchboot mit OBS a/D	00-39.92S 85-15.22W
OBS #11		
1840	Release Command	
1905	Erneutes Release Command	
1930	OBS gesichtet	

1947	OBS a/D	00-44.16S 85-14.61W
OBS #12		
1948	Release Command	
2050	OBS gesichtet	
2056	Schlauchboot z/W	
2103	Schlauchboot mit OBS a/D	00-48.34S 85-14.09W
OBS #13		
2110	Release Command	
2120	Erneutes Release Command	
2136	OBS gesichtet	
2149	OBS a/D	00-52.69S 85-13.62W
OBS #14		
2206	Release Command	
2300	Hydrophon z/W; Erneutes Release Command	
2338	OBS gesichtet	
2341	Schlauchboot z/W	
2345	Schlauchboot mit OBS a/D	00-56.89S 85-13.11W
OBS #15		
2350	Release Command	
29.08.01		
0011	OBS gesichtet	
0033	OBS a/D	01-01.25S 85-12.83W
OBS #16		
0053	Release Command	
0110	Hydrophon z/W; Erneutes Release Command	
0156	OBS gesichtet	
0204	Schlauchboot z/W	
0211	Schlauchboot mit OBS a/D	01-05.77S 85-12.07W
OBS #17		
0211	Release Command	
0232	OBS gesichtet	
0256	OBS a/D	01-10.08S 85-11.84W
OBS #18		
0316	Release Command	
0331	Hydrophon z/W;div. Release Command; ohne Erfolg	
	Schiff auf Stand by	
0500	OBS nicht aufgetaucht	
OBS #19		
0505	Release Command	

0540	OBS gesichtet		
0600	OBS a/D	01-18.48S	85-10.70W

OBS #20

0620	Release Command		
0641	Hydrophon z/W; Erneutes Release Command		
0737	OBS gesichtet		
0741	Schlauchboot z/W		
0743	Schlauchboot mit OBS a/D	01-22.67S	85-09.81W

OBS #21

0750	Release Command		
0820	OBS gesichtet		
0828	OBS a/D	01-27.00S	85-09.28W

OBS #22

0856	Release Command		
0912	Hydrophon z/W; Erneutes Release Command		
0913	OBS gesichtet		
0918	Schlauchboot z/W		
0921	Schlauchboot mit OBS a/D	01-31.13S	85-08.68W

OBS #23

0925	Release Command		
1000	OBS gesichtet		
1010	OBS a/D	01-35.39S	85-08.29W

OBS #24

1011	Release Command		
1110	OBS gesichtet		
1118	Schlauchboot z/W		
1120	Schlauchboot mit OBS a/D	01-39.70S	85-07.63W

OBS #25

1121	Release Command		
1151	OBS gesichtet		
1158	OBS a/D	01-44.02S	85-07.05W

OBS #26

1200	Release Command		
1235	Hydrophon z/W; Erneutes Release Command		
1312	OBS gesichtet		
1320	Schlauchboot z/W		
1327	Schlauchboot mit OBS a/D	01-48.37S	86-06.46W

OBS #27

1327	Release Command		
1403	OBS gesichtet		

1416	OBS a/D	01-52.58S 85-06.03W
OBS #28		
1420	Release Command	
1434	Erneutes Release Command	
1533	OBS gesichtet	
1538	Schlauchboot z7W	
1544	Schlauchboot mit OBS a/D	01-56.82S 85-05.41W
OBS #29		
1544	Release Command	
1615	OBS gesichtet	
1625	OBS a/D	02-01.14S 85-04.95W
OBS #30		
1625	Release Command	
1642	Erneutes Release Command	
1700	Erneutes Release Command	
1820	OBS nicht aufgetaucht	
OBS #31		
1825	Release Command	
18455	Erneut div. Release Commands	
1910	Hydrophon z/W; Erneutes Release Command	
1949	OBS gesichtet	
2001	OBS a/D	02-09.61S 85-03.87W
OBS #32		
2020	Release Command	
2047	Hydrophon z/W; Erneutes Release Command	
2120	OBS gesichtet	
2128	Schlauchboot z/W	
2131	Schlauchboot mit OBS a/D	02-13.80S 85-03.23W
OBS #33		
2133	Release Command	
2201	OBS gesichtet	
2208	OBS a/D	02-18.21S 85-02.68W
OBS #34		
2226	Release Command	
2257	Hydrophon z/W; Erneutes Release Command	
2339	OBS gesichtet	
2348	Schlauchboot z/W	
2351	Schlauchboot mit OBS a/D	02-22.37S 85-02.21W
OBS #35		
2352	Release Command	

FS SONNE Stationsprotokoll SO 159

30.08.01

0031	OBS gesichtet		
0050	OBS a/D		02-26.71S 85-01.79W

OBS #36

0050	Release Command		
0130	OBS gesichtet		
0135	Schlauchboot z/W		
0151	Schlauchboot mit OBS a/D		02-31.11S 85-01.32W

OBS #37

0151	Release Command		
0232	OBS gesichtet		
0248	OBS a/D		02-35.36S 85-00.56W

OBS #38

0248	Release Command		
0320	Hydrophon z/W; Erneutes Release Command		
0330	Erneutes Release Command		
0335	OBS gesichtet		
0350	OBS a/D		02-38.86S 85-00.12W

Profil MAG 109

0405	Beginn Profil, Magnetom. z/W LT = 3167m		02-38.81S 85-00.09W
0413	Magnetometer ausgesteckt SL 180 m; V = 10Kn		
0725	Ende Profil	22 sm	02-17.30S 84-54.20W

Profil MAG 110

0725	Beginn Profil		02-17.30S 84-54.20W
0850	Ende Profil	24 sm	02-17.30S 84-30.00W

Profil MAG 111

0850	Beginn Profil		02-17.30S 84-30.00W
0943	Ende Profil	8 sm	02-08.60S 84-30.00W

Profil MAG 112

0943	Beginn Profil		02-08.60S 84-30.00W
1213	Ende Profil	24 sm	02-08.55S 84-55.08W

Profil MAG 113

1213	Beginn Profil		02-08.55S 84-55.08W
1300	Ende Profil	8 sm	02-00.86S 84-56.33W

Profil MAG 114

1300	Beginn Profil		02-00.86S 84-56.33W
1449	Ende Profil	19 sm	02-00.00S 84-37.20W

Profil MAG 115

1449	Beginn Profil		02-00.00S 84-37.20W

1535	Ende Profil	8 sm	01-52.20S 84-38.50W

Profil MAG 116

1535	Beginn Profil		01-52.20S 84-38.50W
1724	Ende Profil	19 sm	01-52.20S 84-58.00W

Profil MAG 117

1724	Beginn Profil		01-52.20S 84-58.00W
1844	Ende Profil	14 sm	02-05.00S 85-02.20W
1857	Magnetometer a/D		

OBS # 30

1905	Schiff auf Aussetzposition; Stand by; warten auf Auftauchen (Zeitrelea-ser)		02-05.34S 85-04.24W
1932	OBS nicht aufgetaucht		

Profil SIM 118

1933	Beginn Profil		02-05.34S 85-04.24W
2014	Ende Profil	9 sm	02-06.17S 85-13.09W

Profil SIM 119

2014	Beginn Profil		02-06.17S 85-13.09W

31.08.01

0005	Ende Profil	47 sm	01-19.00S 85-17.00W

Profil SIM 120

0005	Beginn Profil		01-19.00S 85-17.00W
0043	Ende Profil	8 sm	01-14.60S 85-11.31W

OBS #18

0050	Schiff auf Aussetzposition, Stand by; warten auf Auftauchen (Zeitrelea-ser)		01-13.95S 85-10.92W
0130	OBS nicht aufgetaucht		

Profil SIM 121

0133	Beginn Profil		01-14.40S 85-10.73W
0212	Ende Profil	8 sm	01-11.61S 85-03.62W

Profil SIM 122

0212	Beginn Profil		01-11.61S 85-03.62W
0508	Ende Profil	39 sm	00-33.05S 85-08.72W

Profil SIM 123

0508	Beginn Profil		00-33.05S 85-08.72W
0540	Ende Profil	8 sm	00-31.42S 85-15.87W

OBS #08

0600	Schiff auf Aussetzposition; Stand by; warten auf Auftauchen (Zeitrelea-ser)		00-31.25S 85-16.38W
0630	OBS nicht aufgetaucht		

Profil SIM 124

0631	Beginn Profil		00-31.31S 85-16.26W
0737	Ende Profil	13 sm	00-20.00S 85-10.00W

Profil SIM 125

0737	Beginn Profil		00-20.00S 85-10.00W
1117	Ende Profil	42 sm	00-45.00S 84-36.00W

Profil SIM 126

1117	Beginn Profil		00-45.00S 84-36.00W
1936	Ende Profil	91 sm	

Profil SIM 127

1936	Beginn Profil		00-45.00S 84-36.00W

01.09.01

0200	Ende Profil	74 sm	02-24.00S 82-13.00W

Profil SIM 128

0200	Beginn Profil		02-24.00S 82-13.00W
0420	Ende Profil	28 sm	02-40.00S 81-50.00W

0445	OBS #39 z/W	LT = 3193 m	02-36.82S 81-47.71W
0514	OBS #40 z/W	LT = 3283 m	02-37.87S 81-44.90W
0536	OBS #41 z/W	LT = 3436 m	02-38.97S 81-42.12W
0600	OBS #42 z/W	LT = 3586 m	02-40.07S 81-39.34W
0624	OBS #43 z/W	LT = 4024 m	02-41.15S 81-36.52W
0646	OBS #44 z/W	LT = 4231 m	02-42.24S 81-33.75W
0708	OBS #45 z/W	LT = 4440 m	02-43.32S 81-30.96W
0729	OBS #46 z/W	LT = 4057 m	02-44.41S 81-28.14W
0753	OBS #47 z/W	LT = 3033 m	02-45.61S 81-25.04W
0818	OBS #48 z/W	LT = 2122 m	02-46.77S 81-22.00W
0843	OBS #49 z/W	LT = 1766 m	02-47.86S 81-19.19W
0906	OBS #50 z/W	LT = 1458 m	02-48.94S 81-16.43W
0929	OBS #51 z/W	LT = 1055 m	02-50.04S 81-13.61W
0956	OBS #52 z/W	LT = 777 m	02-51.12S 81-10.80W
1017	OBS #53 z/W	LT = 687 m	02-52.20S 81-08.00W
1039	OBS #54 z/W	LT = 612 m	02-53.60S 81-05.19W
1100	OBS #55 z/W	LT = 525 m	02-54.38S 81-02.40W
1123	OBS #56 z/W	LT = 436 m	02-55.47S 80-59.60W
1144	OBS #57 z/W	LT = 238 m	02-56.55S 80-56.79W
1213	OBS #58 z/W	LT = 108 m	02-57.63S 80-53.98W

FS SONNE Stationsprotokoll SO 159

Profil SM 02

1419	Bb-Airgun z/W		
1428	Stb-Airgun z/W		
1433	Beginn Profil SM 02	LT = 68m	03-05.64S 80-33.39W
1443	Magnetometer z/W SL 180 m		
1610	Mitte-Airgun z/W		

02.09.01

0956	Ende Profil 86 sm		02-34.00S 81-55.00W
1009	Mitte-Airgun a/D		
1020	Bb-Airgun a/D		
1029	Stb-Airgun a/D		

Profil MAG 129

1030	Beginn Profil		02-33.37S 81-56.35W
1134	Ende Profil 8 sm		02-36.90S 81-48.62W
1141	Magnetometer a/D		

OBS #39

1235	Hydrophon z/W; Release Command		02-36.62S 81-47.87W
1250	Fahren div. Suchkurse		
1405	OBS nicht aufgetaucht		

OBS #40

1330	Release Command		
1438	Erneutes Release Command		
1520	Schiff fährt div. Suchkurse		
1600	OBS nicht aufgetaucht		
1615	Schiff fährt div. Suchkurse		
1635	Suchkurse abgebrochen		

OBS #42

1612	Release Command		
1705	OBS gesichtet		02-39.83S 81-39.45W
1715	OBS a/D		

OBS #43

1705	Release Command		
1747	OBS gesichtet		02-41.07S 81-36.65W
1758	OBS a/D		

OBS #44

1730	Release Command		
1827	OBS gesichtet		02-42.17S 81-33.84W
1835	OBS a/D		

OBS #45

1827	Release Command		
1929	OBS gesichtet		

1932	OBS a/D		02-43.24S 81-31.04W
OBS #46			
1858	Release Command		
1945	OBS gesichtet		
1959	OBS a/D		02-44.21S 81-28.20W
OBS #47			
1953	Release Command		
2038	OBS gesichtet		
2048	OBS a/D		02-45.49S 81-25.14W
OBS #49			
2100	Release Command		
2136	Erneutes Release Command		
2154	OBS gesichtet		
2200	OBS a/D		02-47.76S 81-19.23W
OBS #51			
2226	Release Command		
2240	OBS gesichtet		
2249	OBS a/D		02-49.97S 81-13.65W
OBS #54			
2330	Release Command		
2336	OBS gesichtet		
2352	OBS a/D		02-53.06S 81-05.18W
03.09.01			
0012	Release Command		
0019	OBS gesichtet		
0029	OBS a/D		02-54.23S 81-02.41W
0225	OBS #59 z/W	LT = 1969 m	02-41.23S 81-20.06W
0248	OBS #60 z/W	LT = 2071 m	02-43.98S 81-21.01W
0328	OBS #61 z/W	LT = 2315 m	02-49.60S 81-22.92W
0352	OBS #62 z/W	LT = 2544 m	02-52.46S 81-23.92W
0417	OBS #63 z/W	LT = 3251 m	02-55.35S 81-24.92W
0442	OBS #64 z/W	LT = 2544 m	02-58.21S 81-25.91W
0506	OBS #65 z/W	LT = 3428 m	03-01.07S 81-26.89W
0529	OBS #66 z/W	LT = 2915 m	03-03.68S 81-27.80W
Profil SM 03			
0606	Bb-Airgun z/W		
0614	Stb-Airgun z/W		
0617	Beginn Profil		03-06.01S 81-28.58W
0635	Magnetometer z/W		
1403	Ende Profil 36 sm		02-32.66S 81-17.12W

Profil MAG 129

1434	Beginn Profil	02-31.66S 81-16.32W
1745	Ende Profil 32 sm	02-55.73S 80-54.52W
1755	Magnetometer a/D	

OBS #58

1800	Schiff auf Aussetzposition; Stand by; Zeitreleaser; div. Suchkurse	02-56.83S 80-53.88W
1810	OBS gesichtet	
1814	Schlauchboot z/W	
1816	Schlauchboot mit OBS a/D	02-57.62S 80-53.94W

OBS #57

1833	Auf Aussetzposition; Release Command; Warten auf Auftauchen	02-56.53S 80-56.75W
1955	OBS nicht aufgetaucht	

OBS #56

2017	OBS gesichtet (Zeitrelease)	
2023	Schlauchboot z/W	
2027	Schaluchboot mit OBS a/D	02-55.43S 80-59.61W

OBS #52

2128	OBS gesichtet (Zeitrelease)	
2135	Schlauchboot z/W	
2138	Schlauchboot mit OBS a/D	02-51.01S 81-10.84W

OBS #50

2231	OBS gesichtet (Zeitreleaser)	
2235	Schlauchboot z/W	
2238	Schlauchboot mit OBS a/D	02-48.95S 81-16.36W

04.09.01

OBS #41

0035	OBS gesichtet (Zeitreleaser)	
0055	Schlauchboot z/W	
0103	Schlauchboot mit OBS a/D	02-37.58S 81-42.50W

OBS #40

0120	Auf Aussetzpos.; Warten auf Auftauchen; div. Suchkurse	02-37.87S 81-44.90W
0140	OBS nicht aufgetaucht	

OBS #39

0200	Auf Aussetzpos.; Warten auf Auftauchen; div. Suchkurse	02-36.60S 81-47.68W
0230	OBS nicht aufgetaucht	

OBS #59			
0441	Release Command		
0512	OBS gesichtet		
0524	OBS a/D		02-41.03S 81-20.04W
OBS #60			
0512	Release Command		
0535	OBS gesichtet		
0554	OBS a/D		02-43.69S 81-21.03W
OBS #48			
0600	Release Command		
0623	OBS gesichtet		
0629	Schlauchboot z/W		
0631	Schlauchboot mit OBS a/D		02-46.61S 81-22.04W
OBS #61			
0625	Release Command		
0653	OBS gesichtet		
0703	OBS a/D		02-49.41S 81-22.92W
OBS #62			
0653	Release Command		
0725	OBS gesichtet		
0732	OBS a/D		02-52.35S 81-23.95W
OBS #63			
0725	Release Command		
0747	OBS gesichtet		
0757	OBS a/D		02-55.08S 81-25.01W
OBS #64			
0751	Release Command		
0824	OBS gesichtet		
0833	OBS a/D		02-58.08S 81-26.00W
OBS #65			
0827	Release Command		
0918	OBS gesichtet		
0924	OBS a/D		03-01.02S 81-26.96W
OBS #66			
0917	Release Command		
0954	OBS gesichtet		
1004	OBS a/D		03-03.46S 81-27.89W
1209	OBS #67 z/W	LT = 1291 m	03-21.06S 81-16.42W
1234	OBS #68 z/W	LT = 1065 m	03-18.06S 81-15.53W
1254	OBS #69 z/W	LT = 1158 m	03-15.23S 81-14.74W

1315	OBS #70 z/W	LT = 1170 m	03-12.38S 81-13.91W
1335	OBS #71 z/W	LT = 1223 m	03-09.52S 81-12.99W
1356	OBS #72 z/W	LT = 1294 m	03-06.62S 81-12.18W
1416	OBS #73 z/W	LT = 1129 m	03-03.69S 81-11.33W
1441	OBS #74 z/W	LT = 1234 m	03-00.79S 81-10.48W
1506	OBS #75 z/W	LT = 889 m	02-57.98S 81-09.68W
1531	OBS #76 z/W	LT = 760 m	02-55.11S 81-08.80W
1552	OBS #82 z/W	LT = 692 m	02-52.17S 81-07.94W
1612	OBS #77 z/W	LT = 703 m	02-49.34S 81-07.13W
1633	OBS #78 z/W	LT = 678 m	02-46.43S 81-06.27W
1653	OBS #79 z/W	LT = 600 m	02-43.57S 81-05.39W
1714	OBS #80 z/W	LT = 632 m	02-40.68S 81-04.56W
1736	OBS #81 z/W	LT = 540 m	02-37.70S 81-03.70W

Profil SM 04 :

1826	Bb-Airgun z/W	
1833	Stb-Airgun z/W	
1836	Beginn Profil	02-30.77S 81-01.70W
1843	Mitte Airgun z/W	
1855	Magnetometer z/W	
1944	Mitte-Airgun a/D	
2223	Mitte Airgun z/W	
2237	Mitte Airgun a/D	

05.09.01

0222	Mitte-Airgun z/W		
0455	Mitte-Airgun a/D		
0507	Stb-Airgun a/D		
0653	Ende Profil	59 sm	03-23.00S 81-17.00W
0712	Bb-Airgun a/D		

OBS #67

0712	Release Command	
0726	OBS gesichtet	03-20.83S 81-16.50W
0737	OBS a/D	

OBS #68

0727	Release Command	
0753	OBS gesichtet	03-17.70S 81-15.63W
0805	OBS a/D	

OBS #69

0802	Release Command	
0820	OBS gesichtet	03-14.87S 81-14.80W
0831	OBS a/D	

OBS #70

0827	Release Command

FS SONNE Stationsprotokoll SO 159

0847	OBS gesichtet	
0856	OBS a/D	03-12.02S 81-13.97W
OBS #71		
0852	Release Command	
0912	OBS gesichtet	
0919	OBS a/D	03-09.27S 81-13.05W
OBS #72		
0919	Release Command	
0943	OBS gesichtet	
0954	OBS a/D	03-06.32S 81-12.24W
OBS #73		
1000	Relaese Command	
1012	OBS gesichtet	
1021	OBS a/D	03-03.33S 81-11.35W
OBS #74		
1020	Release Command	
1040	OBS gesichtet	
1048	OBS a/D	03-00.64S 81-10.50W
OBS #75		
1040	Release Command	
1102	OBS gesichtet	
1125	OBS a/D	02-57.56S 81-09.75W
OBS #76		
1114	Release Command	
1144	OBS gesichtet	
1149	Schlauchboot z/W	
1151	Schlauchboot mit OBS a/D	02-54.85S 81-08.79W
OBS #53		
1151	Release Command	
1236	Auf Aussetzposition; OBS nicht aufgetaucht	
OBS #82		
1210	Release Command	
1220	OBS gesichtet	
1216	OBS a/D	02-52.09S 81-07.86W
OBS #77		
1236	Release Command	
1300	Auf Aussetzposition; Schiff auf Stand by	
1320	OBS gesichtet	
1325	Schlauchboot z/W	
1326	Schlauchboot mit OBS a/D	02-49.25S 81-07.06W

OBS #78

1326	Release Command		
1346	Erneutes Release Command		
1415	Hydrophon z/W; Erneutes Release Command; Warten auf Auftauchen		
1443	OBS nicht aufgetaucht		
1801	Hydrphon z/W; Erneutes Release Command; Warten auf Auftauchen		
1845	OBS nicht aufgetaucht		

OBS #79

1503	Release Command		
1524	OBS gesichtet		
1527	Schlauchboot z/W		
1532	Schlauchboot mit OBS a/D	02-43.42S	81-05.34W

OBS #80

1532	Release Command		
1552	Erneutes Release Command		
1607	OBS gesichtet		
1613	Schlauchboot z/W		
1618	Schlauchboot mit OBS a/D	02-40.69S	81-04.64W

OBS #81

1615	Hydrophon z/W; Release Command		
1636	Erneutes Release Command		
1655	OBS gesichtet		
1700	Schlauchboot z7W		
1705	Schlauchboot mit OBS a/D	02-37.65S	81-03.61W

Profil SIM

1845	Beginn Profil	02-46.37S	81-06.23W

06.09.01

1336	Ende Profil	222 sm	00-44.20N	81-30.71W
1435	OBS #82 z/W	LT = 3019 m	00-46.47N	81-40.47W
1503	OBS #83 z/W	LT = 3055 m	00-41.94N	81-41.31W
1531	OBS #84 z/W	LT = 2988 m	00-37.55N	81-42.12W
1600	OBS #85 z/W	LT = 2746 m	00-33.08N	81-42.95W
1630	OBS #86 z/W	LT = 2579 m	00-28.66N	81-43.81W
1657	OBS #87 z/W	LT = 2869 m	00-24.26N	81-44.64W
1725	OBS #88 z/W	LT = 2946 m	00-19.85N	81-45.46W
1754	OBS #89 z/W	LT = 2147 m	00-15.42N	81-46.30W
1823	OBS #90 z/W	LT = 1511 m	00-11.02N	81-47.10W
1858	OBS #91 z/W	LT = 1625 m	00-05.30N	81-48.22W
1932	OBS #92 z/W	LT = 1155 m	00.00.00N	81-49.23W
1957	OBS #93 z/W	LT = 1105 m	00-03.86S	81-49.96W
2023	OBS #94 z/W	LT = 917 m	00-07.76S	81-50.70W
2052	OBS #95 z/W		00-12.21S	81-51.53W

2120	OBS #96 z/W		00-16.68S 81-52.39W
2148	OBS #97 z/W		00-21.08S 81-53.23W
2216	OBS #98 z/W		00-25.49S 81-54.06W
2244	OBS #99 z/W		00-30.07S 81-54.93W
2312	OBS #100 z/W		00-34.48S 81-55.77W
2339	OBS #101 z/W		00-38.90S 81-56.61W
07.09.01			
0005	OBS #102 z/W		00-43.32S 81-57.35W
0034	OBS #103 z/W		00-47.58S 81-58.22W
0100	OBS #104 z/W		00-51.49S 81-58.97W
Profil SIM			
0100	Beginn Profil		00-51.49S 81-58.97W
0917	Ende Profil	99 sm	02-26.20S 81-34.20W
OBS #1			
1041	Schiff auf Aussetzposition (Zeitrelease) Release Command		02-42.99S 81-31.51W
1106	Hydrophon z/W; div. Release Commands		
1200	OBS gesichtet		
1208	Schlauchboot z/W		
1214	Schlauchboot mit OBS a/D		02-42.77S 81-31.53W
Test Benthoskugel W6			
1218	Beginn Station	LT = 4442 m	02-42.72S 81-31.54W
1220	Benthoskugel z/W		
1244	SImax 1000 m	LT = 4442 m	02-42.55S 81-31.45W
1307	Benthoskugel a/D		
1308	Ende Station		
Profil SIM			
1315	Beginn Profil		02-43.00S 81-31.50W
1930	Ende Profil	83 sm	02-50.00S 81-02.78W
OBS #78			
2000	Schiff auf Aussetzposition Warten auf Auftauchen (Zeitreleaser)		02-46.47S 81-06.32W
2133	OBS nicht aufgetaucht		
Profil SIM			
2133	Beginn Profil		02-46.44S 81-06.38W
08.09.01			
0734	Ende Profil	124 sm	00-55.00S 81-59.55W
OBS #106			
0739	OBS #106 z/W	LT = 1424 m	00-54.82S 81-59.63W

FS SONNE Stationsprotokoll SO 159

Profil SM 05

0816	Bb-Airgun z/W	
0818	Beginn Profil SM05	00-58.24S 82-00.27W
0825	Stb-Airgun z/W	
0834	Stb-Airgun a/D; defekt; Umsetzen Mitte Airgun zur Stb-Seite	
0948	Stb-Airgun z/W	
1031	Magnetometer z/W	
1901	Mitte Airgun z/W	

09.09.01

0403	Stb-Airgun a/D	
0632	Mitte-Airgun a/D	
0720	Stb-Airgun z7W	
1300	Ende Profil 120 sm	00-59.97N 81-37.88W
1307	Magnetometer a/D	
1311	Mitte-Airgun a/D	
1323	Bb-Airgun a/D	
1331	Stb-Airgun a/D	

OBS #83

1433	Release Command	
1514	OBS gesichtet	00-46.53N 81-40.59W
1523	OBS a/D	

OBS #84

1514	Release Command	
1547	OBS gesichtet	00-42.03N 81-41.43W
1600	OBS a/D	

OBS #85

1552	Release Command	
1637	OBS gesichtet	00-37.70N 81-42.13W
1646	OBS a/D	

OBS #86

1637	Release Command	
1710	OBS gesichtet	00-33.14N 81-43.04W
1721	OBS a/D	

OBS #87

1718	Release Command	
1746	OBS gesichtet	00-28.69N 81-43.85W
1756	OBS a/D	

OBS #88

1749	Release Command	
1818	OBS gesichtet	00-24.22N 81-44.70W
1828	OBS a/D	

OBS #89		
1825	Release Command	
1902	OBS gesichtet	
1913	OBS a/D	00-19.84N 81-45.55W
OBS #90		
1902	Release Command	
1933	OBS gesichtet	
1951	OBS a/D	00-15.29N 81-46.37W
OBS #91		
1945	Release Command	
2005	OBS gesichtet	
2025	OBS a/D	00-10.92N 81-47.15W
OBS #92		
2046	Release Command	
2108	OBS gesichtet	
2116	OBS a/D	00-05.23N 81-48.27W
OBS #93		
2134	Release Command	
2149	OBS gesichtet	
2156	OBS a/D	00-00.09S 81-49.30W
OBS #96		
2236	OBS gesichtet (Zeitreleaser)	
2309	Schlauchboot z/W	
2313	Schlauchboot mit OBS a/D	00-12.46S 81-51.20W
OBS #97		
2326	OBS gesichtet (Zeitreleaser)	
2339	Schlauchboot z/W	
2342	Schlauchboot mit OBS a/D	00-16.64S 81-52.14W
10.09.01		
OBS #98		
0023	OBS gesichtet (Zeitreleaser)	
0032	Schlauchboot z/W	
0038	Schlauchboot mit OBS a/D	00-21.46S 81-53.20W
OBS #99		
0130	OBS gesichtet (Zeitreleaser)	
0135	Schlauchboot z/W	
0141	Schlauchboot mit OBS a/D	00-25.59S 81-53.95W
OBS #100		
0230	OBS gesichtet (Zeitreleaser)	
0235	Schlauchboot z/W	

FS SONNE Stationsprotokoll SO 159

0239	Schlauchboot mit OBS a/D		00-30.07S 81-54.85W
OBS #101			
0336	OBS gesichtet (Zeitreleaser)		
0341	Schlauchboot z/W		
0347	Schlauchboot mit OBS a/D		00-34.50S 81-55.72W
OBS #102			
0438	OBS gesichtet (Zeitreleaser)		
0444	Schlauchboot z/W		
0448	Schlauchboot mit OBS a/D		00-38.85S 81-56.57W
OBS #103			
0532	OBS gesichtet (Zeitreleaser)		
0536	Schlauchboot z/W		
0542	Schlauchboot mit OBS a/D		00-43.29S 81-57.23W
OBS #104			
0640	OBS gesichtet (Zeitreleaser)		
0646	Schlauchboot z/W		
0650	Schlauchboot mit OBS a/D		
OBS #105			
0741	OBS gesichtet (Zeitreleaser)		
0748	Schlauchboot z/W		
0752	Schlauchboot mit OBS a/D		00-51.44S 81-58.76W
OBS #106			
0748	Release Command		
0817	OBS gesichtet		
0823	OBS a/D		00-54.84S 81-59.55W
Profil SIM			
0823	Beginn Profil		00-54.84S 81-59.55W
1238	Ende Profil	53 sm	00-09.29S 81-45.61W
OBS #95			
1255	Release Command		
1308	OBS gesichtet		
1320	OBS a/D		00-07.75S 81-50.70W
OBS #94			
1330	Release Command		
1345	OBS gesichtet		
1352	OBS a/D		00-03.86S 81-50.00W
Profil SIM			
1352	Beginn Profil		00-03.86S 81-50.00W
1735	Ende Profil	62 sm	00-30.45N 81-24.76W

FS SONNE Stationsprotokoll SO 159

Profil MAG 130

1735	Beginn Profil		00-30.45N 81-24.76W
	Magnetometer z/W; SL 180 m		

11.09.01

0430	Ende Profil 110 sm		01-57.57N 80-10.41W
0443	Magnetometer a/D		
0506	OBS #107 z/W	LT = 3136 m	02-00.48N 80-07.74W
0527	OBS #108 z/W	LT = 3161 m	01-58.52N 80-05.45W
0549	OBS #109 z/W	LT = 3155 m	01-56.60N 80-03.20W
0613	OBS #110 z/W	LT = 3139 m	01-54.64N 80-00.90W
0635	OBS #111 z/W	LT = 3078 m	01-52.69N 79-58.64W
0656	OBS #112 z/W	LT = 3026 m	01-50.77N 79-56.38W
0718	OBS #113 z/W	LT = 2972 m	01-48.88N 79-54.16W
0739	OBS #114 z/W	LT = 2887 m	01-46.96N 79-51.92W
0802	OBS #115 z/W	LT = 2043 m	01-45.05N 79-49.66W
0822	OBS #116 z/W	LT = 2143 m	01-43.12N 79-47.41W
0841	OBS #117 z/W	LT = 1344 m	01-41.23N 79-45.20W
0908	OBS #118 z/W	LT = 957 m	01-39.28N 79-42.91W
0932	OBS #119 z/W	LT = 740 m	01-37.36N 79-40.64W
0954	OBS #120 z/W	LT = 877 m	01-35.43N 79-38.38W
1016	OBS #121 z/W	LT = 871 m	01-33.52N 79-36.17W
1039	OBS #122 z/W	LT = 720 m	01-31.58N 79-33.89W
1113	OBS #123 z/W	LT = 668 m	01-29.71N 79-31.70W
1145	OBS #124 z/W	LT = 629 m	01-27.77N 79-29.45W
1226	OBS #125 z/W	LT = 700 m	01-25.84N 79-27.17W
1248	OBS #126 z/W	LT = 720 m	01-23.89N 79-24.88W
1310	OBS #127 z/W	LT = 716 m	01-21.97N 79-22.65W
1328	OBS #128 z/W	LT = 644 m	01-20.54N 79-20.96W
1345	OBS #129 z/W	LT = 548 m	01-19.21N 79-19.43W
1401	OBS #130 z/W	LT = 446 m	01-17.93N 79-17.94W

Profil SIM

1419	Beginn Profil		01-19.08N 79-16.18W
1645	Ende Profil 30 sm		01-12.71N 79-14.84W

Profil SM06

1710	Beginn Profil, Bb-Airgun z/W		01-14.25N 79-13.57W
1720	Mitte-Airgun z/W		
1725	Mitte-Airgun a/D		
1820	Magnetometer z/W		
1945	Mitte-Airgun z/W		

12.09.01

0937	Ende Profil 73 sm		02-01.80N 80-09.30W
0954	Magnetometer a/D		
1003	Mitte-Airgun a/D		
1011	Bb-Airgun a/D		

1021	Stb-Airgun a/D	
OBS #107		
1022	Release Command	
1106	OBS gesichtet	
1113	OBS a/D	02-00.52N 80-07.83W
OBS #108		
1106	Release Command	
1156	OBS gesichtet	
1206	OBS a/D	01-58.62N 80-05.57W
OBS #109		
1157	Release Command	
1234	OBS gesichtet	
1243	OBS a/D	01-56.65N 80-03.27W
OBS #110		
1234	Release Command	
1317	OBS gesichtet	
1326	OBS a/D	01-54.72N 80-00.98W
OBS #111		
1317	Release Command	
1358	OBS gesichtet	
1403	OBS a/D	01-52.76N 79-58.67W
OBS #112		
1358	Release Command	
1430	OBS gesichtet	
1441	OBS a/D	01-50.84N 79-56.41W
OBS #113		
1430	Release Command	
1510	OBS gesichtet	
1520	OBS a/D	01-48.91N 79-54.17W
OBS #114		
1510	Release Command	
1554	OBS gesichtet	
1600	OBS a/D	01-46.94N 79-51.95W
OBS #115		
1554	Release Command	
1620	OBS gesichtet	
1630	OBS a/D	01-45.00N 79-49.66W

FS SONNE Stationsprotokoll SO 159

OBS #116

1625	Release Command	
1654	OBS gesichtet	
1702	OBS a/D	01-43.08N 79-47.48W

OBS #117

1658	Release Command	
1718	OBS gesichtet	
1732	OBS a/D	01-41.21N 79-45.25W

OBS #118

1736	Release Command	
1755	Erneutes Relaese Command	
1805	OBS gesichtet	
1809	OBS a/D	01-39.29N 79-42.92W

OBS #119

1810	Release Command	
1825	OBS gesichtet	
1837	OBS a/D	01-37.32N 79-40.60W

OBS #120

1841	Release Command	
1854	OBS gesichtet	
1904	OBS a/D	01-35.42N 79-38.36W

OBS #121

1909	Release Command	
1941	OBS gesichtet	
1946	Schlauchboot z/W	
1949	Schlauchboot mit OBS a/D	01-33.57N 79-36.09W

OBS #122

1954	Release Command	
2024	OBS gesichtet	
2031	Schlauchboot z7W	
2033	Schlauchboot mit OBS a/D	01-31.67N 79-33.84W

OBS #123

2038	Release Command	
2111	OBS gesichtet	
2116	Schlauchboot z7W	
2119	Schlauchboot mit OBS a/D	01-29.75N 79-31.65W

OBS #124

2124	Release Command
2214	Hydrophon z/W; Erneutes Release Command
2240	OBS nicht aufgetaucht

OBS #125
2257 Release Command
2400 OBS nicht aufgetaucht

13.09.01
OBS #124
Von Mitternacht bis 0100 div. Suchkurse auf Aussetzposition; OBS nicht aufgetauc
0624 Auf Aussetzposition OBS; div. Suchkurse
0725 Abbruch Sucjkurse; OBS nicht aufgetaucht.

OBS #125
0120 OBS gesichtet (Zeitrelease)
0128 Schlauchboot z/W
0132 Schlauchboot mit OBS a/D 01-25.88N 79-27.15W

OBS #126
0220 OBS gesichtet (Zeitreleaser)
0228 Schlauchboot z/W
0232 Schlauchboot mit OBS a/D 01-23.93N 79-24.85W

OBS #127
0320 OBS gesichtet (Zeitreleaser)
0326 Schlauchboot z/W
0330 Schlauchboot mit OBS a/D 01-22.02N 79-22.62W

OBS #128
0400 OBS gesichtet (Zeitreleaser)
0404 Schlauchboot z/W
0408 Schlauchboot mit OBS a/D 01-20.60N 79-20.96W

OBS #129
0423 Release Command
0436 OBS gesichtet
0440 Schlauchboot z/W
0445 Schlauchboot mit OBS a/D 01-19.23N 79-19.46W

OBS #130
0500 Release Command
0512 OBS gesichtet
0517 Schlauchboot z/W
0522 Schlauchboot mit OBS a/D 01-17.96N 79-17.97W

Profil SIM 01-26.38N 79-39.96W
0735 Beginn Profil 01-45.00N 80-03.50W
1112 Ende Profil 40 sm

Station CTD 03 W4 01-45.00N 80-03.50W
1112 Beginn Station LT = 3147 m

FS SONNE Stationsprotokoll SO 159

1222	CTD z/W			
1315	SImax 3050 m		LT = 3146 m	01-44.94N 80-03.49W
1416	CTD a/D			
1418	Ende Station			
Profil MAG 131				
1434	Magnetometer z/W			
1440	Beginn Profil			01-43.95N 80-02.73W
1507	Ende Profil	6 sm		01-40.00N 80-00.00W
Profil MAG 132				
1507	Beginn Profil			01-40.00N 80.00.00W
1837	Ende Profil	38 sm		01-09.00N 80-19.32W
Profil MAG 133				
1837	Beginn Profil			01-09.00N 80-19.32W
14.09.01				
0048	Ende Profil	65 sm		00-26.00N 81-02.00W
Profil MAG 134				
0048	Beginn Profil			00-26.00N 81-02.00W
0700	Ende Profil	65 sm		00-35.00S 81-26.00W
0713	Magnetometer a/D			
Station CTD 04	W4			
0849	Beginn Station		LT = 1727 m	00-49.01S 81-37.97W
0854	CTD z/W			
0945	SImax 1600 m		LT = 1750 m	00-48.97S 81-37.51W
1024	CTD a/D			
1025	Ende Station			
Profil SIM				
1025	Beginn Profil			00-48.92S 81-37.34W
1324	Ende Profil	36 sm		01-24.00S 81-44.20W
Profil SIM				
1324	Beginn Profil			01-24.00S 81-44.20W
1404	Ende Profil	8 sm		01-16.00S 81-47.00W
Profil SIM				
1404	Beginn Profil			01-16.00S 81-47.00W
1620	Ende Profil	30 sm		00-47.00S 81-47.50W
Profil SIM				
1620	Beginn Profil			00-47.00S 81-47.50W
1642	Ende Profil	4 sm		00-47.00S 81-46.00W

FS SONNE Stationsprotokoll SO 159

Profil SIM			
1642	Beginn Profil		00-47.00S 81-46.00W
1843	Ende Profil	25 sm	01-11.80S 81-50.00W
Profil SIM			
1843	Beginn Profil		01-11.80S 81-50.00W
1930	Ende Profil	10 sm	01-02.17S 81-51.38W
Profil SIM			
1930	Beginn Profil		01-02.17S 81-51.38W
1950	Ende Profil	4 sm	00-58.24S 81-52.75W
Profil SIM			
1950	Beginn Profil		00-58.24S 81-52.75W
2043	Ende Profil	10 sm	01-01.30S 82-02.00W
Profil SIM			
2043	Beginn Profil		01-01.30S 82-02.00W
2216	Ende Profil	19 sm	01-20.00S 82-04.50W
Profil SIM			
2216	Beginn Profil		01-20.00S 82-04.50W
2308	Ende Profil	12 sm	01-20.00S 81-53.00W
Profil SIM			
2308	Beginn Profil		01-20.00S 81-53.00W
15.09.01			
0100	Ende Profil	24 sm	01-43.00S 81-48.00W
Profil SIM			
0100	Beginn Profil		01-43.00S 81-48.00W
0203	Ende Profil	13 sm	01-54.50S 81-41.30W
Profil SIM			
0203	Beginn Profil		01-54.50S 81-41.30W
0325	Ende Profil	17 sm	02-06.50S 81-54.00W
Profil SIM			
0325	Beginn Profil		02-06.50S 81-54.00W
0545	Ende Profil	29 sm	02-32.00S 81-40.80W
Profil SIM			
0545	Beginn Profil		02-32.00S 81-40.80W
0723	Ende Profil	19 sm	02-47.00S 81-55.00W
Profil SIM			
0723	Beginn Profil		02-47.00S 81-55.00W
1030	Ende Profil	37 sm	03-12.00S 82-22.30W

FS SONNE Stationsprotokoll SO 159

Profil SIM			
1030	Beginn Profil		03-12.00S 82-22.30W
1230	Ende Profil	18 sm	03-23.00S 82-08.50W
Profil SIM			
1230	Beginn Profil		03-23.00S 82-08.50W
1515	Ende Profil	37 sm	02-58.50S 81-41.30W
Profil SIM			
1515	Beginn Profil		02-58.50S 81-41.30W
1750	Ende Profil	31 sm	03-23.00S 81-21.50W
Profil SIM			
1750	Beginn Profil		03-23.00S 81-21.50W
1832	Ende Profil	6 sm	03-23.00S 81-13.50W
Profil SIM			
1832	Beginn Profil		03-23.00S 81-13.50W
2159	Ende Profil	39 sm	02-45.64S 81-02.15W
Profil SIM			
2159	Beginn Profil		02-45.64S 81-02.15W
2311	Ende Profil	15 sm	02-34.28S 81-04.35W
Profil SIM			
2311	Beginn Profil		02-34.28S 81-04.35W
16.09.01			
0043	Ende Profil	18 sm	02-18.73S 81-16.72W
Profil SIM			
0043	Beginn Profil		02-18.73S 81-16.72W
0100	Ende Profil	3 sm	02-16.89S 81-17.55W
Profil SIM			
0100	Beginn Profil		02-16.89S 81-17.55W
0236	Ende Profil	22 sm	02-34.94S 81-01.28W
Profil SIM			
0236	Beginn Profil		02-34.94S 81-01.28W
0330	Ende Profil	12 sm	02-37.78S 80-50.00W

MS SONNE KAPITÄN

Appendix II.1a **SALIERI SO159 - PROFILE 01**

INSTRUMENT	LAT (S)	LON (W)	DIST. TO	DEPTH	RELEASER-	ANT.	RECORDER	SKEW	REMARKS
	D:M	D:M	NEXT (nm)	(m)	CODE	CH.	NUMBER	(ms)	
OBS01	0 : 05,595	85 : 19,563	4.43	2910	10.0D	A	98-2	0	-
OBS02	0 : 10,016	85 : 18,968	4.21	3085	3614	D	01001	-3	battery low, no data
OBS03	0 : 14,207	85 : 18,393	4.32	3208	13.0E	B	94-5	0	-
OBH04	0 : 18,504	85 : 17,843	4.29	2736	4A44 (ModeB)	D	980901	23	
OBS05	0 : 22,782	85 : 17,283	4.29	2754	11.5F	C	94-1	0	-
OBH06	0 : 27,053	85 : 16,763	4.26	1992	0386 + 0355	B	1005	5	-
OBS07	0 : 31,318	85 : 16,266	4.29	2323	7.0B	D	93-15	0	not recovered
OBH08	0 : 35,580	85 : 15,677	4.32	2414	039A + 0355	C	980401	-8	
OBS09	0 : 39,941	85 : 15,148	4.30	2408	7.5B	A	92-3	0	-
OBH10	0 : 44,163	85 : 14,534	4.27	2341	0398 + 0355	C	1003	7	-
OBS11	0 : 48,455	85 : 14,025	4.25	2317	10.0C	B	94-12	0	-
OBH12	0 : 52,692	85 : 13,512	4.25	2544	6334	A	001002	-9	-
OBS13	0 : 56,921	85 : 12,947	4.35	2300	11.0E	C	94-16	0	-
OBH14	1 : 01,247	85 : 12,423	4.30	2347	B495	C	991292	-6	-
OBS15	1 : 05,543	85 : 11,851	4.30	2352	8.5B	D	92-7	0	-
OBH16	1 : 09,834	85 : 11,337	4.30	2369	0397 + 0355	C	001006	90	-
OBS17	1 : 14,137	85 : 10,810	4.22	2457	12.0F	A	92-5	0	-
OBH18	1 : 18,321	85 : 10,237	4.28	2398	3659	C	980906	4	-
OBS19	1 : 22,585	85 : 09,710	4.32	2357	14.5H	C	94-7	0	not recovered
OBH20	1 : 26,886	85 : 09,163	4.25	2402	3609	D	000614	-12	-

Appendix II.1b **SALIERI SO159 - PROFILE 01**

INSTRUMENT	LAT (S)	LON (W)	DIST. TO	DEPTH	RELEASER-	ANT.	RECORDER	SKEW	REMARKS
	D:M	D:M	NEXT (nm)	(m)	CODE	CH.	NUMBER	(ms)	
OBS21	1 : 31,129	85 : 08,593	4.30	2426	9.0C	D	94-2	0	-
OBH22	1 : 35,396	85 : 08,030	4.27	2472	0399 + 0355	C	000612	6	-
OBS23	1 : 39,735	85 : 07,500	4.35	2427	10.5C	A	93-10	0	-
OBH24	1 : 43,994	85 : 06,971	4.28	2407	D634	B	991252	-12	-
OBS25	1 : 48,263	85 : 06,395	4.32	2437	7.5A	B	94-8	0	-
OBH26	1 : 52,574	85 : 05,869	4.32	2484	C444	D	971202	-11	-
OBS27	1 : 56,884	85 : 05,302	4.27	2662	9.5D	B	94-10	0	-
OBH28	2 : 01,134	85 : 04,790	4.22	2573	D629	C	991247	1	no data
OBS29	2 : 05,334	85 : 04,273	4.32	2671	15.0H	D	94-18	0	not recovered
OBH30	2 : 09,641	85 : 03,711	4.30	2760	5929	C	991235	0	-
OBS31	2 : 13,922	85 : 03,166	4.32	2968	8.0B	B	94-11	0	-
OBH32	2 : 18,229	85 : 02,620	4.27	2796	3624	D	991247	1	-
OBS33	2 : 22,480	85 : 02,084	4.29	2973	11.5E	C	92-2	0	-
OBH34	2 : 26,776	85 : 01,534	4.24	3028	0387 + 0355	C	000707	-	battery low, no data
OBS35	2 : 31,009	85 : 01,000	4.32	3103	3674	D	000708	-18	Seismometer not working
OBH36	2 : 35,325	85 : 00,444	3.34	3146	4979	D	000616	-6	-
OBH37	2 : 38,660	85 : 00,013		3170	6959	D	010401	-11	
Streamer							980902	0	-
Trigger							990901	2	-

Appendix II.2

SALIERI SO159 - PROFILE 02

INSTRUMENT	LAT (S)	LON (W)	DIST. TO	DEPTH	RELEASER	ANT.	RECORDER	SKEW	REMARKS
	D:M	D:M	NEXT (nm)	(m)	CODE	CH.	NUMBER	(ms)	
OBS39	2 : 36,83	81 : 47,72	2,98	3197	13.0_F	D		0	not recovered
OBS40	2 : 37,84	81 : 44,9	3,03	3285	14.0_H	A	94-3	0	not recovered
OBS41	2 : 38,95	81 : 42,11	2,97	3438	9.5_C	B	94-4	0	-
OBH42	2 : 40,070	81 : 39,341	3,01	3587	0397+0355 B	D	000616	-3	no data
OBS43	2 : 41,144	81 : 36,507	2,98	4021	3614 B	C	001001	-3	no data
OBH44	2 : 42,248	81 : 33,759	3,00	4230	3624 B	D	000707	-2	-
OBS45	2 : 43,323	81 : 30,959	3,02	4441	3674 B	C	000708	-7	-
OBH46	2 : 44,411	81 : 28,138	3,29	4063	6334 B	D	001005	4	-
OBH47	2 : 45,615	81 : 25,034	3,29	3043	0398+0355 B	D	980901	11	-
OBS48	2 : 46,773	81 : 22,007	3,01	2124	10.5_C	C	93-10	0	-
OBH49	2 : 47,864	81 : 19,193	2,96	1766	039A+0355 B	C	991235	0	DPG
OBS50	2 : 48,938	81 : 16,420	3,01	1460	11.5_F	D	94-1	0	-
OBH51	2 : 50,044	81 : 13,608	3,01	1053	0386+0355 B	D	971202	-4	-
OBS52	2 : 51,124	81 : 10,803	3,01	777	7.5_B	A	92-3	0	-
OBS53	2 : 52,196	81 : 07,995	3,01	689	14.5_H	B	94-7	0	not recovered
OBH54	2 : 53,297	81 : 05,189	3,00	612	4A44 B	C	010401	-3	-
OBH55	2 : 54,372	81 : 02,402	3,00	524	0399+0351 B	D	980401	-4	-
OBS56	2 : 55,475	80 : 59,604	3,01	445	10.0_D	C	98-2	0	-
OBS57	2 : 56,551	80 : 56,789	3,01	238	14.5_G	D	93-16	0	not recovered
OBS58	2 : 57,624	80 : 53,979		108	8.5_B	B	92-7	0	-
Trigger							971201	-1	

Appendix II.3 **SALIERI SO159 - PROFILE 03**

INSTRUMENT	LAT (S)		LON (W)		DIST. TO	DEPTH	RELEASER-	ANT.	RECORDER	SKEW	REMARKS
	D:M		D:M		NEXT (nm)	(m)	CODE	CH.	NUMBER	(ms)	
OBH59	2 :	41,219	81 :	20,062	2,88	1971	0399+0355	D	980401	-3	Disk-Error
OBH60	2 :	43,966	81 :	20,995	2,98	2071	4A44	C	010401	-2	-
OBS48	2 :	46,773	81 :	22,007	2,95	**2124**	10.5_C	C	93-10		-
OBH61	2 :	49,589	81 :	22,91	3,02	2306	0386+0355	D	000707	-3	-
OBH62	2 :	52,442	81 :	23,928	3,03	2075	0398+0355	C	991235	nn	DPG
OBH63	2 :	55,339	81 :	24,935	3,02	3250	039A+0355	C	971202	-3	-
OBH64	2 :	58,200	81 :	25,921	3,01	2534	6334	C	001005	3	-
OBH65	3 :	01,075	81 :	26,896	2,74	3425	3624	D	980901	8	-
OBH66	3 :	03,662	81 :	27,831		2916	0397+0355	D	000616	2	HT-Hydrophon
Trigger									971201	0	

Appendix II.4

SALIERI SO159 - PROFILE 04

INSTRUMENT	LAT (S) D:M		LON (W) D:M		DIST. TO NEXT (nm)	DEPTH (m)	RELEASER-CODE	ANT. CH.	RECORDER NUMBER	SKEW (ms)	REMARKS
OBH67	3 :	21,06	81 :	16,42	3,04	1270	6334	C	000616	-1	
OBH68	3 :	18,06	81 :	15,53	2,99	1066	0398+0355	D	001005	1	
OBH69	3 :	15,188	81 :	14,756	2,97	1157	0397+0355	C	971202	-2	
OBS70	3 :	12,34	81 :	13,99	2,94	1166	3614	D	001001	-2	
OBH71	3 :	09,524	81 :	12,988	3,02	1225	039A+0355	C	991235	0	DPG
OBH72	3 :	06,626	81 :	12,180	3,04	1294	0386+0355	D	980901	5	
OBH73	3 :	03,693	81 :	11,333	2,97	1124	4A44	C	000707	-2	
OBH74	3 :	00,750	81 :	10,465	2,95	1219	0399+0355	D	000614	-2	
OBH75	2 :	57,950	81 :	09,687	2,99	890	3609	C	010401	-2	recorder reboot at "end"
OBS76	2 :	55,115	81 :	08,806	3,00	747	11.5_F	A	94-1		
OBS53	2 :	52,196	81 :	07,995	0,04	689	14.5_H	B	94-7		not recovered
OBH82	2 :	52,174	81 :	07,941	2,96	692	3659	C	001003	1	
OBS77	2 :	49,335	81 :	07,136	3,05	694	7.5_B	B	92-3		
OBS78	2 :	46,423	81 :	06,273	2,98		10.0_D	C	98-2		picked up by fisher boat
OBS79	2 :	43,573	81 :	05,395	3.00	597	8.5_B	D	92-7		
OBS80	2 :	40,677	81 :	04,650	3,07	627	10.0_C	B	94-12		
OBS81	2 :	37,693	81 :	03,697		538	8.0_B	C	94-11		
Trigger									971201	0	

Appendix II.5a

SALIERI SO159 - PROFILE 05

INSTRUMENT	LAT (S)		LON (W)		DIST. TO	DEPTH	RELEASER-	ANT.	RECORDER	SKEW	REMARKS
	D:M		D:M		NEXT (nm)	(m)	CODE	CH.	NUMBER	(ms)	
OBH83	0 :	46,448	81 :	40,52	4,59	3013	3609	C	010401	-6	
OBS84	0 :	41,929	81 :	41,33	4,45	3058	3.614	D	001001	-5	
OBH85	0 :	37,556	81 :	42,118	4,52	2958	0399+0355	C	980901	25	
OBH86	0 :	33,075	81 :	42,96	4,50	2755	4A44	D	000616	-5	Streifen
OBH87	0 :	28,649	81 :	43,813	4,46	2579	0386+0355	D	980401	-6	
OBH88	0 :	24,259	81 :	44,644	4,47	2869	039A+0355	C	991235	2	DPG
OBH89	0 :	19,852	81 :	45,468	4,49	2947	0397+0355	D	001005	7	Streifen
OBH90	0 :	15,433	81 :	46,296	4,46	2148	0398+0355	C	971202	-7	
OBH91	0 :	11,037	81 :	47,115	5,79	1518	6334	D	000707	-8	reboot at "skew"
OBH92	0 :	05,305	81 :	48,225	5,38	1629	3659	C	000713	0	
OBH93	0 :	00,001	81 :	49,236	3,90	1156	3624	D	001006	-2	
OBH94	0 :	03,862	81 :	49,958	3,96	1106	d634	C	001002	6	
OBH95	0 :	07,751	81 :	50,705	4,49	917	C444	D	000614	-10	
OBS96	0 :	12,216	81 :	51,523	4,52	800	9.5_D	B	94-10		
OBS97	0 :	16,685	81 :	52,360	4,49	800	7.5_A	C	94-8		
OBS98	0 :	21,117	81 :	53,197	4,45	900	11.5_E	D	92-2		
OBS99	0 :	25,512	81 :	54,034	4,62	1275	9.0_C	A	94-2		
OBS100	0 :	30,053	81 :	54,943	4,49	1315	10.5_C	B	93-10		
OBS101	0 :	34,485	81 :	55,780	4,48	1350	11.5_F	C	94-1		
OBS102	0 :	38,917	81 :	56,544	4,48	1400	7.5_B	B	92-3		

Appendix II.5b

SALIERI SO159 - PROFILE 05

INSTRUMENT	LAT (S)	LON (W)	DIST. TO	DEPTH	RELEASER-	ANT.	RECORDER	SKEW	REMARKS
	D:M	D:M	NEXT (nm)	(m)	CODE	CH.	NUMBER	(ms)	
OBS103	0 : 43,360	81 : 57,284	4,32	1425	8.5_B	C	92-7		
OBS104	0 : 47,612	81 : 58,158	3,96	1425	10.0_C	B	94-12		
OBS105	0 : 51,500	81 : 59,000	3,32	1430	8.0_B	A	94-11		
OBH106	0 : 54,829S	81 : 59,637		1425	d629	C	971201	-7	
Trigger							991252	0	

Appendix II.6a

SALIERI SO159 - PROFILE 06

INSTRUMENT	LAT (S)	LON (W)	DIST. TO	DEPTH	RELEASER-	ANT.	RECORDER	SKEW	REMARKS
	D:M	D:M	NEXT (nm)	(m)	CODE	CH.	NUMBER	(ms)	
OBH107	2 : 00,486	80 : 7,732	3,03	3137	3624	C	000616	-3	
OBH108	1 : 58,522	80 : 5,443	2,97	3160	3.659	D	001005	3	
OBH109	1 : 56,593	80 : 03,194	3,01	3156	6334	C	000614	-4	
OBH110	1 : 54,648	80 : 0,921	2,98	3139	0398+0355	D	010401	-3	
OBH111	1 : 52,695	79 : 58,64	2,96	3078	0397+0355	C	971202	-3	
OBH112	1 : 50,780	79 : 56,387	2,91	3026	039A+0355	D	991235	0	DPG
OBH113	1 : 48,881	79 : 54,161	2,95	2973	d634	C	980401	-3	
OBH114	1 : 46,966	79 : 51,921	2,95	2887	C444	D	980901		no answer from recorder
OBS115	1 : 45,054	79 : 49,647	2,96	2060	3614	D	001001	-3	
OBH116	1 : 43,124	79 : 47,413	2,89	2143	d629	C	000707	-3	
OBH117	1 : 41,250	79 : 45,220	2,99	1355	0386+0355	D	991252	-4	
OBS118	1 : 39,272	79 : 42,913	2,98	959	3674	C	000708	-6	
OBH119	1 : 37,361	79 : 40,647	2,97	738	4A44	D	001006	-1	
OBH120	1 : 35,433	79 : 38,390	2,93	877	0399+0355	C	991247		
OBS121	1 : 33,522	79 : 36,159	2,94	871	8.0_B	A	94-11		
OBS122	1 : 31,581	79 : 33,896	2,93	750	10.0_C	B	94-12		
OBS123	1 : 29,714	79 : 31,688	2,96	660	8.5_B	C	92-7		
OBS124	1 : 27,773	79 : 29,438	2,98	?	7.5_B	D	92-3		
OBS125	1 : 25,821	79 : 27,172	2,98	703	11.5_F	A	94-1		
OBS126	1 : 23,869	79 : 24,880	2,94	730	10.5_C	B	93-10		

Appendix II.6b

SALIERI SO159 - PROFILE 06

INSTRUMENT	LAT (S)		LON (W)		DIST. TO	DEPTH	RELEASER-	ANT.	RECORDER	SKEW	REMARKS
	D:M		D:M		NEXT (nm)	(m)	CODE	CH.	NUMBER	(ms)	
OBS127	1 :	21,960	79 :	22,637	2,22	721	11.5_E	C	92-2		
OBS128	1 :	20,543	79 :	20,960	2,01	648	7.5_A	B	94-8		
OBS129	1 :	19,186	79 :	19,422	1,99	565	9.5_C	C	94-4		
OBS130	1 :	17,930	79 :	17,940		450	10.5_D	B	94-5		
Trigger									971201	0	

Appendix III

Airgun - Pulserstation

Project: Salieri Line: P01 Airgun: 32 l

Date	Time UTC	Latitude	Longitude	Speed [kn]	Course o.G./GPS	Guns	Depth [m]	Trigger Interval [s]	Remarks Operator
26.08.2001	11:55	03°02,629 S	84°56,98 W	3,3	354	1	3235	60	port gun first shot
26.08.2001	12:08	03°01,851 S	84°57,062 W	3,6	352	2	3234	60	starboard gun first shot
26.08.2001	12:19	03°01,137 S	84°57,157 W	4,7	351	3	3221	60	center gun first shot
26.08.2001	12:22					2		60	only starboard and port gun are ok
26.08.2001	21:32	02°20,234 S	84°02,207 W	4,6	349	2	3221	60	1 extra shot
27.08.2001	07:04	01°37,699 S	85°07,800 W	4,5	352	2	2569	60	starboard side: back buoys lost
27.08.2001	07:10					1		60	starboard gun switched off
27.08.2001	07:38					2		60	starboard gun on
27.08.2001	07:41	01°35,936 S	85°08,020 W	4,2	355	2	2435	60	port side: front buoy lost
27.08.2001	16:09	00°57,480 S	85°12,510 W			2		60	trigger not recording
27.08.2001	17:41	00°50,500 S	85°13,440 W			2		60	trigger ok
27.08.2001	19:11	00°44,110 S	85°14,350 W			2		60	trigger not recording

Sheet - No.: 1

Appendix III

Airgun - Pulserstation

Project: Salieri Line: P01 / P02 Airgun: 32 l

Date	Time UTC	Latitude	Longitude	Speed [kn]	Course o.G./GPS	Guns	Depth [m]	Trigger Interval [s]	Remarks Operator
27.08.2001	21:51	00°32,090 S	85°16,060 W			2		60	trigger ok
28.08.2001	04:35	00°01,699 S	85°19,997 W	4,5	354	2	3176	60	streamer on board
28.08.2001	07:03	00°09,413 N	85°21,404 W	4,4	359	2	2989		last shot
Profile 01									total number of shots = 2603
Profile 02	19:21	03°05,899 S	80°32,787 W	2	296	1		60	port gun first shot
01.09.2001	19:30	03°05,768 S	80°33,105 W	3	292	2		60	stb gun first shot
01.09.2001	21:23	03°02,611 S	80°41,141 W	4,4	292	3	77	60	center airgun first shot
02.09.2001	14:59	02°33,929 S	81°55,169 W	3,9	279	3	3114		last shot
Profile 02									total number of shots = 1172

Sheet - No.: 2

Appendix III

Airgun - Pulserstation

Project: Salieri Line: P03 / P04 Airgun: 32 l

Date	Time UTC	Latitude	Longitude	Speed [kn]	Course o.G./GPS	Guns	Depth [m]	Trigger Interval [s]	Remarks Operator
03.09.2001	11:08	03°06,513 S	81°28,767 W	3,1		1	3017	60	port gun first shot
03.09.2001	11:17	03°06,415 S	81°28,062 W	4,6	22	2	2901	60	stb gun first shot
03.09.2001	12:59	02°58,632 S	81°26,057 W	4,6	28	2	2480	40	ok
03.09.2001	19:04	02°32,584 S	81°17,102 W	3,7	27	2	1701		last shot
Profile 03									total number of shots = 649
Profile 04	23:28	02°30,3266 S	81°01,537 W	3	203	1		60	port gun first shot
04.09.2001	23:34	02°30,663 S	81°01,664 W	3,8	198	2		60	stb gun first shot
04.09.2001	23:45	02°31,371 S	81° 01,8634 W	4,2	199	3	77	60	center gun first shot
05.09.2001	00:30	02°34,035 S	81°02,5829 W	4,5	198	2		60	center gun switched off
05.09.2001	03:34	02°46,995 S	81°06,443 W	4,4	196	3	697	60	center gun back into water
05.09.2001	03:35	02°47,878	81°06,698 W	4,3	199	3	706	60	

Sheet - No.: 3

Airgun - Pulserstation

Project: Salieri Line: P04 / P05 Airgun: 32 l

Date	Time UTC	Latitude	Longitude	Speed [kn]	Course o.G./GPS	Guns	Depth [m]	Trigger Interval [s]	Remarks Operator
05.09.2001	07:24	3°04,071 S	81°11.452 W	3,0	196	3	1137	60	center gun back into water
05.09.2001	09:31	03°13,270 S	81°14,136 W	4,5	194	2	1138	60	starbord gun off
05.09.2001	09:35					1		60	center gun off
05.09.2001	11:56	03°23,235 S	81°17,058 W	3,32	191	1	1256		last shot Profile 04
Profile 04									total number of shots: 743
Profile 05	13:19	00°58,251 S	82°00,270 W	2,7	16	1	1378	60	port gun first shot
08.09.2001	13:28	00°57,688 S	82°00,164 W	4,4	11	2	1382	60	stb gun first shot
08.09.2001	13:31	00°57,454 S	82°00,119 W	4,6	15	1	1382	60	stb gun is leaking / off
08.09.2001	14:50	00°53,152 S	81°59,313 W	3,5	8	2	1444	60	stb gun first shot
09.09.2001	00:03	00°10,580 S	81°51,990 W	4,0	12	3	741	60	center gun first shot
09.09.2001	08:00	00°18,750 S	81°45,684 W	4,2	8	3	2895	60	reduced pressure 125 bar

Sheet - No.: 4

Appendix III

Airgun - Pulserstation

Project: Salieri Line: P05 / P06 Airgun: 32 l

Date	Time UTC	Latitude	Longitude	Speed [kn]	Course o.G./GPS	Guns	Depth [m]	Trigger Interval [s]	Remarks Operator
09.09.2001	08:00	00°18,750 N	81°45,684 W	4,2	8	3	2895	60	reduced pressure 125 bar
09.09.2001	08:30	00°20,741 N	81°45,305 W	4,1	11	3	2989	60	reduced pressure 100 bar
09.09.2001	08:34	00°21,039 N	81°45,349 W	4,1	11	2	2970	60	stb gun dead
09.09.2001	10:40	00°29,731 N	81°43,582 W	4,0	11	1	2535	60	center gun not triggering
09.09.2001	12:24	00°36,789 N	81°42,273 W	4,1	10	2	2932	60	stb gun first shot
09.09.2001	18:14	01°00,592 N	81°37,740 W	2,1	11	2	2920		last shot
Profile 05									total number of shots = 1644
Profile 06	22:10	01°14,230 N	79°13,61 W	3,0	299	1	57	60	port gun first shot
11.09.2001	22:18	01°14,230 N	79°13,911 W	2,9	298	2	62	60	starboard gun first shot
12.09.2001	00:48	01°21,629 N	79°22,235 W	4,5	309	3	668	60	center gun first shot
12.09.2001	14:54	02°02,416 N	80°04,986 W	2,9	307	3	3104		last shot
Profile 06									total number of shots = 1004

Sheet - No.: 5

Salieri/SO159 - Magnetic Profiles

Profile Number	Date UTC	Time UTC	Lat	Lon	Profile Length [km]	Magnetic Field Strength [nT]	Remarks
Start P101	23.08.01	07:10	2,8816°S	80,6951°W	18,802	29439	
End P101	23.08.01	08:13	2,9568°S	80,8468°W		29414	
Start P102	23.08.01	08:14	2,9575°S	80,4890°W	119,973	29415	
End P102	23.08.01	12:32	2,9007°S	81,5668°W		29477	
Start P103	23.08.01	23:20	2,7035°S	81,5446°W	510,333	29495	
End P103	25.08.01	05:34	0,0923°S	85,3268°W		30885	
Start P105	26.08.01	03:42	2,6320°S	84,9918°W	27,48	29647	
End P105	26.08.01	05:16	2,4425°S	84,8319°W		29980	
Start P106	26.08.01	05:17	2,4426°S	84,8300°W	27,335	29921	
	26.08.01	05:39	2,4437°S	84,7682°W		29923	short break for sensor inspection due to too large spikes
	26.08.01	07:02	2,4470°S	84,5909°W		29776	magnetometer recording again
End P106	26.08.01	07:16	2,4600°S	84,5848°W		29693	
Start P107	26.08.01	07:17	2,4608°S	84,5854°W	77,347	29701	
End P107	26.08.01	11:34	3,0577°S	84,9482°W		29545	
Start S1	26.08.01	12:30	3,0052°S	84,9544°W	354,977 + 29,242	29538	
	27.08.01	07:32	0,1789°N	85,3629°W		30205	Greatest distance from beginning of profile before going back to recover instruments
End S1	28.08.01	09:18	0,0830°S	85,3263°W		30953	
Start P108	30.08.01	17:32	2,0908°S	84,9277°W	12,724	30221	
End P108	30.08.01	23:45	2,0842°S	85,0419°W		30173	
Start S2	01.09.01	19:46	3,0884°S	80,5699°W	150,089	29343	
End S2	02.09.01	16:19	2,6087°S	81,8329°W		29655	

Appendix IV

Salieri/SO159 - Magnetic Profiles

Profile Number	Date UTC	Time UTC	Lat	Lon	Profile Length [km]	Magnetic Field Strength [nT]	Remarks
Start S3	03.09.01	11:34	3,0802°S	81,4700°W	62,101	29425	
End S3	03.09.01	18:57	2,5494°S	81,2874°W		29611	
Start S4	04.09.01	23:52	2,5312°S	81,0337°W	98,243	29480	
End S4	05.09.01	11:53	3,3835°S	81.2835°W		29256	
Start S5	08.09.01	15:22	0,8330°S	81,9783°W	206,583	30306	
End S5	09.09.01	18:03	1,0023°N	81,6304°W		31204	
Start S6	11.09.01	23:31	1,2990°N	79,2984°W	125,57	31014	
End S6	12.09.01	14:43	2,0337°N	80,1591°W		31512	
Start P13	13.09.01	19:43	1,7263°N	80,0415°W	298,71	31408	
End P13	14.09.01	12:00	0,5836°S	81,4336°W		30341	